Metabolic regulation of the plasma membrane calcium pump in pancreatic ductal adenocarcinoma

A thesis submitted to The University of Manchester for the degree of DOCTOR OF PHILOSOPHY in the Faculty of Life Sciences

2015

ANDREW DAVID JAMES

Table of Contents

Table of Figures

Chapter 1 Figures

Chapter 2 Figures

Chapter 3 Figures

Chapter 4 Figures

Chapter 5 Figures

Table of Supplementary Figures

Chapter 2 Supplementary Figures

Chapter 3 Supplementary Figures

Chapter 4 Supplementary Figures

List of Supplementary Tables

Chapter 4 Supplementary Tables

Word Count: 79,407

Abstract

Institution: The University of Manchester
Name: Andrew David James
Degree title: PhD Pharmacology
Thesis Title: Metabolic regulation of the plasma membrane calcium pump in pancreatic ductal adenocarcinoma
Date: 2015

Pancreatic ductal adenocarcinoma (PDAC) is an aggressive form of cancer with poor prognosis and limited treatment options. Since many patients present with metastatic disease and are thus ineligible for surgical resection, PDAC is almost ubiquitously fatal; new treatment options are therefore needed to combat this disease. A key hallmark of many cancers, including PDAC, is metabolic reprogramming and a shift towards a high glycolytic rate, known as the Warburg effect. This allows cancer cells to generate ATP in the face of hypoxia and to meet the increased metabolic requirements associated with rapid proliferation. We hypothesised that this shift towards glycolytic metabolism has important implications for the regulation of cytosolic Ca^{2+} ($[Ca^{2+}]_i$) in PDAC, since the plasma membrane Ca^{2+} ATPase (PMCA), which is critical for maintaining low $[Ca^{2+}]_i$ and thus cell survival, is dependent on ATP to extrude cytosolic Ca^{2+}. The relative contributions of mitochondrial vs glycolytic ATP in fuelling the PMCA in human PDAC cell lines (PANC-1 and MIA PaCa-2) were therefore assessed. Moreover, the effects of numerous mechanistically distinct metabolic inhibitors on key readouts of cell death, $[Ca^{2+}]_i$ and ATP were investigated. Treatment with glycolytic inhibitors induced significant ATP depletion, PMCA inhibition, $[Ca^{2+}]_i$ overload and cell death in both PANC-1 and MIA PaCa-2 cells, while mitochondrial inhibitors had no effect. Subsequently, these experiments were repeated on PDAC cells cultured in media formulated to “switch” their highly glycolytic phenotype back to one more reliant on mitochondrial metabolism. Culture in nominal glucose-free media supplemented with either galactose (10 mM) or α-ketoisocaproate (KIC, 2 mM) resulted in a switch in metabolism in MIA PaCa-2 cells, where proliferation rate and glycolysis were significantly decreased, and in the case of cells cultured in KIC, oxidative phosphorylation rate was preserved (assessed using Seahorse XF technology). Following culture of MIA PaCa-2 cells in either galactose or KIC, glycolytic inhibition failed to recapitulate the profound ATP depletion, PMCA inhibition and $[Ca^{2+}]_i$ overload observed in glucose-cultured MIA PaCa-2 cells. These data demonstrate that in PDAC cells exhibiting a high rate of glycolysis, glycolytically-derived ATP is important for fuelling $[Ca^{2+}]_i$ homeostasis and thus is critical for survival. Finally, using a cell surface biotinylation assay, the key glycolytic enzymes LDHA, PFKP, GAPDH, PFKFB3 and PKM2 were all found to associate with the plasma membrane in MIA PaCa-2 cells, possibly in a tyrosine phosphorylation-dependent manner. To investigate whether the dynamic membrane-association of glycolytic enzymes provides a privileged supply of ATP to the PMCA in PDAC, the effects of tyrosine kinase inhibitors was assessed on PMCA activity. However, while these inhibited PMCA activity, this occurred without accompanying global ATP depletion. These data indicate that glycolytic ATP is critical for the regulation of $[Ca^{2+}]_i$ by the PMCA in PDAC, and that the glycolytic regulation of the PMCA may be an important therapeutic locus. However, further research is required to determine whether membrane-bound glycolytic enzymes regulate its activity.

Declaration

No portion of the work referred to in the thesis has been submitted in support of an application for another degree or qualification of this or any other university or other institute of learning.

Copyright Statement

List of Abbreviations

~	Approximately
$[ATP]_i$	Cytosolic ATP concentration
$[Ca^{2+}]_i$	Cytosolic Ca^{2+} concentration
2-DG	2-deoxyglucose
2-DG-6-P	2-deoxyglucose-6-phosphate
505LP	505 nm long pass
AA	Antimycin A
acetyl CoA	Acetyl Coenzyme A
AE1	Anion exchanger 1
AM	Antimycin A
AMPK	AMP-activated protein kinase
ASCT2	ASC amino-acid transporter 2
AU	Absorbance units
AUC	Area under the curve
BNIP3	BCL2/adenovirus E1B 19 kDa protein-interacting protein 3
BrPy	3-bromopyruvate
Ca^{2+}	Calcium
CaM	Calmodulin
CCCP	Carbonyl cyanide m-chlorophenyl hydrazine
CCE	Capacitative Ca^{2+} entry
CDKs	Cyclin-dependent kinases
CICR	Ca^{2+}-induced Ca^{2+}-release
COX	Cytochrome c oxidase
CPA	Cyclopiazonic acid
CPA	Cyclopiazonic acid
CRAC	Ca^{2+} release activated Ca^{2+} channels
Cyt C	Cytochrome C
DAG	Diacylglycerol
DMEM	Dulbecco's modified Eagle's medium
DTT	Dithiothreitol
ECAR	Extracellular acidification rate
EGFR	EGFR
ER	Endoplasmic reticulum
F6P	Fructose-6-phosphate
FBP	Fructose-1,6-bisphosphate
FDG-PET	^{18}F-fluorodeoxyglucose positron emission tomography
G	Genistein
G+T	genistein and tyrphostin A23
G6PD	Glucose-6-phosphate dehydrogenase
GAPDH	Glyceraldehyde 3-phosphate dehydrogenase
GAPs	GTPase activating proteins
GEFs	Guanine nucleotide exchange factors
GFR	Growth factor receptor
GLDH	Glutamate dehydrogenase
GLS	Glutaminase
GLUT	Glucose transporter

GPCR	G-protein coupled receptor
GTP	Guanosine triphosphate
HEPES-PSS	HEPES-buffered physiological saline solution
HIF	Hypoxia inducible factor
HK	Hexokinase
HKI	Hexokinase I
HKII	Hexokinase II
HPH	HIF-1α prolyl hydroxylase
IAA	Sodium iodoacetate
IGFBP3	Insulin-like growth factor-binding protein 3
IP_3	Inositol trisphosphate
IP_3Rs	Inositol trisphosphate receptors
IPMN	Intraductal papillary mucinous neoplasias
KIC	α-ketoisocaproate
LDH	Lactate dehydrogenase
LDHA	Lactate dehydrogenase A
LDHB	Lactate dehydrogenase B
LGCC	Ligand-gated Ca2+ channel
LKB1	Liver kinase B1
MAM	Mitochondria-associated ER membrane
Max-$\Delta[Ca^{2+}]_i$	Maximum change in $[Ca^{2+}]_i$
MCN	Mucinous cystic neoplasias
MCT	Monocarboxylate transporter
MCU	Mitochondrial calcium uniporter
MDM2	Murine double minute
mNCX	Mitochondrial Na^+/Ca^{2+}-exchanger
mTOR	Mammalian target of rapamycin
mTORC1/2	Mammalian target of rapamycin complex 1/2
MUC1	Mucin 1
Na^+ free/NMDG	Na^+-free/138mM N-methyl D-glucamine HEPES-PSS
NCX	Na^+/Ca^{2+} exchanger
NCX	Na^+/Ca^{2+} exchanger
NFAT	Nuclear factor of activated T cells
NF-κB	Nuclear factor kappa-light-chain-enhancer of activated B cells
NHERF	Na^+/H^+ exchanger regulatory factor-2
NMDG	*N*-Methyl-D-glucamine
OCR	O2 consumption rate
OM	Oligomycin
OXPHOS	Oxidative phosphorylation
p16INK4A	Cyclin-dependent kinase inhibitor 2A
p19ARF	Alternate reading frame tumor suppressor
PanIN	Pancreatic intraepithelial neoplasias
PBS	Phosphate buffered saline
PDAC	Pancreatic ductal adenocarcinoma
PDH	Pyruvate dehydrogenase
PDK1	Pyruvate dehydrogenase kinase 1
PFK	Phosphofructokinase

PFK1	Phosphofructokinase 1
PFKFB3	6-phosphofructo-2-kinase/fructose-2,6-biphosphatase 3
PFKP	Phosphofructokinase, platelet
PGI	Phosphoglucose isomerase
PGK	Phosphoglycerate kinase
PGM	Phosphoglycerate mutase
PI	Phosphatidylinositol
PI3K	Phosphoinositide 3-kinase
PIP_2	Phospholipid phosphatidylinositol-4,5-bisphosphate
PIP_3	Phosphatidylinositol 3,4,5-trisphosphate
PKC-α	Protein kinase C-α
PKM1	Pyruvate kinase muscle 1 isoform
PKM2	Pyruvate kinase muscle 2 isoform
PLB	Phospholamban
PMCA	Plasma membrane Ca^{2+} ATPase
PMCA NS	PMCA (isoform nonspecific)
pO_2	Oxygen partial pressure
PPP	Pentose phosphate pathway
PSC	Pancreatic stellate cell
PS	Phosphatidylserine
PTEN	Phosphatase and tensin homolog
PV	Pervanadate
Q	Coenzyme Q
R_0	Baseline ratio
R_{min}	Minimum ratio
ROS	Reactive oxygen species
Rot	Rotenone
Rsmad	Receptor-regulated Smads
RyR	Tyanodine receptor
SCO2	Synthesis of Cytochrome c Oxidase 2
SERCA	Sarcoplasmic/endoplasmic reticulum Ca2+-ATPase
Smad	Mothers against decapentaplegic homolog
SPCA	Secretory pathway Ca^{2+} ATPase
SR	Sarcoplasmic reticulum
STIM1	Stromal interacting molecule 1
T	Tyrphostin A23
TCA cycle	Tricarboxylic acid cycle
TGF-β	Transforming growth factor β
TIGAR	TP53-inducible glycolysis and apoptosis regulator
TMC	Time-matched control
TPI	Triosephosphate isomerase
TRP	Transient receptor potential
TSC2	Tuberous sclerosis 2
VDAC	Voltage dependant anion channel
VEGF	Vascular endothelial growth factor
VHL	von Hippel–landau tumour suppressor
VOCC	Voltage-dependent Ca2+ channel
α-KG	α-ketoglutarate

ΔR_{max}	Maximum decrease in ratio
$\Delta \Psi m$	Mitochondrial membrane potential
τ	Tau, relative time constant

Acknowledgements

Firstly, I would like to thank my supervisor Dr Jason Bruce for all his help and guidance throughout my PhD project. His support has been invaluable in my progression, and the time, effort and advice he has contributed to my project has been key in ensuring it was both a productive and enjoyable venture.

Secondly, I would also like to thank all members of the Bruce lab past and present for their help with my studies, and all those who have contributed to the work contained within this thesis. Special thanks go to Parini Mankad, Ayse Latif, Carolina Uggenti, Anthony Chan, James Wong Donald Ward, Martin Steward and Svetoslav Kalaydjiev for their help and advice with the experimental methods used throughout my project.

I would like to thank both the Biotechnology and Biological Sciences Research Council and AstraZeneca plc, whose funding to support my project was valued and greatly appreciated, and all our collaborators at both AstraZeneca and Manchester Royal Infirmary, in particular Prof. Chris Womack, Prof. Ajith Siriwardena and Dr. Asela Bandera.

Finally, I would also like to thank my family and friends for their support throughout my PhD project. Most especially, I would like to thank my parents, whose never-ending support and encouragement has been invaluable throughout the challenges of the past 4 years, and to whom I dedicate this thesis.

Chapter 1 - Introduction

1.1 - Thesis Overview

The term “cancer” denotes a group of often fatal diseases which are characterised by the uncontrolled proliferation of cells, their invasion and destruction of surrounding tissue, and subsequently their metastasis through the blood stream and lymphatic system to tissues distant from the original tumour. Over a quarter of all deaths in the UK are attributed to cancer (Cancer Research UK, 2014), with over 7.6 million cancer related deaths in total worldwide in 2008 (Jemal et al., 2011). Characterising the underlying mechanisms by which cancers originate and progress has long been the aim of researchers searching for novel ways to combat this group of diseases. However, due to the many numerous subtypes of cancer and their inherent complexity and heterogeneity, there is still an unmet clinical need for ways to treat cancer and prognosis remains poor for many tumour subtypes. One such form of cancer is pancreatic cancer, which while relatively uncommon is almost universally fatal within a matter of months. Due to such poor prognosis, research has focused on potential new treatment avenues for these illnesses, and of particular interest is the aberrant metabolism exhibited by tumours. Many cancers, including pancreatic cancer, exhibit an abnormally high glycolytic rate and a corresponding downregulation of mitochondrial metabolism, and it has been suggested that this may be an “Achilles’ heel” with which to target these cancers selectively (Kroemer and Pouyssegur, 2008). The theme of this thesis is the role of altered metabolism in pancreatic cancer in regulating the plasma membrane calcium (Ca^{2+}) pump (PMCA), an energy driven pump on the plasma membrane that is responsible for extruding Ca^{2+} from the cytosol and maintaining the homeostatic regulation of Ca^{2+} levels within the cell. PMCA action is critical for cell survival; as such, this thesis aims to evaluate its regulation by metabolism in pancreatic cancer as a potential as a novel therapeutic locus.

The following introductory chapter will provide a broad overview of:

- The energy generating metabolic pathways in human cells; glycolysis and oxidative phosphorylation.
- The pathophysiology of pancreatic ductal adenocarcinoma (PDAC).
- The shift towards glycolytic metabolism in cancer (“Warburg Effect”) and its advantages for cancer cells.
- The underlying mechanisms responsible for reprogramming metabolic pathways in PDAC.
- The targeting of glycolytic metabolism in cancer.
- The general mechanisms of intracellular intracellular calcium (Ca^{2+}) signalling.
- The PMCA and its regulation by ATP.

1.2 - Glycolysis and Oxidative Phosphorylation: The metabolic pathways for generating energy in human cells

Glucose is a 6 carbon monosaccharide and is the main source of energy used by eukaryotic cells. Conversion of glucose to energy in the form of ATP occurs via two respiratory mechanisms, glycolysis and oxidative phosphorylation (Figure 1.1), with the abundance of oxygen being a deciding factor as to which of these mechanisms predominantly operates (Alberts, 2004). Once transported into the cell via glucose transporters, glucose is converted to pyruvate via glycolysis (from glycose, an older term for glucose, and lysis, from the Greek “to separate”), a 10 step process that occurs within the cytoplasm. During the first three reactions of glycolysis, 2 molecules of ATP are consumed, and glucose is converted from one six-carbon glucose molecule to two three-carbon glyceraldehyde-3-phosphate molecules. The remainder of the glycolytic cascade generates two molecules of ATP and one of pyruvate for each molecule of glyceraldehyde-3-phosphate, with two molecules of NAD^+ reduced to NADH to fuel the fifth step catalysed by glyceraldehyde 3-phosphate dehydrogenase. Glycolysis therefore results in a net yield of two moles ATP and pyruvate for every mole of glucose.

Under aerobic conditions, pyruvate generated by glycolysis is transported to the matrix of the mitochondria, where a single molecule of pyruvate is acetylated to acetyl coenzyme A (acetyl CoA) by pyruvate dehydrogenase (PDH). Acetyl-CoA then enters the tricarboxylic acid (TCA) cycle where it is further oxidised over a series of steps to generate 3 NADH molecules in addition to a single molecule of both guanosine triphosphate (GTP) and $FADH_2$. The NADH and $FADH_2$ then enter the electron transport chain where they are oxidised by protein complexes I to IV, each of which concomitantly translocates protons from the mitochondrial matrix into the intermembrane space. These protons move down their concentration gradient through protein complex V, also known as ATP synthase, which harnesses the energy of the moving protons to phosphorylate ADP to ATP. This ultimately generates between 30 and 36 molecules of ATP for each molecule of glucose via a process known as oxidative phosphorylation.

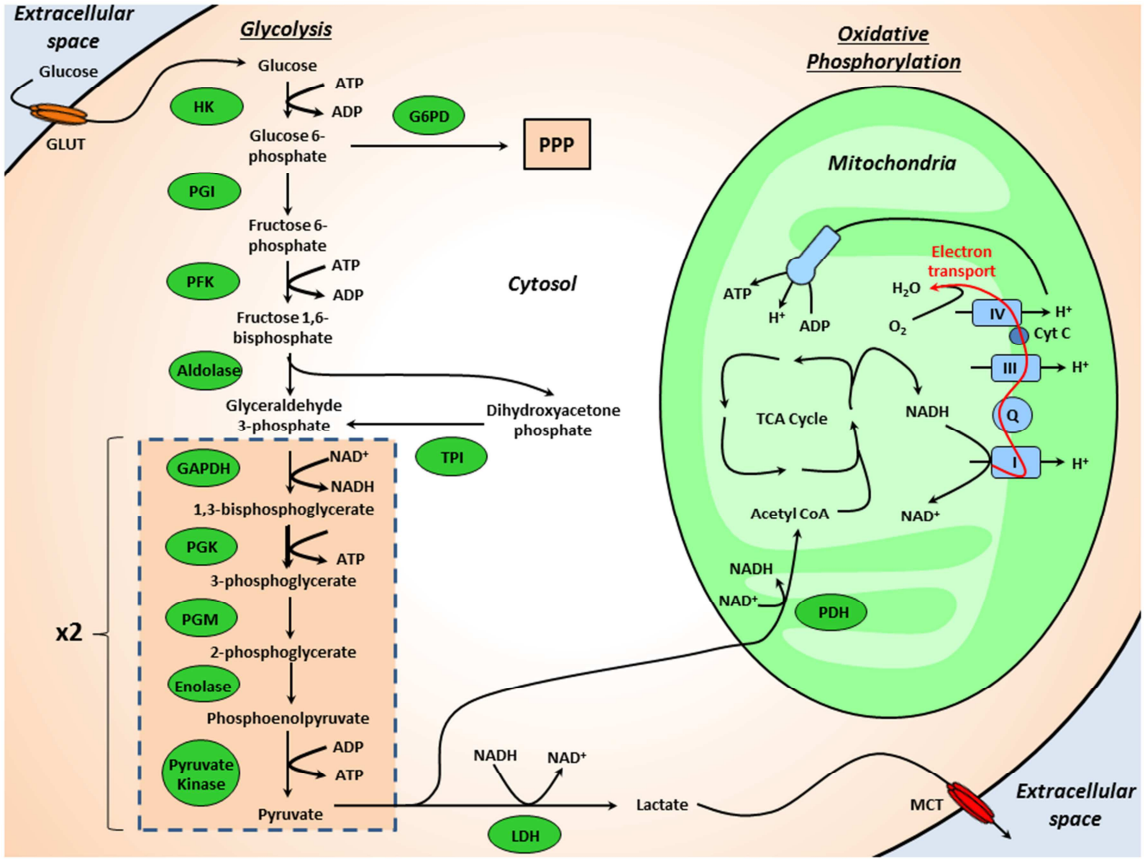

Figure 1.1 – ATP generation by glycolysis and oxidative phosphorylation

Metabolic enzymes are shown in green, and electron transport chain proteins in blue. Additional abbreviations: HK, hexokinase; PGI, phosphoglucose isomerase; PFK, phosphofructokinase; TPI, triosephosphate isomerase; GAPDH, glyceraldehyde 3-phosphate dehydrogenase; PGK, phosphoglycerate kinase; PGM, phosphoglycerate mutase; LDH, lactate dehydrogenase; PDH, pyruvate dehydrogenase. Q, Coenzyme Q; Cyt C, Cytochrome C. TCA, tricarboxylic acid cycle. MCT, monocarboxylate transporter; GLUT, glucose transporter; PPP, pentose phosphate pathway.

Conversely, under anaerobic conditions, insufficient oxygen is present to drive the electron transport chain and instead ATP is generated by fermentation of glucose. The pyruvate generated by glycolysis is converted to lactic acid by lactate dehydrogenase (LDH) with the concomitant generation of NAD^+ from NADH. This NAD^+ is used to fuel further generation of ATP via glycolysis. Despite a much smaller net yield of ATP than oxidative phosphorylation (2 moles of ATP per mole of glucose rather than 36) ATP synthesis in this manner occurs at a much faster rate (Curi et al., 1988, Pfeiffer et al., 2001).

Typically, in normal cells, the conditions to which the cell is exposed dictate how pyruvate is utilized by the cell, and under normoxia the majority generated enters the TCA cycle to fuel oxidative phosphorylation. However, following oncogenic transformation, the fate of pyruvate generated by glycolysis is significantly influenced by the metabolic reprogramming of cancer cells in order to fuel cell proliferation and survival (See *1.4 - The Warburg Effect – Why do cancers exhibit high glycolysis?*).

1.3 - Pancreatic cancer: a silent killer

Cancer of the pancreas is the fourth and fifth most common cause of cancer-related death in men and women, respectively (Krejs, 2010), and risk factors include smoking (Fuchs et al., 1996), family history of the disease (Hassan et al., 2007), advanced age, chronic and hereditary pancreatitis (Bansal and Sonnenberg, 1995), diabetes mellitus (Huxley et al., 2005) and obesity (Berrington de Gonzalez et al., 2003). Pancreatic ductal adenocarcinoma (PDAC) is the most common form of pancreatic cancer, accounting for 85% of pancreatic tumours (Warshaw and Fernandez-del Castillo, 1992, Li et al., 2004), and as its nomenclature suggests is derived from the ductal tissue of the exocrine pancreas. This form of pancreatic cancer typically occurs at the head of the pancreas, from where it can infiltrate the lymphatic system, spleen and peritoneal cavity, thereby facilitating metastasis to the lungs and liver (Hezel et al., 2006). Treatment options are severely limited, and surgical removal of the tumour is the most common course of action. PDAC has become dubbed a “silent killer” due to its rapid progression in the absence of obvious clinical symptoms, and as a result patients often present with the disease at a stage when the cancer has already metastasized (Amin et al., 2006). As a result, only 10 – 20% of patients diagnosed with PDAC present with resectable disease (Loos et al., 2008). Nevertheless, PDAC is almost uniformly fatal; the five year survival rate for patients with pancreatic cancer has been estimated at below 1% (Gudjonsson, 2009). Such poor prognosis and a lack of effective treatment advocates research into new ways to combat this aggressive cancer.

The pathophysiology of cancer is characterised by the development of premalignant neoplasms, which develop into malignant cells as oncogenic transformation progresses. Likewise, prior to the development of frank PDAC, progressive precursor lesions appear in the pancreas tissue (Hruban et al., 2004). Histopathological studies focusing on the cellular origins of PDAC have identified three forms of precursor lesion; pancreatic intraepithelial neoplasias (PanINs), mucinous cystic neoplasias (MCN), and intraductal papillary mucinous neoplasias (IPMN) (Hezel et al., 2006). The most common and well characterised of these precursor lesions are PanINs. These are asymptomatic papillary or flat lesions less than 5 mm that occur in the pancreatic ducts, and are classified as grades 1, 2 and 3 dependent on increasing morphological atypia (Hruban et al., 2004, Hruban et al., 2001). IPMNs are also papillary tumours of the duct epithelium, however these are characterised by mucin production and the subsequent dilatation of the affected ducts (Brugge et al., 2004). MCNs on the other hand, are the least common precursor lesion, and due to their cystic morphology and relatively large size are often found incidentally (Distler et al., 2014). Although the development and morphology of these precursor lesions is beyond the scope of this article (for a recent review, see Distler et al., 2014), these precursor lesions harbour progressive genetic changes that influence metabolic reprogramming and their transformation into in PDAC.

Early mutations implicated in the formation of PDAC precursor lesions (Figure 1.2) include the activation of oncogenic K-Ras in more than 90% of cases (Hezel et al., 2006) and the loss the tumour suppressor protein p16INK4A. Increasing numbers of mutations are

observed as a lesion progresses in severity towards PDAC (Morris et al., 2010), such as the inactivation of the tumour suppressor proteins p53 and SMAD4 (Hezel et al., 2006, Bardeesy and DePinho, 2002) by the PanIN3 stage. In addition, the PanIN sequence is characterised by telomere shortening, which leads to chromosomal instability and therefore can facilitate transformation (Hong et al., 2011, van Heek et al., 2002). In addition to acquired changes in protein function or expression, it is estimated that hereditary mutations contribute to around 10% of pancreatic cancers (Petersen and Hruban, 2003).

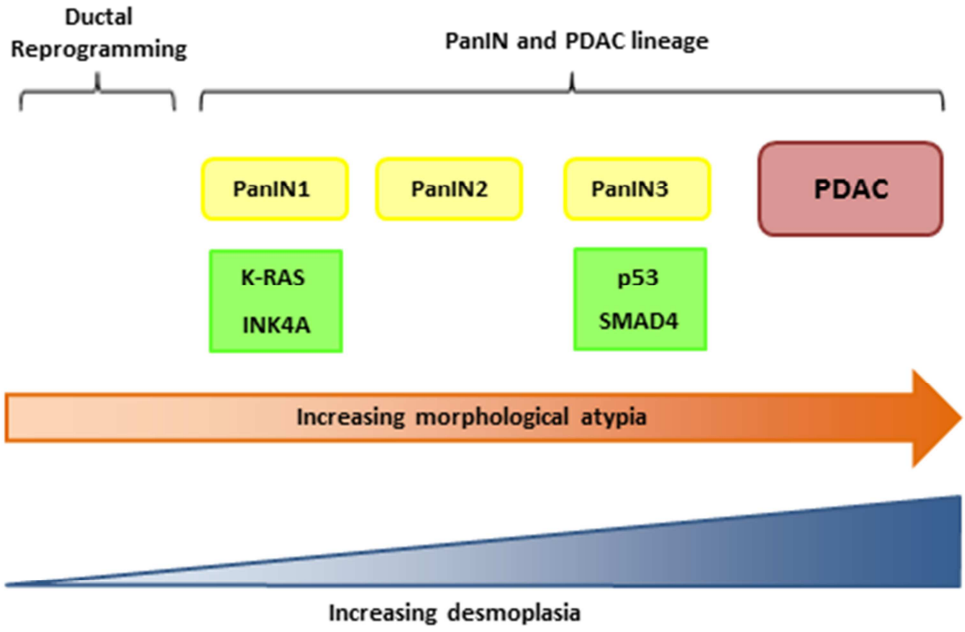

Figure 1.2 – The progression of PanINs to PDAC

Progression of pancreatic intraepithelial neoplasias (PanINs) to pancreatic ductal adenocarcinoma (PDAC) is associated with increasing morphological atypia, an increased desmoplasic response and the cumulative acquisition of oncogenic mutations (commonly implicated proteins shown in green boxes). Additional abbreviations: Cyclin-dependent kinase inhibitor 2A, INK4A; Kirsten rat sarcoma viral oncogene homolog, K-RAS; mothers against decapentaplegic homolog 4, Smad4; tumour protein 53, p53. Adapted from Morris et al., 2010.

Frank PDAC is characterised by tumour desmoplasia, that is, the formation of a dense matrix of connective tissue typically consisting of collagen and fibronectin (Mollenhauer et al., 1987). This dense stroma is particularly rich in PDAC, with stromal components often outnumbering cancer cells, and the contributing factors to this heterogeneous PDAC microenvironment have been extensively reviewed elsewhere (Feig et al., 2012). However, it appears that pancreatic stellate cells (PSCs) play a key role in its formation. PSCs are a subpopulation of pancreatic cells with similar characteristics to fibroblasts which appear to have a key role in facilitating the desmoplastic response in PDAC (Jaster, 2004). Using paracrine

signalling via fibroblast growth factor 2 and transforming growth factor β, PDAC cells stimulate the deposition of connective tissue by PSCs, which in turn facilitates and accelerates tumour growth (Bachem et al., 2005). *In vitro* studies have also indicated that secretions from PSCs stimulate cancer cell proliferation, invasion and metastasis while inhibiting cancer cell apoptosis (Vonlaufen et al., 2008). Furthermore, studies modelling PDAC metastasis in mice suggest that PSCs can stimulate angiogenesis and accompany PDAC cells to metastatic sites to aid secondary tumour growth (Xu et al., 2010b). In response to the hypoxic environment, PDAC cells stimulate further deposition of extracellular matrix by PSCs via sonic hedgehog signalling; this exacerbates the hypoxic core of the tumour in a feed forward loop (Spivak-Kroizman et al., 2013). Importantly, the resulting dense fibrotic network prevents neovascularisation of tumour, limiting the formation of new blood vessels and the efficient delivery of oxygen and nutrients (Koong et al., 2000). As a result, a key characteristic of PDAC is a highly hypoxic tumour core with restricted access for drug delivery (Feig et al., 2012). Indeed, a highly hypoxia tumour core is correlated with resistance to therapy, increased metastasis and poorer prognosis (Zhang et al., 2010).

1.4 - The Warburg Effect – Why do cancers exhibit high glycolysis?

In the 1920's Otto Warburg observed that cancer cells exhibited an abnormally high production of lactic acid in comparison to normal respiring tissues, even in the presence of abundant O_2 (Warburg, 1956). This high glycolytic flux in cancer has since become known as the "Warburg effect" and has become a key hallmark of many tumours (Hanahan and Weinberg, 2011). Warburg hypothesised that this "aerobic glycolysis" was a causative factor in oncogenic transformation, and stemmed from impaired mitochondrial function. Although it is now appreciated that mitochondria are in fact functional in most tumour types (Frezza and Gottlieb, 2009), and can also contribute to ATP synthesis (Zu and Guppy, 2004), aberrant glucose metabolism and upregulated glycolysis remain a common feature of many tumour types (Gillies and Gatenby, 2007). Indeed, it is the increased glucose uptake exhibited by highly glycolytic cells which is exploited by ^{18}F-fluorodeoxyglucose positron emission tomography (FDG-PET) for the detection of primary tumours and metastases (Gambhir, 2002). It is now understood that the Warburg phenotype is instead driven by oncogene-induced metabolic reprogramming (Cairns et al., 2011); the numerous signalling pathways responsible for inducing the Warburg phenotype in PDAC will be considered in the following sections. Despite being an energetically unfavourable means of generating ATP in comparison to oxidative phosphorylation, the shift towards glycolysis has since been hypothesised to confer numerous survival advantages to tumour cells, including resistance to hypoxia, promotion of metastasis, and the increased generation of glycolytic intermediates to allow the incorporation of glucose carbon into anabolic processes and cell proliferation (Kroemer and Pouyssegur, 2008, Vander Heiden et al., 2009, DeBerardinis et al., 2008a).

Numerous studies have established that PDAC has a highly glycolytic phenotype typical of those exhibiting the Warburg effect. This is primarily due to changes in the expression of

numerous key glycolytic enzymes (Dong et al., 2011a, Dong et al., 2011b, Zhou et al., 2012, Zhou et al., 2011, Mikuriya et al., 2007, Chaika et al., 2012b) and glucose transporter 1 (GLUT1), which is responsible for shuttling hexose sugars such as glucose into the cell. These expressional changes are in part driven by severe hypoxia at the core of PDAC tumours (Guillaumond et al., 2013), however, numerous oncogenic mutations contribute in pushing PDAC cells towards this highly glycolytic phenotype. Moreover, both the tumour microenvironment and oncogenic signalling are themselves influenced in response to the changing metabolic phenotype of PDAC (Figure 1.3). Understanding this shift in metabolism towards glycolysis, and the underlying mechanisms that initiate this metabolic reprogramming, has become the aim of numerous studies searching for novel treatment avenues for PDAC (Le et al., 2012, Blum and Kloog, 2014).

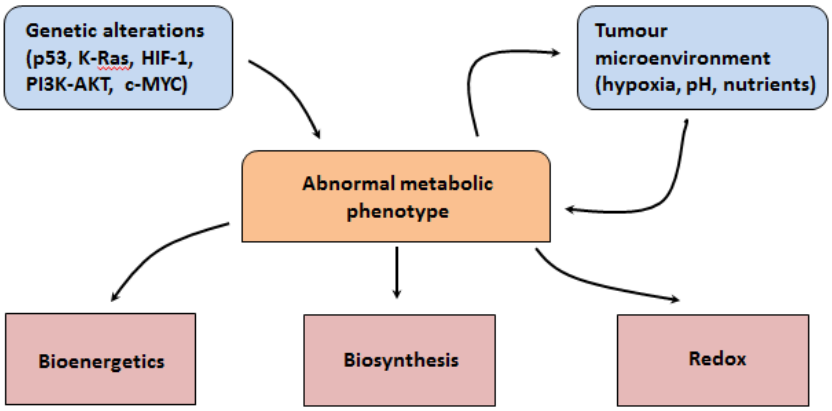

Figure 1.3 – Factors determining the metabolic phenotype in PDAC

The metabolic phenotype of PDAC is controlled by alterations in metabolic gene expression and the response of PDAC cells to the tumour microenvironment. Loss-of-function mutations in tumour suppressors (such as p53) and aberrant activation of oncogenic signalling pathways (such as the PI3K-AKT pathway) results in altered metabolism to meet the metabolic requirements of the rapidly dividing cancer cell. The resulting changes in metabolism that drive uncontrolled cell proliferation and lactate efflux (as a byproduct of increased glycolysis) lead to hypoxia, low pH and nutrient deprivation in the tumour microenvironment. This in turn induces a metabolic response within the PDAC cells, further influencing their metabolic phenotype. This altered metabolic phenotype allows cells to maintain production of ATP and biosynthetic substrates while balancing redox status. Adapted from Cairns et al., 2011.

Whilst Warburg initially hypothesised that the high glycolytic rate in cancer was responsible for generating the majority of ATP in the face of mitochondrial dysfunction, it is now appreciated that mitochondria are in fact functional in cancer (Frezza and Gottlieb, 2009). Instead, it is now thought that cancer cells upregulate glycolysis primarily to allow more glycolytic intermediates to be used for fuelling cell proliferation (DeBerardinis et al., 2008a). A high glycolytic flux results in an increased abundance of glycolytic intermediary products, which can then be diverted toward anabolic processes and utilized for cell proliferation (Tong et al., 2009). For example, glucose-6-

phosphate (G6P) can be shuttled into the pentose phosphate pathway (PPP) by the enzyme glycose-6-phosphate dehydrogenase (G6PD). The PPP uses the glucose-6-phosphate carbons to synthesise ribose-5-phosphate for the backbone of DNA/RNA, and generates reducing equivalents in the form of NADPH to maintain the intracellular redox state (Deberardinis et al., 2008b). This removes nucleotide abundance and synthesis as rate limiting factors for cell proliferation (Tong et al., 2009). Furthermore, in addition to providing precursors for the anabolic processes required for tumour growth, the increased generation of NADPH via the PPP provides an increased reducing potential with which to neutralise cytosolic reactive oxygen species (ROS), providing a survival advantage to cancer cells (Brand and Hermfisse, 1997, Kondoh et al., 2007, Vousden and Ryan, 2009).

Cancer cells also exhibit a degree of metabolic plasticity in order to adapt to the spatial heterogeneity of O_2 abundance within a tumour (Rodriguez-Enriquez et al., 2008, Cardenas-Navia et al., 2008), such that cancer cells with a high glycolytic flux are less sensitive to fluctuating oxygen levels and can survive in hypoxic conditions (Pouyssegur et al., 2006). An increased distance from blood vessels correlates with lower pH and oxygen partial pressure (pO_2) in tumours (Helmlinger et al., 1997), and hypoxia at the centre of primary tumours (pO_2 < 10 mmHg) is associated with an increased risk of metastasis and mortality (Vaupel and Mayer, 2007, Vaupel et al., 2004). It has been suggested that the hypoxia present in solid tumours selects for those cells most adapted to survive in those conditions, thereby driving the growth of highly glycolytic and aggressive cancer cells (Gatenby and Gillies, 2004). Furthermore, the increased production of lactic acid as a byproduct of high glycolysis leads to acidification of the extracellular matrix, which in turn facilitates tumour cell migration and invasion (Stock and Schwab, 2009, Gatenby et al., 2006) and suppresses anticancer immune functions (Fischer et al., 2007, Lardner, 2001) and therefore favours the metastatic phase of cancer. Interestingly, in addition to exhibiting metabolic plasticity, evidence also suggests that aerobic tumour cells proximal to blood vessels can take up the lactate produced by cells in hypoxic regions of the tumour and utilise it for mitochondrial oxidative phosphorylation. This phenomenon increases the availability of glucose to glycolytically-dependent cells at the hypoxic tumour core, forming a metabolic symbiosis between cells in a heterogeneous tumour bed (Sonveaux et al., 2008, Semenza, 2008).

In addition to increasing glucose flux through glycolysis, cancer cells exhibiting the Warburg effect commonly show an increased consumption of glutamine. Glutaminase (GLS) catalyses the conversion of glutamine to glutamate, which in turn is converted by glutamate dehydrogenase (GLDH) to α-ketoglutarate, a key intermediate in the TCA cycle (Vander Heiden et al., 2009). Studies have shown that glutamine consumption exceeds that required to meet the demands of nucleotide synthesis and to maintain nonessential amino acid pools (DeBerardinis et al., 2007), suggesting that glutamine acts an anapleurotic precursor for replenishing the metabolic intermediates of the TCA cycle. Additionally, cancer cells utilise glutamine to compensate for decreased pyruvate entry into the TCA cycle, which would otherwise leave cancer cells lacking citrate with which to generate fatty acids. This is achieved by converting glutamine-derived α-ketoglutarate to citrate via the TCA cycle, thereby

maintaining citrate levels for fatty acid synthesis in the face of decreased glucose flux into the mitochondria (Semenza, 2013, DeBerardinis et al., 2007). Consistent with this, the enzyme responsible for converting acetyl-CoA into fatty acids, fatty acid synthase (FAS), has also found to be upregulated in cancer (Wang et al., 2005). Finally, to complement the PPP, glutaminolysis is a robust means of generating NADPH, which provides a source of carbon and nitrogen amino acid synthesis and reducing power for fatty acid synthesis (Wise et al., 2008). Interestingly, numerous studies indicate that glutamine is the main carbon source utilised by the TCA cycle in mouse models of PDAC (Gao et al., 2009, Wise et al., 2008, Ying et al., 2012).

1.5 - Oncogenic Signalling Pathways Responsible for Metabolic Reprogramming in PDAC

An oncogene is a gene which has the potential to cause cancer, either due to overexpression or mutation of its gene product. Many oncogenic mutations and changes in protein expression are implicated in the pathogenesis and metabolic reprogramming of PDAC. The affected signalling pathways regulate many diverse cellular processes, including cell death, cell proliferation, cell cycle control and metabolism, and the mechanisms by which these contribute to the progression of the disease have been reviewed in detail elsewhere (Hanahan and Weinberg, 2011, Hezel et al., 2006, Hruban et al., 2008). However, a common feature of many tumours is a dependency on upregulated oncogenic pathways for the cancer cells' continued survival and proliferation, a phenomenon that has since been termed "oncogenic addiction" (Weinstein, 2000). As a result, understanding the role and regulation of these oncogenic pathways has become a key research aim of many research groups, with the goal of identifying novel treatment strategies that can discriminate between cancer cells and healthy cells.

The following section will focus specifically on those oncogenic signalling pathways in PDAC that influence cancer cell metabolism, and in particular those that impact on ATP-generating mechanisms in PDAC cells. These pathways are summarised in Figure 1.4, and the common transcription factor targets that contribute to the glycolytic phenotype of PDAC are summarised in Figure 1.5

1.5.1 - K-Ras

K-Ras is a member of the Ras family of guanosine triphosphate (GTP)-binding proteins that regulates cell survival and proliferation via downstream signalling of growth factor receptors (Malumbres and Barbacid, 2003). The Ras family of small GTPases (H-Ras, N-Ras, K-Ras4A and K-Ras4B, the latter two being splice variants) undergo conformational changes upon the binding of GTP or GDP, which confer the active and inactive states of Ras, respectively. When bound to GDP, Ras is inactive, and activation of Ras is achieved upon the binding of GTP after guanine nucleotide exchange factors (GEFs) induce the dissociation of GDP (Cullen and Lockyer, 2002). Inactivation of Ras signalling occurs upon hydrolysis of GTP to GDP. Importantly, the intrinsic GTPase activity of Ras is low, and Ras requires GTPase activating proteins (GAPs) to promote GTP hydrolysis by enhancing its intrinsic GTPase activity, in order

to revert Ras to its inactive state (di Magliano and Logsdon, 2013). Downstream of KRas are numerous signalling cascades including the RAF/MAPK and Ral GDS signalling cascades, however, it is the PI3K-mTOR (see *1.5.3 - PI3K-AKT*) pathway that is primarily responsible for the metabolic effects of oncogenic K-Ras signalling (Hruban et al., 2008, Gysin et al., 2011).

As the earliest known genetic change in noninvasive PDAC precursor lesions (Klimstra and Longnecker, 1994), K-Ras appears to be an important initiating factor in the development of PanINs and facilitating their subsequent progression into PDAC. Indeed, genetically engineered mice expressing oncogenic K-Ras acquire PanINs early in life before developing PDAC, indicating that K-Ras is a key driver of PDAC initiation *in vivo* (Aguirre et al., 2003, Guerra et al., 2003, Hingorani et al., 2003). Furthermore, activating mutations of the KRAS gene are present in more than 90% of PDAC, typically manifesting as mutations on codon 12 (Hruban et al., 2008, Morris et al., 2010, Hezel et al., 2006). Mutations in KRAS which lower or abolish the sensitivity of its protein product K-Ras to GAPs subsequently result in an inability to inactivate KRAS (Scheffzek et al., 1997). *In vitro* studies showed that transfection of cultured cell lines with oncogenic K-Ras led to increased phosphofructokinase 1 (PFK1) activity (Kole et al., 1991), increased production of lactate (Racker et al., 1985) and an upregulated expression of GLUT1 (Yun et al., 2009, Fleming et al., 2005), suggesting that K-Ras contributes to upregulated glycolysis in cancer.

Further advances in our understanding of the role of K-Ras specifically in PDAC metabolism came from genetically engineered mouse models of PDAC which express an oncogenic point mutation in KRAS. These showed that doxycycline-induced expression of oncogenic KRAS ($KRAS^{G12D}$) resulted in a decrease in cellular G6P, fructose-6-phosphate (F6P) and fructose-1,6-bisphosphate (FBP). Subsequent extinction of oncogenic KRAS upon withdrawal of doxycycline resulted in a decrease in glucose uptake and lactate production, and downregulation of GLUT1, HK1, HK2, PFK1, enolase and lactate dehydrogenase A (LDHA) gene transcription (Ying et al., 2012). In the same study, oncogenic KRAS was shown to promote anabolic glucose metabolism via the nonoxidative pentose phosphate pathway and hexosamine biosynthesis pathway in order to fuel cell proliferation. Concomitant to upregulating glucose flux through glycolysis, K-Ras has also been shown to be responsible for upregulating glutamine consumption in PDAC cells (Son et al., 2013).

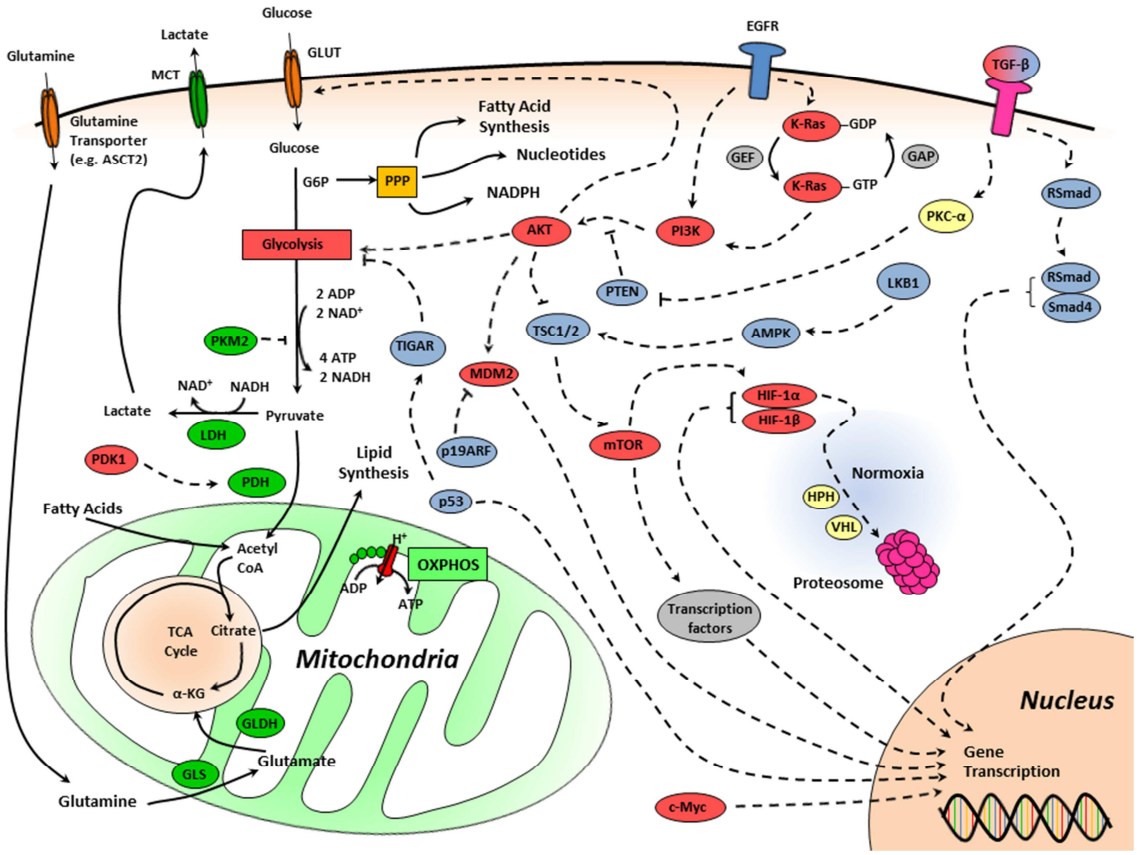

Figure 1.4 - Oncogenic signalling pathways involved in metabolic reprogramming in PDAC

Metabolic enzymes are shown in green. Signalling proteins that promote a high glycolytic rate in PDAC are shown in red, while those that oppose it (tumour suppressors) are shown in blue. electron transport chain proteins in blue. Additional abbreviations: AMPK, AMP-activated protein kinase; ASCT2, ASC amino-acid transporter 2; EGFR, epidermal growth factor receptor; GAP, GTPase-activating protein; GEF, guanine nucleotide exchange factor; G6P, glucose-6-phosphate; GLDH, glutamate dehydrogenase; GLS, glutaminase; GLUT, glucose transporter; HIF-1α/β, hypoxia inducible factor subunit α/subunit β; HPH, HIF-1α prolyl hydroxylase; α-KG, α-ketoglutarate; LDH, lactate dehydrogenase; LKB1, liver kinase B1; MCT, monocarboxylate transporter; MDM2, murine double minute 2; mTOR, mammalian target of rapamycin; OXPHOS, oxidative phosphorylation; PKC-α, protein kinase C-α; PDH, pyruvate dehydrogenase; PKC-α, protein kinase C α; PI3K, phosphoinositide 3-kinase; PKM2, pyruvate kinase M2 isoform; PPP, pentose phosphate pathway; PTEN, phosphatase and tensin homolog; RSmad, receptor-regulated Smads; Smad, mothers against decapentaplegic homolog; TIGAR, TP53-inducible glycolysis and apoptosis regulator; TGF-β, transforming growth factor β; TSC1/2, tuberous sclerosis complex; VHL, von Hippel–landau tumour suppressor.

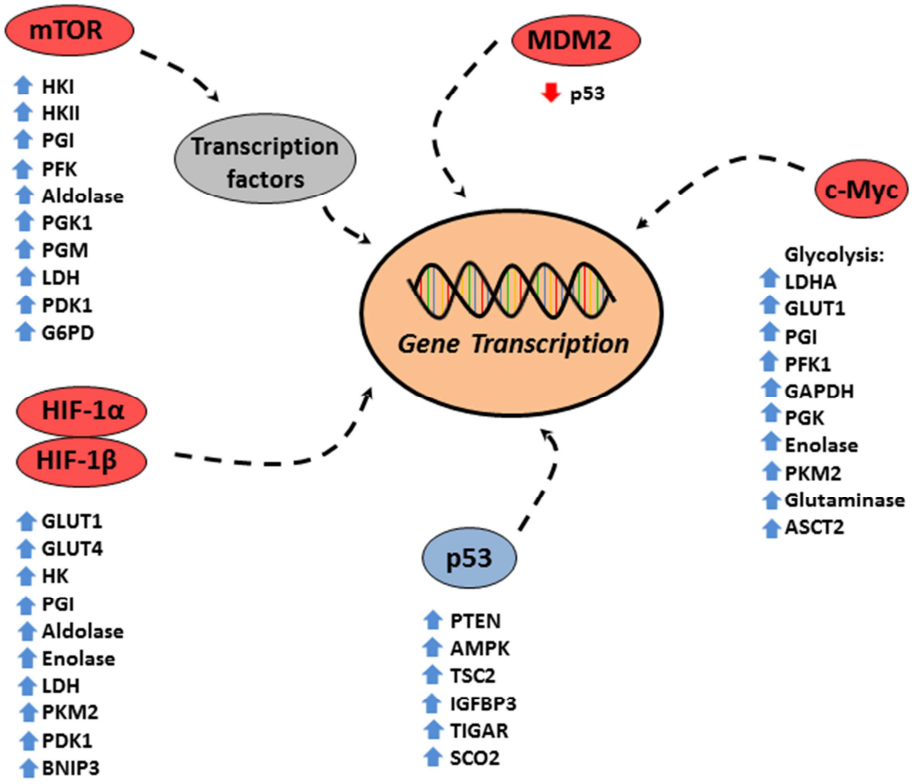

Figure 1.5 - Common transcription factor targets involved in driving the highly glycolytic phenotype in PDAC

Signalling proteins and transcription factors that contribute to a highly glycolytic rate are shown in red circles, while those that oppose this are shown in blue. Additional abbreviations: AMPK, AMP-activated protein kinase; ASCT2, ASC amino-acid transporter 2; BNIP3, BCL2/adenovirus E1B 19 kDa protein-interacting protein 3; GLDH, glutamate dehydrogenase; GLUT1/GLUT4, glucose transporter 1/4; HKI, hexokinase I; HKII, hexokinase II; IGFBP3, insulin-like growth factor-binding protein 3; PDK1, pyruvate dehydrogenase kinase 1; PFK, phosphofructokinase; PGI, phosphoglucose isomerase; PGK1, phosphoglycerate kinase 1; PGM, phosphoglycerate mutase; PTEN, phosphatase and tensin homolog; LDH, lactate dehydrogenase; LDHA, lactate dehydrogenase A isoform; G6PD, glucose-6-phosphate dehydrogenase; GFBP3, insulin-like growth factor-binding protein 3; SCO2, synthesis of cytochrome c oxidase 2; TIGAR, TP53-inducible glycolysis and apoptosis regulator; TSC2, tuberous sclerosis complex 2.

1.5.2 - HIF-1

The hypoxia inducible factor (HIF) complexes are the principal transcription factors responsible for instigating the cellular responses to hypoxia, and in particular drive glycolytic flux at the expense of mitochondrial metabolism (Bristow and Hill, 2008, Cairns et al., 2011). Indeed, increased HIF-1α expression is correlated with poor prognosis in numerous cancers (Semenza, 2010). *In vitro* experiments using human pancreatic cancer cell lines indicate that HIF-1 is upregulated in PDAC (Akakura et al., 2001, Buchler et al., 2003), as have studies evaluating its expression in samples from resected pancreatic tumours (Zhang et al., 2010, Cui et al., 2009b).

The active HIF-1 complex is a heterodimer of stable beta (HIF-1β) and unstable alpha (HIF-1α and HIF-2α) subunits, both of which are constitutively expressed. During normoxia the alpha subunit is hydroxylated by O_2-dependent HIF-1α prolyl hydroxylase (HPH) and subsequently recognised and ubiquitinated by von Hippel–landau tumour suppressor (VHL), an e3 ubiquitin ligase, and undergoes proteosomal degredation (Kroemer and Pouyssegur, 2008). HPH is itself inactivated by hypoxia, allowing the active heterodimer of HIF-1 to stabilise (Stiehl et al., 2006), and is regulated by its reaction substrate α-ketoglutarate (Semenza, 2013). Transcription of both the alpha and beta subunits of HIF-1 has been shown to exponentially increase as the O_2 level in a cell decreases (Jiang et al., 1996). As a result, the findings that HIF-1 is upregulated in PDAC are somewhat to be expected, since pancreatic tumours are known to be highly hypoxic (Koong et al., 2000). While hypoxia is the major driver of HIF-1 stabilisation, single nucleotide polymorphisms in HIF-1 which result in the stabilisation of the active HIF-1 complex have been correlated with both the risk and severity of PDAC (Wang et al., 2011). Furthermore, mitochondrial defects have also been proposed as an indirect activator of HIF-1. Tumorigenic loss of function mutations in fumarate hydratase and succinate dehydrogenase lead to an increase in the TCA intermediates fumarate and succinate, respectively, which in turn inhibit the α-ketoglutarate dependent HIF-1α prolyl hydroxylase responsible for degrading HIF-1 under normoxic conditions (Gottlieb and Tomlinson, 2005).

HIF-1 has widespread regulatory effects on cancer cell metabolism that bring about the Warburg phenotype and allow cancer cells to survive under hypoxic conditions (Semenza, 2013, Lum et al., 2007). The expression of virtually all glycolytic enzymes and glucose transporters are induced by HIF-1, resulting in increased glucose flux through glycolysis to lactate (Semenza et al., 1994, Wang and Semenza, 1993, Gordan and Simon, 2007, Semenza et al., 2006). It has been well documented that HIF-1α upregulates GLUT1 and GLUT4 (Behrooz and Ismail-Beigi, 1999, Ebert et al., 1995, Seagroves et al., 2001), and the gene promoters for HK (Mathupala et al., 2001), glucose-6-phosphate isomerase (Mole et al., 2009), aldolase, enolase and LDH (Semenza et al., 1996) all contain binding sites for activation by HIF-1. Furthermore, HIF-1 and induces the expression of the M2 isoform of pyruvate kinase (PKM2, see *1.5.6 – The Role of Glycolytic Enzymes in the Warburg Phenotype*), which is thought to be key in cancer; interestingly, PKM2 itself functions as a transcriptional coactivator for HIF-1 expression in a feed-forward loop (Luo et al., 2011).

In addition to upregulating glucose flux through glycolysis, HIF-1 attenuates mitochondrial metabolism by numerous mechanisms. HIF-1 induces expression of pyruvate dehydrogenase kinase 1 (PDK1) which in turn inactivates pyruvate dehydrogenase (PDH) (Kim et al., 2006). PDH is the key enzyme required for the conversion of pyruvate to acetyl CoA in the mitochondria. The inactivation of PDH by PDK1 prevents flux of acetyl CoA into the TCA cycle, ultimately inhibiting oxidative phosphorylation and shunting pyruvate towards reduction by LDH (Gottlieb and Tomlinson, 2005). The increased conversion of pyruvate to lactate, rather than its oxidation by PDH to acetyl CoA, results in the production of NAD^+, which in turn can be used to further fuel the glycolytic enzyme GAPDH and promote glycolytic flux (Fantin et al., 2006). HIF-1 signalling further suppresses mitochondrial respiration by preventing c-Myc from stimulating mitochondrial biogenesis (Zhang et al., 2007) and by promoting the transcription of a Bcl-2 family protein BCL2/adenovirus E1B 19 kDa protein-interacting protein 3 (BNIP3), that initiates mitochondrial autophagy (Zhang et al., 2008). This ultimately leads to a decrease in mitochondrial mass within cancer cells. The downregulation of oxidative phosphorylation facilitated by HIF-1 also serves to maintain redox homeostasis within the tumour cells under hypoxia (Zhang et al., 2008, Kim et al., 2006).

1.5.3 - PI3K-AKT

Downstream of K-Ras, phosphoinositide 3-kinase (PI3K) and its main downstream effector, the serine/threonine kinase AKT (also known as Protein Kinase B), appear to play a key role in driving the metabolic alterations present in many cancers. The family of PI3K proteins consists of a group of intracellular signal transducer enzymes that induce strong survival and proliferation signals and changes in cell metabolism (Vivanco and Sawyers, 2002). PI3Ks are lipid and serine/threonine kinases, of which three classes of PI3K have been identified, each consisting of multiple isoforms and subunits. Importantly, class IA PI3Ks, which are coupled to receptor tyrosine kinases (RTKs, sometimes via K-Ras), are the only PI3K isoforms implicated in carcinogenesis (future use of the abbreviation PI3K in this thesis will refer solely this subclass). Upon activation, PI3K phosphorylates the membrane bound phospholipid phosphatidylinositol-4,5-bisphosphate (PIP_2) to form phosphatidylinositol 3,4,5-trisphosphate (PIP_3), and AKT (the primary oncogenic downstream effector of PI3K) is recruited to the plasma membrane via direct interaction with PIP_3 via its pleckstrin-homology domain. AKT is subsequently activated when phosphorylated at threonine 308 by 3-phosphoinositide-dependent protein kinase-1 (Bellacosa et al., 1998). However, maximal AKT activation is achieved by additional phosphorylation at serine 473 by the mTORC2 complex (Sarbassov et al., 2005b, see *1.5.4 – mTOR*). Three isoforms of AKT exist, with AKT2 being the isoform most commonly implicated in driving the Warburg phenotype and cancer progression (Plas and Thompson, 2005, Robey and Hay, 2009). Other signalling proteins downstream of PI3K include protein kinase C and the Rho family of GTPases; however, unlike AKT or c-Myc, these proteins do not appear to play a key role in promoting metabolic transformation (Hennessy et al., 2005).

AKT activates numerous downstream signalling cascades responsible for the reprogramming metabolism in PDAC (Hennessy et al., 2005, Robey and Hay, 2009, Vivanco and Sawyers, 2002), and increased expression of activated AKT is correlated with poorer prognosis in PDAC (Yamamoto et al., 2004). Activated AKT increases glycolytic flux in cancer cells (Elstrom et al., 2004), regulates hexokinase (Gottlob et al., 2001) and 6-phosphofructo-2-kinase/fructose-2,6-biphosphatase 3 (PFKFB3) activity (Deprez et al., 1997), and can also stimulate increased glucose uptake via glucose transporters at the plasma membrane (Wieman et al., 2007). Furthermore, the PI3K/AKT pathway indirectly promotes the Warburg phenotype by regulating various downstream effectors. AKT phosphorylates and inactivates tuberous sclerosis 2 (TSC2), a protein responsible for inactivating the kinase mTOR, thus AKT indirectly activates signalling through the mTOR pathway, which itself can promote the glycolytic phenotype of cancer (Robey and Hay, 2009, see *1.5.4 – mTOR*). Similarly PI3K appears to regulate c-Myc (see *1.5.5 – c-Myc*) expression, which also regulates cancer metabolism and in particular glutamine addiction (Asano et al., 2004). On the other hand, in addition to facilitating pro-Warburg signalling AKT downregulates the expression of the tumour suppressor protein p53 (see *1.6.1 – p53*) that can act to oppose glycolysis by phosphorylating the p53 regulator protein murine double minute (MDM2, Mayo and Donner, 2002).

A hyperactivation and upregulation of AKT is commonly observed in PDAC (Stoll et al., 2005, Ruggeri et al., 1998, Cheng et al., 1996, Altomare et al., 2002, Yamamoto et al., 2004), and can occur for numerous reasons. Regulating the activation of AKT by PI3K is the tumour suppressor phosphatase and tensin homolog (PTEN), which opposes the effects of PI3K by converting the AKT activator PIP_3 back to PIP_2 (Di Cristofano and Pandolfi, 2000); loss-of-function mutations within PTEN or the downregulation of PTEN expression allows for unopposed AKT signalling in cancer. Aberrant expression of PTEN and the downregulation of PTEN mRNA have both been observed in PDAC, suggesting that there may be reduced opposition of PI3K signalling by PTEN in this cancer (Ebert et al., 2002, Asano et al., 2004). Other mechanisms that induce aberrant PI3K-AKT signalling in cancer include intrinsic mutations in PI3K complex subunits that render it constitutively active, and altered receptor tyrosine kinase signalling upstream of PI3K, such as oncogenic K-Ras (Wong et al., 2010). Indeed, in the context of PDAC, the major upstream activator of PI3K is K-Ras, and as mentioned above, activating mutations in the KRAS gene are present in >90% of PDAC. Importantly, in mouse models of PDAC arising from oncogenic KRAS ($KRAS^{G12D}$), loss of function of PTEN is associated with accelerated acquisition of PanINs and progression to PDAC (Hill et al., 2010, Xu et al., 2010a, Kennedy et al., 2011), indicating that PTEN acts as a tumour suppressor in PDAC.

1.5.4 - mTOR

Mammalian target of rapamycin (mTOR) is a serine threonine kinase that acts as the catalytic component of the rapamycin and nutrient-sensitive multiprotein complexes (mTORC1 and mTORC2). mTORC1 is a major downstream effector of AKT, while mTORC2 is involved in actin cytoskeleton organisation and its upstream regulators remain unknown (Loewith, 2011,

Wullschleger et al., 2006). mTORC1 acts to stimulate protein and lipid biosynthesis and cell growth when nutrients are abundant, and achieves this by activating numerous transcription factors and transcription suppressors. These have the combined effect of stimulating metabolism and inducing lipid and protein synthesis while simultaneously suppressing autophagy (Wullschleger et al., 2006, Sarbassov et al., 2005a, Shimobayashi and Hall, 2014). In the context of tumour metabolism, mTORC1 drives a highly glycolytic phenotype by activating metabolic gene transcription through HIF-1 (Yecies and Manning, 2011).

Besides mTOR, the mTORC1 complex contains numerous regulatory proteins such as regulatory-associated protein of mTOR (RPTOR, Hara et al., 2002) and proline-rich AKT1 substrate 1, (PRAS40, Wang et al., 2007) that mediate mTOR activity. While the molecular physiology of mTORC1 is beyond the scope of this article and has been reviewed elsewhere (Guertin and Sabatini, 2007), two important negative regulators of mTORC1 are TSC1 and TSC2 (Orlova and Crino, 2010). TSC2 is negatively regulated by AKT (Inoki et al., 2002), thus inhibition of the TSC1/2 complex by AKT and subsequent activation of mTOR may contribute to PDAC tumour progression. Indeed, mTOR is activated in the majority of PDAC cases (Ito et al., 2006) and it appears that tumours that depend on AKT activation also rely on mTORC1 activation for progression (Grewe et al., 1999, Shah et al., 2001). Of relevance to tumour progression, studies in $TSC1^{-/-}$ and $TSC2^{-/-}$ mouse embryonic fibroblasts have revealed that activated mTORC1 stimulates glycolysis by inducing the transcription of various enzymes involved in glycolysis, the oxidative arm of the PPP, and de novo lipid synthesis (Duvel et al., 2010). Moreover, mTORC1 has been shown to induce the expression of the key glycolytic enzymes HKI, HKII, PGI, PFK, aldolase, PGK1, PGM, LDH and PDK1 and G6PD (Duvel et al., 2010). Moreover, it was determined that mTORC1 achieved this via induction of HIF-1α expression, providing a mechanism by which activated mTOR facilitates the switch towards a glycolytic phenotype in PDAC.

1.5.5 - c-Myc

The proto-oncogene c-Myc is a transcription factor widely expressed during embryogenesis in tissues exhibiting high rates of proliferation, and deregulated expression of c-Myc has been implicated in a broad range of cancers (Pelengaris et al., 2002). c-Myc induces cell growth and proliferation via changes at the transcription level, and evidence indicates that aberrant regulation of PI3K due to the decreased expression of PTEN leads to a sustained activation of c-Myc in PDAC (Asano et al., 2004, Schild et al., 2009). Indeed, studies in PDAC cell lines (PANC-1 and MIA PaCa-2) using siRNA against mutant KRAS have shown that expression of c-Myc is, at least in part, induced by oncogenic K-Ras (Fleming et al., 2005). c-Myc can promote the Warburg phenotype by inducing the expression of LDHA (Shim et al., 1997) GLUT1, PGI, PFK1, GAPDH, PGK, and enolase (Osthus et al., 2000) and facilitates the preferential expression of PKM2 via alternative exon splicing (David et al., 2010). However, despite its ability to increase aerobic glycolysis at the expense of mitochondrial respiration, in recent years c-Myc has been shown to play a role in driving mitochondrial biogenesis (Li et al., 2005, Kim et

al., 2008). While initially counterintuitive to the metabolic phenotype of cancer and at direct odds with Warburg's initial hypothesis that aerobic glycolysis in cancer stems from mitochondrial dysfunction (Warburg, 1956), it has become apparent that by upregulating certain facets of mitochondrial metabolism c-Myc drives a highly proliferative cancer phenotype. In addition to its effects on the glycolytic cascade, c-Myc has been shown to induce the expression of glutaminase and the plasma membrane glutamine transporter ASC amino-acid transporter 2 (ASCT2, Gao et al., 2009), thereby increasing mitochondrial metabolism of glutamine (Wise et al., 2008). The resulting upregulation of glutaminolysis fuels the generation of anabolic substrates for use in accelerated cell proliferation (Morrish et al., 2009, Morrish et al., 2008).

1.5.6 - The role of glycolytic enzymes in the Warburg phenotype

Numerous studies have shown the expression and activity of metabolic enzymes is often emphatically altered in cancer as a result of aberrant signalling through the pathways discussed above. Of these, a wealth of evidence indicates that enzymes involved in the glycolytic cascade are commonly overexpressed in PDAC. These include HKII, aldolase, triose phosphate isomerase (TPI), PGK1, GAPDH, PDK1, lactate dehydrogenase A and B (LDHA and LDHB), enolase 2, pyruvate kinase muscle isoforms 1 and 2 (PKM1 and PKM2), and PFKFB3 (Bobarykina et al., 2006, Zhou et al., 2012, Zhou et al., 2011, Akakura et al., 2001, Guillaumond et al., 2013, Rong et al., 2013, Mikuriya et al., 2007, Ishihara et al., 1999, Cui et al., 2009a, Hwang et al., 2006, Schek et al., 1988). This increase in glycolytic enzyme expression results in a robust increase in glycolytic capacity in these cells, as evidenced by the increased production of lactic acid by PDAC cells (Guillaumond et al., 2013). However, numerous glycolytic enzymes contribute to cancer progression via mechanisms other than increased activity due to protein overexpression.

Interestingly, the studies have shown that the HK isoform most commonly overexpressed by cancer cells is the HKII isoform, which appears to facilitate the accelerated glycolytic rate of cancer cells (Pedersen, 2007). It has been found that in cancer cells HKII associates tightly with the voltage dependant anion channel (VDAC) VDAC on mitochondria (Pedersen, 2007). This tight HK-VDAC interaction inhibits the opening of the mitochondrial permeability transition pore, a key step in facilitating the release of cytochrome c from the mitochondria to signal for apoptosis, resulting in resistance to programmed cell death, a classic hallmark of cancer (Mathupala et al., 2006).

Interestingly, concomitant with its role as an intermediate enzyme in glycolysis, phosphoglucose isomerase (PGI) is known to act as a powerful mitogen and cytokine, stimulating cell survival, migration and invasion (Funasaka and Raz, 2007); thus PGI has also become known as the autocrine motility factor (AMF). Overexpression of PGI has been shown to increase *in vitro* invasion in MIA PaCa-2 cells and tumour size and liver metastasis in mouse models of PDAC (Tsutsumi et al., 2004).

Of particular relevance to cancer cell bioenergetics is the M2 isoform of pyruvate kinase, PKM2. PKM2 catalyses the final step of glycolysis, converting phosphoenolpyruvate to pyruvate while concomitantly generating ATP in the process. While absent in most tissues except those requiring a high rate of nucleic acid synthesis (such as embryonic cells and stem cells), PKM2 is highly expressed in cancer cells, and as a result has been suggested as a potential biomarker for cancer (Mazurek et al., 2005). Indeed, analysis of human PDAC tissue sections by tissue immunohistochemistry and western blotting has shown PKM2 to be expressed in the cytosol of both cancerous cells and pancreatic stellate cells (Wehr et al., 2011). Evidence suggests that PKM2 acts as a “gatekeeper” for pyruvate synthesis in glycolysis, as PKM2 appears to oscillate between a high activity tetrameric and low activity dimeric form. High expression of the low-activity dimeric form facilitates the accumulation of glycolytic intermediates, which can be diverted towards the anabolic processes that fuel cell proliferation rather than energy production (Mazurek et al., 2005). Evidence provided by point mutation assays also suggests that binding of phosphotyrosine peptides to PKM2 regulate its activity by inhibiting binding of its activator FBP, possibly following stimulation by growth factors (Christofk et al., 2008a, Christofk et al., 2008b).

1.6 - Tumour Suppressors opposing metabolic transformation in PDAC

Tumour suppressors are proteins that act as control points within intracellular signalling cascades. Crucially, they act to oppose the action of signalling cascades that would otherwise promote cancer development if not tightly regulated. Thus development of cancer is often a combination of pathologically increased activity within oncogenic signalling pathways coupled with a loss of function within the tumour suppressor mechanisms that control them. While the mechanisms described above act to drive the highly glycolytic phenotype of PDAC, loss of function mutations within the tumour suppressor pathways that regulate and control these signalling cascades leads to their unopposed action, and therefore their loss can indirectly promote the glycolytic phenotype in PDAC. We will now consider the key tumour suppressors implicated in the development of PDAC, and how disrupted tumour suppressor function can facilitate induction of the Warburg phenotype.

1.6.1 - p53

p53 is a transcription factor which serves to induce apoptosis and inhibit cell division in response to instances of metabolic stress (Horn and Vousden, 2007, Levine and Oren, 2009). p53 is activated by a low cytosolic ATP/ADP ratio (Okorokov and Milner, 1999) and hypoxia, the latter via a hypoxia-induced suppression of the p53 negative-regulator, MDM2 (Alarcon et al., 1999). Loss of function mutations in p53 appear to be present in around 60 to 70% of PDAC (Moore et al., 2001, Redston et al., 1994) and occur in later stage, advanced PanINs progressing to frank PDAC (Maitra et al., 2003). Evidence suggests that the loss of p53 in PDAC helps promote cancer progression, as p53 loss in $KRAS^{G12D}$ mouse models of PDAC has been shown to cooperate with oncogenic KRAS to drive metastatic disease (Hingorani et al., 2005). Furthermore, upregulation of the MDM2 transcription promoter in resected human PDAC tissue has been associated with a 6-fold increased risk of tumour related death, and the concomitant suppression of p53 expression correlated with worse prognosis (Grochola et al., 2011). It appears therefore that loss of function mutations in p53 are an important contributor to PDAC progression.

The loss of p53 function can facilitate metabolic transformation in cancer cells, as p53 serves to oppose the Warburg phenotype via numerous mechanisms. p53 facilitates the expression of PTEN, AMP-activated protein kinase (see *1.6.3 – LKB1 and AMPK*), TSC2 and insulin-like growth factor-binding protein 3 (IGFBP3), each of which acts to suppress the PI3K-AKT-mTOR pathway that is commonly upregulated in cancer (Feng et al., 2007). Furthermore, p53 inhibits glycolysis by lowering the levels of fructose-2,6-bisphosphate, a potent allosteric activator of the key glycolytic enzyme PFK1, via the metabolic regulator TP53-induced glycolysis and apoptosis regulator (TIGAR, Bensaad et al., 2006).

In addition to suppressing glycolysis, evidence suggests that p53 promotes mitochondrial metabolism. p53 regulates electron transport chain activity by inducing the expression of an assembly protein encoded by the synthesis of cytochrome c oxidase 2 (SCO2) gene. This

protein is then targeted to the inner mitochondrial membrane, where it facilitates the formation of the cytochrome c oxidase (COX) complex (Ma et al., 2007). Indeed, disruption of SCO2 gene in human colorectal cancer cells expressing wild-type p53 (HCT116) has been shown to induce the glycolytic Warburg phenotype (Matoba et al., 2006).

1.6.2 - TGF-β and SMAD4

Signalling via the transforming growth factor β (TGF-β) pathway regulates apoptosis and cellular growth (Massague, 2008). TGF-β is a ligand for the type I and type II TGF-β serine/threonine kinase receptors, which when activated form a tetrameric complex of receptors with the type II receptor phosphorylating the type I receptor. TGF-β achieves its tumour suppressor activity by activating the mothers against decapentaplegic homolog (Smad) proteins; upon receptor activation and tetramer formation, the type I TGF-β serine/threonine kinase receptor phosphorylates the receptor substrates Smad2 and Smad3. Activated receptor-regulated Smads (RSmads) then form a complex with Smad4 and translocate to the nucleus, where the complex regulates target gene transcription (Shi and Massague, 2003). TGF-β signalling typically acts as a tumour suppressor in the early stages of tumour development. However, unlike other tumour suppressors, the TGF-β pathway can also act to promote tumour progression, depending on the stage of tumour progression (Bierie and Moses, 2006). Similarly, evidence suggests that TGF-β signalling can act to both promote and suppress the Warburg phenotype in PDAC.

Genetic alterations in the TGF-β/Smad4 pathway are observed in almost all instances of PDAC (Holloway et al., 2003) with deletion or loss-of-function mutations in Smad4 present in around 50% of pancreatic cancers (Hahn et al., 1996). Evidence suggests that loss of Smad4 is critical for the progression of pancreatic cancer and its loss is most commonly observed in later stage PanINs (Wilentz et al., 2000). Smad4 loss had no effect on pancreatic development yet is associated with accelerated PDAC progression in mice expressing activated K-Ras (Bardeesy et al., 2006b, Izeradjene et al., 2007). Conditional knock-out of Smad4 in the pancreas of mice is associated with an increased expression of an inactive form of PTEN, and disruption of both Smad4 and PTEN is associated with accelerated malignancy and an increased expression AKT and mTOR (Xu et al., 2010a).

Mutations within the TGF-β/Smad4 pathway in the later stages of tumour development frequently lead to the loss of growth-inhibitory responses in cancer cells. This is commonly accompanied by an increase in the production of TGF-β by other cells present in the tumour microenvironment (fibroblasts, immune cells). Under these conditions, it appears that TGF-β can also function as a tumour promoter (Bierie and Moses, 2006, Yang and Moses, 2008). TGF-β has been shown to be overexpressed in pancreatic cancer and is linked with poor prognosis (Friess et al., 1993). Studies using PANC-1 cells treated with TGF-β and mice overexpressing TGF-β have both suggested that PTEN expression in the pancreas, which is significantly reduced in PDAC, is negatively regulated by TGF-β (Ebert et al., 2002). Further

evidence suggests that TGF-β signalling via the Ca^{2+}-dependent action of protein kinase C-α (PKC-α) suppresses the transcription of PTEN (Chow et al., 2008) and promotes the invasive phenotype of pancreatic cancer (Dong et al., 2010). Taken together, these studies suggest that the loss of Smad4 and upregulation TGF-β signalling in the latter stages of tumour progression can facilitate the Warburg phenotype via effects on the AKT regulation PTEN.

1.6.3 - LKB1 and AMPK

AMP-activated protein kinase (AMPK) plays an important role in detecting the energy status of a cell and in regulating catabolic energy-generating response pathways. AMPK is activated by a low cytosolic ATP/AMP ratio and subsequently inhibits cell proliferation while stimulating mitochondrial respiration (Shackelford and Shaw, 2009). AMPK also phosphorylates and activates the mTOR negative regulator TSC2, and therefore opposes the actions of mTOR-activating role of AKT in response to energy starvation (Inoki et al., 2003). As a result, aberrant changes in AMPK signalling that prevent it from performing these tasks are thought to contribute to promoting the Warburg phenotype.

Liver kinase B1 (LKB1) is an upstream kinase that facilitates the activation of AMPK, and evidence suggests that its loss may have a role in the development of PDAC. Peutz-Jeghers syndrome is a hereditary disease caused by a mutation in LKB1 and is associated with a 130-fold increased risk of developing PDAC (Canto et al., 2006). LKB1 deletion in mouse pancreatic epithelium *in vivo* is associated with AMPK inactivation, disrupted acinar function and the development of pancreatic cystadenomas (Hezel et al., 2008). In the context of the Warburg phenomenon, it is likely that mutation of LKB1 leads to a loss of AMPK activation and a subsequent loss of mTOR inhibition and HIF-1 opposition.

1.6.4 - INK4A and ARF

INK4A and ARF are two overlapping genes at the 9q21 locus that encode for the tumour suppressor proteins cyclin-dependent kinase inhibitor 2A (p16INK4A) and alternate reading frame tumor suppressor (p19ARF, Sherr, 2001). Loss of p16INK4A transcription is the most common tumour suppressor inactivation in PDAC and occurs in more than 95% of cases (Moore et al., 2001, Schutte et al., 1997). p16INK4A inhibits cyclin-dependent kinases (CDKs) and prevents the DNA synthesis stage of the cell cycle and, despite no apparent role in driving the Warburg phenotype, the almost ubiquitous abrogation of p16INK4A signalling in PDAC is worthy of note, especially in the light of animal studies indicating that p16INK4A cooperates with activated K-Ras to drive metastatic PDAC progression (Aguirre et al., 2003, Bardeesy et al., 2006a). p19ARF, on the other hand, acts to suppress proteolysis of p53 by MDM2 by promoting the degradation of MDM2 (Zhang et al., 1998), and studies using animal models of PDAC indicate that p19ARF function is lost following the development of frank PDAC (Ying et al., 2011). p19ARF therefore may play a role in facilitating the suppressive effects of p53 on glycolysis.

1.7 - Targeting glycolytic metabolism in PDAC

As research has continued to characterise the signalling cascades underpinning altered metabolism in tumours, numerous studies have attempted to target these as a means of selectively killing cancer cells whilst sparing healthy cells, with numerous compounds progressing to clinic. These strategies have been covered in detail by numerous excellent reviews elsewhere (Tennant et al., 2010, Vander Heiden, 2011, Hennessy et al., 2005, Semenza, 2003, Wise and Thompson, 2010), with some focusing on their promise in PDAC (Le et al., 2012, Blum and Kloog, 2014). While it is beyond the scope of this thesis to consider the many diverse attempts to target the altered metabolic signalling pathways in cancer, it is pertinent to the overall theme of this thesis to consider those that have aimed to inhibit the glycolytic cascade in tumours exhibiting the Warburg phenotype. As previously discussed above (see *1.5.6 - The role of glycolytic enzymes in the Warburg phenotype*), many glycolytic enzymes are commonly overexpressed in cancer cells, and have subsequently been targeted by studies aiming to exploit the metabolic phenotype of tumours with small molecule inhibitors, both as pharmacological tools to assess the cancer metabolic phenotype and as potential clinical therapies (Pelicano et al., 2006). These drugs are summarised in Figure 1.6.

Studies with the lactate/pyruvate analogue 3-bromopyruvate (BrPy), which acts to inhibit HK, have shown that BrPy depletes ATP in cancer cells and can selectively eradicate tumours in mouse xenograft models of cancer (Ko et al., 2004). Further studies with BrPy indicate that it is particularly effective in killing those cancer cells in hypoxic conditions, since these cells exhibit a dependency on a high glycolytic rate (Xu et al., 2005). Similarly, 2-deoxyglucose (2-DG) also acts to inhibit HK. This drug is not further metabolised once converted to 2-deoxyglucose-6-phosphate (2-DG-6-P) by HK, and 2-DG-6-P accumulates within the cytosol and inhibits both HK (Chen and Gueron, 1992) and glucose-6-phosphate isomerase (Wick et al., 1957). 2-DG has been shown to induce cell death in cancer cells in *in vitro* studies, and similar to BrPy, 2-DG has a particularly potent effect on those cells with defects in mitochondrial metabolism or in hypoxic conditions (Liu et al., 2001, Liu et al., 2002, Maher et al., 2004). *In vivo* studies have also revealed that 2-DG can potentiate the efficacy of adriamycin and paclitaxel in mouse xenograft models of cancer (Maschek et al., 2004). Lonidamine is another drug that is thought to inhibit HK and has been investigated as a potential cancer treatment. Evidence suggests lonidamine selectively inhibits glycolysis in cancer cells (Floridi et al., 1981), and it has been shown to cause ATP depletion in a human breast cancer cell line while also enhancing the cytotoxic effects of other anticancer agents (Floridi et al., 1998). PDK has been targeted for inhibition by numerous drugs, including AZD7545, dichloroacetate (DCA) and radicicol (Kato et al., 2007); by inhibiting PDK DCA promotes mitochondrial metabolism of pyruvate and a downregulation of glycolysis, thus reversing the Warburg phenotype and suppression of apoptosis while slowing tumour growth (Michelakis et al., 2008). Sodium iodoacetate (IAA) is well known to inhibit GAPDH, and while unsuitable for the clinical treatment of cancer due to its toxicity, IAA is an important tool for inhibiting glycolysis in experimental systems (Schmidt and Dringen, 2009). Indeed, similar to BrPy, IAA has been shown to deplete ATP and induce necrosis in PDAC cell lines (Bhardwaj et al., 2010). At the terminal end of the glycolytic

cascade, shRNA knockdown of PKM2 has been shown to reverse the Warburg phenotype and to reduce the ability of cancer cells to form tumours in xenograft models (Christofk et al., 2008a). Isoform selective inhibition of PKM2 has also been shown to slow glycolytic flux and to have cytotoxic effects (Vander Heiden et al., 2010). Similarly, inhibition of LDH using either siRNA or the small molecule inhibitor FX11 has also been shown to inhibit glycolytic flux, resulting in ATP depletion, an increase in oxidative stress and a decrease in tumour progression (Le et al., 2010). This is possibly due to a decrease in NAD^+ availability, which is a crucial electron acceptor generated by the LDHA reaction and is required to sustain flux through the GAPDH step of glycolysis (Seidler, 2013).

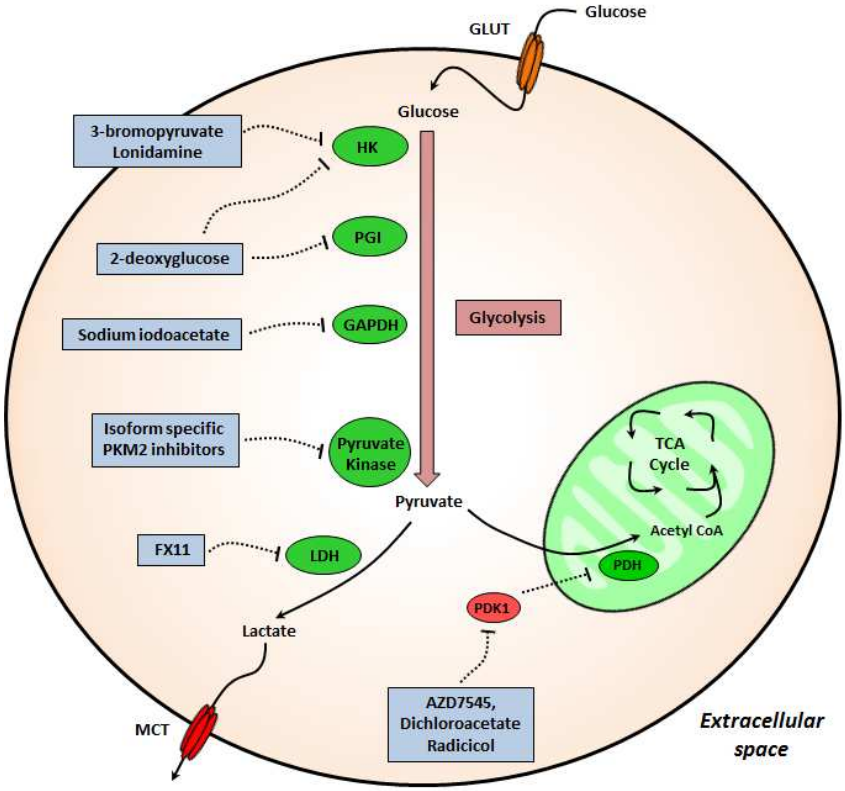

Figure 1.6 – Drugs for targeting glycolysis in cancer cells.

Numerous drugs have been studied for their inhibitory effects on the glycolytic cascade in cancer (blue boxes). Although not necessarily applicable in the clinic due to toxicity, these have become useful tools for studying tumour metabolism. Metabolic enzymes are shown in green ovals, kinases in red ovals. Additional abbreviations: MCT, monocarboxylate transporter; GLUT, glucose transporter.

Taken together, these numerous studies indicate the feasibility and indeed the potential of targeting the glycolytic cascade in cancer cells, and in particular those which are dependent on a high glycolytic rate for survival. Given the hypoxic core and the high glycolytic rate exhibited by PDAC tumours, the selective targeting of glycolysis is an attractive strategy for this disease. However, as glycolysis is a key cellular process in all cells, the selectivity of any potential treatment for malignant cells over their healthy counterparts is paramount to its potential as a therapy. The targeting of those glycolytic enzyme isoforms preferentially expressed in cancer cells is one potential way to overcome this problem, and more recent studies have begun to employ this strategy for targets such as PKM2 (Vander Heiden et al., 2010).

1.8 - Metabolic Regulation of Ca^{2+} Signalling: a Novel Treatment Avenue for PDAC?

The major hallmarks of cancer include a resistance to apoptosis resulting in limitless cell replication, sustained proliferation, evasion of growth suppression pathways, induction of angiogenesis and the promotion of invasion and metastasis (Hanahan and Weinberg, 2011). Most current chemotherapeutic drugs target the cell cycle (paclitaxel), DNA replication (etoposide/gemcitibine), DNA damage (doxorubicin) and growth factor receptor (GFR) signalling (Iressa, erlotinib), with the aim of preventing cell division and inducing cell death (Stevens and Rodriguez, 2014). However, the identification of novel therapeutic avenues for the treatment of cancer, such as cancer metabolism as discussed above, is a key focus within the cancer field. Another potential target for the treatment of cancer is Ca^{2+} signalling. As will be covered in the following sections, Ca^{2+} signals manifest as oscillations in intracellular Ca^{2+} concentration ($[Ca^{2+}]_i$) and the diverse nature of these signals allows Ca^{2+} to control a vast repertoire of intracellular signalling pathways (Berridge et al., 2000). Moreover, Ca^{2+} signals have a critical role in controlling all the above-mentioned cancer-hallmark processes. For example, Ca^{2+} signals can regulate transcription factors responsible for the control of cell proliferation, such as nuclear factor of activated T cells (NFAT, Hogan et al., 2003) and nuclear factor kappa-light-chain-enhancer of activated B cells (NF-κB, Dolmetsch et al., 1998), and play a key role in mediating vascular endothelial growth factor (VEGF)-induced angiogenesis (Li et al., 2011). Of particular interest to PDAC, Ca^{2+} signals can activate Ras (Kupzig et al., 2005, Rosen et al., 1994) and regulate its actions via Ca^{2+} activated GAPs. Furthermore, Ca^{2+} has many diverse roles in regulating cell motility, invasion (Prevarskaya et al., 2011) and cell death (Orrenius et al., 2003, Roderick and Cook, 2008). Given the role of Ca^{2+} signals in regulating the key hallmark processes in cancer, it is somewhat surprising that none of the mainstay cancer treatments target proteins involved in regulating Ca^{2+} signals. Indeed, studies indicate that the expression of many proteins involved in regulating Ca^{2+} signals is altered in cancer (Monteith et al., 2012), and recent evidence also suggests that Ca^{2+} signals themselves are altered in their nature following oncogenic transformation, although our understanding of how these are related to the cancer phenotype is still in its infancy (Stewart et al., 2014). As we shall discuss in the following sections, Ca^{2+} signalling is regulated by many factors, and this may provide a smörgåsbord of therapeutic targets for modulating the Ca^{2+}-dependent signalling processes underlying the cancer phenotype, as has been reviewed elsewhere (Prevarskaya et al., 2011, Monteith et al., 2007). However, the selective targeting of Ca^{2+} signalling in cancer cells while leaving healthy cells unharmed presents a significant challenge to this approach.

While the perturbation of Ca^{2+} signalling in cancer cells would likely be an effective means of inducing cell death, Ca^{2+} signals also regulate many critical intracellular processes in non-cancerous cells. Thus any attempts to target the Ca^{2+} signalling machinery in tumour cells must consider the selectivity of the treatment for cancer cells over healthy cells. Any treatment targeting the Ca^{2+} signalling machinery in cancer cells would therefore need to target either uniquely expressed components of the Ca^{2+} signalling toolkit, or those that have an entirely new function in cancer cells. This dilemma of the selectivity of any putative therapy targeting Ca^{2+} signalling for cancer cells is similar to that faced by attempts to target glycolysis globally, as

described in the previous section, since these processes are ubiquitously important in normal healthy cells. However, the metabolic phenotype of PDAC may provide a means to target Ca^{2+} signalling while achieving the desired selectivity for cancer cells over healthy cells. Rather than attempt to target glycolysis globally, one could instead target processes that critically rely on metabolism in cancer cells. In other words, certain ATP-dependent mechanisms critical for maintaining cell survival may be more reliant on a glycolytic ATP supply in cancer cells, rendering them exquisitely sensitive to targeted glycolytic inhibition in comparison to the same mechanisms in healthy cells. This could provide a novel and selective therapeutic locus. Moreover, the tight control of Ca^{2+} signalling is one such ATP-dependent process, and an inability to maintain the energy-dependent regulation of Ca^{2+} signals is cytotoxic to any cell.

The following sections will discuss how Ca^{2+} signals are propagated and controlled, how cells maintain Ca^{2+} homeostasis, and will consider potential avenues to perturb Ca^{2+} handling selectively in cancer cells by exploiting its dependency on ATP and the metabolic phenotype of PDAC.

1.8.1 - Ca^{2+} - a versatile and ubiquitous cell signalling agent

The Ca^{2+} ion is one of the most important signalling entities utilised by cells, and is crucial for the coordination of a vast array of intracellular processes. These span from the moment an ovum is fertilized by a sperm until the death of an organism, and include muscle contraction, exocytosis, synaptic transmission and cell proliferation (Berridge et al., 1998). Moreover, Ca^{2+} signals are stimulated by numerous intracellular and extracellular events, such as membrane depolarisation, receptor stimulation by agonists, endoplasmic reticulum (ER) Ca^{2+} store depletion and stretch. Ca^{2+} signals manifest as oscillations in intracellular Ca^{2+} concentration ($[Ca^{2+}]_i$, Thul et al., 2008) and are both propagated and controlled by a diverse range of Ca^{2+} channels, pumps, transporters and binding proteins. Collectively these mechanisms are known as the Ca^{2+} signalling machinery (Figure 1.7). The spatial and temporal properties of these dynamic Ca^{2+} signals determine their downstream effects, and differences in location, amplitude, frequency and duration allow them to control a wide range of distinct cellular processes (Berridge et al., 2000). Ca^{2+} signals can present as slow oscillations with a frequency of seconds or hours, or a brief spike, depending on what signal is to be conveyed. Ca^{2+} oscillations can be propagated globally, or restricted to a single subcellular location to focus the signal within a particular microdomain. Moreover, distinct cytosolic Ca^{2+} signals can be coordinated so that they form Ca^{2+} waves that pass throughout the cell.

The Ca^{2+} signalling machinery has been covered extensively by numerous review articles (Berridge et al., 2000, Berridge et al., 2003, Clapham, 2007, Berridge et al., 1998), and primarily consists of channels, pumps and transporters (Figure 1.7). Moreover, these mechanisms exist in a number of different isoforms and are regulated by numerous second messengers, allowing cells to tailor Ca^{2+} signals to fulfil their requirements (Berridge et al., 2000). The mechanisms that propagate and regulate Ca^{2+} signals can be broadly categorised into those that increase

$[Ca^{2+}]_i$, and those that decrease $[Ca^{2+}]_i$. We will consider those mechanisms responsible for elevating $[Ca^{2+}]_i$, before focusing in detail on the mechanisms responsible for reducing $[Ca^{2+}]_i$.

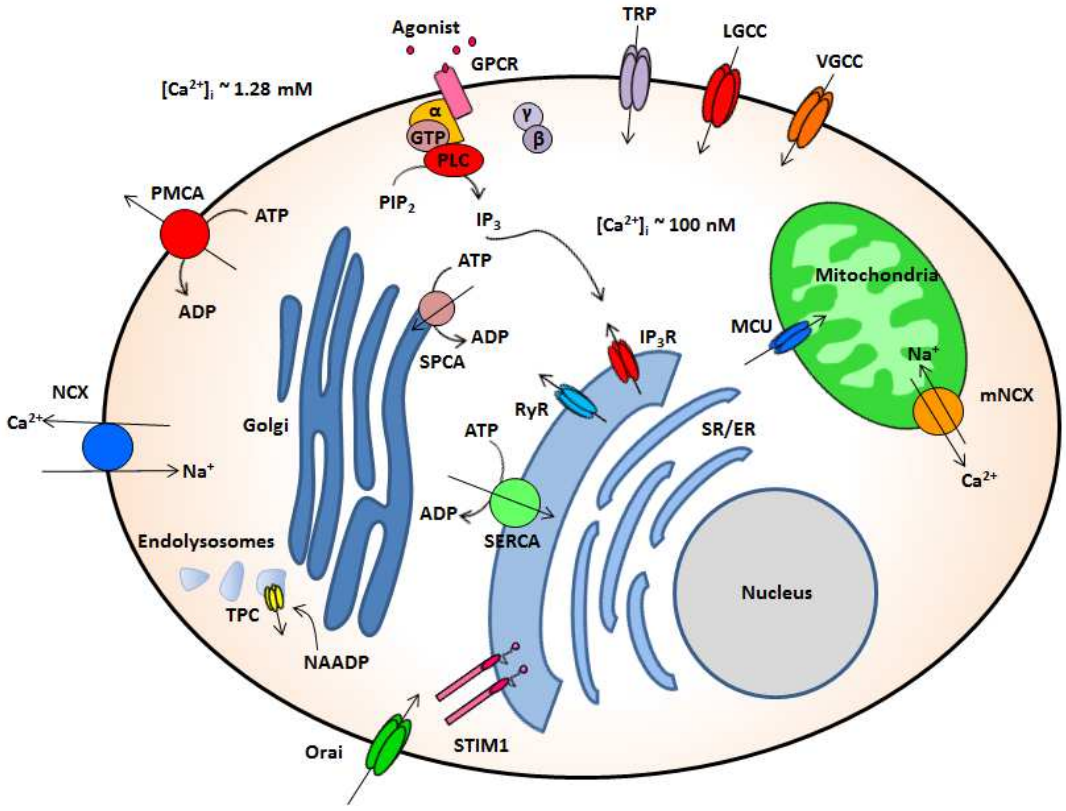

Figure 1.7 - The Ca^{2+} signalling machinery

Numerous mechanisms control intracellular $[Ca^{2+}]_i$. to elevate $[Ca^{2+}]_i$, Ca^{2+} can enter the cytosol from the extracellular space via ligand-gated Ca^{2+} channels (LGCCs), voltage-dependent Ca^{2+} channels (VOCCs) transient receptor potential (TRP) channels, and store operated Ca^{2+} entry channels (SOCE). SOCE channels are activated via an interaction with stromal interacting molecule 1 (STIM1) on the sarcoplasmic reticulum/endoplasmic reticulum (SR/ER) membrane, which senses SR/ER luminal Ca^{2+} concentration via an EF hand domain. Ca^{2+} is also released from the SR/ER via inositol trisphosphate (IP_3) receptors (IP_3Rs) and ryanodine receptors (RyR). IP_3Rs are activated by IP_3 downstream of G-protein coupled receptors (GPCRs) upon stimulation by an agonist. Ca^{2+} can also be released from the mitochondria by the mitochondrial Na^+/Ca^{2+}-exchanger (mNCX), and from the Golgi apparatus by two-pore channels (TPC), which are activated by nicotinic acid adenine dinucleotide (NAADP). To lower $[Ca^{2+}]_i$, Ca^{2+} can sequestered into the SR/ER by the sarcoplasmic/endoplasmic reticulum Ca^{2+}-ATPase (SERCA), into the Golgi by the secretory pathway Ca^{2+}-ATPase, and into the mitochondria via the mitochondria Ca^{2+} uniporter. Ca^{2+} is also extruded from the cell across the plasma membrane via the Na^+/Ca^{2+}-exchanger (NCX) and the plasma membrane Ca^{2+}-ATPase.

1.8.2 - Mechanisms responsible for elevating $[Ca^{2+}]_i$

Increases in $[Ca^{2+}]_i$ typically occur via Ca^{2+} channels, with Ca^{2+} moving from either the extracellular space (Ca^{2+} entry) or from intracellular Ca^{2+} stores (Ca^{2+} release) to the cytosol. Ca^{2+} entry channels facilitates Ca^{2+} entry into the cell, and can be categorised into voltage-dependent Ca^{2+} channels (VOCCs), ligand-gated Ca^{2+} channels (LGCCs), transient receptor potential (TRP) channels, and store operated Ca^{2+} entry channels (SOCE). VOCCs, including the L, T, N, and P/Q-type Ca^{2+} channels are primarily expressed in excitable cells such as cardiac myocytes and neurons (Dolphin, 2006) and are activated by membrane depolarisation (Catterall et al., 2005). LGCCs, on the other hand, are activated and opened following the binding of an exogenous ligand, and include glutamate-gated N-Methyl D-glutamate (NMDA) receptors and ATP-gated purinergic P2X receptors (Burnashev, 1998). The transient receptor potential (TRP) family of ion channels are a diverse group of Ca^{2+}-permeable, non-selective ion channels that act as cellular sensors of the environment, and are categorised into the TRPC (TRPC1-C7), TRPV (TRPV1-6), TRPM (TRPM1-8), and the more obscure muculipin (TRPML) and polycystin (TRPP1-2) families (Wu et al., 2010). TRP channels respond to diverse stimuli, including temperature (Bautista et al., 2007, Caterina et al., 1997), pain, osmolality, pheromones, touch, redox state and metabolism (Sumoza-Toledo and Penner, 2011, Clapham, 2003). SOCE channels, also known as Ca^{2+} release activated Ca^{2+} channels (CRAC) or capacitative Ca^{2+} entry (CCE) channels, were first described in the 1980s (Putney, 1986) and are plasma membrane Ca^{2+} channels that open following depletion of the ER/SR Ca^{2+} store. ER Ca^{2+} store depletion is detected by stromal interacting molecule 1 (STIM1), which is located on the ER membrane and senses the ER Ca^{2+} content via a luminal EF hand domain (Liou et al., 2005, Roos et al., 2005). Upon ER Ca^{2+} store depletion, STIM1 oligomerises, forms puncta and translocates to form junctions between the ER and the plasma membrane (Zhang et al., 2005) via a direct interaction with the pore forming subunit of SOCE channels, Orai (Prakriya et al., 2006, Yeromin et al., 2006). This interaction opens the SOCE channels, allowing for ER Ca^{2+} to be refilled. While ubiquitously expressed, two STIM and three Orai isoforms exist, respectively, thus allowing for cells to tailor SOCE responses to tissue specific functions (Carrasco and Meyer, 2010, Frischauf et al., 2008).

In addition to Ca^{2+} entry from the extracellular space, elevation of $[Ca^{2+}]_i$ is also achieved via the release of Ca^{2+} from intracellular stores (Berridge et al., 2003). Most commonly, intracellular Ca^{2+} release occurs from the ER (or SR in muscle cells) via Ca^{2+} release channels, including inositol-1,4,5-triphosphate (IP_3)-gated channels (IP_3 receptors, IP_3Rs) and ryanodine receptors, both of which are expressed on the ER membrane (Berridge, 2009). IP_3 is generated upon activation of G protein-coupled receptors (GPCRs) coupled to the Gq heterotrimeric G protein. Following activation, the α-subunit of this G-protein activates phospholipase C (PLC), which in turn hydrolyses the membrane-bound (PIP_2) to diacylglycerol (DAG) and IP_3. While DAG remains bound to the plasma membrane, IP_3 is free to diffuse through the cell to the ER membrane where it binds to and stimulates the IP_3R, which is a ligand-gated ion channel, allowing Ca^{2+} to be released from the ER store and into the cytoplasm. This released Ca^{2+} from an individual receptor (a Ca^{2+} "blip") can then act to promote further Ca^{2+} release from other

nearby IP_3Rs (Ca^{2+} "puffs") in a feed-forward fashion (Yao et al., 1995), stimulating further Ca^{2+} release from the ER in a process known as Ca^{2+}-induced Ca^{2+}-release (CICR). These Ca^{2+} "puffs" can continue to increase in intensity to generate global Ca^{2+} waves, until a threshold $[Ca^{2+}]_i$ is reached that inhibits the IP_3Rs and terminates the Ca^{2+} release (Bootman et al., 1997). CICR also occurs via Ca^{2+} sensitive ryanodine receptors (RyRs) on the ER membrane, which also sense and are activated by Ca^{2+} on the cytosolic side of the ER membrane (Smith et al., 1988, Imagawa et al., 1987). Thus, IP_3 acts as a trigger for the Ca^{2+} signal, whereas Ca^{2+} acts as both an amplifier (CICR) and terminator of the Ca^{2+} signal (inhibition of IP_3Rs at high $[Ca^{2+}]_i$). This represents an intrinsic oscillatory mechanism in many non-excitable cells (Fedorenko et al., 2014, Mikoshiba, 2007). Besides the release from the ER store, additional Ca^{2+} release channels have been identified in organelles such as the Golgi and lysosomes, with evidence suggesting that this Ca^{2+} release from acidic stores is mediated by two-pore channels (TPCs) that are gated by nicotinic acid adenine dinucleotide (NAADP, Michelangeli et al., 2005, Galione and Chuang, 2012, Patel et al., 2011).

While Ca^{2+} release from the ER store is actively mediated by the above-mentioned channels, there exists a constitutive, slow release of Ca^{2+} from the ER store. This leak can be revealed upon selective inhibition of the sarco/endoplasmic reticulum Ca^{2+}-ATPase (SERCA) with cyclopiazonic acid (CPA, Seidler et al., 1989) or thapsigargin (Thastrup et al., 1990), however, the molecular identity of the leak pathway remains controversial (Camello et al., 2002). Evidence suggests IP_3Rs and RyRs may play a role (Szlufcik et al., 2006), while previous conflicting studies indicate that the Ca^{2+} leak pathway is independent of both these channels (Hofer et al., 1996) and may be mediated by other putative Ca^{2+} channels (Giunti et al., 2007). However, evidence suggests that the translocon complex, which is responsible for the transport of nascent polypeptides into the ER lumen, is the most likely candidate (Ong et al., 2007, Van Coppenolle et al., 2004).

1.8.3 - Mechanisms responsible for lowering $[Ca^{2+}]_i$

To ensure Ca^{2+} signals are tightly controlled and carefully coordinated and to prevent the cytotoxic effects of a prolonged elevated $[Ca^{2+}]_i$ (Berliocchi et al., 2005, Criddle et al., 2007), cells have numerous mechanisms which act to reduce $[Ca^{2+}]_i$. These Ca^{2+} homeostasis mechanisms typically involve extrusion of Ca^{2+} across the plasma membrane into the extracellular space (Ca^{2+} efflux) or sequestration of Ca^{2+} into intracellular compartments (Ca^{2+} uptake) via transporters or ATPases. Together, Ca^{2+} efflux and Ca^{2+} uptake work to maintain resting $[Ca^{2+}]_i$ relatively low at ~100 nM, some 5 orders of magnitude lower than that present outside the cell *in vivo* (~1.28 mM). Failure to properly control resting $[Ca^{2+}]_i$ can be catastrophic for a cell, and can result in the inappropriate and deleterious activation of Ca^{2+} sensitive processes. Indeed, aberrant Ca^{2+} handling leading to a prolonged elevation in $[Ca^{2+}]_i$ is known to be pathological and cytotoxic (Berliocchi et al., 2005, Criddle et al., 2007). Thus, the homeostatic mechanisms responsible for the maintenance a low resting $[Ca^{2+}]_i$ are critical for cell survival.

The following section will consider those mechanisms involved in lowering $[Ca^{2+}]_i$ and maintaining $[Ca^{2+}]_i$ homeostasis. Particular attention will afforded to the role and regulation of the plasma membrane Ca^{2+} ATPase (PMCA), an ATP driven membrane-bound pump critically responsible for Ca^{2+} efflux into the extracellular space, before focusing on the potential link between cancer metabolism and this ATP-dependent Ca^{2+} pump.

1.8.3.1 - The sarcoplasmic/endoplasmic reticulum Ca^{2+}-ATPase

The endoplasmic reticulum (ER) is a membrane enclosed organelle within eukaryotic cells that is important for the correct processing of newly synthesised proteins. The ER is formed from interconnected tubes (cisternae), and contains a relatively high concentration of Ca^{2+} ions thought to be in the mM range (Bygrave and Benedetti, 1996). The ER achieves a high luminal Ca^{2+} concentration via the sarco/endoplasmic reticulum Ca^{2+}-ATPase (SERCA), a Ca^{2+} pump which resides in the ER membrane that acts to take Ca^{2+} into the ER. Thus, the ER forms a dynamic intracellular reservoir of Ca^{2+} ions, with Ca^{2+} uptake performed by SERCA and Ca^{2+} release by IP_3Rs and RyRs; the similar sarcoplasmic reticulum plays a similar role as Ca^{2+} store in muscle cells. SERCA is a P-Type ATPase and was the first ATP-driven Ca^{2+} pump to be identified (MacLennan, 1970). Since then, 3 major isoforms have since been characterised (Wuytack et al., 2002)), each with numerous splice variants to allow for further functional diversity. SERCA uses energy from the hydrolysis of ATP to move Ca^{2+} against its electrochemical gradient into the ER lumen, and is important for replenishing the ER Ca^{2+} store following Ca^{2+} release from the ER. In addition, constitutive SERCA activity opposes a passive Ca^{2+} leak from the ER in order to maintain the high luminal Ca^{2+} concentration (Hofer et al., 1996). For every ATP hydrolysed, SERCA transports 2 Ca^{2+} ions into the ER lumen. This is coupled to the export of 3 H^+ ions, and as a consequence SERCA activity is electrogenic (Yu et al., 1993). One of the main regulators of SERCA activity is phospholamban (PLB), which when dephosphorylated associates with SERCA and lowers its affinity for Ca^{2+}, thereby inhibiting SERCA activity without affecting the V_{max} (Simmerman and Jones, 1998, MacLennan and Kranias, 2003). SERCA is an energy efficient means of clearing $[Ca^{2+}]_i$ as 2 Ca^{2+} ions are transported into the ER lumen for every ATP hydrolysed (Inesi et al., 1978); nevertheless, the ER's capacity for Ca^{2+} is finite, and the passive movement of Ca^{2+} out of the ER via the Ca^{2+} leak pathway counteracts the action of SERCA.

1.8.3.2 - The secretory pathway Ca^{2+} ATPase

In addition to ER sequestration of Ca^{2+}, Ca^{2+} uptake can also occur in the Golgi apparatus. This occurs via both SERCA and the less well understood secretory pathway Ca^{2+} ATPase (SPCA), which can also contribute to the shaping of cytosolic signals (Dolman and Tepikin, 2006). The SPCA is a P-type ATPase similar to SERCA and PMCA. However, unlike these related pumps, it can also transport Mn^{2+}, which is important for protein glycosylation and sorting (Durr et al., 1998), Furthermore, in addition to influencing Golgi function, Mn^{2+} uptake is important mechanism to prevent toxicity associated with excessively high cytoplasmic Mn^{2+} concentrations (Van Baelen et al., 2004).

1.8.3.3 - Mitochondrial Ca^{2+} uptake

In addition to generating ATP by oxidative phosphorylation, mitochondria play a role in numerous other intracellular processes, including β-oxidation of fatty acids (McBride et al., 2006), reactive oxygen species signalling (Li et al., 2013) and programmed cell death (Green, 1998). They are also a key component of the Ca^{2+} signalling machinery (Duchen, 2000). Mitochondrial uptake of Ca^{2+} is largely driven by the negative potential across the inner mitochondrial membrane. While Ca^{2+} can cross the outer mitochondrial membrane freely, Ca^{2+} entry into the mitochondrial matrix is facilitated by the recently identified mitochondrial calcium uniporter (MCU), a low affinity (Bragadin et al., 1979) Ca^{2+} transporter that resides in the inner mitochondrial membrane (De Stefani et al., 2011, Baughman et al., 2011). Furthermore, Ca^{2+} transport via MCU is regulated by numerous accessory proteins found at the inner mitochondrial membrane (Marchi and Pinton, 2014), including mitochondrial calcium uptake 1 (MICU1, Perocchi et al., 2010) and mitochondrial calcium uptake 2 (MICU2, Patron et al., 2014). Thus, since they can sequester Ca^{2+}, mitochondria contribute to the shaping the amplitude and spatiotemporal aspects of Ca^{2+} signals (Budd and Nicholls, 1996, Duchen, 1999, Jouaville et al., 1995). Mitochondria also express a Na^{+} -dependent Ca^{2+} efflux mechanism (Carafoli et al., 1974), known as the mitochondrial Na^{+}/Ca^{2+} exchanger, mNCX. This transporter operates with a stoichiometry of $3Na^{+}:Ca^{2+}$ (Jung et al., 1995) and can operate in reverse mode (Smets et al., 2004), similar to the plasma membrane Na^{+}/Ca^{2+} exchanger (see *1.8.3.4 - NCX*).

Studies also indicate that the ER is adjoined to mitochondria by tethers that are between 10 and 25 nm in distance (Csordas et al., 2006), in an interaction known as the mitochondria-associated ER membrane (MAM). This physical coupling provides an interface for the selective transmission of Ca^{2+} signals between these two organelles (Patergnani et al., 2011), and the close positioning of mitochondria to ER release channels (IP_3Rs and RyRs) allows for the efficient transfer of Ca^{2+} (Kopach et al., 2008, Decuypere et al., 2011). This allows mitochondria to spatially restrict Ca^{2+} signals to a specific microdomain. Moreover, Ca^{2+} buffering proximal to Ca^{2+} sensitive channels (such as SOCE channels and the IP_3 receptor) allows mitochondria to modulate the activity of these channels and to act as a Ca^{2+} buffer following large increases in $[Ca^{2+}]_i$ (Pinton et al., 2008, Parekh, 2003). However, mitochondria cannot store high $[Ca^{2+}]_i$ within the mitochondrial matrix for prolonged periods of time as this leads to precipitation of Ca^{2+} phosphate (Kristian et al., 2007), and beyond a certain threshold mitochondrial Ca^{2+} stimulates the intrinsic pathway of apoptosis (Pinton et al., 2008, Orrenius et al., 2003, Rizzuto et al., 2009).

Of note with respect to cell metabolism, evidence from numerous studies indicates that Ca^{2+} uptake regulates numerous mitochondrial enzymes and that mitochondrial Ca^{2+} stimulates an increase in respiratory rate and ATP production (Glancy and Balaban, 2012, McCormack et al., 1990, Patergnani et al., 2011), and isolated enzyme studies have identified Ca^{2+} as a regulator of PDH (Denton et al., 1972), isocitrate dehydrogenase (Denton et al., 1978), glycerol-3-phosphate dehydrogenase (Rutter et al., 1992) and the α-ketoglutarate dehydrogenase complex (Armstrong et al., 2014, McCormack and Denton, 1979).

1.8.3.4 - NCX

The Na^+/Ca^{2+} exchanger (NCX) is a Ca^{2+} transport molecule found in the plasma membrane that uses the Na^+ gradient generated by the Na^+/K^+ ATPase to extrude Ca^{2+} from the cytosol (Berridge et al., 2003). NCX countertransports one Ca^{2+} ion for 3 Na^+ ions, and due to its low affinity for Ca^{2+} (Carafoli et al., 2001) coupled with a high capacity for Ca^{2+} transport, NCX is important for rapidly removing cytosolic Ca^{2+} following large increases in $[Ca^{2+}]_i$, such as those observed in cardiac cells. Three isoforms (NCX1 - 3) have been identified (Linck et al., 1998), and the physiological roles of these transporters has been reviewed in detail elsewhere (Blaustein and Lederer, 1999). Although NCX typically acts to export Ca^{2+} from cells, it can also operate in reverse to facilitate Ca^{2+} entry (Blaustein and Lederer, 1999). Indeed, NCX has been shown to be expressed in numerous pancreatic cancer cell lines (Hansen et al., 2009), where it can contribute to TGF-β-induced motility by working in Ca^{2+} entry mode (Dong et al., 2010). However, while it has been suggested that NCX contributes to Ca^{2+} efflux in isolated rat pancreatic ducts (Ankorina-Stark et al., 2002, Hug et al., 1996), evidence suggests that NCX does not contribute to $[Ca^{2+}]_i$ clearance in pancreatic acinar cells, as replacement of extracellular Na^+ with *N*-Methyl-D-glucamine (NMDG, thus removing the driving force for NCX) has no effect on $[Ca^{2+}]_i$ clearance in these cells (Muallem et al., 1988). It remains to be determined whether the NCX contributes to $[Ca^{2+}]_i$ clearance in PDAC.

1.8.3.5 - The Plasma Membrane Ca^{2+} ATPase and its regulation by ATP

The plasma membrane Ca^{2+} ATPase (PMCA) is an ATP-driven Ca^{2+} pump that is essential for extruding Ca^{2+} from the cell across the plasma membrane following Ca^{2+} entry or release of Ca^{2+} from the ER store. The PMCA was first identified and its activity measured in the 1960s (Dunham and Glynn, 1961, Schatzmann, 1966), and is ubiquitously expressed in all eukaryotic cells. Similarly to SERCA, the PMCA is a member of the P-type ATPase family. Typically, the PMCA exchanges one Ca^{2+} ion for two H^+ ions per ATP molecule hydrolysed, and as a result PMCA flux is electroneutral (Niggli et al., 1982, Thomas, 2009). However, evidence suggests the PMCA can exhibit variable Ca^{2+}:H^+ coupling to behave in an electrogenic fashion (Hao et al., 1994, Salvador et al., 1998), and may even uncouple Ca^{2+} efflux from H^+ influx at alkaline pH in order to extrude Ca^{2+} independent of H^+ transport (Milanick, 1990). Due to its high affinity for Ca^{2+} (K_d, ~200 nM) despite a low Ca^{2+} transport capacity, the PMCA is critically important for the fine tuning of $[Ca^{2+}]_i$ below 300 nM (Carafoli, 1994, Carafoli, 1991, Szasz et al., 1978). Therefore, in contrast to the NCX, which is key for controlling large dynamic Ca^{2+} signals during stimulation, the PMCA is more responsible for the moment-to-moment maintenance of a low resting $[Ca^{2+}]_i$ at around ~100 nM (Clapham, 2007, Carafoli et al., 2001). However, in cells where NCX is absent or not functional, the PMCA is the major Ca^{2+} efflux pathway (Bruce, 2010). Nevertheless, in cells where NCX is responsible for the bulk of Ca^{2+} efflux, such as excitable cells, the PMCA is still critical for the fine tuning of resting $[Ca^{2+}]_i$ below the threshold of NCX Ca^{2+} sensitivity (Carafoli et al., 2001). Indeed, while the PMCA was once thought play only a “housekeeping” role in Ca^{2+} homeostasis, it has become apparent that different PMCA isoforms play a multifaceted role in other intracellular processes, and can influence processes

such as programmed cell death (Brini, 2009, Curry et al., 2012), which has implications for apoptosis-resistant cancer cells, and cardiac contractility (Schuh et al., 2001, Oceandy et al., 2007). Isoform-specific PMCA expression has been reported to be deregulated in numerous cancers, including breast (Lee et al., 2002, Lee et al., 2005), colon (Aung et al., 2007), gastric (Ribiczey et al., 2007) and oral cancer (Saito et al., 2006). These findings suggest that changes in PMCA expression and function could contribute to the remodelling of Ca^{2+} signals in cancer, although the nature and impact of this is currently not known and research in this field is currently still in its infancy (Roberts-Thomson et al., 2010).

Since it was first identified, four PMCA isoforms have been characterised (PMCA1 - 4); PMCA 1 and 4 are ubiquitously expressed in all tissues, while PMCA 2 and 3 are predominantly expressed only in excitable cells. Each isoform has numerous splice variants, allowing for functional diversity and differences in tissue and subcellular localisation (Monteith et al., 1998, Strehler and Zacharias, 2001a). Of note, different PMCA isoforms exhibit varying affinities for the PMCA regulator calmodulin (CaM), can operate at different rates (Elwess et al., 1997), are differentially regulated by the rate of change of Ca^{2+} and can display memory of previous Ca^{2+} signals (Caride et al., 2001a, Caride et al., 2001b). The PMCA protein comprises of 10 transmembrane domains (TM) with 4 cytosolic loops and both the N and C termini residing on the cytosolic side of the plasma membrane (Bruce et al., 2003, Di Leva et al., 2008). Importantly, the cytosolic N terminal domain exhibits the greatest diversity among isoforms (Stauffer et al., 1995). The two-dimensional structure of the PMCA is presented in Figure 1.8.

The PMCA is regulated by numerous intracellular messengers, most notably ATP and CaM (Strehler and Zacharias, 2001a, Di Leva et al., 2008), and three major cytosolic domains are the loci of PMCA regulation by these agents; the intracellular loops between TM2 and TM3, TM4 and TM5 and the C terminal domain. The C terminus is notable as the site of an autoinhibitory mechanism that is regulated by the main activator of the PMCA, CaM (James et al., 1988). The cytosolic loop between the TM2 and TM3 domains contains part of the binding site for this autoinhibitory domain (Falchetto et al., 1992), with the other half present on the second cytosolic loop between the TM4 and TM5. This second loop also contains the major catalytic site, comprised of the ATP binding site and the aspartate residue that forms the acyl phosphate intermediate during the reaction cycle of Ca^{2+} transport (Falchetto et al., 1991). The autoinhibitory domain blocks the catalytic site when $[Ca^{2+}]_i$ is low and the PMCA operates in a low-activity state (Figure 1.8A), while at a higher $[Ca^{2+}]_i$ Ca^{2+}-bound CaM prevents this interaction by binding to the autoinhibitory site and reducing its affinity for the catalytic domain (Figure 1.8B, Carafoli, 1994). In doing so, binding of Ca^{2+}-bound CaM to the PMCA at this site increases the rate of Ca^{2+} transport via the PMCA (Jeffery et al., 1981) by dramatically increasing its affinity for Ca^{2+} (Muallem and Karlish, 1981).

In addition to the CaM binding site, the extended C-terminal domain contains the phosphorylation site for PKA (Strehler and Zacharias, 2001a) and PKC (Penniston and Enyedi, 1998, Monteith et al., 1998), which results in increased CaM binding (Gromadzinska et al., 2001) and enhanced PMCA activity (Neyses et al., 1985, Smallwood et al., 1988, Zylinska et al.,

1998). Other proteins that interact with the PMCAs act to stabilise and traffic them to specific regions of the cell, including membrane-associated guanylate kinase (MAGUK) and Na^+/H^+ exchanger regulatory factor-2 (NHERF) which interact with the PDZ domain (named after three proteins which were first found to share the domain, **p**ost synaptic density protein, **d**rosophila disc large tumor suppressor, and **z**onula occludens-1 protein) in the C-terminus (Di Leva et al., 2008).

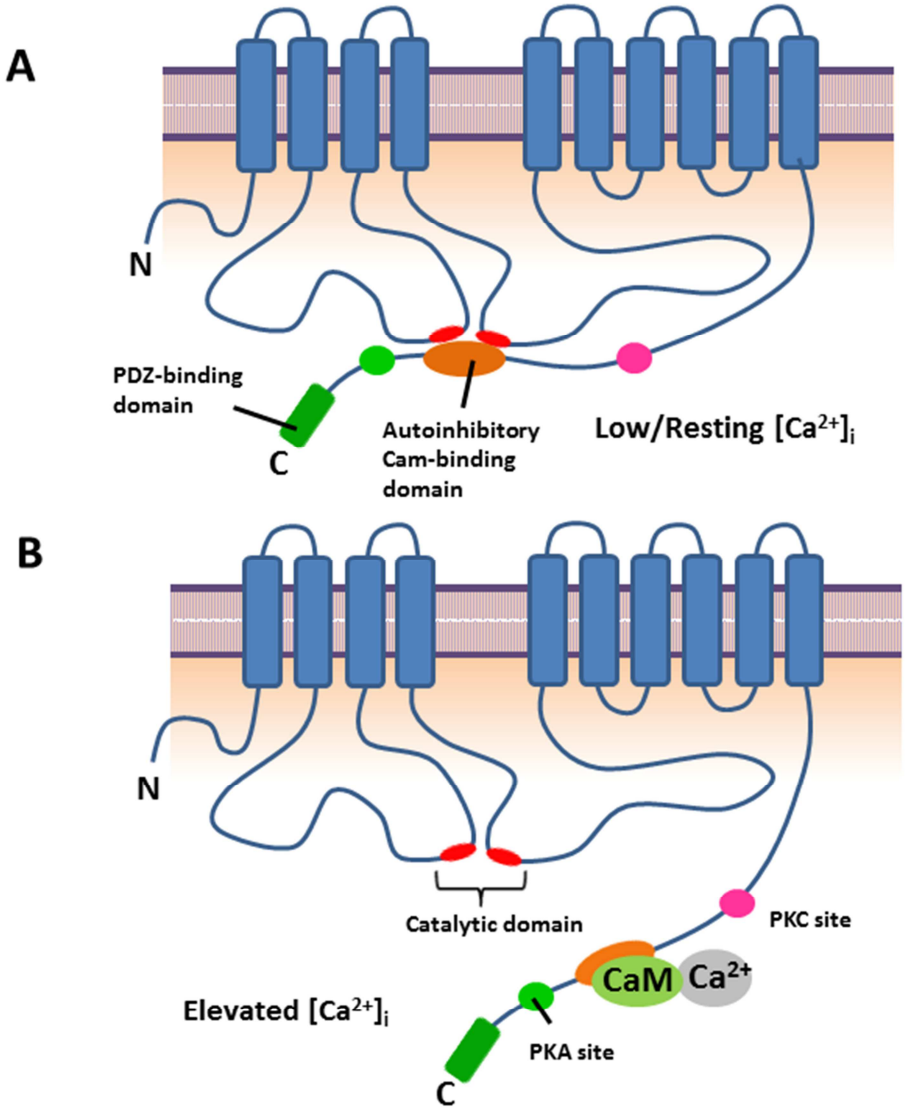

Figure 1.8 - Structure of the plasma membrane Ca^{2+} ATPase (PMCA) at both resting and elevated $[Ca^{2+}]_i$

Depicted is the two dimensional structure of the PMCA when $[Ca^{2+}]_i$ is low at resting (***A***) and elevated during a $[Ca^{2+}]_i$ transient (***B***). The PMCA is comprised of 10 transmembrane (TM) domains, The catalytic site, including the ATP binding domain, is found at an interface between the TM2-TM3 and TM4-TM5 intracellular loops (red). The extended intracellular C-terminal domain contains the binding site for protein kinase C (PKC) and protein kinase A (PKA), and the PDZ-binding domain (named after three proteins which were first found to share the domain, **p**ost synaptic density protein, **d**rosophila disc large tumor suppressor, and **z**onula occludens-1 protein). It also contains the autoinhibitory domain which occupies the active site at low $[Ca^{2+}]_i$. This autoinhibition of the PMCA active site is relieved upon Ca^{2+}-bound calmodulin (CaM) binding to the autoregulatory site. Adapted from Bruce et al., 2003.

Early studies in human erythrocytes established that two binding sites exist for ATP on the PMCA (Richards et al., 1978). It was proposed that the higher affinity site (Km, 2.5 µM) was the catalytic site; however, occupation of this site conferred only 10% of the maximum activity attainable when the ATP concentration was not limiting. Maximum PMCA activity was achieved upon occupation of the second, lower affinity binding site (K_m, 145 µM) in an Mg^{2+} dependent manner, suggesting this site plays a regulatory role. However, more recent studies have suggested that the ATP regulation of the PMCA is in fact more complex (Echarte et al., 2007). The ATP sensitivity of the PMCA is dynamically regulated by many factors, including $[Ca^{2+}]_i$, $[Mg^{2+}]_i$, CaM and the phospholipid composition of the plasma membrane. In particular, acidic phospholipids are important in regulating the ATP sensitivity of the PMCA. The C terminal domain of the PMCA contains binding sites for acidic phospholipids such as phosphatidylinositol (PI) and phosphatidylserine (PS), which have long been known to increase affinity of the PMCA for Ca^{2+} and ATP, and are thought to be responsible for the permanent activation of the PMCA to 50% of its maximal activity (Niggli et al., 1981a, Niggli et al., 1981b). PS is known to relocate to the outer leaflet of the membrane during apoptosis (Fadok et al., 1992), a process that allows detection of apoptotic cells using Annexin V-based assays (van Engeland et al., 1998), and this loss of acidic phospholipids from the inner envelope of the plasma membrane corresponds with a decrease in PMCA affinity for ATP. Cell free assays have determined that the affinity of the regulatory site for ATP decreases dramatically (K_m, 5 - 10 mM) when PI or PS were absent from the phospholipid bilayer (Lehotsky et al., 1992, Rossi and Rega, 1989). This decrease in affinity for ATP would be expected to leave the PMCA exquisitely sensitive to even modest decreases in cytosolic ATP. Indeed, loss of phosphatidylserine from the inner envelope of the plasma membrane following cholesterol depletion by β-methyl-cyclodextran treatment has been shown to cause PMCA inhibition (Zhang et al., 2009). Although intuitively one might expect ATP depletion to have a profound effect on PMCA activity, the absolute ATP sensitivity of the PMCA *in vivo* remains poorly characterised, therefore the threshold concentration at which ATP depletion affects the PMCA is not currently known. Nevertheless, given that cancer cells undergo a shift towards glycolysis following oncogenic transformation, drugs designed to cut off the glycolytic ATP supply to the PMCA might be expected to inhibit PMCA, resulting in $[Ca^{2+}]_i$ overload and cell death. It is therefore tempting to speculate that regulation of the PMCA by glycolytic ATP may be an untapped therapeutic avenue for the treatment of cancer.

In addition to the action of numerous regulatory agents on the ATP sensitivity of the PMCA, it has been suggested that a critical [ATP] threshold exists where Na^+ efflux via the Na^+-K^+-ATPase becomes more favourable than maintenance of Ca^{2+} extrusion via the PMCA (Castro et al., 2006). This study proposed that below this threshold ATP concentration the Na^+-K^+-ATPase can 'steal' ATP from the PMCA, suggesting that the ATP dependency of the PMCA is not isolated from the actions of other ion pumps present in the plasma membrane. Furthermore, evidence also suggests that the PMCA has a preferential supply of ATP derived from a local, submembrane glycolytic cascade. Studies in inside out plasma membrane vesicles isolated from porcine smooth muscle have shown that a complete glycolytic cascade beginning at

aldolase is associated with the membrane fraction and is able to fuel Ca^{2+} transport via the PMCA by generating a submembrane pool of glycolytically-derived ATP from glycolytic substrates (Paul et al., 1989). Further extensions of this study established that the PMCA preferentially utilised this glycolytically-derived submembrane ATP pool despite the addition of exogenous ATP (Hardin et al., 1992).

It has long been established that glycolytic enzymes colocalise with the PMCA in human erythrocytes by associating with the membrane protein anion exchanger 1, also known as band 3 (Puchulu-Campanella et al., 2013, Campanella et al., 2005, Campanella et al., 2008). This is regulated by tyrosine phosphorylation of AE1 (Low et al., 1987), and influences the activity of the glycolytic enzymes involved (Harrison et al., 1991). Moreover, while little is known about putative plasma membrane-bound glycolytic enzymes in other cell types, evidence suggests this is likely of importance to cells other than erythrocytes. Studies using highly glycolytic endothelial cells have shown that silencing PFKFB3 abolishes the generation of a submembrane pool of glycolytically-derived ATP required for cell migration (De Bock et al., 2013), thus highlighting the potential importance of a submembrane glycolytic cascade in invasive cancer. However, unlike erythrocytes, the putative binding sites for glycolytic enzyme association with the plasma membrane have not yet been identified in other cells. Nevertheless, mucin 1 (MUC1), a membrane bound glycoprotein important for protecting cells by binding extracellular pathogens, has recently been shown to both bind to and regulate PKM2, and that this interaction is regulated by tyrosine phosphorylation (Kosugi et al., 2011). As mentioned in an earlier chapter, PKM2 is overexpressed in PDAC (Chaika et al., 2012b), and this provides a potential mechanism by which glycolytic enzymes critical for the Warburg phenotype associate with the plasma membrane in PDAC Moreover, MUC1 is overexpressed in pancreatic cancer (Hinoda et al., 2003) and regulates HIF-1α signalling to promote the highly glycolytic phenotype of PDAC (Chaika et al., 2012a). As such, a submembrane supply of glycolytically-derived ATP might be critical for fuelling PMCA activity, and may represent a key weakness in cancer cells exhibiting the Warburg phenotype. Could this be a means to selectively target PDAC whilst sparing healthy cells?

1.9 - Summary

To summarize, PDAC is an aggressive cancer with extremely poor prognosis and limited treatment options. Clearly a radical approach to treating this illness is urgently required. Cancer cells often proliferate rapidly and are resistant to cell death due, in part, to a switch from mitochondrial metabolism towards a highly glycolytic phenotype, which is common of cancer cells exhibiting the Warburg phenotype. This shift in metabolism typically results from a combination of oncogenic mutations, a hypoxic tumour microenvironment and the metabolic demands of the rapidly proliferating cancer cells. Although this shift in metabolism is considered to confer numerous survival advantages for cancer cells and to provide them with a robust means of generating energy in the face of tumour hypoxia, their increased reliance on glycolysis as a major source of ATP may prove to be a weakness that can be exploited therapeutically. This is because ATP is required to fuel numerous energy-dependent mechanisms critical for cell survival. One such mechanism is the ATP-driven PMCA, which is critical for maintaining a low resting $[Ca^{2+}]_i$. Moreover, Ca^{2+} efflux via the PMCA is critical for cell survival, since inhibition of the PMCA leads to a cytotoxic $[Ca^{2+}]_i$ overload. Regulation of the PMCA by glycolytic ATP may therefore be critical for cell survival in highly glycolytic PDAC cells, and may therefore represent a novel therapeutic locus that can be targeted with drugs to selectively kill PDAC cells while sparing healthy tissue.

Experimental Aims

The central theme of this thesis is the metabolic regulation of the PMCA in highly glycolytic PDAC cells. This will be addressed by three separate results chapters, each with a different aim that contributes to the overarching theme. Supplementary methods and supporting data will be presented in a separate chapter.

Specific aims:

- **Results Chapter 1**
  Specific aim: To investigate the importance of glycolytic ATP supply to the PMCA in PDAC.
  This will be achieved by comparing the effects of mechanistically distinct metabolic inhibitors (mitochondrial vs glycolytic) on key readouts of cell function including cell death, cytosolic ATP, resting $[Ca^{2+}]_i$ and PMCA activity in human PDAC cell lines.

- **Results Chapter 2**
  Specific aim: To investigate the effect of "reversing" the Warburg Effect on metabolic regulation of the PMCA in PDAC cells.
  This will be achieved by culturing PDAC cells in nominal glucose-free media supplemented with alternative substrates with the intention of "refuelling" the mitochondria, thereby shifting their metabolic phenotype from a high glycolytic rate to one more reliant on mitochondrial metabolism. We will assess the effects these culture regimens on the metabolic phenotype in these cells, and then investigate the effects of

glycolytic vs mitochondrial inhibitors on cytosolic ATP, resting $[Ca^{2+}]_i$ and PMCA activity in human PDAC cell lines.

- **Results Chapter 3**

  Specific aim: **To investigate the putative dynamic association of glycolytic enzymes with the plasma membrane in PDAC.**

  This will be achieved by using a combination of western blotting with a biotinylation assay to isolate the plasma membrane fraction of PDAC cells. The nature of any dynamic association will be tested using drugs that regulate protein tyrosine phosphorylation. Furthermore, functional assays will assess the effects of these drugs on cytosolic [ATP] and PMCA activity.

1.10 - Alternative Format

This thesis is presented in the Alternative Format in accordance with the Rules and Regulations of the University of Manchester. While the results chapters presented within have been written in the style of the journal for which they are intended to be submitted, some aspects of each chapter have been reformatted to ensure that the thesis is presented as a cohesive body of work. Moreover, following each results chapter, a supplementary methods and results section has been included to provide a detailed description and critical analysis of the methods employed.

The details of each results chapter, its intended journal and the contribution of each other authors are specified below.

- **Results Chapter 1**

  Title: Glycolytic ATP fuels the plasma membrane calcium pump critical for pancreatic cancer cell survival

  Authors: Andrew D. James, Anthony Chan, Oihane Erice, Ajith K. Siriwardena, Jason I. E. Bruce

  Intended Journal: Published in Journal of Biological Chemistry, October 24 2013

  Contribution of Authors: This study was devised, conducted and the paper written by myself with guidance from Jason Bruce. I obtained the majority of data and contributed to all figures in this paper. Additional $[Ca^{2+}]_i$ clearance experiments performed by Anthony Chan and Oihane Erice Azparren. All data was analysed by me.

- **Results Chapter 2**

  Title: The plasma membrane calcium pump in pancreatic cancer cells exhibiting the "Warburg Effect" is reliant on a glycolytic ATP supply

  Authors: Andrew D. James, Waseema Patel, Zohra Butt, Magretta Adiamah, Raga Dakhel, Carolina Uggenti, Lisa Swanton, Hiromi Imamura, and Jason I. E. Bruce

  Intended Journal: Journal of Biological Chemistry

  Contribution of Authors: This study was devised, conducted and the paper written by myself with guidance from Jason Bruce. I performed the majority of experiments included in this paper, and contributed to all figures. All data was analysed by me. However, while all experiments were devised by me, some experiments within the data set were performed by numerous masters and undergraduate students and performed under my supervision. Waseema Patel and Raga Dakhel contributed to the luciferase and GO-ATeam-based ATP assays, respectively, and Zohra Butt and Magretta Adiamah made an equal contribution to the calcium overload data set. These co-authors were also taught their respective techniques by me. On the other hand, the cell proliferation assays were performed by myself under guidance from Ayse Latif; similarly, the preparation of MIA PaCa-2 cells stably expressing GO-ATeam was

performed by myself under guidance from Carolina Uggenti and Lisa Swanton. The GO-ATeam plasmid was developed, validated and supplied by Hiromi Imamura.

- **Results Chapter 3**

  Title: The regulation of the plasma membrane calcium pump by membrane-bound glycolytic enzymes in pancreatic cancer

  Authors: Andrew James, James Wong, Bobby Chow, Joseph Dent, Jonathan Briggs, Hannah Tierney, Hiromi Imamura, Donald Ward and Jason I. E. Bruce

  Intended Journal: Journal of Biological Chemistry

  Contribution of Authors: This study was devised, conducted and the paper written by myself with guidance from Jason Bruce. I performed most of experiments included in this paper, and contributed to all figures and analysis. All data was analysed by me. James Wong contributed to some of the early western blotting experiments, which were repeated and expanded by me. Aside from this, all sample preparation, reprobing of membranes, and western blotting were all performed by me, although some later western blots were performed by Jonathan Briggs and Hannah Tierney under my supervision. For the imaging experiments, all cell culture and the preparation of cells stably expressing GO-ATeam was performed by me, and some experiments within the data set were performed under my supervision by Bobby Chow and Joseph Dent. This study was devised, conducted and the paper written by myself with guidance from Jason Bruce. The GO-ATeam plasmid was developed, validated and supplied by Hiromi Imamura, and Donald Ward provided initial advice on preparing the tyrosine kinase and tyrosine phosphatase inhibitors in addition to support with general western blotting techniques.

Chapter 2 - Glycolytic ATP Fuels the Plasma Membrane Calcium Pump Critical for Pancreatic Cancer Cell Survival

Andrew James[1], Anthony Chan[2], Oihane Erice Azparren[1], Ajith Siriwardena[2], Jason Bruce[1]

From the [1]Faculty of Life Sciences, The University of Manchester, Michael Smith Building, Oxford Road, Manchester, M13 9PT, United Kingdom and the [2]Hepatobiliary Surgery Unit, Manchester Royal Infirmary, Manchester, M13 9NT, United Kingdom

2.1 - Abstract

Pancreatic cancer is an aggressive cancer with poor prognosis and limited treatment options. Cancer cells rapidly proliferate and are resistant to cell death due, in part, to a shift from mitochondrial metabolism to glycolysis. We hypothesised that this shift is important in regulating cytosolic Ca^{2+} ($[Ca^{2+}]_i$), since the ATP-dependent plasma membrane Ca^{2+} ATPase (PMCA) is critical for maintaining low $[Ca^{2+}]_i$ and thus cell survival. The present study aimed to determine the relative contribution of mitochondrial vs glycolytic ATP in fuelling the PMCA in human pancreatic cancer cells. We report that glycolytic inhibition induced profound ATP depletion, PMCA inhibition, $[Ca^{2+}]_i$ overload and cell death in PANC-1 and MIA PaCa-2 cells. Conversely, inhibition of mitochondrial metabolism had no effect, suggesting that glycolytic ATP is critical for $[Ca^{2+}]_i$ homeostasis and thus survival. Targeting the glycolytic regulation of the PMCA may therefore be an effective strategy for selectively killing pancreatic cancer, whilst sparing healthy cells.

2.2 - Introduction

Pancreatic ductal adenocarcinoma (PDAC) is an aggressive form of cancer that originates in the glandular ductal tissue of the exocrine pancreas. Treatment options are severely limited, with surgical removal of the tumour being the most common course of action. While its incidence is relatively low, mortality in PDAC is almost 100% (Krejs, 2010); pancreatic cancer is the 4th and 5th most common cause of cancer-related death in men and women, respectively. PDAC often progresses to metastasis in the absence of obvious clinical symptoms (Amin et al., 2006), resulting in late diagnosis and a five year survival rate of 1% (Gudjonsson, 2009).

A hallmark of cancer cells, including PDAC, is a shift from predominantly mitochondrial metabolism towards glycolysis, even when oxygen is abundant (the 'Warburg Effect', Hanahan and Weinberg, 2011, Zhou et al., 2011). Such a metabolic shift seems counterintuitive, as the textbook view is that glycolytic ATP synthesis is an energetically unfavourable method of meeting the presumably high ATP demand of rapidly proliferating cancer cells. However, a shift towards glycolysis appears to confer a number of survival advantages for tumour cells (Gatenby and Gillies, 2004). These include resistance to hypoxia, which is prevalent in PDAC tumours (Koong et al., 2000), and an increased availability of glycolytic intermediates for use in the anabolic pathways that drive cell proliferation (Kroemer and Pouyssegur, 2008).

It is therefore unlikely that cancer cells exhibit the Warburg phenotype primarily for bioenergetic purposes, despite exhibiting an increased reliance on glycolytic ATP (Nakashima et al., 1984). However, the homeostatic maintenance of a low resting cytosolic calcium (Ca^{2+}) concentration ($[Ca^{2+}]_i$, ~100nM) is an ATP dependant process that is critical for cell survival. Of particular importance is the ubiquitously expressed plasma membrane Ca^{2+} ATPase (PMCA), an ATP-dependent pump with a high affinity for Ca^{2+} that extrudes cytosolic Ca^{2+} (Carafoli, 1991). The PMCA has been suggested as the major efflux pathway in non-excitable cells (such as epithelial cells) where the Na^{+}/Ca^{2+} exchanger (NCX) is either lacking or expressed with low abundance (Carafoli, 1987). In these cells, impaired PMCA function quickly results in $[Ca^{2+}]_i$ overload and cell death, indicating that PMCA function is critical for cell survival. Under physiological conditions when ATP is abundant, the source of ATP to fuel the PMCA is not likely to be important, provided that the cytosolic [ATP] is maintained above a critical threshold. The classical view is that the bulk of ATP comes from the mitochondria, and evidence suggests that inhibition of mitochondrial metabolism in non-cancerous cells impairs Ca^{2+} homeostasis and leads to cell death (Baggaley et al., 2008, Criddle et al., 2006, Criddle et al., 2007). However, in cancer cells where there is a shift towards glycolytic metabolism, this relationship may be very different. Importantly, the PMCA has been reported to have its own localised glycolytic ATP supply (Campanella et al., 2005, Hardin et al., 1992). It could, therefore, be hypothesised that glycolytic ATP is critical for fuelling the PMCA and confers a survival advantage to cancer cells.

The present study shows that in human PDAC cell lines (PANC-1 and MIA PaCa-2), inhibition of glycolysis induced severe ATP depletion, cytosolic Ca^{2+} overload, inhibition of PMCA activity and cell death. In contrast, inhibition of mitochondrial metabolism had almost no effect on $[Ca^{2+}]_i$

handling, ATP depletion or cell death. Glycolytic regulation of the PMCA may therefore be a critical pro-survival mechanism in PDAC, and thus may represent a previously untapped therapeutic avenue for selectively killing PDAC cells whilst sparing normal cells.

2.3 - Experimental Procedures

2.3.1 - Cell Culture

MIA PaCa-2 and PANC-1 cells (ATCC) were grown in DMEM (D6429, Sigma-Aldrich, supplemented with 10% FBS, 100 units/ml penicillin and 100 µg/ml streptomycin) in a humidified atmosphere of air/CO2 (95%:5%) at 37°C. Cells were used up to passage 30 and then discarded.

2.3.2 - Fura-2 fluorescence Ca^{2+} imaging

Cells were seeded onto glass coverslips in a 6-well culture plate and grown to >30% confluency. To load cells with fura-2 dye, seeded coverslips were rinsed with HEPES-buffered physiological saline solution (HEPES-PSS: 138 mM NaCl, 4.7 mM KCl, 1.28 mM $CaCl_2$, 0.56 mM $MgCl_2$, 5.5 mM glucose, 10mM HEPES, pH 7.4). Rinse buffer was replaced with 4 µM fura-2 AM in 1 ml HEPES-PSS and incubated for 40 minutes at room temperature. Cells were then rinsed with HEPES-PSS, followed by a further 20 minutes in dye-free HEPES-PSS to allow uncleaved dye to re-equilibrate. Fura-2 loaded cells were mounted onto imaging systems and $[Ca^{2+}]_i$ measured as previously described (Baggaley et al., 2008, Bruce and Elliott, 2007, also see *2.8.1 – Fura-2 fluorescence microscopy and measurement of intracellular $[Ca^{2+}]_i$* in *2.8 – Chapter 2 Supplementary Methods and Results*). Experiments were performed using a Nikon Diaphot fitted with a x40 oil immersion objective (numerical aperture 1.3) and an Orca CCD camera (Hamamatsu), while the PANC-1 $[Ca^{2+}]_i$ clearance assays were performed using a Nikon TE2000 microscope fitted with a x40 oil immersion objective (numerical aperture 1.3) and a CoolSNAP HQ interline progressive-scan CCD camera (Roper Scientific Photometrics, Tucson, AZ). Both systems used a monochromator illumination system (Cairn Research, Kent, UK) and were controlled by MetaFluor image acquisition and analysis software (Molecular Devices, Downington, CA). Cells were continually perfused with HEPES-PSS using a gravity-fed perfusion system (Harvard apparatus) and were excited at 340nm and 380nm (50ms exposure). Emitted light was separated from excitation using a 400nm dichroic with 505LP filter. Background-subtracted images of a field of view of cells were acquired every 5 seconds for both excitation wavelengths (340 nm and 380 nm). For all experiments, $[Ca^{2+}]_i$ was measured as fura-2 340/380nm fluorescence ratio. $[Ca^{2+}]_i$ clearance was measured using an *in situ* $[Ca^{2+}]_i$ clearance assay as previously described (Mankad et al., 2012). Unless stated, $0Ca^{2+}$ HEPES-PSS contained 1 mM EGTA. Experiments (between 5 and 32 cells) were performed at room temperature.

2.3.3 - Preparation of test reagents

Na^+-free HEPES-PSS was prepared by replacing NaCl with equimolar N-methyl D-glucamine (Na^+ free/NMDG). Stocks of La^{3+}, 3-bromopyruvate (BrPy), sodium iodoacetate (IAA) and ATP

(Mg^{2+} salt) were prepared in MilliQ water. Stocks of oligomycin (OM), carbonyl cyanide m-chlorophenyl hydrazine (CCCP) and cyclopiazonic acid (CPA) were prepared in DMSO. Fura-2 AM (Invitrogen, TEFLabs) was prepared in 50:50 DMSO (Sigma-Aldrich) and 0.1% Pluronic® F-127 (Molecular Probes, Invitrogen). Working solutions in HEPES-PSS were prepared from frozen stocks immediately prior to an experiment. Reagents were prepared in media for the ATP and cell death experiments.

2.3.4 - Cell Death Assays

PANC-1 cells were seeded into black walled, clear-bottom 96 well plates at 70% confluency and allowed to adhere overnight. Cells were then incubated in culture conditions with blank media or ascending concentrations of CCCP (1 - 10 µM), BrPy (100 - 1000 µM), or a combination (3 µM and 500 µM, respectively) for 0.5 - 6 hours. Cells were then stained with propidium iodide (PI, cell death, 2 µg/ml, Fluka) and Hoechst 33342 (cell count, 20 µg/ml, Invitrogen). PI-positive cell count was normalised to Hoechst 33342-positive cell count (%). Assays were run in duplicate on a Thermo Fisher Scientific Cellomics® ArrayScan® VTI HCS Reader fitted with Hamamatsu ORCAR-ER camera and both x10 and x20 objectives. Imaging was performed by Imagen Biotech Ltd. Image analysis was assessed using the Compartmental Analysis Bioapplication (Thermo Fisher Scientific) whereby a threshold gate was set (~500 levels of grey) along an intensity histogram plot to distinguish positive PI fluorescent cells (~5000 levels of grey) from background noise (~10 levels of grey).

2.3.5 - ATP Measurements

Cultured MIA PaCa-2 and PANC-1 cells were seeded into white-walled, clear-bottom 96 well plates (1x 10^5 cells/ml) and allowed to adhere overnight. Cells were then treated with varying concentrations of metabolic inhibitors and incubated for 15 minutes in culture conditions. Each experiment included untreated cells (control), which represented total ATP, and a positive control with cells treated with an ATP depletion cocktail (4 µM CCCP, 10 µM OM, 500 µM BrPy, 2 mM IAA) to achieve maximal ATP depletion. Following treatment, cells were lysed and ATP determined using the luciferase-based ViaLight® Plus kit (Lonza, Rockland, ME, UK). Luminescence was measured using a Synergy HT multiwell reader (BioTEK). Each experiment was run in duplicate; the luminescence counts of each duplicate pair were averaged. To correct for background luminescence under conditions of maximal ATP depletion, the averaged luminescence count from the ATP depletion cocktail duplicates was subtracted from all other values. These values were normalised to the corresponding control (%).

2.3.6 - Calibration of resting $[Ca^{2+}]_i$

$[Ca^{2+}]_i$ calibrations were performed by first applying 10µM ionomycin in the absence of external Ca^{2+} to naïve fura-2 loaded PANC-1 (n=30 cells), and MIA PaCa-2 cells (n=25 cells). Once

$[Ca^{2+}]_i$ reached a minimum (R_{min}), cells were perfused with 20mM Ca^{2+} to induce a maximum increase in $[Ca^{2+}]_i$ (R_{max}). Fura-2 ratios were then calibrated to determine $[Ca^{2+}]_i$ as previously described (Grynkiewicz et al., 1985). Fura-2 ratios were plotted against calibrated $log[Ca^{2+}]_i$, with all cells from each cell line treated as a single data series A single sigmoidal curve was then fitted, representative of calibrated $[Ca^{2+}]_i$ in an average cell. The equation derived from this curve was used to estimate $[Ca^{2+}]_i$ and was extrapolated for each cell line. 100µM ATP was used to test cell viability, with viable cells eliciting a $[Ca^{2+}]_i$ spike (for a more detailed consideration of this method, please refer to *2.8.2 – Calibration of resting $[Ca^{2+}]_i$* in *2.8 – Chapter 2 Supplementary Methods and Results*)

2.3.7 - Measurement of $[Ca^{2+}]_i$ clearance

Repeated measurements of $[Ca^{2+}]_i$ clearance rate were performed, in parallel, on cells from the same passage in the presence or absence of test reagents during the second $[Ca^{2+}]_i$ clearance phase. The linear clearance rate over 60 seconds for the first influx-clearance phase was determined in fura-2 ratio units/second. This was repeated for the second influx-clearance phase (measured from the same standardised fura-2 value) and the second rate normalised to the first. Values were averaged for all cells in an experiment, and the resulting experimental means for each condition were averaged to give the presented group means ± SEM. To measure % recovery to baseline, difference was first calculated between the first fura-2 value used to measure linear clearance during the second clearance phase and the plateau subsequently reached. This was then normalised (%) to the difference between the same initial fura-2 ratio and the baseline observed after addition to CPA, before the first Ca^{2+} influx phase was initiated (for a more detailed description of both clearance and recovery analysis methods, please refer to *2.8.3 – Measurement of $[Ca^{2+}]_i$ clearance rate* and *2.8.4 – Measurement of % recovery of $[Ca^{2+}]_i$ clearance to baseline*.

2.3.8 - Data Analysis

Cell death was statistically assessed using a 2-way ANOVA with a post-hoc Bonferroni correction. Changes in resting $[Ca^{2+}]_i$ were quantified by measuring area under the curve (AUC) and the maximum increase in $[Ca^{2+}]_i$ over 30 minutes and compared using a one-way ANOVA with post hoc Dunnetts' test for multiple comparisons. Cell viability was quantified as the percentage of cells responding to 100µM ATP and compared using a Mann-Whitney U test. Changes in $[Ca^{2+}]_i$ clearance rate were compared using a Mann-Whitney U test. ATP depletion was assessed using a one sample t-test against the hypothetical control value of 100%. Presented data are the mean ± S.E.M of the indicated number (n) of independent experiments.

2.4 - Results

2.4.1 - Inhibition of glycolysis but not mitochondrial metabolism induces cell death in human PANC-1 cells

To determine whether PANC-1 cells functionally exhibit the Warburg Effect with respect to cell viability, the effects of both a mitochondrial and a glycolytic inhibitor on cell death were measured using propidium iodide (PI) fluorescence. PANC-1 cells were treated for 0.5 – 6 hours with either 3-bromopyruvate (BrPy), an inhibitor of the glycolytic enzyme hexokinase (Ko et al., 2001), or CCCP, a protonophore that collapses the mitochondrial membrane potential (Mankad et al., 2012).

Inhibition of mitochondrial metabolism with all three concentrations of CCCP (1, 3 and 10 µM) had no effect on cell death at any time point compared to corresponding control experiments (Figure 2.1A, n=5). In contrast, inhibition of glycolysis with BrPy resulted in a time-dependent increase in cell death at higher concentrations of BrPy. After 6 hours treatment, 300 µM BrPy caused significant cell death, with 37 ± 6% of cells positive for PI (n=5) compared to 6 ± 1 % for corresponding control cells (Figure 2.1B, P<0.001, n=5). Similar effects were observed at higher concentrations of BrPy and longer treatment periods. The combination of 3 µM CCCP and 500 µM BrPy caused a similar cell death to BrPy alone over a similar time frame, with 27 ± 6% of cells staining for PI (Figure 2.1A, P<0.001, n=5); no difference in cell death was observed between 6 hours treatment with 300 µM BrPy alone or a combination of 3 µM CCCP and 500 µM BrPy. These results strongly suggest that PANC-1 cells are sensitive to inhibition of glycolysis by BrPy, yet are unaffected by inhibition of mitochondrial metabolism by CCCP.

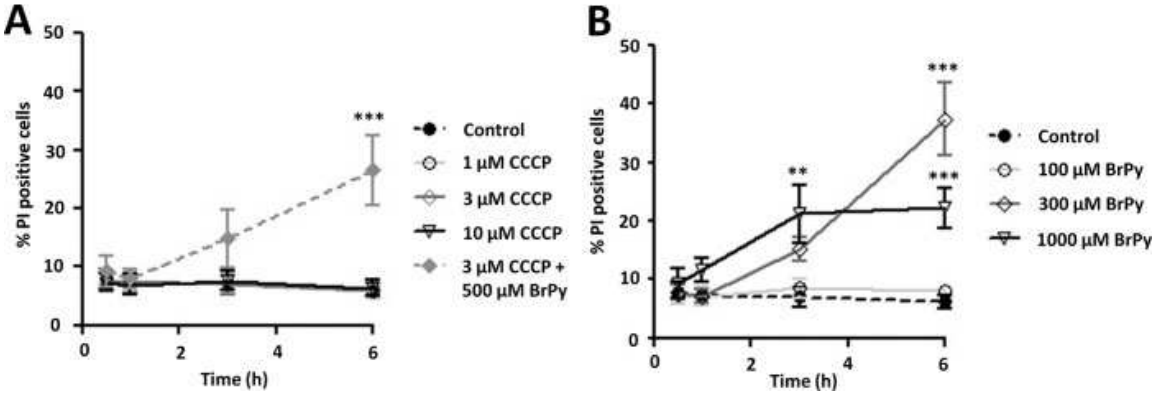

Figure 2.1 - Inhibition of glycolysis, but not mitochondrial metabolism, induces cell death in pancreatic cancer cells.

PANC-1 cells were treated with either the mitochondrial inhibitor, CCCP (1-10 µM, ***A***), the glycolytic inhibitor, 3-bromopyruvate (BrPy; 100-1000 µM, ***B***) or a combination of both (***A***, filled diamond) for varying times (0.5-6 hours). Cell death was determined using high content propidium iodide fluorescence (PI) on a Cellomics®. ArrayScan® VTI HCS Reader (Imagen Biotech). PI-positive cells (dead) were normalized to Hoechst-positive cells (cell count) to determine % cell death (n=5). *, p<0.05; **, p<0.01; ***, p<0.001 compared with control (2-way ANOVA, post-hoc Bonferroni correction).

2.4.2 - Inhibitors of glycolytic but not mitochondrial metabolism induce cytosolic Ca^{2+} overload in human PDAC cells

We next tested the effects of glycolytic and mitochondrial inhibitors on resting $[Ca^{2+}]_i$ in the human PDAC cell lines PANC-1 and MIA PaCa-2 using fura-2 fluorescence imaging (See *2.8.1 – Fura-2 fluorescence microscopy and measurement of intracellular $[Ca^{2+}]_i$*). The PANC-1 and MIA PaCa-2 cell lines were selected since these cell lines express oncogenic KRAS mutations at codon 12 (Berrozpe et al., 1994). This mutation is a key hallmark of clinical PDAC (Hruban et al., 1993), and has been shown to both initiate and drive PDAC in transgenic mouse models (Hingorani et al., 2003). Inhibition of glycolytic metabolism was achieved using iodoacetate (IAA, 2 mM), which inhibits glyceraldehyde-3-phosphate dehydrogenase (Schmidt and Dringen, 2009), or BrPy (500 µM). Conversely, inhibition of mitochondrial ATP production was achieved using either oligomycin (OM, 10 µM), an inhibitor of the mitochondrial F_1/F_0-ATP synthase (Shchepina et al., 2002), or CCCP (4 µM). Cells were perfused with HEPES-PSS, and metabolic inhibitors applied for 30 minutes. At 30 minutes cells were treated with 100 µM ATP to activate purinergic receptors, thereby testing for reversibility of responses and thus viability. For a detailed description of how resting $[Ca^{2+}]_i$ was calculated, please see *2.8.2 – Calibration of resting $[Ca^{2+}]_i$* in *2.8 – Chapter 2 Supplementary Methods and Results*. Statistical comparisons were carried out using a one-way ANOVA with post hoc Dunnetts' test for multiple comparisons or Mann Whitney U test.

Treatment with BrPy (500 µM) for 30 minutes induced an irreversible $[Ca^{2+}]_i$ overload, with an average maximum increase in $[Ca^{2+}]_i$ of 531 ± 32 nM in MIA PaCa-2 cells (n=5) and 425 ± 134 nM in PANC-1 cells (n=5, Figures 2.2B and 2F). Similarly, treatment with 2 mM IAA induced an average maximum increase in $[Ca^{2+}]_i$ of 261 ± 29 nM in MIA PaCa-2 cells (n=7) and 160 ± 26 nM in PANC-1 cells (n=6, Figures 2.2D and 2F). These responses were significant compared to corresponding time-matched control cells for both MIA PaCa-2 (26 ± 12 nM, n=5, $p<0.0001$ for both BrPy and IAA) and PANC-1 cells (BrPy alone, 3 ± 2 nM, n=4, $p<0.01$).

Similarly, BrPy (500 µM) increased area under the curve (AUC) to 485 ± 104 µM.s in MIA PaCa-2 cells and 399 ± 86 µM.s in PANC-1 cells, while IAA (2 mM) elevated AUC to 421 ± 44 µM.s in MIA PaCa-2 cells and 213 ± 28 µM.s in PANC-1 cells (Figure 2.2E). These responses were significantly elevated compared to control MIA PaCa-2 (71 ± 9 µM.s. BrPy, $p<0.001$; IAA, $p<0.0001$) and PANC-1 cells (BrPy alone, 52 ± 14 µM.s, $p<0.001$). AUC represents a measure of not only the magnitude of $[Ca^{2+}]_i$ increase but also recovery of response.

In contrast, OM (10 µM, Figure 2.2A) and CCCP (4 µM, Figure 2.2C) had no effect on the maximum increase in $[Ca^{2+}]_i$ observed in either MIA PaCa-2 cells (Figure 2.2F, n=7 and n=5, respectively) or PANC-1 cells (Figure 2.2F, n=4 and n=4, respectively). Interestingly, CCCP elicited a small but significant increase in AUC to 128 ± 16 µM.s (n=5) in MIA PaCa-2 cells (n=5, $p<0.05$), but not in PANC-1 cells (n=4, Figure 2.2E). Despite this, OM had no effect on AUC in either MIA PaCa-2 or PANC-1 cells (n= 7 and n-4, respectively, Figure 2.2E).

In addition to their effects on $[Ca^{2+}]_i$, BrPy (500 µM) and IAA (2 mM) abolished the ability of both cell lines to elicit Ca^{2+} responses to 100 µM ATP (Figures 2.2B, 2.2D and 2.2G). In healthy cells, ATP evoked robust spike-like increases in $[Ca^{2+}]_i$, indicating that these cells were viable. In contrast to the glycolytic inhibitors, ATP-evoked Ca^{2+} responses were observed in the majority of cells treated with the mitochondrial inhibitors OM (10 µM, Figure 2.2A) or CCCP (4 µM, Figure 2.2C). Together these results suggest that glycolysis, but not mitochondrial metabolism, is critically important for maintaining a low resting $[Ca^{2+}]_i$ in human PDAC cells.

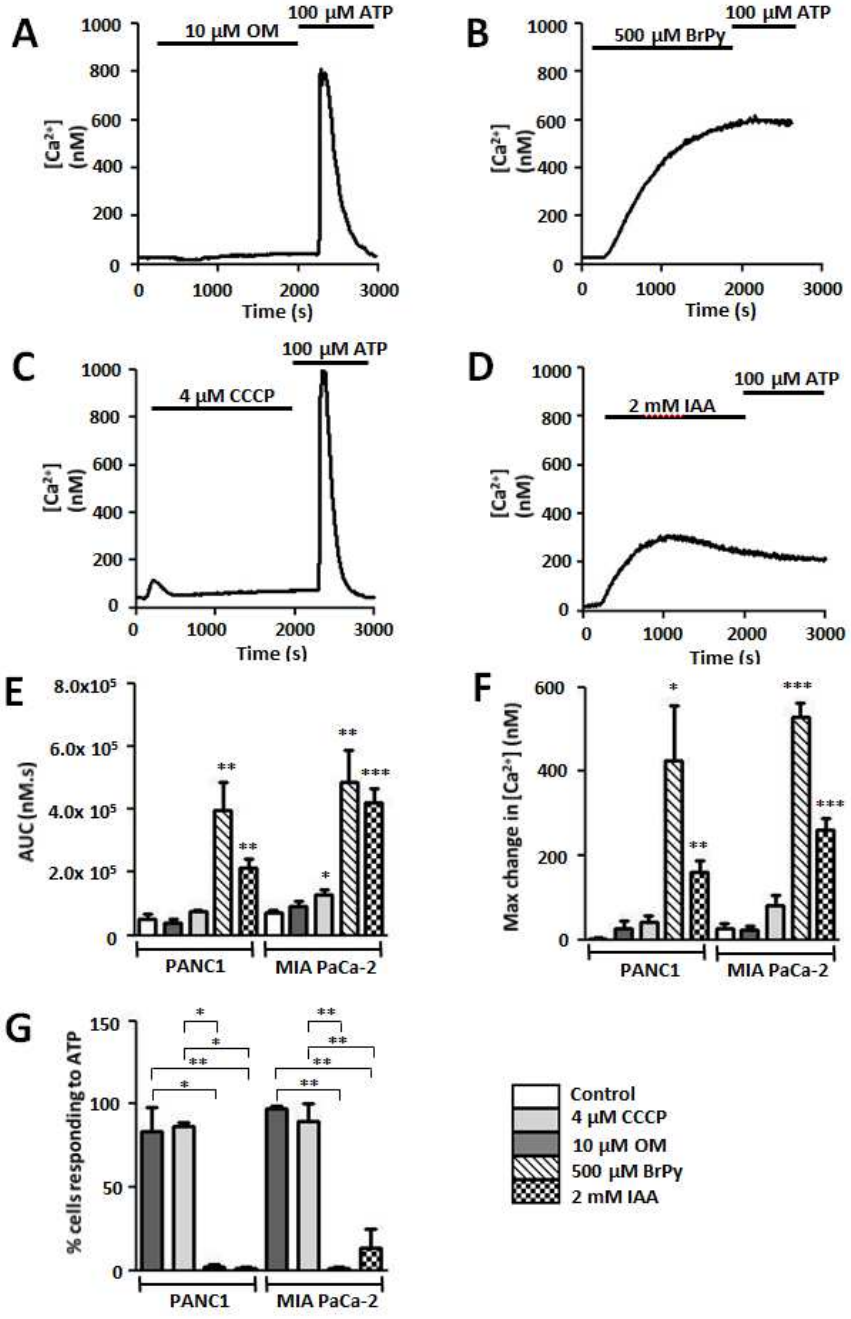

Figure 2.2 - Glycolytic inhibitors but not mitochondrial inhibitors induce an irreversible cytosolic $[Ca^{2+}]_i$ overload in pancreatic cancer cells.

Using fura-2 fluorescence imaging, cytosolic Ca^{2+} concentration ($[Ca^{2+}]_i$) was measured in PANC-1 or Mia PaCa-2 cells**. *A-D*,** representative traces showing the effect of various metabolic inhibitors on $[Ca^{2+}]_i$ in PANC-1 cells. Cells were treated for 30 minutes with either mitochondrial inhibitors (10 µM oligomycin, ***A***; 4 µM CCCP, ***C***) or glycolytic inhibitors (500 µM bromopyruvate (BrPy), ***B***; 2 mM iodoacetate (IAA), ***D***) followed by stimulation with the purinergic agonist, ATP (100 µM) to test for cell viability. Similar qualitative results were obtained for MIA PaCa-2 cells. Responses were quantified by measuring the area under the curve (AUC, ***E***) for the 30 minute treatment with drug, maximum change in $[Ca^{2+}]_i$ (***F***). Recovery from metabolic inhibitor was assessed by measuring the % cells that subsequently responded to ATP (***G***). n=4-7 for all conditions. *, $p<0.05$; **, $p<0.01$; ***, $p<0.001$ (***E*** and ***F***, one-way ANOVA with post hoc Dunnetts' test for multiple comparisons; ***G***, Mann-Whitney U), compared with control.

2.4.3 - Validation that in situ $[Ca^{2+}]_i$ clearance assay represents PMCA activity in PDAC

We have previously developed an *in situ* $[Ca^{2+}]_i$ clearance assay in pancreatic acinar cells in which PMCA activity is pharmacologically and functionally isolated (Baggaley et al., 2008, Mankad et al., 2012). Briefly, sarcoplasmic/endoplasmic reticulum Ca^{2+} ATPase (SERCA) activity was blocked by continuous application of cyclopiazonic acid (CPA) in the absence of extracellular Ca^{2+} and the presence of 1 mM EGTA, leading to ER Ca^{2+} store depletion. Rapid store-operated Ca^{2+} entry was then induced upon perfusion with 20 mM Ca^{2+}. The subsequent removal of extracellular Ca^{2+} resulted in clearance of $[Ca^{2+}]_i$, presumably via the PMCA. This influx-clearance phase was repeated and test reagents or manoeuvres were applied during the second influx-clearance phase. Thus, the resulting paired experimental design controlled for cell-to-cell and temporal variability.

$[Ca^{2+}]_i$ clearance can be quantified either by fitting the falling phase to a single exponential decay or by measuring the initial linear clearance rate from a standardised $[Ca^{2+}]_i$ value. However, fitting to an exponential decay is only valid if the $[Ca^{2+}]_i$ clears to approximately the same baseline $[Ca^{2+}]_i$ (asymptote) and is not accurate if clearance approaches a slow linear phase. This was almost always the case when clearance was severely inhibited. We therefore normalised the linear clearance rate over 60 seconds during the second clearance phase to that of the first, both measured from the same $[Ca^{2+}]_i$ value (%). A detailed description of this assay protocol and analysis method can be found in *2.8.3 – Measurement of $[Ca^{2+}]_i$ clearance rate* in *2.8 – Chapter 2 Supplementary Methods and Results*. Prior to assessing the effects of metabolic inhibitors on $[Ca^{2+}]_i$ clearance during our *in situ* $[Ca^{2+}]_i$ clearance assay, control experiments revealed that clearance rate was maintained between sequential influx-clearance phases in untreated PANC-1 (100 ± 3%, n=18, Figure 2.3A and 3G) and MIA PaCa-2 cells (98 ± 5%, n=17, Figure 2.3B and 2.3H).

Whilst the Na^+/Ca^{2+} exchange (NCX) is not thought to contribute to $[Ca^{2+}]_i$ clearance in pancreatic acinar cells (Muallem et al., 1988, Tepikin et al., 1992, Wolff et al., 1993), evidence suggests it may play a role in rat pancreatic ductal cells (Ankorina-Stark et al., 2002, Hug et al., 1996). Furthermore, NCX is reported to be expressed in human PDAC cells (Dong et al., 2010, Hansen et al., 2009, Hug et al., 1996). To determine whether NCX contributed to Ca^{2+} clearance in PANC-1 and MIA PaCa-2 cells under the conditions of our *in situ* $[Ca^{2+}]_i$ clearance assay, we replaced extracellular Na^+ with equimolar N-methyl D-glucamine (Na^+ free/NMDG). NMDG is not transported by NCX yet maintains the osmotic balance, thereby removing the Na^+ gradient required for NCX-mediated Ca^{2+} efflux.

Na^+ free/NMDG had no effect on $[Ca^{2+}]_i$ clearance in PANC-1 (Figure 2.3C and 2.3G, n=7) or MIA PaCa-2 cells (Figure 2.3D and 2.3H, n=4) compared to control cells (PANC-1, Figure 2.3A, n=18; MIA PaCa-2, Figure 2.3B, n=17). These data indicate that NCX does not contribute to $[Ca^{2+}]_i$ clearance in these cell lines under the current experimental conditions.

Furthermore, to test whether the PMCA is responsible for $[Ca^{2+}]_i$ clearance in PANC-1 and MIA PaCa-2 cells during the *in situ* $[Ca^{2+}]_i$ clearance assay, 1 mM La^{3+} was applied during the

second clearance phase. La^{3+} inhibits Ca^{2+} efflux (PMCA) at millimolar concentrations (Baggaley et al., 2007). However, since La^{3+} also inhibits store-operated Ca^{2+} entry (SOCE) at micromolar concentrations (Bouron, 2000), La^{3+} was applied at the peak of the Ca^{2+} influx, first for 1 minute in the presence of 20 mM Ca^{2+} before removal of external Ca^{2+} under the continued application of La^{3+}. These experiments were performed using HEPES-PSS devoid of EGTA as this also chelates La^{3+} (Wakasugi et al., 1981). 1 mM La^{3+} dramatically inhibited linear clearance rate to 10 ± 3% in PANC-1 cells (Figures 2.3E and 2.3G, n=5) and 18 ± 5% in MIA PaCa-2 cells (Figure 2.3F and 2.3H, n=7), compared to 100±3% (n=18) and 98 ± 5% (n=17) in corresponding time-matched control cells, respectively (PANC-1, Figures 2.3A and 2.3G; MIA PaCa-2, Figures 2.3B and 2.3H; P<0.001, Mann-Whitney U).

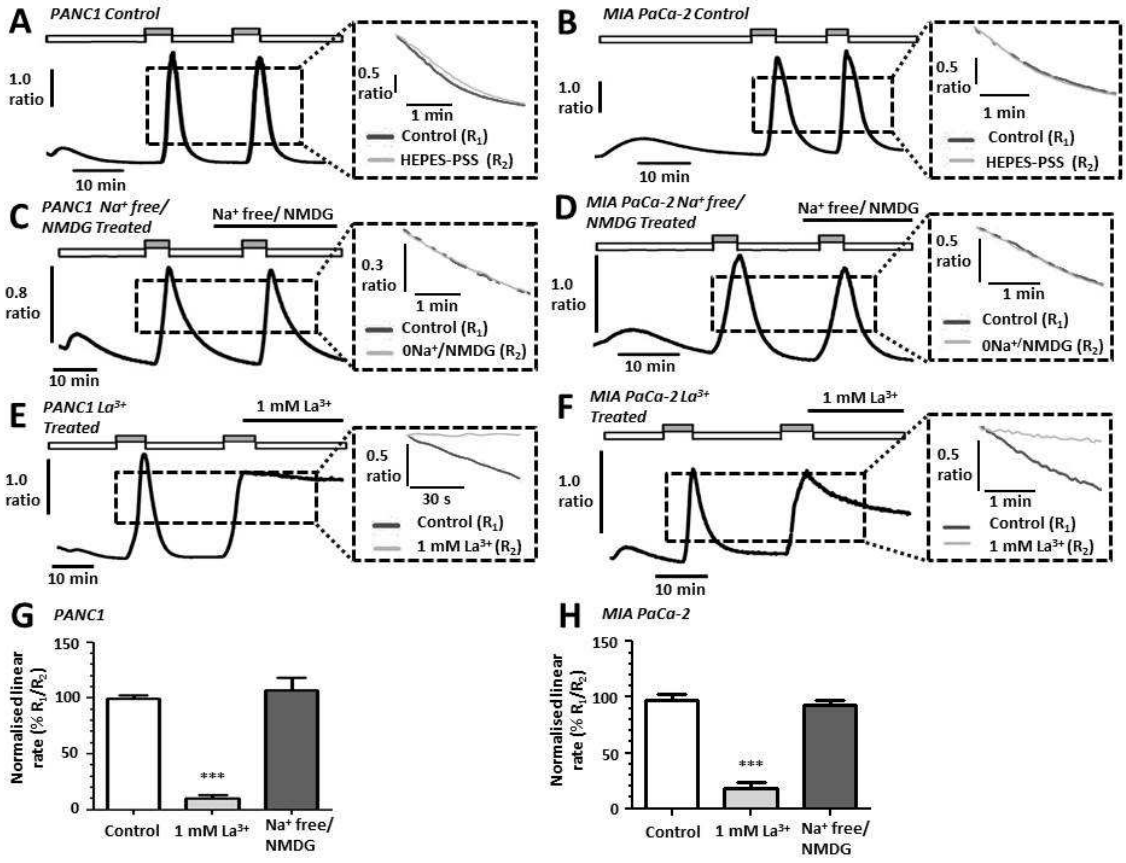

Figure 2.3 - PMCA is the main mechanism of $[Ca^{2+}]_i$ clearance in human PDAC cell lines.

A-F, Representative traces showing the *in situ* $[Ca^{2+}]_i$ clearance assay (PMCA activity) for control PANC-1 (***A***) and MIA PaCa-2 (***B***) cells, Na^+ free/NMDG treated PANC-1 (***C***) and MIA PaCa-2 (***D***) cells, and La^{3+} treated PANC-1 (***E***) and MIA PaCa-2 (***F***) cells. Cells were treated with 30 µM cyclopiazonic acid (CPA) in the absence of external Ca^{2+} with 1mM EGTA (*white box*) or 20mM Ca^{2+} (*grey box*) to induce store-operated Ca^{2+} influx. Subsequent removal of external Ca^{2+} allowed $[Ca^{2+}]_i$ clearance. This influx-clearance phase was repeated under conditions where extracellular Na^+ was replaced with equimolar N-methyl D-glucamine (Na^+ free/NMDG) or in the presence of 1mM La^{3+}. La^{3+} was prepared in HEPES-PSS devoid of EGTA chelating of the La^{3+}. The inset of each trace shows expanded time courses comparing the second (grey trace) with the first clearance phase (black trace) in the presence of each treatment. The linear clearance rate over 60 seconds (in the presence of each treatment) was normalized to the initial clearance rate in each cell (% relative clearance). Mean percentage relative clearance (± S.E.M) is presented for PANC-1 (***G***) and MIA PaCa-2 (***H***) cells. n=4-18 for all conditions. *, p<0.05; **, p<0.01; ***, p<0.001 (Mann-Whitney U), compared with time-matched control experiments (*white bar).*

Collectively these data confirm that the PMCA is the major Ca^{2+} clearance pathway and that NCX plays no role in $[Ca^{2+}]_i$ clearance in these cells under these conditions. Any inhibition of $[Ca^{2+}]_i$ clearance observed using this experimental design can therefore be interpreted as an effect on PMCA activity, consistent with our previous studies (Baggaley et al., 2008, Mankad et al., 2012).

2.4.4 - Inhibitors of glycolytic but not mitochondrial metabolism inhibit PMCA activity in human PDAC cells

After establishing that inhibition of glycolysis results in $[Ca^{2+}]_i$ overload, we aimed to determine whether this was due at least in part to inhibition of the PMCA. To test this, we applied the glycolytic inhibitors (IAA, 2 mM, and BrPy, 500 µM) or mitochondrial inhibitors (OM, 10 µM and CCCP, 4 µM) during the second Ca^{2+} clearance phase of our *in situ* $[Ca^{2+}]_i$ clearance assay. In PANC-1 cells, both IAA and BrPy markedly decreased PMCA activity to 57 ± 4% (Figures 2.4B and 2.4F, n=5) and 63 ± 5% (Figures 2.4D and 2.4F, n=8), respectively, compared to time matched control cells (103 ± 4%, Figures 2.4A and 2.4F, n=11, $p<0.005$, Mann-Whitney U). In contrast, the mitochondrial inhibitors CCCP and OM had no effect (CCCP, n=8, Figures 2.4E and 2.4F; OM, n=5, Figures 2.4C and 2.4F).

Similarly, in MIA PaCa-2 cells, IAA (2 mM) and BrPy (500 µM) also inhibited PMCA activity. We first attempted to repeat the $[Ca^{2+}]_i$ clearance experiments in MIA PaCa-2 cells using an identical protocol to that used for PANC-1 cells. BrPy (500 µM, Figure 2.5D) and IAA (2 mM, Figure 2.5B) both significantly decreased PMCA activity to 10 ± 10% (n=4, 2.5F) and 23 ± 10% (n=5, Figure 2.5F), respectively, compared to corresponding time-matched control cells (92 ± 3%, Figure 2.5A and 2.5F, n=6, $p<0.001$ for both BrPy and IAA, Mann-Whitney U)**.** Interestingly, CCCP decreased PMCA activity to 58 ± 6% (Figures 2.5E and 2.5F, $p<0.01$, Mann-Whitney U); OM on the other hand had no effect (Figures 2.5C and 2.5F, n=3). However, application of IAA and BrPy prior to Ca^{2+} influx resulted in inhibition of Ca^{2+} entry and dramatically reduced the plateau from which $[Ca^{2+}]_i$ clearance was initiated and subsequently measured (Figures 2.5B and 2.5D). As a result, $[Ca^{2+}]_i$ clearance could only be measured over a very narrow range of Ca^{2+} concentrations. Furthermore, the slowed Ca^{2+} influx meant it took longer to achieve a sufficient increase in $[Ca^{2+}]_i$ from which to measure $[Ca^{2+}]_i$ clearance rate. Using the current protocol where metabolic inhibitors were applied prior to Ca^{2+} influx, this resulted in prolonged exposure (>15 minutes) to the glycolytic inhibitors prior to initiation of $[Ca^{2+}]_i$ clearance. These confounding factors cast doubt on the validity of the $[Ca^{2+}]_i$ clearance data obtained from MIA PaCa-2 cells with the current experimental design.

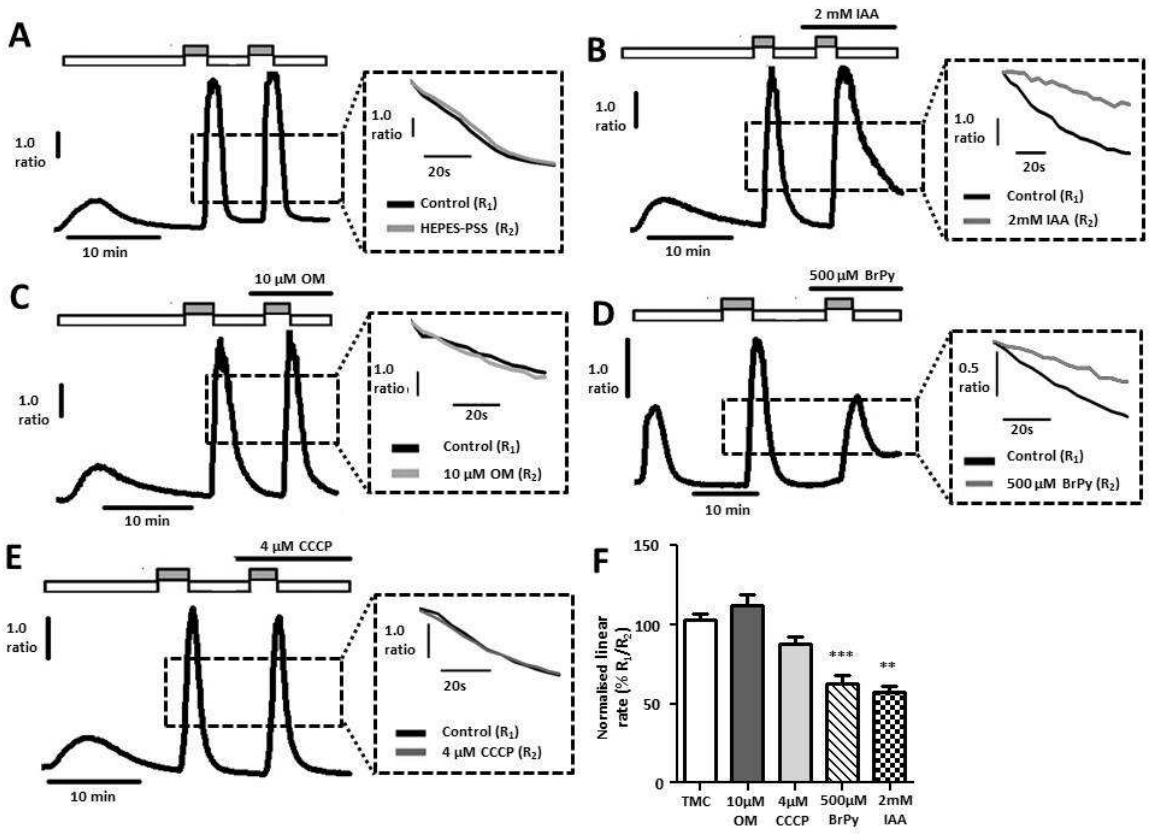

Figure 2.4 - Glycolytic inhibitors, but not mitochondrial inhibitors, inhibit PMCA activity in PANC-1 cells.

A–E, representative traces showing the *in situ* $[Ca^{2+}]_i$ clearance assay (PMCA activity) in fura-2-loaded PANC-1 cells. Cyclopiazonic acid (CPA, 30 µM) was applied in the absence of external Ca^{2+} with 1mM EGTA (*white box*) or 20mM Ca^{2+} (*grey box*) to induce store-operated Ca^{2+} influx. Subsequent removal of external Ca^{2+} allowed $[Ca^{2+}]_i$ clearance. This influx-clearance phase was repeated using a paired experimental design and metabolic inhibitors were applied during this second influx-clearance phase. Each inset trace shows expanded time courses comparing the second (grey trace) with the first clearance phase (black trace) in the presence of each metabolic inhibitor. ***A,*** time-matched control (TMC); ***B***, 2 mM iodoacetate (IAA); ***C***, 10 µM oligomycin (OM); ***D***, 500 µM bromopyruvate (BrPy,); ***E***, 4 µM CCCP. Linear clearance rate over 60 seconds during the second clearance phase was normalized to that of the first (% relative clearance). ***F***, mean percentage relative clearance (± S.E.M). n=5-11 for all conditions. *, $p<0.05$; **, $p<0.01$; ***, $p<0.001$ (Mann-Whitney U), compared with TMC.

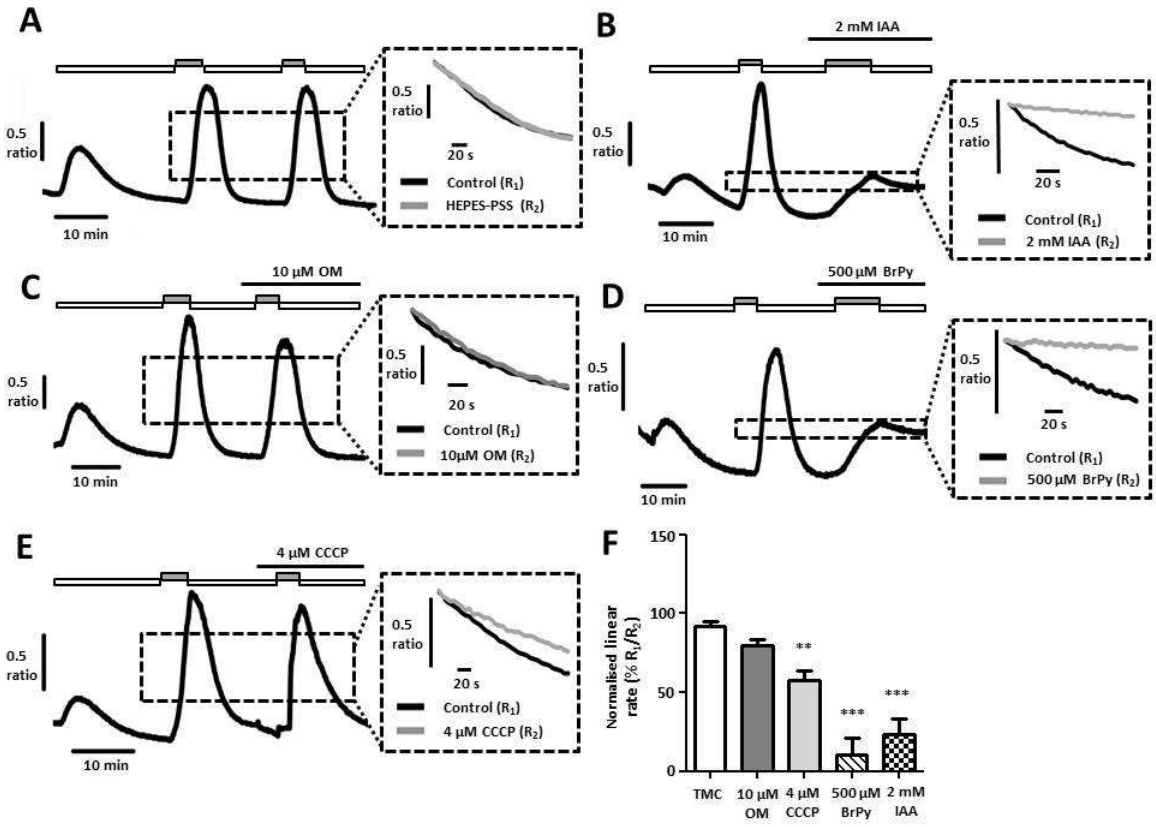

Figure 2.5 - Glycolytic inhibitors, but not mitochondrial inhibitors, inhibit PMCA activity and store-operated Ca^{2+} entry in MIA PaCa-2 cells.

A–E, representative traces showing the *in situ* $[Ca^{2+}]_i$ clearance assay (PMCA activity) in fura-2-loaded MIA PaCa-2 cells. Cyclopiazonic acid (CPA, 30 µM) was applied in the absence of external Ca^{2+} with 1 mM EGTA (*white box*) or 20mM Ca^{2+} (*grey box*) to induce store-operated Ca^{2+} influx. Subsequent removal of external Ca^{2+} allowed $[Ca^{2+}]_i$ clearance. This influx-clearance phase was repeated using a paired experimental design and metabolic inhibitors were. applied during this second influx-clearance phase. The inset of each trace shows expanded time courses comparing the second (grey trace) with the first clearance phase (black trace) in the presence of each metabolic inhibitors. ***A,*** time-matched control (TMC); ***B***, 2 mM iodoacetate (IAA); ***C***, 10 µM oligomycin (OM); ***D***, 500 µM 3-bromopyruvate (BrPy); ***E***, 4 µM CCCP. Linear clearance rate over 60 seconds during the second clearance phase was normalized to that of the first (% relative clearance). ***F***, mean percentage relative clearance (± S.E.M). n=3-5 for all conditions. *, p<0.05; **, p<0.01; ***, p<0.001 (Mann-Whitney U), compared with TMC.

We therefore modified our $[Ca^{2+}]_i$ clearance protocol to isolate the effects of the drugs on PMCA activity and to control for the duration of drug exposure prior to initiating $[Ca^{2+}]_i$ clearance. To achieve this, 1 mM La^{3+} was applied in the absence of Ca^{2+} and EGTA at the peak of $[Ca^{2+}]_i$ influx. This inhibited Ca^{2+} influx and efflux, and thereby effectively clamped $[Ca^{2+}]_i$ within the cell. Test reagents were applied simultaneously with La^{3+} at the peak of $[Ca^{2+}]_i$ influx, rather than prior to $[Ca^{2+}]_i$ influx. Following 5 minutes treatment with a metabolic inhibitor, La^{3+} was rapidly removed using 1 mM EGTA, which has a high affinity for La^{3+} (Putney, 2006). The addition of EGTA and removal of La^{3+} allows initiation of $[Ca^{2+}]_i$ clearance, and thus clearance can be assessed as before, without the confounding factors of a reduced Ca^{2+} influx rate and a prolonged drug exposure time influencing $[Ca^{2+}]_i$ clearance.

Similar to previous experiments, $[Ca^{2+}]_i$ clearance rate during the second clearance phase of this amended protocol was reasonably well maintained at 91 ± 5% in control MIA PaCa-2 cells (Figures 2.6A and 2.6F, n=9). Similar to PANC-1 cells, BrPy (500 µM, Figure 2.6D) and IAA (2 mM, Figure 2.6B) both significantly decreased PMCA activity to 25 ± 8% (Figure 2.6F, n=6) and 40 ± 6% (Figure 2.6F, n=6), respectively, compared to corresponding time-matched control cells ($p<0.001$ for both BrPy and IAA, Mann-Whitney U)**.** In contrast, 10 µM OM had no effect on $[Ca^{2+}]_i$ clearance (n=5, Figures 2.6C and 2.6F). Interestingly, however, CCCP caused a significant decrease in $[Ca^{2+}]_i$ clearance (60 ± 7%, $p<0.001$, n=8, Mann-Whitney U, Figures 2.6E and 2.6F).

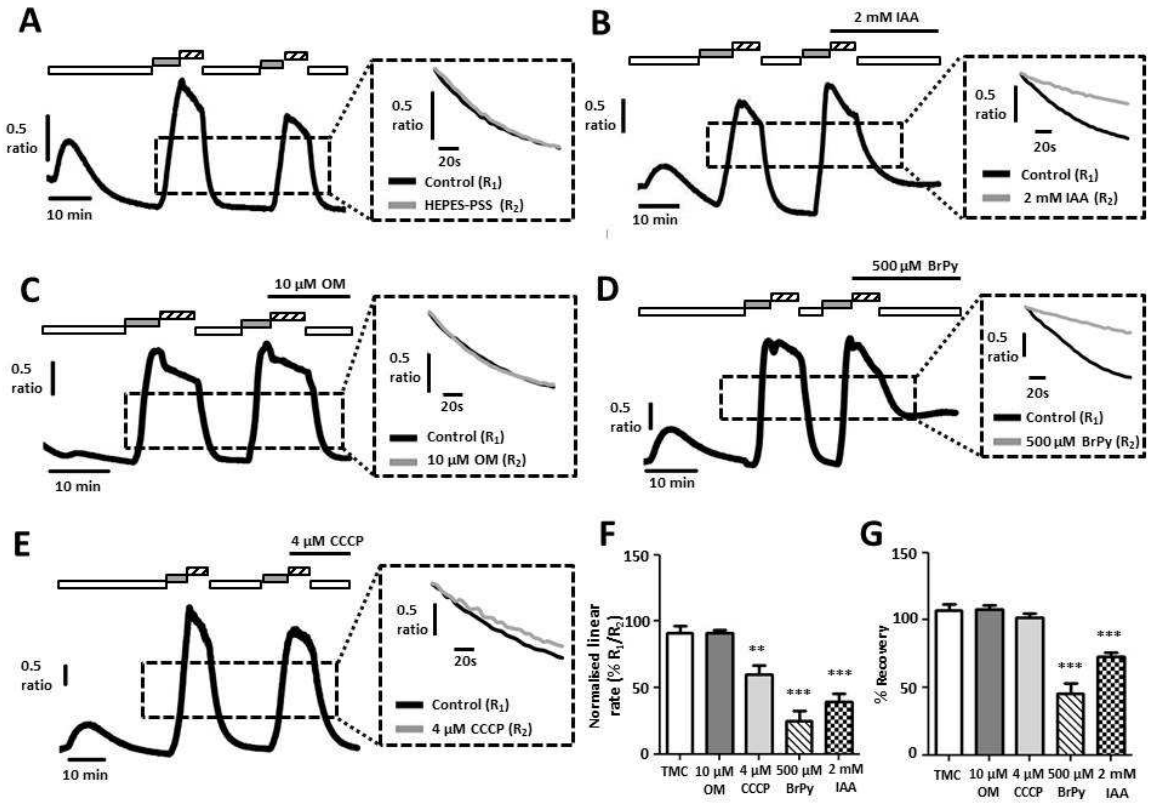

Figure 2.6 - Glycolytic inhibitors, but not mitochondrial inhibitors, inhibit PMCA activity in MIA PaCa-2 cells.

A–E, representative traces showing a modified protocol *in situ* $[Ca^{2+}]_i$ clearance assay (PMCA activity) in fura-2-loaded MIA PaCa-2 cells. Ca^{2+} influx was induced prior to application of test reagents to isolate their effects on clearance. 30 µM cyclopiazonic acid (CPA) was applied in the absence of external Ca^{2+} with 1mM EGTA (*white box*), or 20mM Ca^{2+} (*grey box*) to induce store-operated Ca^{2+} influx. 1mM La^{3+} was then applied at the peak of Ca^{2+} influx (*striped box*). Subsequent removal of external La^{3+} and readdition of 1mM EGTA after 5 minutes allowed $[Ca^{2+}]_i$ clearance. This influx-clearance phase was repeated and metabolic inhibitors applied during this second influx-clearance phase. Each inset trace shows expanded time courses comparing the second clearance phase (grey trace) with the first (black trace) in the presence of each metabolic inhibitor. ***A,*** time-matched control (TMC); ***B***, 2 mM iodoacetate (IAA); ***C***, 10 µM oligomycin (OM); ***D***, 500 µM bromopyruvate (BrPy); ***E***, 4 µM CCCP. Linear clearance rate over 60 seconds during the second clearance phase was normalized to that of the first (% relative clearance). To determine recovery, the baseline Ca^{2+} value prior to influx was subtracted from that upon removal of La^{3+}, and recovery normalised to this value. ***F***, mean percentage relative clearance (± S.E.M). G, mean percentage relative recovery (± S.E.M). n=5-9 for all conditions. *, $p<0.05$; **, $p<0.01$; ***, $p<0.001$ (Mann-Whitney U), compared with TMC.

We therefore also assessed the degree of recovery to baseline $[Ca^{2+}]_i$ following each treatment. To measure recovery, the difference was calculated between the fura-2 ratio upon removal of La^{3+} during the second influx-clearance phase and minimum value the steady state plateau subsequently reached. This was then normalised to the difference between the fura-2 ratio upon removal of La^{3+} during the second influx-clearance phase and the lowest fura-2 ratio value observed prior to the first influx-clearance phase (see *2.8.2 – Measurement of % recovery of $[Ca^{2+}]_i$ to baseline* in *2.8 – Chapter 2 Supplementary Methods and Results*). BrPy (500 µM, Figure 2.6D) and IAA (2 mM, Figure 2.6B) both significantly inhibited recovery to 45 ± 8% (n=6, Figure 2.6G) and 73 ± 3% (n=6, Figure 2.6G), respectively, compared to 107 ± 4% for corresponding time-matched control cells (107 ± 4%, Figures 2.6A and 2.6G, n=9, $p<0.001$, Mann Whitney U). In contrast, following treatment with the mitochondrial inhibitors, cells were able to fully recover $[Ca^{2+}]_i$ to baseline values; neither OM (10 µM, Figures 2.6C and 2.6G, 108 ± 3%, n=5) nor CCCP (4 µM, Figures 2.6E and 2.6G, 102 ± 4%, n=7) had any effect on recovery compared to corresponding control cells.

Taken together, these data suggest that glycolysis, but not mitochondrial metabolism, is critically important for both maintaining PMCA $[Ca^{2+}]_i$ clearance rate and for ensuring full recovery to a low resting $[Ca^{2+}]_i$.

2.4.5 - Inhibition of glycolysis, but not mitochondrial metabolism, induces ATP depletion in PDAC cells

To assess the effects of glycolytic and mitochondrial inhibitors on ATP depletion, cells were treated with varying concentrations of BrPy. CCCP, IAA or OM for 15 minutes prior to addition of ViaLight® Plus ATP kit assay reagents (see *2.3.5 – ATP Measurements* in *2.3 - Experimental Procedures*). These concentrations were chosen as they were below, equal to and higher than those used in the $[Ca^{2+}]_i$ clearance experiments. Moreover, 15 minutes incubation was chosen because it was sufficient to induce $[Ca^{2+}]_i$ overload and inhibition of the PMCA during our *in situ* $[Ca^{2+}]_i$ clearance assays. Cells were also treated with a combination of all four metabolic inhibitors to induce maximum ATP depletion (ATP depletion cocktail: BrPy, 500 µM; CCCP, 4 µM; IAA, 2 mM; OM, 10 µM). Raw luminescence counts obtained from those cells treated with the ATP depletion cocktail were subtracted from each individual treatment, prior to normalisation to the luminescence counts of untreated control cells (%). On average, the raw luminescence count in control cells was 37994 ± 5976 in PANC-1 (n=7) and 56974 ± 10865 in MIA PaCa-2 cells (n=8), and in those treated with the ATP depletion cocktail was 2923 ± 519 in PANC-1 and 4036 ± 1032 in MIA PaCa-2 cells. Thus, the ATP depletion cocktail reduced global ATP to 8 ± 1% in PANC-1 cells and 9 ± 3% in MIA PaCa-2 cells over 15 minutes. All statistical comparisons were made using a one-sample t-test against the hypothetical control value of 100%.

The glycolytic inhibitors BrPy and IAA caused a profound decrease in ATP in both MIA PaCa-2 and PANC-1 cells. IAA caused a significant decrease in ATP at all three concentrations in both

MIA PaCa-2 (0.7 mM, 25 ± 5%; 2 mM, 17 ± 3%; 7 mM, 20 ± 3%, P<0.001, n=8, Figure 2.7A) and PANC-1 cells (0.7 mM, 24 ± 3%; 2 mM, 23 ± 3%; 7 mM, 23 ± 3%, P<0.001, n=7, Figure 2.7B). Likewise, the intermediate and high concentrations of BrPy caused a significant decrease in ATP in both MIA PaCa-2 (500 µM, 21 ± 13%; 1mM, 6 ± 5%, P<0.001, n=8, Figure 2.7A) and PANC-1 cells (500 µM, 55 ± 10%; 1 mM, 19 ± 5%, P<0.001, n=7, Figure 2.7B). Conversely, OM and CCCP had only a modest effect at concentrations higher than those used in our $[Ca^{2+}]_i$ clearance experiments; 10 µM CCCP caused a significant decrease in ATP in both MIA PaCa-2 (89 ± 3%, n=8, P<0.01, Figure 2.7A) and PANC-1 cells (73 ± 8%, n=8, P<0.05, Figure 2.7B), while 30 µM OM only caused a significant decrease in ATP in PANC-1 cells (82 ± 5%, n=8, P<0.01, Figure 2.7B).

These data suggest that glycolysis is the major mechanism of ATP synthesis in PANC-1 and MIA PaCa-2 cells under these conditions, and that inhibition of glycolysis is an effective means of inducing ATP depletion. On the other hand, it appears that mitochondrial metabolism contributes far less to ATP production. Thus, the $[Ca^{2+}]_i$ overload and PMCA inhibition observed following treatment with mechanistically distinct glycolytic inhibitors is most likely due to ATP depletion, as all these phenomena occur over a similar time course.

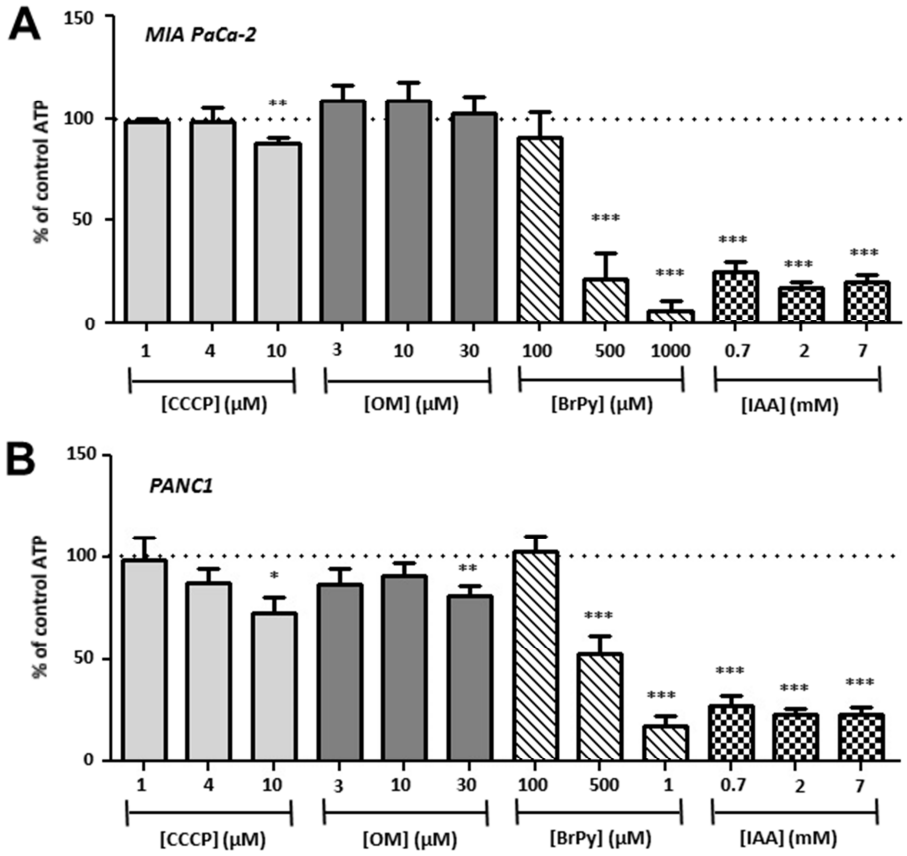

Figure 2.7 - Inhibition of glycolysis, but not mitochondrial metabolism, induces ATP depletion in PDAC cells.

PANC-1 (***A***) and MIA PaCa-2 cells (***B***) were treated with either mitochondrial inhibitors (CCCP, 1 - 10 µM; oligomycin, 3 - 30 µM) or glycolytic inhibitors (BrPy, 100 - 1000 µM; iodoacetate (IAA), 0.7 - 7 mM) for 15 minutes. ATP depletion was determined using a luciferase-based luminescence assay. To determine ATP depletion (%), luminescence counts were normalized for each condition to untreated time-matched cells (total ATP). n=7-8 for all experiments. *, $p<0.05$; **, $p<0.01$; ***, $p<0.001$ (one-sample t-test), compared to theoretical mean of 100%.

2.5 - Discussion

The present study is the first to show that in human PDAC cell lines (PANC-1 and MIA PaCa-2) both $[Ca^{2+}]_i$ clearance and the maintenance of a low resting $[Ca^{2+}]_i$ are critically dependent on glycolytic rather than mitochondrial metabolism. Inhibition of glycolysis inhibited PMCA activity and induced both substantial ATP depletion and an irreversible increase in cytosolic $[Ca^{2+}]$ ("$[Ca^{2+}]_i$ overload") within minutes, and ultimately caused cell death within 3 to 6 hours. Inhibition of mitochondrial metabolism, on the other hand, had almost no effect on resting $[Ca^{2+}]_i$, PMCA activity, ATP depletion or cell death. This is at variance with studies in non-cancerous pancreatic duct cells and the related pancreatic acinar cells, in which separate inhibition of either glycolysis or mitochondrial metabolism induced ATP depletion (Voronina et al., 2010, Maleth et al., 2011) and inhibited PMCA activity (Mankad et al., 2012). The present study also shows that the PMCA is the major Ca^{2+} efflux pathway in PANC-1 and MIA PaCa-2 cells. Taken together, these data suggest that inhibition of glycolysis compromises PMCA activity as a result of ATP depletion, resulting in an irreversible $[Ca^{2+}]_i$ overload and cell death. These findings are of potential therapeutic importance, since an increased dependence of the PMCA on glycolytically-derived ATP may be a unique feature in tumour cells. PMCA activity is critical for the maintenance of a low resting $[Ca^{2+}]_i$ (Bruce, 2010, Carafoli, 1987), and even if other $[Ca^{2+}]_i$ clearance pathways such as SERCA are inhibited (for example, following treatment with CPA), $[Ca^{2+}]_i$ will recover so long as the PMCA remains active. On the other hand, an inability to extrude $[Ca^{2+}]_i$ via the PMCA would render $[Ca^{2+}]_i$ overload an inevitability, since the ER capacity is finite. This leaves the PMCA as the 'final gatekeeper' for the control of low resting $[Ca^{2+}]_i$ in PDAC. Given that non-cancerous cells have a greater reliance on mitochondrial ATP production, targeting the glycolytic regulation of the PMCA may be an effective strategy to selectively kill PDAC cells whilst leaving non-cancerous cells unharmed. Furthermore, this may be relevant to other similar cancers where the PMCA is the major Ca^{2+} efflux pathway.

It has previously been described that PDAC cells exhibit the highly glycolytic phenotype characteristic of the 'Warburg effect' (Chaika et al., 2012, Zhou et al., 2011). Indeed, in the present study, the glycolytic inhibitors IAA and BrPy both induced profound ATP depletion within 15 minutes, while the mitochondrial inhibitors OM and CCCP had no effect. In line with the present study, previous studies have shown that BrPy causes ATP depletion in cancer cells (Ko et al., 2004). Although BrPy is reported to induce mitochondrial depolarisation and thus impair mitochondrial function (Ihrlund et al., 2008), this is unlikely to be the major mechanism by which BrPy induces ATP depletion in the present study, since CCCP also depolarises $\Delta\Psi m$ (Criddle et al., 2007) and had minimal effect on ATP depletion. This indicates that the mitochondrial ATP production capacity is of minor importance in these cells for maintaining ATP, and suggests that BrPy depletes ATP by inhibiting glycolysis rather than impairing mitochondrial function. Furthermore, the mechanistically distinct glycolytic inhibitor IAA does not target the mitochondria yet depleted ATP regardless. We can therefore conclude from the degree of ATP depletion achieved by IAA and BrPy that glycolysis is the major source of ATP in both PANC-1 and MIA PaCa-2 cells.

ATP depletion is well known to drive necrosis (Leist et al., 1997), and inhibition of glycolysis with BrPy would therefore be expected to induce cell death in glycolytically-dependent PDAC cells as a result of ATP depletion. Indeed, in the present study, BrPy induced cell death in human PDAC cells, while inhibition of mitochondrial metabolism had no effect. Consistent with this, studies have shown that BrPy depletes ATP and induces cell death in highly glycolytic hepatocellular carcinoma cells without affecting normal hepatocytes (Ko et al., 2004). It has, however, been suggested that BrPy can exert its cytotoxic effects by inducing the release of ROS (Kim et al., 2008) or cell death signalling factors (Chen et al., 2009) from the mitochondria. One counterargument to this, however, is that ROS and cell death factors released from the mitochondria will most likely induce apoptosis rather than necrosis unless there is accompanying ATP depletion (Criddle et al., 2007, Slater et al., 1995). Apoptosis is an ATP dependent process, with ATP depletion being critically implicated in promoting necrotic cell death (Kim et al., 2003, Nicotera et al., 1998), and it has been suggested that exogenously supplemented ATP can protect against necrosis in pancreatic ductal cells following metabolic insult (Hegyi et al., 2011). Moreover, in the present study, significant cell death was observed using propidium iodide, which is impermeant to apoptotic cells with an intact membrane. Similarly, BrPy induced cytotoxicity in hepatoma cells has been shown to be ATP-depletion dependent (Kim et al., 2008). While we cannot rule out these alternative mechanisms, we propose that the cytotoxic effects of BrPy in PDAC are driven primarily by ATP depletion.

In addition to ATP depletion, it is likely that the observed cell death was in part driven by $[Ca^{2+}]_i$ overload. A sustained increase in $[Ca^{2+}]_i$ is catastrophic for cells since it leads to the inappropriate activation of cytosolic enzymes such as proteases, phospholipases and nucleases; it has long been known that a prolonged elevation in $[Ca^{2+}]_i$ has cytotoxic and pathological effects (Baggaley et al., 2008, Bruce and Elliott, 2007, Criddle et al., 2007). In the present study, both PANC-1 and MIA PaCa-2 cells were able to maintain a low resting $[Ca^{2+}]_i$ following treatment with CCCP or OM, whilst treatment with either BrPy or IAA induced $[Ca^{2+}]_i$ overload. Furthermore, $[Ca^{2+}]_i$ overload was irreversible and associated with impaired ATP-induced $[Ca^{2+}]_i$ responses, suggesting that glycolytic ATP is required for Ca^{2+} homeostasis and signalling. It is likely that profound ATP depletion would inhibit Ca^{2+} extrusion via the PMCA, thereby inducing the irreversible $[Ca^{2+}]_i$ overload observed. However, since both ATP depletion and $[Ca^{2+}]_i$ overload occurred over a similar timeframe (minutes), we are presented with a conundrum with respect to the sequence of events, as either could be expected to promote cell death. Furthermore, in addition to PMCA inhibition, ATP depletion would also be expected to inhibit the Na^+/K^+ ATPase. The Na^+/K^+ ATPase consumes a large fraction (>20%) of intracellular ATP to maintain the resting membrane potential of the cell (Milligan and McBride, 1985), and thus its failure following ATP depletion would be expected to lead to cell membrane depolarisation. This would result in the disruption of the maintenance of ion gradients, intracellular pH and cell volume, and decrease the driving force for Ca^{2+} entry. Since these effects could all contribute to the observed cell death, we cannot rule out inhibition of the Na^+/K^+ ATPase as a contributing factor to $[Ca^{2+}]_i$ overload in driving necrosis.

In addition to PMCA inhibition, it is likely that ATP depletion would also inhibit SERCA, leading to net ER Ca^{2+} leak, ER Ca^{2+} store depletion and subsequent activation of SOCE. Thus, the effects of ATP depletion on SERCA and SOCE likely contributed to the rise in $[Ca^{2+}]_i$ observed in our $[Ca^{2+}]_i$ overload assays. However, inhibition of SERCA is unlikely to be the sole mechanism responsible due to the irreversible nature of the $[Ca^{2+}]_i$ overload response. This is because inhibition of SERCA alone using CPA nearly always results in a transient rather than irreversible increase in $[Ca^{2+}]_i$. This strongly implies that $[Ca^{2+}]_i$ efflux via the PMCA is also abolished during the irreversible $[Ca^{2+}]_i$ overload response. Furthermore, although studies have shown that NCX is expressed in several (CFPAC-1, PANC-1 and Capan-1) human PDAC cell lines, (Hansen et al., 2009), the present study shows that NCX has no role during our *in situ* $[Ca^{2+}]_i$ clearance assay and that Ca^{2+} efflux is achieved solely by the PMCA in PANC-1 and MIA PaCa-2 cells. This makes glycolytic regulation of the PMCA all the more relevant to the survival phenotype of these cells, since PMCA inhibition would be expected to induce an irreversible $[Ca^{2+}]_i$ overload.

The present study is also the first to show that glycolytically-derived ATP is critical for PMCA function in PDAC cells and is therefore crucial for the maintenance of a low resting $[Ca^{2+}]_i$ and thus cell survival. Interestingly, although OM had no effect on the rate or degree of $[Ca^{2+}]_i$ clearance, CCCP caused PMCA inhibition in MIA PaCa-2 cells. However, despite this decrease in $[Ca^{2+}]_i$ clearance rate, cells could still recover $[Ca^{2+}]_i$ to baseline. One explanation for this is that CCCP collapses $\Delta\Psi m$, thereby decreasing the driving force for mitochondrial Ca^{2+} uptake (Duchen, 1999), which could appear during our *in situ* $[Ca^{2+}]_i$ clearance assay as a modest reduction in $[Ca^{2+}]_i$ clearance rate. Nevertheless, the PMCA was still capable of recovering a low resting $[Ca^{2+}]_i$, and CCCP had no effect on resting $[Ca^{2+}]_i$, ATP depletion or cell death in our other experiments. In contrast to CCCP, $[Ca^{2+}]_i$ never fully recovered to baseline during our $[Ca^{2+}]_i$ clearance assays on MIA PaCa-2 cells treated with BrPy or IAA.

Evidence suggests that glycolysis can contribute as much as half of the total ATP generated in tumour cells under aerobic conditions (Nakashima et al., 1984), and although the source of ATP to fuel the PMCA is likely unimportant provided the cytosolic [ATP] is maintained above a critical threshold, the glycolytic dependence of PDAC may render the PMCA exquisitely sensitive to inhibition of glycolysis in these cells. It is important to consider that the rate of ATP depletion following inhibition of glycolysis is likely to be much faster during our *in situ* $[Ca^{2+}]_i$ clearance assay compared to our luciferase-based assays, as ATP is also being rapidly consumed due to the PMCA operating at full capacity. Nevertheless, inhibition of glycolysis resulted in an irreversible $[Ca^{2+}]_i$ overload in resting PDAC cells, suggesting that glycolytic inhibition alone causes ATP depletion sufficient to compromise PMCA activity.

This poses the question as to what degree of ATP depletion would be required to inhibit the PMCA. Early studies in red blood cells showed that the PMCA has a high (μM) affinity for ATP (Richards et al., 1978). However, ATP regulation of the PMCA is more complex than previously thought (Echarte et al., 2007), and can be influenced by $[Ca^{2+}]_i$, $[Mg^{2+}]_i$, calmodulin and the phospholipid composition of the plasma membrane. For example, studies in human erythrocyte

membranes have shown that the absence of phosphatidylserine decreases the affinity of the PMCA for ATP (Rossi and Rega, 1989), presumably making the PMCA exquisitely sensitive to ATP depletion. Furthermore, functional studies in intact cells indicate that the PMCA is inhibited by the loss of phosphatidylserine from the inner leaflet of the plasma membrane (Zhang et al., 2009), supporting evidence that phosphatidylserine plays a role in regulating the ATP sensitivity of the PMCA. It is important to note, however, that the majority of studies have used cell-free assays to examine the relationship between ATP and PMCA activity. It is therefore difficult to extrapolate the results of these studies to physiological PMCA activity in live intact cells, since dynamic changes in the lipid composition of the membrane, $[Ca^{2+}]_i$ and protein-protein interactions could profoundly alter these complex mechanisms. As such, the absolute threshold at which ATP depletion inhibits PMCA activity in intact cells is not currently known.

Despite this, evidence (including the current study) suggests that ATP depletion-induced inhibition of the PMCA impairs the maintenance of resting $[Ca^{2+}]_i$. We have previously shown that an acute insulin-induced switch from mitochondrial to glycolytic metabolism in rat pancreatic acinar cells is sufficient to prevent ATP depletion and to protect PMCA activity in the face of oxidant-induced impaired mitochondrial function (Mankad et al., 2012). This has important implications for the current study. Similarly, combined inhibition of both mitochondrial and glycolytic metabolism in mouse pancreatic acinar cells resulted in ATP depletion and corresponded with a decrease in Ca^{2+} extrusion rate (Barrow et al., 2008). $[Ca^{2+}]_i$ overload following inhibition of mitochondrial ATP production has also been shown to be prevented by maintaining cytosolic [ATP] via a patch pipette (Criddle et al., 2006). Collectively these studies suggest that impairment of $[Ca^{2+}]_i$ clearance due to ATP depletion can occur regardless of whether glycolysis or mitochondrial metabolism is perturbed, providing that global ATP depletion is sufficient. Importantly, however, in the present study, inhibition of glycolysis alone was sufficient to induce substantial ATP depletion in PDAC cells, and resulted in both inhibition of the PMCA and a profound effect on resting $[Ca^{2+}]_i$. Unlike previous studies conducted in acutely isolated pancreatic cells, inhibition of mitochondrial metabolism had little or no effect on global ATP or $[Ca^{2+}]_i$ clearance in the present study. Therefore, in addition to supporting the hypothesis that PMCA inhibition following metabolic stress is likely due to ATP depletion, the present study suggests that the PMCA in PDAC cells is sensitive to the depletion of glycolytic rather than mitochondrially-derived ATP.

In light of these findings, it is tempting to speculate that glycolytic regulation of the PMCA may be an important pro-survival mechanism in PDAC tumours. Previous experiments using human erythrocyte membranes suggest that glycolytic enzymes associate with the plasma membrane (Campanella et al., 2005), and that this affects their catalytic activity (Tsai et al., 1982). Importantly, evidence suggests that these enzymes may be colocalised to the PMCA (Campanella et al., 2005, Hardin et al., 1992), thereby potentially providing the PMCA with a privileged glycolytic ATP supply. Moreover, the aberrant metabolic profile and in particular the unique overexpression of key glycolytic enzymes in PDAC (Zhou et al., 2011) may provide an "Achilles' heel" that could be targeted to disrupt $[Ca^{2+}]_i$ homeostasis in PDAC selectively.

Collectively the present study suggests that glycolytic ATP synthesis is critically important for maintaining PMCA activity and a low resting $[Ca^{2+}]_i$ in human PDAC cell lines. Furthermore, these findings are translational and provide insights into a potentially new therapeutic avenue for the treatment of PDAC. While targeting the glycolytic regulation of the PMCA in PDAC alone may be insufficient to eradicate the cancer unless part of a combination chemotherapy regimen, the link between the Warburg effect and $[Ca^{2+}]_i$ homeostasis is an avenue previously unexplored. Moreover, glycolytic regulation of the PMCA might represent a critical pro-survival phenotype in other cancer types, particularly those derived from cells that rely on the PMCA as the major Ca^{2+} efflux pathway. Targeting key glycolytic enzymes that are upregulated or uniquely expressed in highly glycolytic tumours such as PDAC could result in selective PMCA inhibition, thereby inducing $[Ca^{2+}]_i$ overload-induced cell death in the tumour whilst sparing adjacent non-cancerous cells.

2.6 - Acknowledgements

We thank Prof. M. Dunne for use of the BioTek Synergy HT luminescent multi-plate reader.

2.7 - References

AMIN, Z., THEIS, B., RUSSELL, R. C., HOUSE, C., NOVELLI, M. & LEES, W. R. 2006. Diagnosing pancreatic cancer: the role of percutaneous biopsy and CT. *Clin Radiol,* 61**,** 996-1002.

ANKORINA-STARK, I., AMSTRUP, J. & NOVAK, I. 2002. Regulation of the Na^+/Ca^{2+} exchanger in rat pancreatic ducts. *J Membr Biol,* 186**,** 43-53.

BAGGALEY, E., MCLARNON, S., DEMETER, I., VARGA, G. & BRUCE, J. I. 2007. Differential regulation of the apical plasma membrane Ca^{2+}-ATPase by protein kinase A in parotid acinar cells. *J Biol Chem,* 282**,** 37678-93.

BAGGALEY, E. M., ELLIOTT, A. C. & BRUCE, J. I. 2008. Oxidant-induced inhibition of the plasma membrane Ca^{2+}-ATPase in pancreatic acinar cells: role of the mitochondria. *Am J Physiol Cell Physiol,* 295**,** C1247-60.

BARROW, S. L., VORONINA, S. G., DA SILVA XAVIER, G., CHVANOV, M. A., LONGBOTTOM, R. E., GERASIMENKO, O. V., PETERSEN, O. H., RUTTER, G. A. & TEPIKIN, A. V. 2008. ATP depletion inhibits Ca^{2+} release, influx and extrusion in pancreatic acinar cells but not pathological Ca^{2+} responses induced by bile. *Pflugers Arch,* 455**,** 1025-39.

BERROZPE, G., SCHAEFFER, J., PEINADO, M. A., REAL, F. X. & PERUCHO, M. 1994. Comparative analysis of mutations in the p53 and K-ras genes in pancreatic cancer. *Int J Cancer,* 58**,** 185-91.

BOURON, A. 2000. Activation of a capacitative $Ca(^{2+})$ entry pathway by store depletion in cultured hippocampal neurones. *FEBS Lett,* 470**,** 269-72.

BRUCE, J. 2010. Plasma membrane calcium pump regulation by metabolic stress. *World J Biol Chem,* 1**,** 221-8.

BRUCE, J. I. & ELLIOTT, A. C. 2007. Oxidant-impaired intracellular Ca^{2+} signaling in pancreatic acinar cells: role of the plasma membrane Ca^{2+}-ATPase. *Am J Physiol Cell Physiol,* 293**,** C938-50.

CAMPANELLA, M. E., CHU, H. & LOW, P. S. 2005. Assembly and regulation of a glycolytic enzyme complex on the human erythrocyte membrane. *Proc Natl Acad Sci U S A,* 102**,** 2402-7.

CARAFOLI, E. 1987. Intracellular calcium homeostasis. *Annu Rev Biochem,* 56**,** 395-433.

CARAFOLI, E. 1991. Calcium pump of the plasma membrane. *Physiol Rev,* 71**,** 129-53.

CHAIKA, N. V., YU, F., PUROHIT, V., MEHLA, K., LAZENBY, A. J., DIMAIO, D., ANDERSON, J. M., YEH, J. J., JOHNSON, K. R., HOLLINGSWORTH, M. A. & SINGH, P. K. 2012. Differential expression of metabolic genes in tumor and stromal components of primary and metastatic loci in pancreatic adenocarcinoma. *PLoS One,* 7**,** e32996.

CHEN, Z., ZHANG, H., LU, W. & HUANG, P. 2009. Role of mitochondria-associated hexokinase II in cancer cell death induced by 3-bromopyruvate. *Biochim Biophys Acta,* 1787**,** 553-60.

CRIDDLE, D. N., GERASIMENKO, J. V., BAUMGARTNER, H. K., JAFFAR, M., VORONINA, S., SUTTON, R., PETERSEN, O. H. & GERASIMENKO, O. V. 2007. Calcium signalling and pancreatic cell death: apoptosis or necrosis? *Cell Death Differ,* 14**,** 1285-94.

CRIDDLE, D. N., MURPHY, J., FISTETTO, G., BARROW, S., TEPIKIN, A. V., NEOPTOLEMOS, J. P., SUTTON, R. & PETERSEN, O. H. 2006. Fatty acid ethyl esters cause pancreatic calcium toxicity via inositol trisphosphate receptors and loss of ATP synthesis. *Gastroenterology,* 130**,** 781-93.

DONG, H., SHIM, K. N., LI, J. M., ESTREMA, C., ORNELAS, T. A., NGUYEN, F., LIU, S., RAMAMOORTHY, S. L., HO, S., CARETHERS, J. M. & CHOW, J. Y. 2010. Molecular mechanisms underlying Ca^{2+}-mediated motility of human pancreatic duct cells. *Am J Physiol Cell Physiol,* 299**,** C1493-503.

DUCHEN, M. R. 1999. Contributions of mitochondria to animal physiology: from homeostatic sensor to calcium signalling and cell death. *J Physiol,* 516 (Pt 1)**,** 1-17.

ECHARTE, M. M., ROSSI, R. C. & ROSSI, J. P. 2007. Phosphorylation of the plasma membrane calcium pump at high ATP concentration. On the mechanism of ATP hydrolysis. *Biochemistry,* 46**,** 1034-41.

GATENBY, R. A. & GILLIES, R. J. 2004. Why do cancers have high aerobic glycolysis? *Nat Rev Cancer,* 4**,** 891-9.

GRYNKIEWICZ, G., POENIE, M. & TSIEN, R. Y. 1985. A new generation of Ca^{2+} indicators with greatly improved fluorescence properties. *J Biol Chem,* 260**,** 3440-50.

GUDJONSSON, B. 2009. Pancreatic cancer: survival, errors and evidence. *Eur J Gastroenterol Hepatol,* 21**,** 1379-82.`

HANAHAN, D. & WEINBERG, R. A. 2011. Hallmarks of cancer: the next generation. *Cell,* 144**,** 646-74.

HANSEN, M. R., KRABBE, S., ANKORINA-STARK, I. & NOVAK, I. 2009. Purinergic receptors stimulate Na^{+}/Ca^{2+} exchange in pancreatic duct cells: possible role of proteins handling and transporting Ca^{2+}. *Cell Physiol Biochem,* 23**,** 387-96.

HARDIN, C. D., RAEYMAEKERS, L. & PAUL, R. J. 1992. Comparison of endogenous and exogenous sources of ATP in fueling Ca^{2+} uptake in smooth muscle plasma membrane vesicles. *J Gen Physiol,* 99**,** 21-40.

HEGYI, P., PANDOL, S., VENGLOVECZ, V., & RAKONCZAY, Z. 2010. The acinar-ductal tango in the pathogenesis of acute pancreatitis. *Gut*, 60, 544-552.

HINGORANI, S. R., PETRICOIN, E. F., MAITRA, A., RAJAPAKSE, V., KING, C., JACOBETZ, M. A., ROSS, S., CONRADS, T. P., VEENSTRA, T. D., HITT, B. A., KAWAGUCHI, Y., JOHANN, D., LIOTTA, L. A., CRAWFORD, H. C., PUTT, M. E., JACKS, T., WRIGHT, C. V., HRUBAN, R. H., LOWY, A. M. & TUVESON, D. A. 2003. Preinvasive and invasive ductal pancreatic cancer and its early detection in the mouse. *Cancer Cell,* 4**,** 437-50.

HRUBAN, R. H., VAN MANSFELD, A. D., OFFERHAUS, G. J., VAN WEERING, D. H., ALLISON, D. C., GOODMAN, S. N., KENSLER, T. W., BOSE, K. K., CAMERON, J. L. & BOS, J. L. 1993. K-ras oncogene activation in adenocarcinoma of the human pancreas. A study of 82 carcinomas using a combination of mutant-enriched polymerase chain reaction analysis and allele-specific oligonucleotide hybridization. *Am J Pathol,* 143**,** 545-54.

HUG, M., PAHL, C. & NOVAK, I. 1996. Evidence for a Na^{+}-Ca^{2+} exchanger in rat pancreatic ducts. *FEBS Lett,* 397**,** 298-302.

IHRLUND, L. S., HERNLUND, E., KHAN, O. & SHOSHAN, M. C. 2008. 3-Bromopyruvate as inhibitor of tumour cell energy metabolism and chemopotentiator of platinum drugs. *Mol Oncol,* 2**,** 94-101.

KIM, J. S., AHN, K. J., KIM, J. A., KIM, H. M., LEE, J. D., LEE, J. M., KIM, S. J. & PARK, J. H. 2008. Role of reactive oxygen species-mediated mitochondrial dysregulation in 3-bromopyruvate induced cell death in hepatoma cells : ROS-mediated cell death by 3-BrPA. *J Bioenerg Biomembr,* 40**,** 607-18.

KIM, J. S., QIAN, T. & LEMASTERS, J. J. 2003. Mitochondrial permeability transition in the switch from necrotic to apoptotic cell death in ischemic rat hepatocytes. *Gastroenterology,* 124**,** 494-503.

KO, Y. H., PEDERSEN, P. L. & GESCHWIND, J. F. 2001. Glucose catabolism in the rabbit VX2 tumor model for liver cancer: characterization and targeting hexokinase. *Cancer Lett,* 173**,** 83-91.

KO, Y. H., SMITH, B. L., WANG, Y., POMPER, M. G., RINI, D. A., TORBENSON, M. S., HULLIHEN, J. & PEDERSEN, P. L. 2004. Advanced cancers: eradication in all cases using 3-bromopyruvate therapy to deplete ATP. *Biochem Biophys Res Commun,* 324**,** 269-75.

KOONG, A. C., MEHTA, V. K., LE, Q. T., FISHER, G. A., TERRIS, D. J., BROWN, J. M., BASTIDAS, A. J. & VIERRA, M. 2000. Pancreatic tumors show high levels of hypoxia. *Int J Radiat Oncol Biol Phys,* 48**,** 919-22.

KREJS, G. J. 2010. Pancreatic cancer: epidemiology and risk factors. *Dig Dis,* 28**,** 355-8.

KROEMER, G. & POUYSSEGUR, J. 2008. Tumor cell metabolism: cancer's Achilles' heel. *Cancer Cell,* 13**,** 472-82.

LEIST, M., SINGLE, B., CASTOLDI, A. F., KUHNLE, S. & NICOTERA, P. 1997. Intracellular adenosine triphosphate (ATP) concentration: a switch in the decision between apoptosis and necrosis. *J Exp Med,* 185**,** 1481-6.

MALETH, J., VENGLOVECZ, V., RAZGA, Z., TISZLAVICZ, L., RAKONCZAY, Z., JR. & HEGYI, P. 2011. Non-conjugated chenodeoxycholate induces severe mitochondrial damage and inhibits bicarbonate transport in pancreatic duct cells. *Gut,* 60**,** 136-8.

MANKAD, P., JAMES, A., SIRIWARDENA, A. K., ELLIOTT, A. C. & BRUCE, J. I. 2012. Insulin protects pancreatic acinar cells from cytosolic calcium overload and inhibition of the plasma membrane calcium pump. *J Biol Chem,* 287**,** 1823-36.

MILLIGAN, L. P. & MCBRIDE, B. W. 1985. Energy costs of ion pumping by animal tissues. *J Nutr,* 115**,** 1374-82.

MUALLEM, S., BEEKER, T. & PANDOL, S. J. 1988. Role of Na^+/Ca^{2+} exchange and the plasma membrane Ca^{2+} pump in hormone-mediated Ca^{2+} efflux from pancreatic acini. *J Membr Biol,* 102**,** 153-62.

NAKASHIMA, R. A., PAGGI, M. G. & PEDERSEN, P. L. 1984. Contributions of glycolysis and oxidative phosphorylation to adenosine 5'-triphosphate production in AS-30D hepatoma cells. *Cancer Res,* 44**,** 5702-6.

NICOTERA, P., LEIST, M. & FERRANDO-MAY, E. 1998. Intracellular ATP, a switch in the decision between apoptosis and necrosis. *Toxicology Lett,* 102-103**,** 139-42.

PUTNEY, J. W. 2006. *Calcium signaling,* Boca Raton, CRC/Taylor & Francis.

RICHARDS, D. E., REGA, A. F. & GARRAHAN, P. J. 1978. Two classes of site for ATP in the Ca^{2+}-ATPase from human red cell membranes. *Biochim Biophys Acta,* 511**,** 194-201.

ROSSI, J. P. & REGA, A. F. 1989. A study to see whether phosphatidylserine, partial proteolysis and EGTA substitute for calmodulin during activation of the Ca^{2+}-ATPase from red cell membranes by ATP. *Biochim Biophys Acta,* 996**,** 153-9.

SCHMIDT, M. M. & DRINGEN, R. 2009. Differential effects of iodoacetamide and iodoacetate on glycolysis and glutathione metabolism of cultured astrocytes*.,* 1**,** 1.

SHCHEPINA, L. A., PLETJUSHKINA, O. Y., AVETISYAN, A. V., BAKEEVA, L. E., FETISOVA, E. K., IZYUMOV, D. S., SAPRUNOVA, V. B., VYSSOKIKH, M. Y., CHERNYAK, B. V. & SKULACHEV, V. P. 2002. Oligomycin, inhibitor of the F_0 part of H^+-ATP-synthase, suppresses the TNF-induced apoptosis. *Oncogene,* 21**,** 8149-57.

SLATER, A. F., STEFAN, C., NOBEL, I., VAN DEN DOBBELSTEEN, D. J. & ORRENIUS, S. 1995. Signalling mechanisms and oxidative stress in apoptosis. *Toxicology Lett,* 82-83**,** 149-53.

TEPIKIN, A. V., VORONINA, S. G., GALLACHER, D. V. & PETERSEN, O. H. 1992. Acetylcholine-evoked increase in the cytoplasmic Ca^{2+} concentration and Ca^{2+} extrusion measured simultaneously in single mouse pancreatic acinar cells. *J Biol Chem,* 267**,** 3569-72.

TSAI, I. H., MURTHY, S. N. & STECK, T. L. 1982. Effect of red cell membrane binding on the catalytic activity of glyceraldehyde-3-phosphate dehydrogenase. *J Biol Chem,* 257**,** 1438-42.

VORONINA, S. G., BARROW, S. L., SIMPSON, A. W., GERASIMENKO, O. V., DA SILVA XAVIER, G., RUTTER, G. A., PETERSEN, O. H. & TEPIKIN, A. V. 2010. Dynamic changes in cytosolic and mitochondrial ATP levels in pancreatic acinar cells. *Gastroenterology,* 138**,** 1976-87.

WAKASUGI, H., STOLZE, H., HAASE, W. & SCHULZ, I. 1981. Effect of La^{3+} on secretagogue-induced Ca^{2+} fluxes in rat isolated pancreatic acinar cells. *Am J Physiol,* 240**,** G281-9.

WOLFF, T., LEIPZIGER, J., FISCHER, K. G., KLAR, B., NITSCHKE, R. & GREGER, R. 1993. Evidence for agonist-induced export of intracellular Ca^{2+} in epithelial cells. *Pflugers Arch,* 424**,** 423-30.

ZHANG, J., XIAO, P. & ZHANG, X. 2009. Phosphatidylserine externalization in caveolae inhibits Ca^{2+} efflux through plasma membrane Ca^{2+}-ATPase in ECV304. *Cell Calcium,* 45**,** 177-84.

ZHOU, W., CAPELLO, M., FREDOLINI, C., RACANICCHI, L., PIEMONTI, L., LIOTTA, L. A., NOVELLI, F. & PETRICOIN, E. F. 2011. Proteomic Analysis Reveals Warburg Effect and Anomalous Metabolism of Glutamine in Pancreatic Cancer Cells. *J Proteome Res,* 11**,** 554-63.

2.8 - Chapter 2 Supplementary Methods and Results

2.8.1 - Fura-2 fluorescence microscopy and measurement of intracellular $[Ca^{2+}]_i$

$[Ca^{2+}]_i$ was measured using fura-2, a ratiometric fluorescent indicator which binds free intracellular Ca^{2+}. Fura-2 is an aminopolycarboxylic acid, however, the fura-2 derivative fura-2-acetoxymethyl ester (fura-2 AM) is used to load a cell with the free-acid form of fura-2. Fura-2 AM is freely permeable across the plasma-membrane, but is cleaved by intracellular esterases to the free-acid form of fura-2, which is membrane impermeable and thus trapped within the cell. When excited, fura-2 emits light at 510 nm. However, fura-2 is excited by two wavelengths (λ) of light, both of which are in the UV range, and the spectral properties of fura-2 change upon Ca^{2+} binding (Supplementary Figure 2.1). Thus, when bound to Ca^{2+}, fura-2 is excited at 340 nm, while Ca^{2+}-free fura-2 is excited at 380 nm. The ratio of the emissions at both excitation wavelengths (F340/380) corresponds to $[Ca^{2+}]_i$. In a typical healthy cell where resting $[Ca^{2+}]_i$ is low, the light emitted by Ca^{2+}-bound fura-2 (F340) will be lower than that of Ca^{2+}-free fura-2 (F380). As $[Ca^{2+}]_i$ increases, the amount of fura-2 bound to Ca^{2+} increases while the amount of Ca^{2+}-free fura-2 decreases, and this is mirrored by a reciprocal change in the emission intensities at the two excitation λ. The opposite is true for decreases in $[Ca^{2+}]_i$, where the amount of Ca^{2+}-bound fura-2 decreases with a corresponding increase in Ca^{2+}-free fura-2. By measuring $[Ca^{2+}]_i$ at a given timepoint as a ratio of the signals emitted by both Ca^{2+}-bound and Ca^{2+}-free fura-2, this technique eliminates numerous otherwise confounding variables that would impair the accurate measurement of $[Ca^{2+}]_i$ if using a non-ratiometric Ca^{2+} dye. These include subtle drift in optical focus, dye leakage, changes or differences in cell volume and thickness, photobleaching and any other experimental limitations that would otherwise induce changes in fluorescence signal and result in false $[Ca^{2+}]_i$ measurements.

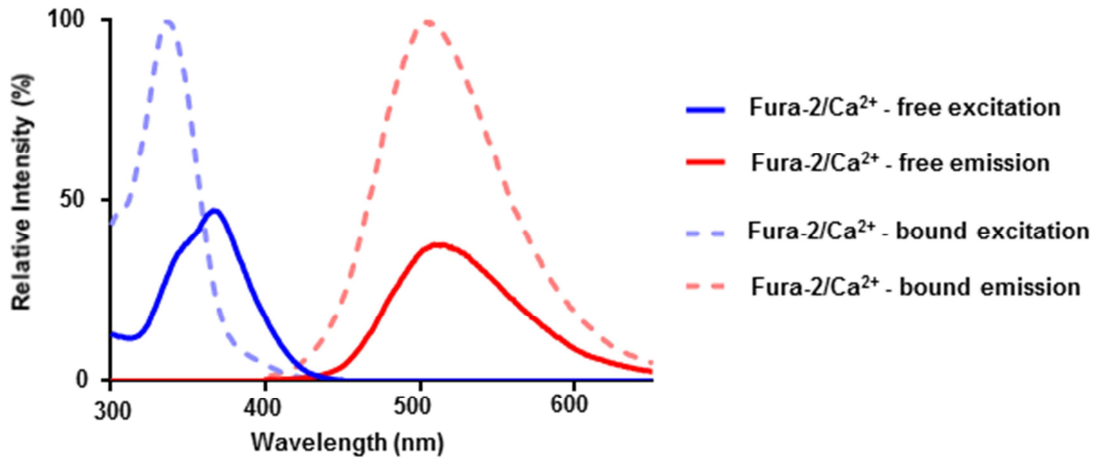

Supplementary Figure 2.1 - The excitation and emission spectra of Ca^{2+}-free and Ca^{2+} bound fura-2.

The decision was made in the present study to use fura-2, as this dye is both ratiometric and has a high affinity for Ca^{2+}. The ratiometric properties of fura-2 cancel out any variables that would lead to fluctuating fluorescence, and thus fura-2 controls for fluorescence changes that are independent of changes in $[Ca^{2+}]_i$. Other ratiometric $[Ca^{2+}]_i$ indicators do exist that could be used in place of fura-2, however these were less-well suited to our particular experimental applications (Vetter, 2012). For example, indo-1 is another effective ratiometric $[Ca^{2+}]_i$ indicator that undergoes a shift in emission peak rather than absorption λ (Takahashi et al., 1999), and evidence suggests indo-1 does not suffer from the same degree of compartmentalisation as fura-2. However, indo-1 exhibits rapid photobleaching by UV light and has a much lower affinity for Ca^{2+}, and is therefore less suited for measuring subtle changes in resting $[Ca^{2+}]_i$ over prolonged periods of time (Scheenen et al., 1996). Moreover, the indo-1 emission spectra overlaps with that of NADH (excitation and emission at 340 and 440 – 470 nm, respectively), making it difficult to distinguish NADH autofluorescence from indo-1 fluorescence (Wahl et al., 1990). While not the primary reason for choosing it for use in our assays, fura-2 also has the advantage of being compatible with GO-ATeam FRET microscopy for the simultaneous measurement of $[Ca^{2+}]_i$ and [ATP] (Nakano et al., 2011). Other derivatives of fura-2 exist that address the problems of compartmentalisation and sensitivity to high $[Ca^{2+}]_i$, however these derivatives have a lower affinity for $[Ca^{2+}]_i$ and are not available as a membrane-permeable form, therefore they require invasive loading techniques (Schlatterer et al., 1992).

Two similar but separate imaging systems were used to carry out the experiments described in this thesis. Supplementary Figure 2.2 depicts the basic setup of these imaging systems. One comprised of a Nikon Diaphot fitted with a x40 oil immersion objective (numerical aperture 1.3) and an Orca charge-coupled device (CCD) camera (Hamamatsu), while the other comprised of a Nikon TE2000 microscope fitted with a x40 oil immersion objective (numerical aperture 1.3) and a CoolSNAP HQ interline progressive-scan CCD camera (Roper Scientific Photometrics, Tucson, AZ). Both systems utilised a monochromator illumination system with a xenon arc lamp light source (Cairn Research, Kent, UK). Light generated by this light source was collimated using a mirror inside the monochromator, and was then separated using a diffraction grating that was mounted on a movable axis. Light at the desired λ was then reflected by a second mirror out of the output slit, and this light was passed along to the microscope via a quartz fibre optic. Excitation light was then reflected up through the objective by a dichroic mirror (400 nm), thus exciting the fura-2 within the cells mounted on the microscope coverslip. Light emitted by fura-2 was then passed back along the objective and transmitted through the same dichroic mirror, at which point it was filtered by an emission filter (505LP), reflected out of the microscope and detected by the CCD camera. Both systems were controlled by MetaFluor image acquisition and analysis software (Molecular Devices, Downington, CA). Cells were excited at 340 nm and 380 nm (50ms exposure), with background-subtracted images acquired every 5 seconds.

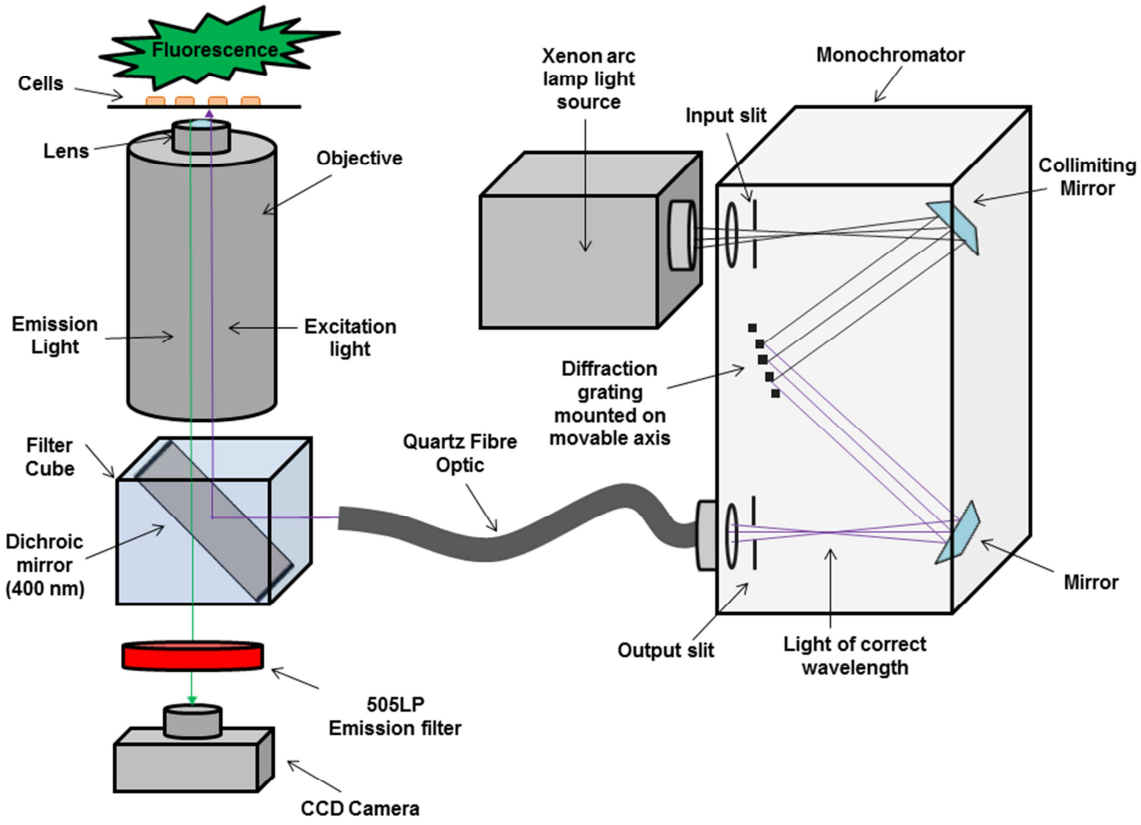

Supplementary Figure 2.2 - An inverted microscope system for fura-2 fluorescence imaging of $[Ca^{2+}]_i$

Light generated by a xenon arc lamp light source enters a monochromator system, where it is first collimited using a collimiting mirror before being separated using a mobile diffraction grating. This light is then reflected through the output slit at the desired excitation wavelengths (λ, 340 nm and 380 nm in the case of fura-2). The light is carried to the microscope using a quartz fibre optic cable, where a dichroic mirror (400 nm) reflects the light through an objective to excite the cells. Fluorescence light emitted following excitation of fura-2 is then carried back through the objective and passed through the dichroic mirror and a 505 nm long pass (505LP) emission filter, and detected using a charged coupled device (CCD) camera system.

2.8.2 - Calibration of resting $[Ca^{2+}]_i$

Since the F340/F380 fura-2 fluorescence ratio is proportional to absolute $[Ca^{2+}]_i$, $[Ca^{2+}]_i$ could be calculated by means of a calibration step. This calibration step was applied to assess for changes in our resting $[Ca^{2+}]_i$ experiments. As previously described (Grynkiewicz et al., 1985), $[Ca^{2+}]_i$ can be derived from fura-2 fluorescence ratio using the following equation:

$$[Ca^{2+}]_i = K_d \times \left(\frac{(R - R_{min})}{(R_{max} - R)} \right) \times \left(\frac{Sf_{380}}{Sb_{380}} \right)$$

Where K_d is the fura-2 binding affinity for Ca^{2+} in the cytosolic environment (225 nM, Grynkiewicz et al., 1985), R is the F340/F380 fura-2 fluorescence ratio, and R_{min} and R_{max} are the minimum and maximum calibrated ratios, respectively. Sf_{380} and Sb_{380} are the fluorescence signals elicited by the second excitatory λ (380 nm) in the absence of $[Ca^{2+}]_i$ (the "f" denoting fura-2 in the Ca^{2+}-free state) or the presence of saturating $[Ca^{2+}]_i$ (the "b" denoting fura-2 in the Ca^{2+}-bound state).

Supplementary Figure 2.3A shows a typical calibration protocol. Calibrations were performed by first perfusing cells with Ca^{2+}-free HEPES-PSS (138 mM NaCl, 4.7 mM KCl, 1.28 mM $CaCl_2$, 0.56 mM $MgCl_2$, 5.5 mM glucose, 10mM HEPES, pH 7.4) supplemented with 1 mM EGTA. The perfusion was then stopped and the Ca^{2+} ionophore ionomycin (10 µM) applied to the static bath for 2 minutes, followed by further perfusion in Ca^{2+}-free HEPES-PSS with 1 mM EGTA until R_{min} was reached. At this point, HEPES-PSS containing 20 mM Ca^{2+} was applied to determine R_{max}. These values can then be used in the above equation to determine $[Ca^{2+}]_i$ for a given value of R.

Ideally, one would perform a calibration at the end of an experiment for each individual cell. However, due to limitations in the experimental setup and the cost of ionomycin, this is both unreliable and financially unfeasible. For example, changes in cell volume due to drug treatment or dye leakage during the experiment would lead to inaccurate $[Ca^{2+}]_i$ values were a post-assay calibration applied. We therefore opted to extrapolate calibration values taken from naive cells. This is not without its own limitations, since selection of which cell to extrapolate the calibration values from could lead to skewed calculations of $[Ca^{2+}]_i$ if this cell was not representative of the population. Therefore, it was decided to perform numerous separate calibration experiments, and to construct from this a calibration curve representative of an average cell from which to calculate estimated $[Ca^{2+}]_i$. To do this, cells were loaded with fura-2 and a $[Ca^{2+}]_i$ calibration immediately performed, after which the $[Ca^{2+}]_i$ values were converted to $\log[Ca^{2+}]_i$. The R values between and inclusive of the R_{min} and R_{max} for all cells were then plotted against their respective calibrated $\log[Ca^{2+}]_i$ and treated as a single data series (Supplementary Figure 2.3B). From

here, a sigmoidal curve could be plotted through the data points to give a calibration curve representative of an average cell. By deriving the equation for this curve, $\log[Ca^{2+}]_i$ could be calculated for any given ratio value. This could then be converted into $[Ca^{2+}]_I$ to give an estimated absolute $[Ca^{2+}]_i$. These values were then used to calculate area under the curve (AUC), maximum change in $[Ca^{2+}]_i$ (Max-$\Delta[Ca^{2+}]_i$) and responses to 100 µM ATP ($\Delta[Ca^{2+}]_i$ >100 nM). Since R, R_{min}, R_{max}, Sf_{380} and Sb_{380} are derived from fluorescence values whose intensity depends on the particular setup of the optical system employed, experiments were run on the same imaging system with identical optical settings (i.e. 4x4 binning), and calibration assays run on the same day as the other experiments.

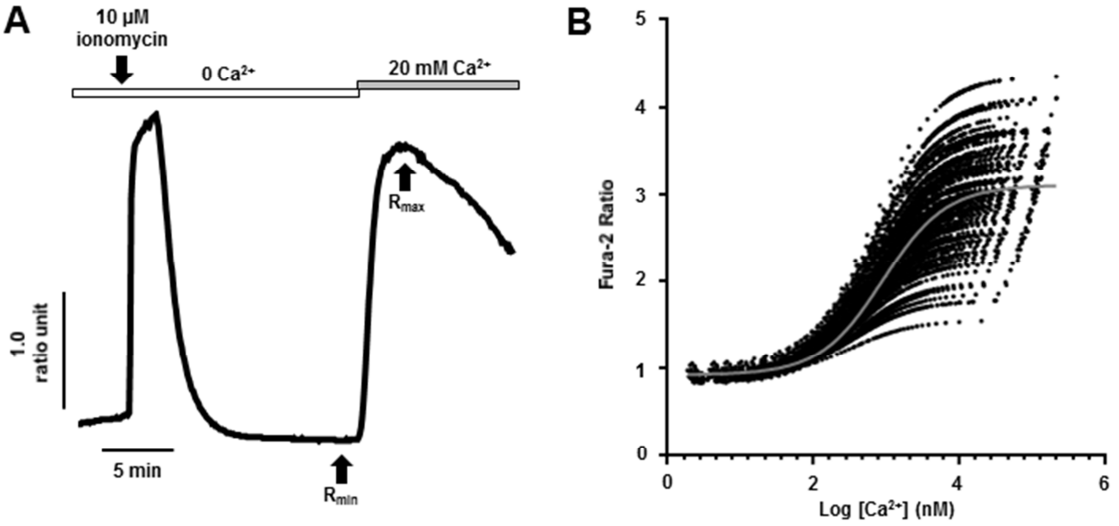

Supplementary Figure 2.3 - Fura-2 calibration and estimation of resting $[Ca^{2+}]_I$

A*,** A representative trace depicting a $[Ca^{2+}]_i$ calibration experiment. To calibrate $[Ca^{2+}]_i$ from fura-2 within a given experiment, cells were perfused with Ca^{2+}-free HEPES-PSS supplemented with 1 mM EGTA. The perfusion was then stopped and the Ca^{2+} ionophore ionomycin (10 µM) applied to the static bath for 2 minutes, followed by further perfusion in Ca^{2+}-free HEPES-PSS with 1 mM EGTA until the minimum fura-2 ratio (R_{min}) was reached. At this point, HEPES-PSS containing 20 mM Ca^{2+} was applied to determine the maximum fura-2 ratio (R_{max}). From these values, $[Ca^{2+}]_i$ can be determined for a given fura-2 ratio (Grynkiewicz et al., 1985). To create a calibration curve representative of an average cell from which to estimate resting $[Ca^{2+}]_i$ (B***), MIA-PaCa-2 cells were loaded with fura-2 and calibrated as in panel A. The log $[Ca^{2+}]_i$ (nM) values between the R_{max} and R_{min} for all cells were plotted as a single data series, and a sigmoidal curve fitted. Using the values of this curve together with the equation for a sigmoidal curve, estimated $[Ca^{2+}]_i$ (nM) was calculated for all subsequent MIA PaCa-2 cells using identical optical settings.

2.8.3 - Measurement of $[Ca^{2+}]_i$ clearance rate

To measure $[Ca^{2+}]_i$ clearance rate by the plasma membrane Ca^{2+} ATPase (PMCA), we employed an *in situ* $[Ca^{2+}]_i$ clearance assay (Supplementary Figure 2.4A) as previously described (Mankad et al., 2012, Baggaley et al., 2008). Cells were perfused with 30 µM cyclopiazonic acid (CPA) in the absence of extracellular $[Ca^{2+}]_i$ and the presence of 1 mM

EGTA. CPA selectively inhibits the sarcoplasmic/endoplasmic reticulum Ca^{2+} ATPase (SERCA), resulting in a transient increase in $[Ca^{2+}]_i$ as the ER Ca^{2+} store is depleted via the Ca^{2+} leak pathway. $[Ca^{2+}]_i$ then returns to a baseline, presumably due to PMCA activity. Upon perfusion with 20 mM Ca^{2+}, store-operated Ca^{2+} entry (SOCE) is induced, and a large increase in $[Ca^{2+}]_i$ is observed. Following Ca^{2+} influx, cells are again perfused with Ca^{2+} free HEPES-PSS containing 1 mM EGTA, and $[Ca^{2+}]_i$ is again cleared. This influx/clearance phase can be repeated in the presence of absence of test reagents or manoeuvres to assess their effects on PMCA $[Ca^{2+}]_i$ clearance rate. CPA is applied throughout the experiment.

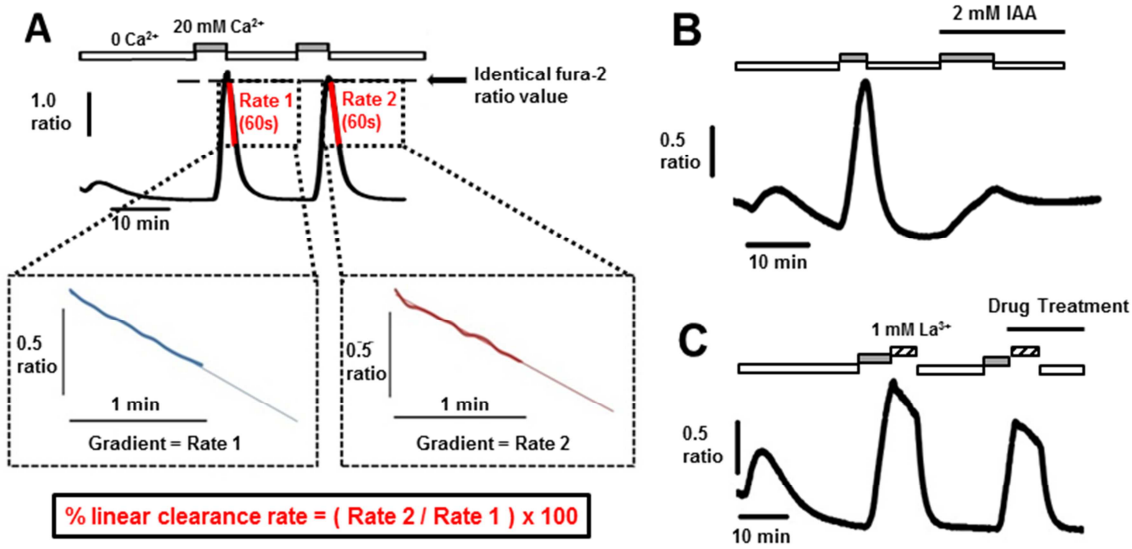

Supplementary Figure 2.4 - Protocols for the *in situ* $[Ca^{2+}]_i$ clearance assay

A, A representative trace depicting the *in situ* $[Ca^{2+}]_i$ clearance assay and measurement of relative linear rate (%). Cells were treated with cyclopiazonic acid (CPA, 30 uM) in zero external Ca^{2+} with 1 mM EGTA (white box) or 20 mM Ca^{2+} (grey box) to induce store-operated Ca^{2+} influx. Subsequent removal of external Ca^{2+} resulted in $[Ca^{2+}]_i$ clearance. This influx-clearance phase was repeated in the presence of test reagents or manoeuvres. To calculate the % linear $[Ca^{2+}]_i$ clearance during the second clearance phase, the fastest 60s segment of both clearance phases was fitted to a nonlinear regression, both starting at the same fura-2 ratio value. The gradient (itself a unit of rate) for the second clearance phase was then normalised to the first (%). ***B***, a representative trace depicting the attenuated store-operated Ca^{2+} entry observed following treatment with certain test reagents, in this case 2 mM iodoacetate (IAA). ***C***, a representative trace of the modified $[Ca^{2+}]_i$ clearance assay where $[Ca^{2+}]_i$ is "clamped" at a high concentration following SOCE using 1 mM La^{3+} (striped box). This allows for the application of a test reagent for a set period of time (5 minutes) after SOCE has been achieved, prior to releasing the inhibition of Ca^{2+} entry and efflux by La^{3+} with 1 mM EGTA, thus initiating $[Ca^{2+}]_i$ clearance.

There are numerous ways in which $[Ca^{2+}]_i$ clearance rate could be measured. One method would be to fit the clearance phase to a single exponential decay, which yields the time constant of the decaying curve (tau, τ). However, previous work in isolated pancreatic acinar cells has found that, under conditions of metabolic inhibition, $[Ca^{2+}]_i$ clearance rate was often inhibited to

such a degree that the clearance phase had a linear nature rather than one that could be fitted to a single exponential decay (Baggaley et al., 2008). Similarly, this was also observed in the present study (Supplementary Figure 2.5A). Thus, if using this method of analysis, any experiments where clearance was linear would need to be excluded despite being valid experiments, since the calculated τ values of the linear clearance curves would be unreliable if fitting to a single exponential decay. Furthermore, fitting two clearance phases to a single exponential decay and comparing the τ assumes that the asymptote reached by each clearance curve is identical. Even when the clearance appeared to follow a single exponential decay, the fura-2 ratio did not always reach the same fura-2 ratio baseline (asymptote) in the presence of test reagents. Moreover, the asymptotes of the two clearance phases were often vastly different following metabolic inhibition (Supplementary Figure 2.5B). In cases where the fura-2 ratio asymptote reached was different, the comparing of τ values would not accurately reflect changes in clearance rate.

After considering the limitations of fitting the clearance phases to a single exponential decay, the measurement of clearance as a linear rate was therefore considered more appropriate. To assess rate, we decided to measure the linear clearance rate during the second influx/clearance challenge in the presence or absence of test reagents, and to normalise this to the first, control influx/clearance phase (Supplementary Figure 2.4A). To achieve this, a linear regression was fitted to the first 60 seconds of clearance in the initial control influx/clearance phase (measurements taken at 5 second intervals), and the gradient of the linear regression line (itself a unit of rate) calculated. The calculation of linear rate was then repeated for the second influx/clearance phase using the same method, however this measurement was taken from the same fura-2 ratio value as that used to measure clearance rate during the first influx/clearance phase (as shown in Supplementary Figure 2.4A). Thus this method controlled for the possibility that a variable $[Ca^{2+}]_i$ might influence clearance rate.

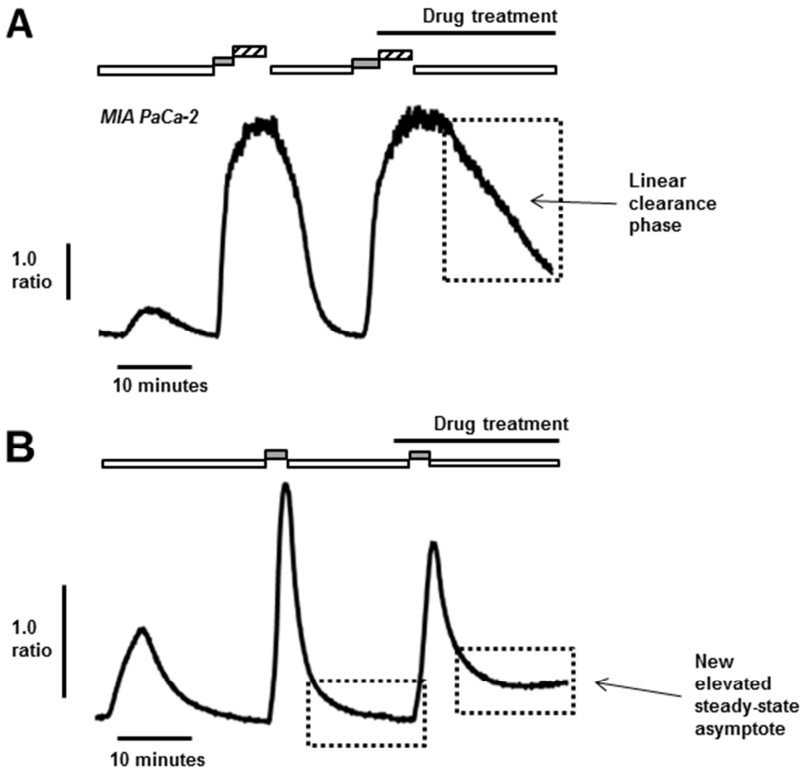

Supplementary Figure 2.5 - The limitations of comparing single exponential decay time-constants in an *in situ* $[Ca^{2+}]_i$ clearance assay

In our *in situ* $[Ca^{2+}]_i$ clearance assay, 30 µM cyclopiazonic acid (CPA) was applied in the absence of external Ca^{2+} with 1 mM EGTA (*white box*), or 20 mM Ca^{2+} (*grey box*) to induce store-operated Ca^{2+} influx. 1 mM La^{3+} was then applied at the peak of Ca^{2+} influx (*striped box*). Subsequent removal of external La^{3+} and readdition of 1 mM EGTA after 5 minutes allowed $[Ca^{2+}]_i$ clearance. This influx-clearance phase was repeated and metabolic inhibitors applied during this second influx-clearance phase. Following treatment with certain drugs, $[Ca^{2+}]_i$ clearance was so profoundly affected that the nature of clearance more resembled a linear rate rather than a single exponential decay (***A***). Moreover, in other experiments, drug treatment resulted in the second $[Ca^{2+}]_i$ clearance phase reaching a new elevated steady-state asymptote compared to that during the first control clearance phase (***B***). Under these conditions, comparison of the single exponential decay time constant (tau, τ) becomes an invalid means of comparing clearance rates between the two phases.

In some experiments, certain drug treatments severely inhibited SOCE as well as $[Ca^{2+}]_i$ clearance (Supplementary Figure 2.4B). This made it difficult to compare $[Ca^{2+}]_i$ clearance because $[Ca^{2+}]_i$ failed to reach a sufficiently high enough short-lived steady state from which $[Ca^{2+}]_i$ clearance could be initiated, and thus dramatically reduced the range over which $[Ca^{2+}]_i$ clearance could be measured. Furthermore, the slowed rate of SOCE following certain treatments meant that these cells had prolonged exposure to drug treatment compared to those where SOCE was unaffected. It therefore became apparent that the current experimental method was insufficient to reliably compare linear clearance rate when $[Ca^{2+}]_i$ influx was inhibited.

To eliminate these confounding factors, we modified the *in situ* $[Ca^{2+}]_i$ clearance assay such that test reagents could be applied for a fixed period of time at the peak of the Ca^{2+} influx phase (Supplementary Figure 2.4C). This was achieved by applying 1 mM La^{3+} in nominal Ca^{2+}-free HEPES-PSS to inhibit both Ca^{2+} influx and Ca^{2+} efflux, thereby effectively clamping $[Ca^{2+}]_i$ high. This allowed test reagents to be applied for a fixed period of time (5 minutes) after achieving sufficient SOCE, while maintaining a high $[Ca^{2+}]_i$ from which to initiate clearance. Removal of La^{3+}, and thus the initiation of $[Ca^{2+}]_i$ clearance, was achieved by addition of 1 mM EGTA, which chelates Ca^{2+} with pM affinity (Putney, 2006). From here, $[Ca^{2+}]_i$ clearance can be assessed as before, without the confounding effects of drug-induced inhibition of Ca^{2+} influx and an associated prolonged drug exposure.

2.8.4 - Measurement of % recovery of $[Ca^{2+}]_i$ to baseline

While linear rate provided a means to compare $[Ca^{2+}]_i$ clearance rate during the fastest portion of the clearance curve, this method of analysis does not take into account the nature of $[Ca^{2+}]_i$ clearance past the initial 60 seconds of the clearance phase and may underestimate the extent of inhibition. Moreover, in some experiments, the clearance rate following drug treatment was often dramatically inhibited and consequently led to an elevated new steady state. In an attempt to quantify this response, we therefore also measured the degree of recovery of $[Ca^{2+}]_i$ to baseline that cells could achieve following treatment with test reagents of manoeuvres. In the current study, we compared the degree of recovery during the second clearance phase to the pre-influx/clearance phase baseline. Using this method (Supplementary Figure 2.6) the difference is calculated between the plateau reached after the second clearance phase and the first fura-2 value used to measure linear $[Ca^{2+}]_i$ clearance rate. This was normalised (%) to the difference between the same starting fura-2 ratio value and the post-CPA baseline prior to the first Ca^{2+} influx phase. This method ignores the influence of the first clearance phase, and is appropriate to calculate the ability of a cell to recover $[Ca^{2+}]_i$ to baseline during the second influx/clearance phase and can be used when recovery during the first influx/clearance phase is 100%.

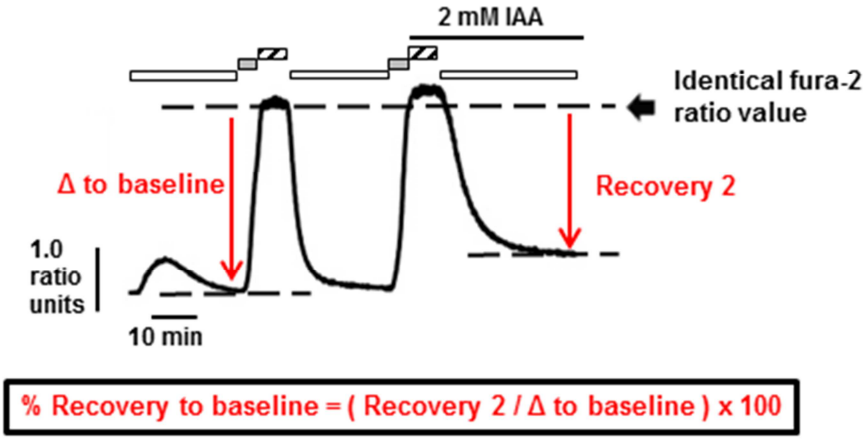

Supplementary Figure 2.6 - Measurement of recovery to baseline in an *in situ* $[Ca^{2+}]_i$ clearance assay

In our *in situ* $[Ca^{2+}]_i$ clearance assay, 30 µM cyclopiazonic acid (CPA) was applied in the absence of external Ca^{2+} with 1 mM EGTA (*white box*), or 20 mM Ca^{2+} (*grey box*) to induce store-operated Ca^{2+} influx. 1 mM La^{3+} was then applied at the peak of Ca^{2+} influx (*striped box*). Subsequent removal of external La^{3+} and readdition of 1 mM EGTA after 5 minutes allowed $[Ca^{2+}]_i$ clearance. This influx-clearance phase was repeated and metabolic inhibitors applied during this second influx-clearance phase. Recovery from Ca^{2+} influx in our *in situ* $[Ca^{2+}]_i$ clearance assay can be measured as the % recovery to the pre-influx/clearance phase baseline, which normalises (%) the recovery during the second clearance phase (Recovery 2) to the change to the post-cyclopiazonic acid treatment baseline (Δ to baseline). Recovery 2 and Δ to baseline are measured from an identical fura-2 ratio value.

2.9 - Supplementary References

BAGGALEY, E. M., ELLIOTT, A. C. & BRUCE, J. I. 2008. Oxidant-induced inhibition of the plasma membrane Ca^{2+}-ATPase in pancreatic acinar cells: role of the mitochondria. *Am J Physiol Cell Physiol,* 295**,** C1247-60.

GRYNKIEWICZ, G., POENIE, M. & TSIEN, R. Y. 1985. A new generation of Ca^{2+} indicators with greatly improved fluorescence properties. *J Biol Chem,* 260**,** 3440-50.

MANKAD, P., JAMES, A., SIRIWARDENA, A. K., ELLIOTT, A. C. & BRUCE, J. I. 2012. Insulin protects pancreatic acinar cells from cytosolic calcium overload and inhibition of plasma membrane calcium pump. *J Biol Chem,* 287**,** 1823-36.

NAKANO, M., IMAMURA, H., NAGAI, T. & NOJI, H. 2011. Ca^{2+} regulation of mitochondrial ATP synthesis visualized at the single cell level. *ACS Chem Biol,* 6**,** 709-15.

PUTNEY, J. W. 2006. *Calcium signaling,* Boca Raton, FL, CRC/Taylor & Francis.

SCHEENEN, W. J., MAKINGS, L. R., GROSS, L. R., POZZAN, T., & TSIEN, R. Y. (1996). Photodegradation of indo-1 and its effect on apparent Ca^{2+} concentrations. Chemistry & biology, 3(9), 765-774.

SCHLATTERER, C., KNOLL, G. & MALCHOW, D. 1992. Intracellular calcium during chemotaxis of Dictyostelium discoideum: a new fura-2 derivative avoids sequestration of the indicator and allows long-term calcium measurements. *Eur J Cell Biol,* 58**,** 172-81.

TAKAHASHI, A., CAMACHO, P., LECHLEITER, J. D. & HERMAN, B. 1999. Measurement of intracellular calcium. *Physiol Rev,* 79**,** 1089-125.

VETTER, I. (2012). Development and Optimization of FLIPR high throughput calcium assays for ion channels and GPCRs. In *Calcium Signaling* (pp. 45-82). Springer Netherlands.

WAHL, M., LUCHERINI, M. J. & GRUENSTEIN, E. 1990. Intracellular Ca^{2+} measurement with Indo-1 in substrate-attached cells: advantages and special considerations. *Cell Calcium,* 11**,** 487-500.

Chapter 3 - The Plasma Membrane Calcium Pump in Pancreatic Cancer Cells Exhibiting the "Warburg Effect" is Reliant on a Glycolytic ATP supply

Andrew James[‡], Waseema Patel[‡], Zohra Butt[‡], Magretta Adiamah[‡], Raga Dakhel[‡], Ayse Latif[§], Carolina Uggenti[‡], Lisa Swanton[‡], Hiromi Imamura[¶], and Jason I. E. Bruce[‡]

From the [‡] Faculty of Life Sciences and the [§] Faculty of Medical and Human Sciences, The University of Manchester, Michael Smith Building, Oxford Road, Manchester, M13 9PT, United Kingdom, and [¶]PRESTO, Japan Science and Technology Agency, Japan.

3.1 - Abstract

Pancreatic ductal adenocarcinoma (PDAC) is an aggressive cancer with poor prognosis. We previously described that the plasma membrane Ca^{2+} ATPase (PMCA), which extrudes cytosolic Ca^{2+} to maintain a low intracellular Ca^{2+} concentration ($[Ca^{2+}]_i$) and thus cell survival, utilises glycolytically-derived ATP in PDAC. However, it is not known whether this glycolytic dependency of the PMCA is a unique feature to highly glycolytic cancer cells, or occurs regardless of glycolytic rate. The present study explored this question by switching PDAC cells from a highly glycolytic phenotype to one more reliant on mitochondrial metabolism, and examining the relative sensitivity of these cells to metabolic inhibitor-induced ATP depletion, PMCA inhibition and $[Ca^{2+}]_i$ overload in comparison to control cells. This switch in metabolism was achieved by culturing PDAC cell lines (MIA PaCa-2 cells and PANC-1) for 21 days in nominal glucose-free media supplemented with either 2 mM α-ketoisocaproate (KIC) or 10 mM galactose. Under these conditions, PDAC cells exhibited a decrease in the rate of glycolytic flux and proliferation, and were less sensitive to ATP depletion by glycolytic inhibitors (3-bromopyruvate and iodoacetate, IAA) while sensitivity to mitochondrial inhibitors (oligomycin and antimycin) was potentiated. Furthermore, in contrast to glucose-cultured cells, inhibition of glycolysis with IAA had no effect on PMCA activity and resting $[Ca^{2+}]_i$ in KIC and galactose-cultured cells. This suggests that the reliance of the PMCA on glycolytic ATP may be a specific feature of PDAC cells exhibiting a high glycolytic rate, and that this may be a vulnerability that can be exploited therapeutically.

3.2 - Introduction

Pancreatic ductal adenocarcinoma (PDAC) is a highly aggressive form of cancer with poor prognosis and severely limited treatment options. Surgical resection of the tumour is often the only available course of action, yet only 10 – 20% of patients diagnosed with PDAC present with resectable disease (Loos et al., 2008). This is often due to the advanced progression of PDAC in the absence of clinical symptoms. As such, the 5-year survival rate of PDAC is estimated at below 5% (Amin et al., 2006), and there is an almost entirely unmet clinical need for novel approaches with which to effectively combat PDAC.

A common hallmark of cancer is an aberrant metabolic profile characterised by a high glycolytic rate even when oxygen is abundant. First observed by Otto Warburg (Warburg, 1956), this phenomenon has since become known as “aerobic glycolysis” (Hanahan and Weinberg, 2011), and has been hypothesised to confer numerous survival advantages for rapidly proliferating tumour cells. These include promotion of metastasis, resistance to hypoxia, and the generation of an abundance of glycolytic intermediates for use in anabolic processes and cell proliferation (Gatenby and Gillies, 2004, Gillies and Gatenby, 2007, Koong et al., 2000, Kroemer and Pouyssegur, 2008). Upregulated glycolysis in cancer cells has been targeted for anticancer treatment by numerous studies with promising results (Pelicano et al., 2006), and inhibition of glycolysis in cancer cells has been shown to be an effective means of depleting intracellular ATP (Ko et al., 2004) in cancer cells. While not an energetically favourable method of ATP production, glycolysis occurs at a high rate in cancer cells, allowing PDAC tumours to meet their metabolic demands in the face of hypoxia (Guillaumond et al., 2013).

Despite this metabolic reprogramming, a robust supply of ATP remains essential for the many energy consuming processes of rapidly dividing cancer cells. One such important energy consuming process is the plasma membrane calcium (Ca^{2+}) ATPase (PMCA), an ATP-driven Ca^{2+} pump on the plasma membrane which is responsible for the maintenance of a low resting cytosolic Ca^{2+} concentration ($[Ca^{2+}]_i$,100 nM). The PMCA is the main and most important Ca^{2+} efflux pathway in human PDAC cells (James et al., 2013), and compromised PMCA activity can lead to an irreversible $[Ca^{2+}]_i$ overload and cell death (Brini and Carafoli, 2009). The contribution of the PMCA to $[Ca^{2+}]_i$ homeostasis is therefore crucial for PDAC cell survival. We have previously provided evidence that a glycolytic ATP supply to the PMCA is crucial for maintaining a low resting $[Ca^{2+}]_i$ in human PDAC cells; MIA PaCa-2 and PANC-1 treated with inhibitors of glycolysis exhibited ATP depletion, $[Ca^{2+}]_i$ overload, PMCA inhibition and cell death, while mitochondrial inhibitors had no effect (*Chapter 2*, James et al., 2013). To further examine the glycolytic dependency of the PMCA in PDAC, the present study sought to reverse the metabolic phenotype of PDAC cells from a glycolytic state to one more reliant on mitochondrial metabolism. This allowed us to determine the importance of the relative source of ATP responsible for fuelling the PMCA in PDAC. We aimed to achieve this by culturing human PDAC cell lines (MIA PaCa-2 and PANC-1) in nominal glucose-free conditions supplemented with substrates for fuelling mitochondrial ATP synthesis. It has been suggested that cells cultured

under such conditions may be a better model of aerobically poised non-cancerous cells *in vivo*, which unlike transformed cells are typically susceptible to mitochondrial toxicants (Marroquin et al., 2007). These “switched” PDAC cells would be derived from an identical genetic background to their glucose-cultured counterparts but would therefore likely resemble a non-cancerous metabolic phenotype, thereby allowing relative importance of glycolytic ATP regulation of the PMCA in PDAC to be further corroborated.

Two substrates that have been suggested to promote mitochondrial metabolism are the monosacharride sugar galactose and the keto-analogue of leucine, α-ketoisocaproate (KIC). Replacement of glucose with galactose in culture medium has been shown to lower glycolytic rate in rat ascites hepatoma cells with a corresponding decrease in lactic acid production (Bustamante and Pedersen, 1977). Galactose is converted via the Leloir pathway to glucose-6-phosphate, thereby bypassing the hexokinase step of glycolysis (Bustamante and Pedersen, 1977). The predominant isoform of hexokinase expressed in human cancers, hexokinase II, has been suggested to promote the highly glycolytic phenotype of cancer (Mathupala et al., 2009). Furthermore, galactose entry into glycolysis occurs at a slower rate than glucose entry into glycolysis (Bustamante and Pedersen, 1977). The circumventing of the hexokinase step coupled with the slower utilisation of galactose compared to glucose results in a slowed glycolytic flux, and cells are ultimately forced to upregulate oxidative phosphorylation to maintain ATP levels (Robinson et al., 1992, Rossignol et al., 2004). Indeed, galactose supplementation has previously been shown to manipulate metabolism in cultured cells by enhancing mitochondrial metabolism while slowing glycolytic flux (Bellance et al., 2009, Marroquin et al., 2007, Rossignol et al., 2004, Shulga et al., 2010, Bustamante and Pedersen, 1977).

In contrast to galactose, KIC is metabolised exclusively by mitochondria, and its metabolism enhances the availability of α-ketoglutarate (Lenzen et al., 1985, Malaisse et al., 1981), acetyl-CoA and the ketone body acetoacetone (Noda and Ichihara, 1974, MacDonald et al., 2005), thereby boosting the capacity of the TCA cycle (Hutton et al., 1979). Ketone bodies have been reported to inhibit tumour growth (Magee et al., 1979), and this is thought to contribute to the antiproliferative effects of the ketogenic diet in numerous cancers (Seyfried et al., 2003, Abdelwahab et al., 2012, Otto et al., 2008). Indeed, evidence suggests that the ketogenic diet slows tumour growth in PDAC by inducing metabolic reprogramming (Shukla et al., 2014), and thus supplementation of PDAC cells with KIC in nominal glucose-free conditions might recapitulate these metabolic changes in an *in vitro* setting.

Based on this evidence, we hypothesised that KIC and galactose would be good candidate substrates as a glucose replacement in order to shift the metabolic phenotype of human PDAC cells back towards mitochondrial metabolism. We report that a relative switch from glycolytic to mitochondrial metabolism can be achieved in human PDAC cell lines by culturing in nominal glucose-free media supplemented with either 2 mM KIC or 10 mM galactose. Moreover, these culture conditions confer a reversal in the sensitivity of PDAC cells to ATP depletion by various

inhibitors of either glycolytic or mitochondrial metabolism when compared to glucose-cultured PDAC cells. Furthermore, the previously reported effects of the glycolytic inhibitor iodoacetate on $[Ca^{2+}]_i$ overload and PMCA activity in glucose-cultured PDAC cells (James et al., 2013) were significantly attenuated in KIC and galactose-cultured cells. This study indicates that PDAC cells rely on glycolytically-derived ATP to fuel the PMCA when glycolytic rate is high, which may represent an important and cancer-specific therapeutic locus for the treatment of PDAC tumours exhibiting the Warburg phenotype.

3.3 - Experimental Procedures

3.3.1 - Cell culture

PANC-1 and MIA PaCa-2 cells (ATCC) were cultured in a humidified atmosphere of air/CO_2 (95%:5%) at 37 °C, in either glucose-containing DMEM (D6429, Sigma) or glucose-free DMEM (11966-025, Life Technologies) containing either 10 mM D-(+)-Galactose (G5388, Sigma) or α-ketoisocaproate (KIC, K0629, Sigma). All media was supplemented with 10% FBS, 100 units/ml penicillin, and 100 g/ml streptomycin. Cells were used up to passage 30 and then discarded.

3.3.2 - Preparation of test reagents

HEPES-buffered physiological saline solution (HEPES-PSS; 138 mM NaCl, 4.7 mM KCl, 1.28 mM $CaCl_2$, 0.56 mM $MgCl_2$, 5.5 mM glucose, 10 mM HEPES, pH 7.4) was used in all imaging experiments using glucose-cultured cells. For KIC and galactose-cultured cells, 5.5 mM glucose was replaced with 2 mM KIC and 10 mM galactose, respectively. Fura-2 AM (Invitrogen, TEFLabs) was prepared in 50:50 DMSO (Sigma), and 0.1% Pluronic F-127 (Molecular Probes, Invitrogen). Stocks of 3-bromopyruvate (BrPy), sodium iodoacetate (IAA) and 2-deoxyglucose (2-DG) were prepared in MilliQ water. Stocks of oligomycin (OM), carbonyl cyanide m-chlorophenyl hydrazine (CCCP), cyclopiazonic acid (CPA) and ionomycin were prepared in DMSO. Antimycin (AM) was prepared in ethanol. Frozen stocks were defrosted and diluted in HEPES-PSS to give working solutions immediately prior to an experiment. For the luciferase-based ATP assays, working solutions were prepared in media rather than HEPES-PSS. Both galactose and KIC were prepared at 50x and 100x stocks, respectively, in Dulbecco's Phosphate Buffered Saline without Ca^{2+} or Mg^{2+} (PBS, D8537, Sigma) prior to supplementation into culture media.

3.3.3 - Luciferase-based ATP assays

ATP was assessed as previously described (James et al., 2013). Briefly, MIA PaCa-2 and PANC-1 cells were seeded into white-walled, clear-bottom 96-well plates (1×10^5 cells/ml) and left to adhere overnight. Cells were treated for 15 minutes with various metabolic inhibitors and ATP determined using the luciferase-based ViaLight Plus kit (Lonza, Rockland, ME) and Synergy HT multiwall reader (BioTEK). Experiments were run in duplicate. To correct for background, luminescence values obtained from a positive control group treated with an ATP depletion cocktail (10 µM OM, 4 µM CCCP, 2 mM IAA and 500 mM BrPy) were subtracted from all other values before normalising to control (%). Differences in ATP depletion (% control, luciferase-based assays) between groups were assessed using a Kruskal-Wallis test with a post-hoc Dunn's test.

3.3.4 - Cell proliferation assay

Glucose, galactose and KIC-cultured MIA PaCa-2 cells were seeded at a constant density of 5000 cells per well into 96 well Costar® cell culture plates (Corning). At 2, 24, 48, 72 and 96 hours post-seeding, one plate for each culture condition was fixed using 10% trichloroacetic acid at 4°C for 1 hour, then rinsed with MilliQ H_2O and dried. Cell biomass was stained using sulforhodamine B. Excess dye was rinsed away using 1% acetic acid, and remaining dye solubilised using a standard volume of 10 mM Tris. Protein content was measured as absorbance at 565 nm. For each culture condition, 8 replicates were performed, and the rate of proliferation between 72 and 96 hours measured as the average rate of increase in absorbance units (AU) per hour between these timepoints. Data presented are the mean ± SEM across all 8 replicates.

3.3.5 - Extracellular flux measurements

An XFe96 Extracellular Flux Analyzer (Seahorse Bioscience) was used to measure mitochondrial and glycolytic function in glucose, galactose and KIC-cultured MIA PaCa-2 cells. Oxygen consumption rate (OCR) and extracellular acidification rate (ECAR) exhibited by adherent MIA PaCa-2 cells were measured using either an XF Cell Mito Stress Test Kit or XF Glycolysis Stress Test Kit (Seahorse Bioscience) to measure key metabolic parameters. These assays were carried out according to the manufacturer's instructions. All materials and reagents were supplied by Seahorse Bioscience. Briefly, glucose, galactose and KIC-cultured MIA PaCa-2 cells were seeded into XF96 V3 PS cell culture plates at an optimised density of 2.5×10^4 cells per well and allowed to adhere overnight at 37 °C with 5% CO_2. The culture medium was then exchanged for XF Base medium (pH 7.35) supplemented with 1 mM L-glutamine. For the XF Cell Mito Stress Test, XF Base was also supplemented with either 10 mM glucose and 1 mM sodium pyruvate, 2 mM KIC or 10 mM galactose depending on the cells' respective culture conditions. Cells were then incubated at 37°C without CO_2 for 1 h prior to commencing the assay, after which cells were transferred to the XFe96 and the assay performed. The XF Cell Mito Stress Test involved sequential addition of oligomycin (1 µM), FCCP (0.5 µM) and then a combination of rotenone and antimycin A (both 1 µM). The XF Glycolysis Stress Test involved the sequential addition of glucose (10 mM), oligomycin (1 µM) and 2-deoxyglucose (100 mM). All assays were performed at 37°C. Drugs were used at concentrations optimised for these XF stress tests. OCR and ECAR were measured simultaneously throughout each experiment. Three sequential measurements were recorded at set interval time points prior to addition of the first drug and then after each sequential drug addition. The final of these three measurements was used to calculate the metabolic parameters reported (Figure 3.4D and 3.5D). OCR and ECAR data for each well were normalised using a sulforhodamine B-based assay for protein content (described above for the proliferation assay) prior to calculation of metabolic parameters. A single experiment was performed for both the XF Cell Mito Stress Test (6 – 8 replicates) and the XF Glycolysis Stress Test (14 - 16 replicates). Calculated metabolic

parameters for all replicates were averaged to give the presented experimental means ± SEM. All statistical comparisons were performed using a one-way ANOVA with post-hoc Bonferroni test for multiple comparisons.

3.3.6 - Stable transfection of GO-ATeam into MIA PaCa-2 cells

MIA PaCa-2 cells were grown to 70% confluency in 35 mm x 10 mm tissue-culture treated culture dishes (Corning) and transfected with 1 µg/ml GO-ATeam (Nakano et al., 2011) cDNA using GeneCellin transfection reagent as per manufacturer's instructions (BioCellChallenge). For a description of GO-ATeam plasmid validation, please see *3.8.2 – Amplification and validation of GO-ATeam plasmid* in *3.8 – Chapter 3 Supplementary Methods and Results*. Following transfection, cells were treated with 500 µM G418 (Sigma) from 24 hours to 21 days post-transfection, with the media replaced every two days. Colonies stably expressing GO-ATeam were then selected using a Zeiss Axio Observer D1 microscope fitted with an Axiocam CCD camera and FITC filter set (Zeiss), isolated using cloning cylinders (Corning) and routinely cultured in glucose-containing DMEM (as described above) supplemented with 500 µM G418. All experiments were performed on cells derived from the same colony. For more details, see *3.8.3 – Generation of MIA PaCa-2 cells stably expressing GO-ATeam* in *3.8 – Chapter 3 Supplementary Methods and Results*.

3.3.7 - GO-ATeam fluorescence ATP imaging

All experiments were carried out using a Nikon TE2000 microscope fitted with a x40 oil immersion objective (numerical aperture 1.3) and a CoolSNAP HQ interline progressive-scan CCD camera (Roper Scientific Photometrics, Tucson, AZ). Both the microscope used for GO-ATeam imaging and that used for fura-2 imaging employed a monochromator illumination system (Cairn Research,Kent, UK) controlled by MetaFluor image acquisition and analysis software (Molecular Devices, Downingtown, PA), and cells were continually perfused with HEPES-PSS using gravity-operated perfusion systems (Harvard Apparatus). Cells were excited at 470 nm (500ms exposure) and excitation light was separated from emitted light using a 505 nm dichroic with a dual band emission filter (59004m ET FITC/TRITC Dual Emitter). Emitted light was simultaneously collected at 510-nm and above 560-nm using an OptoSplit Image Splitter equipped with a JC1 565 nm dichroic (Cairn Research, Kent, UK). All experiments were performed at room temperature. For more details on the GO-ATeam FRET microscopy methods employed, see *3.8.4 – GO-ATeam FRET imaging of cytosolic ATP* in *3.8 – Chapter 3 Supplementary Methods and Results*.

3.3.8 - Fura-2 fluorescence Ca^{2+} imaging

Cells were loaded with fura-2 AM (4 µM) for 40 minutes at room temperature prior to being mounted on an imaging system as previously described (See *Chapter 2*, Baggaley et al., 2008, Bruce and Elliott, 2007, Mankad et al., 2012, James et al., 2013). Experiments were performed on a Nikon Diaphot fitted with a x40 oil immersion objective (numerical aperture 1.3), and an Orca CCD camera (Hamamatsu). Cells were excited at 340 nm and 380 nm (50 ms exposure) and excitation light separated from emitted light using a 400 nm dichroic with a 505LP filter. Cells were continually perfused with HEPES-PSS as described for the GO-ATeam experiments. All experiments were performed at room temperature.

3.3.9 - Calibration of resting $[Ca^{2+}]_i$

Calibration of $[Ca^{2+}]_i$ was performed in MIA PaCa-2 cells (3 experiments, 97 cells) as previously described (See *Chapter 2*, James et al., 2013). Following calibration, fura-2 ratios were plotted against calibrated log$[Ca^{2+}]_i$ values, with values from all cells treated as a single data series. A sigmoidal curve was fitted to these data, representative of calibrated $[Ca^{2+}]_i$ in an average cell. This curve was used to estimate $[Ca^{2+}]_i$ for all cells in our resting $[Ca^{2+}]_i$ experiments. All experiments were performed on an identical imaging setup (4x4 binning).

3.3.10 - Measurement of $[Ca^{2+}]_i$ clearance

$[Ca^{2+}]_i$ clearance was measured using an *in situ* $[Ca^{2+}]_i$ clearance assay as previously described, using the amended protocol to clamp $[Ca^{2+}]_i$ high in cells while applying metabolic inhibitors (see *Chapter 2*, James et al., 2013). Briefly, this involved treating cells with CPA in Ca^{2+} free HEPES-PSS containing 1 mM EGTA followed by sequential pulses of perfusion with 20 mM Ca^{2+} and Ca^{2+} free HEPES-PSS containing 1 mM EGTA to induce rapid phases of Ca^{2+} influx and clearance, respectively. Repeated measurements of $[Ca^{2+}]_i$ clearance rate were performed during these sequential Ca^{2+} influx/clearance phases. Following influx, $[Ca^{2+}]_i$ was clamped inside the cell by application of 1 mM La^{3+} (which blocks both Ca^{2+} influx and Ca^{2+} efflux) for 5 minutes, at which point La^{3+} was removed by addition of 1 mM EGTA, allowing rapid $[Ca^{2+}]_i$ clearance. Metabolic inhibitors were applied during the second influx/clearance phase from the addition of La^{3+}.

3.3.11 - Fluorescence imaging data acquisition, analysis and experimental design

For both GO-ATeam and fura-2 imaging experiments, background-subtracted images of a field of view of cells were acquired every 5 seconds for each emission (GO-ATeam) or excitation (fura-2) wavelength. Data were analysed using Microsoft Excel and Graphpad Prism 6. Data presented are the means ± SEM of the indicated number (n) of experiments. To calculate

relative ATP levels (%) in the GO-ATeam experiments, the maximum decrease in fluorescence from baseline (ΔR_{max}) was first calculated (the mean of the 10 ratios immediately prior to drug perfusion minus the baseline ratio reached following treatment with the ATP depletion cocktail). Baseline-corrected fluorescence values were then normalised to ΔR_{max} and statistical comparisons between culture conditions performed using a two-way ANOVA with post-hoc Bonferroni test for multiple comparisons. Changes in resting $[Ca^{2+}]_i$ were quantified by measuring both the baseline-corrected area under the curve (AUC) and maximum change in $[Ca^{2+}]_i$ (max-$\Delta[Ca^{2+}]_i$) and assessed statistically using a one-way ANOVA with post-hoc Bonferroni's test. Similarly, differences in cell proliferation rate were statistically assessed using a one-way ANOVA with post-hoc Bonferroni's test. Differences in cell viability (% responding to 100 µM ATP) between treatment groups was assessed using a Kruskal-Wallis test with a post-hoc Dunn's test. To quantify $[Ca^{2+}]_i$ clearance rate, the linear rate over 60 seconds during the second influx/clearance phase (fura-2 ratio units/second) was normalised (%) to that of the first influx/clearance phase, beginning at a standardised fura-2 ratio value. % rate was then compared between treatment groups using a Mann Whitney U test. Relative recovery in our $[Ca^{2+}]_i$ clearance assays was measured by normalising (%) the clearance achieved during the second influx/clearance phase to that of the first influx/clearance phase, again from a standardised fura-2 ratio value (this method differed from that used in *Chapter 2* due to recovery during the first influx/clearance phase not reaching 100% in cells cultured in galactose or KIC - see *3.8.1 - Measurement of relative recovery of $[Ca^{2+}]_i$ during in situ $[Ca^{2+}]_i$ clearance assays*). Differences between treatment groups was statistically assessed using a Mann Whitney U test.

3.4 - Results

3.4.1 - Effect of metabolic inhibitors on ATP in galactose and KIC cultured PDAC cells vs those cultured in glucose

We have previously reported that the PMCA is reliant on a glycolytic ATP supply for maintaining a low resting $[Ca^{2+}]_i$ in PDAC, and that this may present a key pro-survival mechanism for this cancer. The aim of the present study was to further investigate the glycolytic dependency of both the PMCA and $[Ca^{2+}]_i$ homeostasis in PDAC. This was achieved by "switching" the metabolism of cultured PDAC cells towards mitochondrial ATP production and subsequently testing the effects of various metabolic inhibitors on cytosolic ATP levels, resting $[Ca^{2+}]_i$ and PMCA activity in these cells. To achieve this "switch" in metabolism from glycolytic to mitochondrial metabolism we employed two approaches; MIA PaCa-2 and PANC-1 cells were cultured in either 10 mM galactose or 2 mM α-ketoisocaproate (KIC) for a minimum of 3 passages and 21 days. The original cells from which these two populations were derived were maintained in glucose-containing DMEM, thereby retaining their highly glycolytic cancer phenotype, and used as a control in all parallel experiments. It is important to note, however, that while glucose-free media was used, supplementation of the media with 10% FCS was expected to result in nominal trace amount of glucose in the final media. Nevertheless, one would expect this to dramatically reduce the glycolytic rate in these cells, and all imaging experiments in these cells were performed in the complete absence of glucose.

Since a common characteristic of highly glycolytic cells is a high proliferation, most likely due to glucose carbon flux into anabolic processes, we first performed a cell proliferation assay to assess the growth rate of MIA PaCa-2 cells when cultured in either glucose, galactose or KIC. Cells seeded at an identical density into 96 well plates were fixed and stained with sulforhodamine B at set timepoints 24 hours apart and up to 96 hours, and protein content determined by solubilising the dye and measuring absorbance at 565 nm (see *3.3.4 – Cell proliferation assay*). Growth curves were then plotted (Figure 3.1A) and average growth rates in absorbance units (AU) per hour were calculated between 72 and 96 hours and compared between groups using a one-way ANOVA with post-post hoc Bonferroni test for multiple comparisons. Compared to glucose-cultured cells (0.0414 ± 0.00181 AU/h, n=8, Figure 3.1B), cell proliferation was significantly decreased in both galactose (0.0113 ± 0.00206 AU/h, n=8, $P<0.0001$, Figure 3.1B) and KIC-cultured cells (0.0147 ± 0.00264 AU/h, n=8, $P<0.0001$, Figure 3.1B). No significant difference in proliferation rate was found between galactose and KIC-cultured cells. These results provide the first indication that a switch in metabolic rate had been achieved under these conditions.

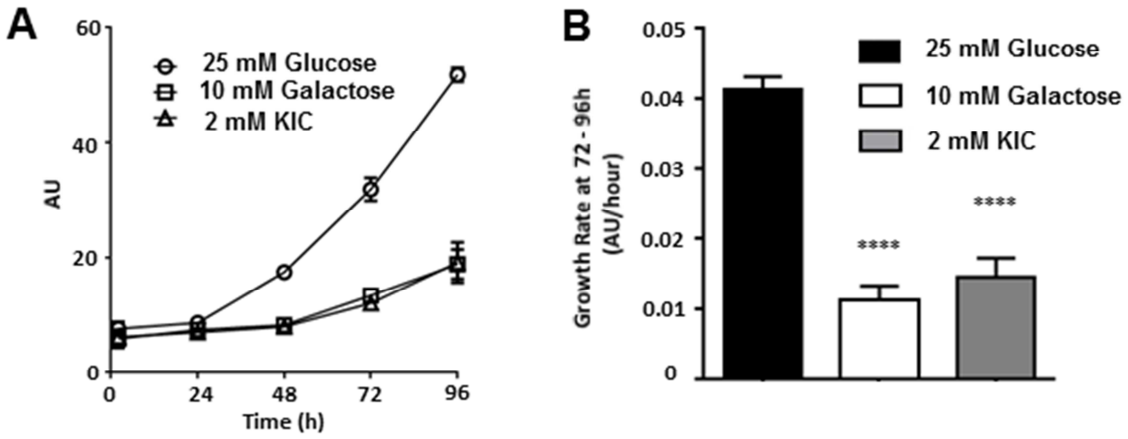

Figure 3.1 - Culture in KIC or galactose slows the growth rate of MIA PaCa-2 cells.

MIA PaCa-2 cells were first cultured in standard Dulbecco's modified Eagle's medium (DMEM) containing glucose or nominal glucose-free DMEM containing galactose (10 mM) and α-ketoisocaproate (KIC, 2 mM) for a minimum of 3 passages and 21 days. Cells were then assayed ***A*** – Growth curves for MIA PaCa-2 cells cultured from an identical starting density in glucose, 10 mM galactose and 2 mM KIC over 96 hours, as measured using a sulforhodamine B protein assay. ***B*** – Growth rate of glucose, galactose and KIC cells between 72 and 96 hours post-seeding. n=8 for each condition *, p<0.05;**, p <0.01; ***, p <0.001; ****, p<0.0001, all statistical comparisons made between galactose or KIC-cultured cells and glucose-cultured cells (one-way ANOVA with post-hoc Bonferroni test for multiple comparisons).

We have previously shown that inhibition of glycolysis, but not mitochondrial metabolism, results in ATP depletion in highly glycolytic PDAC cell lines (James et al., 2013). To test whether refuelling the mitochondria by culturing in galactose or KIC altered the relative source of ATP production, PANC-1 and MIA PaCa-2 cells from each culture condition (KIC, galactose and glucose) were treated with various mechanistically distinct inhibitors of either glycolytic or mitochondrial metabolism for 15 minutes and ATP levels then assessed using the luciferase-based ViaLight®Plus ATP assay kit (see *3.3.3 – Luciferase-based ATP assays*). To inhibit mitochondrial metabolism, cells were treated with oligomycin (OM, 10 µM), antimycin (AM, 0.5 µM) or CCCP (4 µM). OM and AM are well characterised inhibitors of the mitochondrial F_1/F_0-ATP synthase (Shchepina et al., 2002) and cytochrome bc_1 complex (Slater, 1973), respectively, while CCCP is a protonophore which depolarises the mitochondrial membrane potential (Kaftan et al., 2000). Conversely, to inhibit glycolysis, cells were treated with 2-deoxyglucose (2-DG, 10 mM), iodoacetate (IAA, 2 mM) or 3-bromopyruvate (BrPy, 500 µM). 2-DG once converted to 2-deoxyglucose-6-phosphate (2-DG-6-P), is not further metabolised; 2-DG-6-P accumulates in the cell and inhibits hexokinase (Chen and Gueron, 1992) and glucose-6-phosphate isomerase (Wick et al., 1957). Similarly, BrPy inhibits hexokinase (Ko et al., 2001), while IAA inhibits glyceraldehyde-3-phosphate dehydrogenase (Schmidt and Dringen, 2009). In addition to each of these treatments, a positive control was performed, where cells were treated with a combination of OM, CCCP, IAA and BrPy at their respective concentrations. This ATP depletion "cocktail" was considered to induce maximal ATP depletion, and the raw

luminescence counts from this were subtracted from each individual treatment before normalization to that of untreated control cells (%).

KIC and galactose-cultured cells were both sensitive to ATP depletion by mitochondrial inhibitors. In both MIA PaCa-2 and PANC-1 cell lines, treatment with OM caused a significantly greater decrease in ATP in the 'switched' cells (galactose PANC-1, 48 ± 4%, P<0.001, n=12; KIC PANC-1, 58 ± 5%, P<0.01, n=16; galactose MIA PaCa-2, 37 ± 3, P<0.0001, n=12; KIC MIA PaCa-2, 62 ± 4%, P<0.01, n=16, Figures 3.2A and 3.2B) compared to the glucose cells (PANC-1, 91 ± 5%, n=14; MIA PaCa-2, 107 ± 5%, n=16, Figures 3.2A and 3.1B). Similarly, in both cell lines, AM induced a greater ATP depletion in the galactose-grown cells (galactose PANC-1, 47 ± 7%, P<0.01, n=8; galactose MIA PaCa-2, 25 ± 4%, P<0.001, n=8, Figures 3.2A and 3.2B) than in glucose grown cells (PANC-1, 95 ± 5%, n=8; MIA PaCa-2, 91 ± 5%, n=8, Figures 3.2A and 3.2B). However, although the average AM and CCCP-induced ATP depletion in KIC-cultured PANC-1 and MIA PaCa-2 cells appeared less than that in their glucose-cultured counterparts, due to high variability no significant change in ATP depletion was observed in cells treated with these conditions (Figures 3.2A and 3.2B).

In contrast to their increased sensitivity to mitochondrial inhibitors, glycolytic inhibitors became less effective at depleting ATP in MIA PaCa-2 and PANC-1 cells cultured in either galactose or KIC. In both cell lines, treatment with IAA caused a significantly smaller decrease in ATP in the 'switched' cells (galactose PANC-1, 80 ± 4%, P<0.0001, n=12; KIC PANC-1, 61 ± 5%, P<0.01, n=16; galactose MIA PaCa-2, 88 ± 5%, P<0.0001, n=12; KIC MIA PaCa-2, 76 ± 7%, P<0.0001, n=16, Figures 3.2A and 3.2B) than in the glucose cells (PANC-1, 17 ± 3%, n=14; MIA PaCa-2, 14 ± 2%, n=16, Figures 3.2A and 3.2B). However, only in KIC-cultured PANC-1 cells was the ATP depletion induced by BrPy (103 ± 4%, n=8, Figure 3.2A) significantly less than that in glucose-cultured PANC-1 cells (53 ± 9%, P<0.01, n=8, Figure 3.2A); due to high variability, no significant change in ATP depletion was observed in galactose-cultured PANC-1 or galactose or KIC-cultured MIA PaCa-2 cells following BrPy treatment, despite the average ATP depletion appearing much less under these conditions. Interestingly, 2-DG had minimal effect in glucose grown cells, yet induced significant ATP depletion in galactose-grown MIA PaCa-2 cells (galactose MIA PaCa-2, 39 ± 2%, n=8; glucose MIA PaCa-2, 89 ± 6%, n=8, P<0.01, Figure 3.2B).

While a clear cut switch in sensitivity was not observed for every condition tested, overall these data suggest that a relative switch in metabolism has been successfully achieved, since these cells have become less sensitive to ATP depletion following inhibition of glycolysis by IAA, yet exhibit significantly increased sensitivity to inhibition of mitochondrial function by OM and AM. Moreover, the data indicate that in KIC and galactose-cultured cells a significantly higher relative proportion of ATP is derived from mitochondrial oxidative phosphorylation than in glucose-cultured cells. However, an important caveat to consider when interpreting these data is that the luminescence counts following each treatment are normalised to the luminescence

count of their respective controls, which in turn may be different following culture in the three culture conditions due to different starting ATP concentrations.

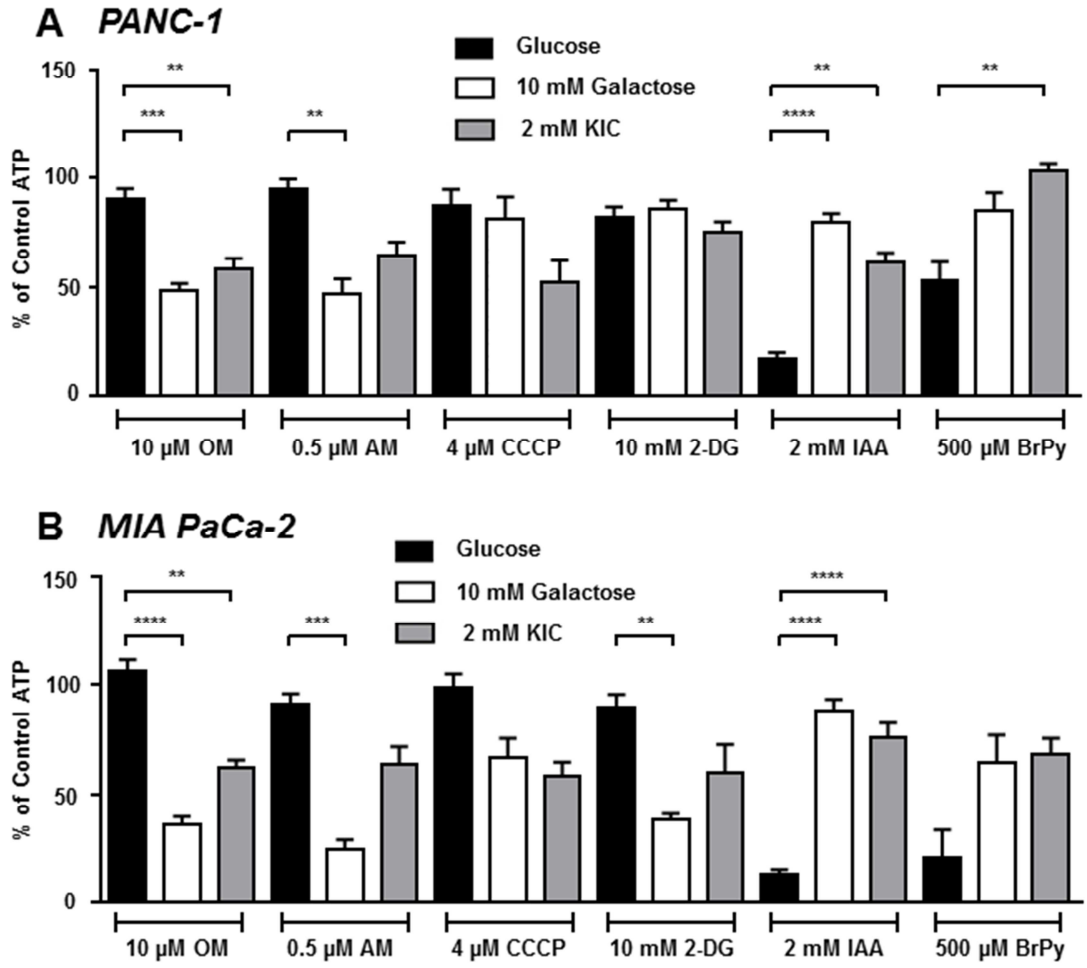

Figure 3.2 - Effect of metabolic inhibitors on ATP in galactose and KIC cultured PDAC cells vs those cultured in glucose.

PANC-1 cells (***A***) and MIA PaCa-2 (***B***) cells were cultured in either glucose-containing media (25 mM) or nominal glucose-free media supplemented with 10 mM galactose or 2 mM KIC for a minimum of 3 passages and 21 days. Both were then treated with either mitochondrial inhibitors (oligomycin, OM, 10 µM; antimycin, AM, 0.5 µM; CCCP, 4 µM) or glycolytic inhibitors (2-deoxyuglucose, 2DG, 10 mM; iodoacetate, IAA, 2 mM; 3-bromopyruvate, BrPy, 500 µM) for 15 minutes. ATP depletion was determined using a luciferase-based biouminescence assay. To determine ATP depletion, luminescence counts for each treatment condition were normalized to untreated time-matched control cells (%). Data presented are mean ± SE, n=8-14. *, p 0.05; **, p 0.01; ***, p 0.001, all data analysed using a Kruskal-Wallis test with a post-hoc Dunn's test for multiple comparisons.

3.4.2 - Real-time imaging of cytosolic ATP using a FRET-based reporter (GO-ATeam)

To further interrogate the temporal effects of metabolic inhibitors on ATP depletion in KIC, galactose and glucose-cultured MIA PaCa-2 cells, cytosolic ATP was measured in these cells using the recombinant ATP reporter GO-ATeam. GO-ATeam is a Förster resonance energy transfer (FRET) reporter developed to allow quantitative measurements of cytosolic ATP to be made in intact cells (Nakano et al., 2011). Briefly, GO-Team is comprised of the ε subunit of the bacterial F_oF_1-ATP synthase sandwiched between green and orange fluorescent proteins. These fluorescent proteins act as the FRET donor and acceptor, respectively, and a conformational change in the structure of GO-ATeam upon occupation of the ATP binding site on the F_oF_1-ATP synthase subunit determines FRET efficiency. MIA PaCa-2 cells stably expressing GO-ATeam (See *3.3 - Experimental Procedures* and *3.8 – Chapter 3 Supplementary Methods and Results*) were first cultured in DMEM or either 2 mM KIC or 10 mM galactose-containing media as described above to induce a switch in metabolism. Cells were then perfused with HEPES-PSS containing either 5.5 mM glucose, 2 mM KIC or 10 mM galactose. Cells were treated for 20 minutes with either 2-DG (10 mM), IAA (2 mM), OM (10 µM) or AM (0.5 µM), followed by an ATP depletion cocktail containing all four drugs at equivalent concentrations until the FRET ratio had reached a plateau (R_{min}, considered maximal ATP depletion, Figure 3.3A). R_{min}–subtracted ratio values at 0, 5, 10, 15 and 20 minutes were then normalised to the maximum decrease in ratio (ΔR_{max}) from the pretreatment baseline (R_0) to give % ATP at these timepoints (see *3.3.11 - Fluorescence imaging data acquisition, analysis and experimental design*). The data for each timepoint were averaged across all cells in an experiment to give the experimental mean of one assay, which were further averaged to give the presented means ± SEM.

In control experiments, no difference was observed between galactose or glucose cultured cells following perfusion with HEPES-PSS (time-matched controls; Figure 3.3B). Similarly, no difference in ATP was observed between KIC or glucose-cultured cells for 15 minutes. However, at 20 minutes post treatment a significant decrease in ATP was observed in KIC-cultured cells (70 ± 9 %, n=3, Figure 3.3B) compared to glucose-cultured counterparts (87 ± 3 %, n=7, $P<0.001$), suggesting that ATP was declining towards the end of these time-matched control experiments.

Culture in galactose or KIC resulted in an increased sensitivity of MIA PaCa-2 cells to ATP depletion by mitochondrial inhibitors. In galactose-cultured cells, 10 µM OM induced significantly greater ATP depletion at 10 (72 ± 8 %, n=4, Figure 3.3C), 15 (57 ± 10 %, n=4, Figure 3.3C) and 20 minutes (42 ± 14 %, n=4, Figure 3.3C) post-treatment compared to the equivalent timepoints in glucose-cultured cells (10 minutes, 104 ± 9 %, n=9, $P<0.05$; 15 minutes, 100 ± 9 %, n=9, $P<0.01$; 20 minutes, 96 ± 9 %, n=9, $P<0.001$, Figure 3.3C). No significant difference was observed in KIC-cultured cells treated with OM compared to glucose-cultured counterparts, however this is likely due to the small sample size for this condition (n=1, Figure 3.3C). Similar to OM, 0.5 µM AM induced significantly greater ATP depletion in galactose-cultured cells at 10

(73 ± 9 %, P<0.01, n=4, Figure 3.3D), 15 (53 ± 12 %, P<0.0001, n=4, Figure 3.3D) and 20 minutes (36 ± 11 %, P<0.0001, n=4, Figure 3.3D) compared to glucose-cultured control cells (10 minutes, 104 ± 5 %, n=6; 15 minutes, 102 ± 6 %, n=6; 20 minutes, 100 ± 7 %, n=6, Figure 3.3D). Similar effects were observed with KIC-cultured cells treated with AM compared to glucose-cultured counterparts, however this could not be compared statistically due to the small sample size for this condition (n=2, Figure 3.3D). These results were comparable to those observed in the previous luciferase based assays.

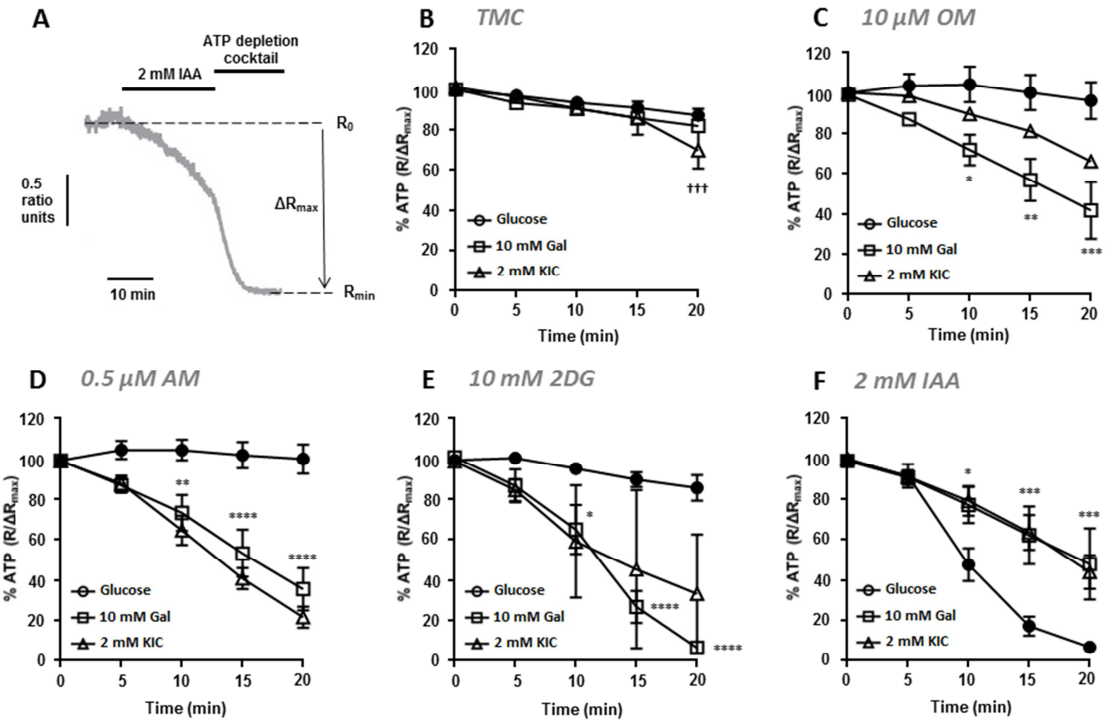

Figure 3.3 - GO-ATeam FRET imaging reveals the effects of glycolytic and mitochondrial inhibitors on ATP in glucose, galactose and KIC cultured cells.

MIA PaCa-2 cells were stably transfected with the ATP probe GO-ATeam and cultured in either glucose-containing (25 mM, closed circles) or nominal glucose-free media supplemented with either 10 mM galactose (open squares) or 2 mM KIC (open triangles) for a minimum of 3 passages and 21 days. Cytosolic ATP was then measured in cells in each culture group in response to various metabolic inhibitors using GO-ATeam FRET imaging. ***A***, a representative trace showing a galactose-cultured cell treated with iodoacetate (IAA). ATP depletion (%) was calculated by subtracting the minimum ratio observed after ATP depletion cocktail addition (R_{min}) from the FRET ratio values throughout drug treatment. These values were then normalised to the difference between the mean of the 10 FRET ratio values immediately prior to drug addition (baseline ratio, R_0) and the R_{min} (ΔR_{max}). Cells were treated with either vehicle alone (***B***, time matched control, TMC), a mitochondrial inhibitor (oligomycin, OM, 10 µM, ***C***; or antimycin, AM, 0.5 µM, ***D***) or a glycolytic inhibitor (2-deoxyuglucose, 2DG, 10 mM, ***E***; IAA, 2 mM, ***F***) for 20 minutes before maximal ATP depletion was induced using an ATP depletion cocktail containing all four drugs at equivalent concentrations. Data presented are mean % ATP ± S.E.M, n=1-9 for all conditions. Comparisons were made between KIC or galactose-cultured cells and glucose-cultured cells at 0, 5, 10, 15 and 20 minutes drug treatment using a two-way ANOVA with post hoc Bonferroni test for multiple comparisons. ***** denotes significance for galactose-cultured cells, while † denotes significance for KIC-cultured cells. *, p<0.05; **, p<0.01; ***, p<0.001.

KIC and galactose-cultured cells exhibited a marked attenuation in the IAA-induced ATP depletion in contrast to glucose-cultured cells. Treatment with 2mM IAA resulted in significantly less ATP depletion in galactose-cultured cells at 10 (33 ± 29 %, n=5, P<0.05, Figure 3.3F) 15 (62 ± 14 %, n=5, P<0.001, Figure 3.3F) and 20 minutes (48 ± 17 %, n=5, P<0.001, Figure 3.3F) compared to glucose-cultured cells (10 minutes, 48 ± 8 %, n=13; 15 minutes, 17 ± 5 %, n=13; 20 minutes, 7 ± 3 %, n=13, Figure 3.3F). Similar effects were observed with KIC-cultured cells treated with IAA compared to glucose-cultured counterparts, however this could not be compared statistically due to the small sample size for this condition (n=2, Figure 3.3F). Interestingly, however, 2-DG (10 mM) appeared to have minimal effects in glucose cultured cells but induced significantly greater ATP depletion in galactose-cultured cells at 10 (33 ± 12 %, n=6, P<0.05, Figure 3.3E) 15 (27 ± 8 %, n=6, P<0.0001, Figure 3.3E) and 20 minutes (6 ± 3 %, n=6, P<0.0001, Figure 3.3E) compared to glucose-cultured cells (10 minutes, 95 ± 2 %, n=6; 15 minutes, 90 ± 4 %, n=6; 20 minutes, 86 ± 6 %, n=6, Figure 3.3E). Similar effects were observed with KIC-cultured cells treated with 2DG compared to glucose-cultured counterparts, however once again this could not be compared statistically due to the small sample size for this condition (n=2, Figure 3.3E). Initially, these observations seemed to be the complete opposite to what was expected according to our hypothesis. However, we reasoned that 2-DG may compete with glucose for uptake via GLUT transporters and thus may take much longer to accumulate and inhibit hexokinase at this concentration.

Taken together, the data obtained from the luciferase and GO-ATeam ATP assays are broadly in line with the notion that long-term culture in glucose free medium containing either 10 mM galactose or 2 mM KIC reverses the sensitivity of PDAC cells to ATP depletion by glycolytic and mitochondrial inhibitors, indicating that a ‘switch’ towards mitochondrial metabolism can be successfully achieved with these culture conditions.

3.4.3 - Mitochondrial and glycolytic metabolism are altered in galactose or KIC cultured cells

Since culture in KIC and galactose resulted in a switch in sensitivity to metabolic inhibitors with respect to ATP depletion, we employed an XFe96 extracellular flux analyser (Seahorse Bioscience) to assess for changes in mitochondrial and glycolytic metabolism within these cells in comparison to glucose-cultured cells. The O_2 consumption rate (OCR) and extracellular acidification rate (ECAR) exhibited by glucose, galactose and KIC cultured MIA PaCa-2 cells were measured following various pharmacological treatments to measure the key components of mitochondrial and glycolytic metabolism.

We first performed an XF Cell Mito Stress Test, depicted in Figure 3.4C. Briefly, this assay employs oligomycin (1 µM) to reveal ATP-linked O_2 consumption, followed by FCCP (0.5 µM) to uncouple the mitochondria and determine the maximal mitochondrial respiration rate and the spare respiratory capacity. All mitochondrial respiration is then inhibited by applying a combination of rotenone (Rot, 1 µM) and AM (1 µM), revealing the non-mitochondrial O_2

consumption. From these values, OM-insensitive mitochondrial respiration, or proton leak, (across the mitochondrial inner membrane, which generates heat rather than ATP) can be determined. Following these measurements, OCR and ECAR measurements were normalised to protein using a sulforhodamine B assay (measured in absorbance units, AU). Basal respiration, ATP production, mitochondrial proton leak, and maximal respiration rate were then calculated (see Figure 3.4C and *3.3.5 – Extracellular flux measurements*).

Figures 3.4A and 3.4B present the OCR and ECAR traces for all three culture types following the XF Cell Mito Stress Test. Average data for the mitochondrial stress test parameters is presented in Figure 3.4D. Compared to the basal respiration exhibited by their glucose-cultured counterparts (52 ± 1 pmol/min/AU, n=15), both galactose and KIC-cultured cells exhibited a significant decrease in basal OCR (galactose, 7 ± 1 pmol/min/AU, P<0.0001, n=16; KIC, 40 ± 1 pmol/min/AU, P<0.0001, n=14). Blockade of the mitochondrial F_1/F_0 ATP synthase with OM (1 µM) revealed ATP production-linked OCR, which was significantly lower in both galactose (3 ± 0 pmol/min/AU, P<0.0001, n=16) and KIC cells (29 ± 1 pmol/min/AU, P<0.0001, n=14) compared to glucose-cultured cells (41 ± 1 pmol/min/AU, n=15). Subsequently, treatment with FCCP (0.5 µM) revealed the spare respiratory capacity, which when compared to glucose-cultured cells (30 ± 2 pmol/min/AU, n=15) was significantly decreased in both galactose (5 ± 1 pmol/min/AU, P<0.0001, n=16) and KIC-cultured cells (6 ± 3 pmol/min/AU, P<0.0001, n=14). Following cessation of all mitochondrial respiration using a combination dose of Rot and AM (1 µM each), only in galactose cells was there a significant change in proton leak-linked OCR. Compared to glucose-cultured cells (11 ± 0 pmol/min/AU, n=15), proton leak-linked OCR was significantly decreased in galactose-cultured cells (4 ± 0 pmol/min/AU, P<0.0001, n=16); no difference was observed in KIC-cultured cells (11 ± 0 pmol/min/AU, n=14).

Surprisingly, these results indicated that glucose-cultured MIA PaCa-2 cells exhibit a higher basal OCR, and consumed more O_2 for ATP generation than galactose or KIC cultured cells. Furthermore, glucose-cultured cells had a greater spare respiratory capacity than their galactose and KIC-cultured counterparts. These data suggest that despite the highly glycolytic phenotype, glucose-cultured cells still retain functional mitochondria. However, despite this apparent decline in mitochondrial respiration rate in galactose and KIC-cultured cells, basal ECAR in these cells was significantly decreased (Figure 3.4B). Compared to glucose-cultured cells (44 ± 2 mpH/min/AU, n=15) the ECAR at the third basal timepoint was significantly lower in cells cultured in galactose (5 ± 1 mpH/min/AU, n=15, P<0.0001, Figure 3.4E) and KIC (9 ± 1 mpH/min/AU, n=14, P<0.0001, Figure 3.4E). Moreover, an ECAR vs OCR plot (Figure 3.4F) revealed that the basal metabolic phenotype of MIA PaCa-2 cells following culture in galactose or KIC (again taken from the third basal timepoint) had indeed shifted from a highly glycolytic phenotype to one exhibiting low glycolytic flux, despite slowed OCR. Interestingly, the KIC cells maintained a relatively high basal OCR despite exhibiting a significantly decreased ECAR. This is not surprising, since KIC is metabolised entirely within the mitochondria and is converted to mitochondrial substrates such as α-ketoglutarate (Lenzen et al., 1985, Malaisse et al., 1981) and acetyl-CoA (Noda and Ichihara, 1974, MacDonald et al., 2005). However, galactose-

cultured cells exhibited a significantly lowered overall metabolism (OCR and ECAR), which is likely due to galactose entering glycolysis from the Leloir pathway at a slower rate than glucose enters glycolysis (Bustamante and Pedersen, 1977).

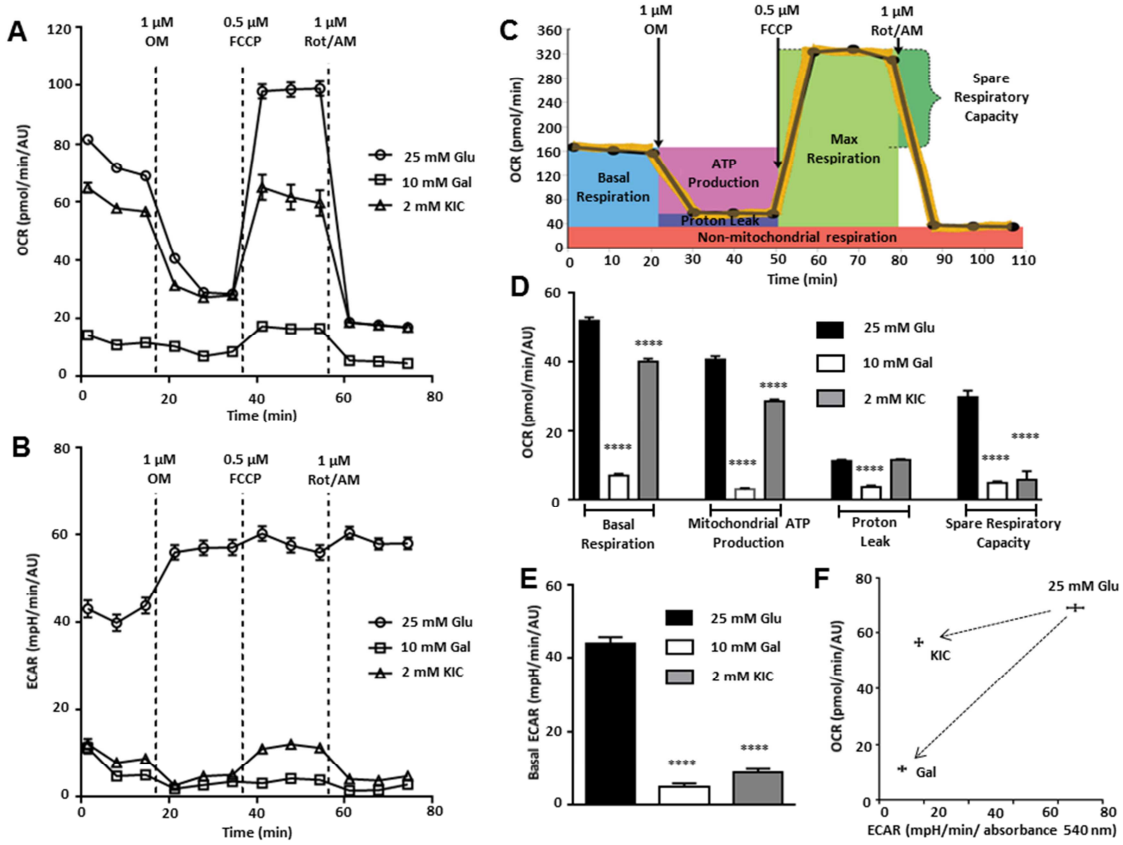

Figure 3.4 - MIA PaCa-2 cells cultured in galactose or KIC exhibit alterations in mitochondrial and glycolytic metabolism and a slowed growth rate compared to glucose-cultured cells

MIA PaCa-2 cells were cultured in standard media containing glucose (Glu, 25 mM) or nominal glucose-free media containing galactose (10 mM Gal) and KIC (2 mM) for a minimum of 3 passages and 21 days. Cells were then assayed using an XFe96 extracellular flux analyser performing an XF Cell Mito Stress Test. This assay involved the sequential addition of oligomycin (OM, 1 µM), FCCP (0.5 µM) and a combination dose of rotenone and antimycin A (Rot/AM, both 1 µM) to reveal the various components of mitochondrial metabolism. O_2 consumption rate (OCR, ***A***) and extracellular acidification rate (ECAR, ***B***) were measured in glucose (open circles), galactose (open squares) and KIC (open triangles) throughout the XF Mito Stress Test. ***C*** – Cartoon (supplied by Seahorse Bioscience) depicting a typical XF Mito Stress Test and accompanying measurement of mitochondrial metabolic parameters. All calculations were made using the third baseline measurement and the third measurement post-addition of each drug. ***D*** – Mean ± SEM measurements from one experiment for each metabolic parameter in glucose (n=15) galactose (n=16) and KIC (n=14). ***E*** – Mean ± SEM basal ECAR in measurements from the third basal measurement in glucose (n=15) galactose (n=15) and KIC (n=14). ***F -*** OCR vs ECAR plot of pooled baseline measurements (mean ± SEM) prior to the addition of OM for glucose (n=45), galactose (n=48) and KIC-cultured cells (n=42) indicates changes in basal metabolism. All measurements were normalised to protein content using a sulforhodamine B assay for protein content, measured in absorbance units (AU). *, p<0.05;**, p <0.01; ***, p <0.001; ****, p<0.0001, all statistical comparisons made between galactose or KIC-cultured cells and glucose-cultured cells (one-way ANOVA with post-hoc Bonferroni test for multiple comparisons).

In the mitochondrial stress test, blockade of mitochondrial ATP generation with OM in glucose-cultured cells resulted in compensatory increase in ECAR, presumably to maintain ATP, as evidenced by a corresponding increase in ECAR upon addition of OM (Figure 3.4B). Crucially, this was absent from galactose or KIC-cultured cells, suggesting these cells could not compensate for blockade of mitochondrial ATP synthesis and are more reliant on mitochondrial metabolism to meet their ATP demands. However, we did not know whether the absent compensatory increase in ECAR could be solely attributed to the absence of glucose, or whether a functional change in the glycolytic capacity of galactose and KIC-cultured cells contributed. To resolve this, we next performed a glycolysis stress test to see whether culture in galactose or KIC affected the ability of MIA PaCa-2 cells to utilise glucose as a substrate for glycolysis upon its readdition. Briefly, this assay (Figure 3.5C) involved starving the cells of all substrates for 2 hours, at which point cells were supplemented with glucose (10 mM) to reveal basal glycolytic rate, measured as ECAR. Mitochondrial respiration was then blocked using OM (1 µM) to reveal the glycolytic reserve capacity, followed by application of 2-DG (100 mM) to block all glycolytic flux. ECAR and OCR values were normalised to protein content as with the mitochondrial stress test, and the glycolytic parameters calculated from the ECAR measurements were basal glycolytic rate, maximum glycolytic capacity and glycolytic reserve (See Figure 3.5C). Differences between glucose and galactose or KIC cultured cells were assessed using a one-way ANOVA with post-hoc Bonferroni test for multiple comparisons.

Figures 3.5A and 3.5B present the OCR and ECAR traces for all three culture types following the XF Glycolysis Stress Test. Following addition of 10 mM glucose, all cells from each culture condition exhibited a sharp increase in ECAR that represented the basal glycolytic rate. No significant difference in basal glycolytic ECAR was observed between glucose-cultured cells (33 ± 2 mpH/min/AU, n=8, Figure 3.5D) and either galactose (30 ± 1 mpH/min/AU, n=8, Figure 3.5D) or KIC-cultured cells (33 ± 1 mpH/min/AU, n=6, Figure 3.5D). However, while maximum glycolytic capacity was significantly reduced in galactose-cultured cells (31 ± 1, mpH/min/AU, n=8, $P<0.0001$, Figure 3.5D) compared to glucose-cultured cells (44 ± 2, mpH/min/AU, n=8, Figure 3.5D), a modest but significant increase in maximum glycolytic capacity was observed in KIC-cultured cells (51 ± 2, mpH/min/AU, n=6, $P<0.05$, Figure 3.5D). This was reflected in the spare glycolytic capacity, which was significantly increased in KIC-cultured cells (19 ± 1, mpH/min/AU, n=6, $P<0.0001$, Figure 3.5D) and decreased in galactose-cultured cells (1 ± 0 mpH/min/AU, n=8, $P<0.0001$, Figure 3.4D) compared to glucose-cultured cells (12 ± 0 mpH/min/AU, n=8, Figure 3.5D). Thus, while galactose and KIC-cultured cells exhibited a decreased ECAR in the XF Cell Mito Stress Test, these data suggest that these cells largely retained their ability to utilise glycolysis upon exposure to glucose, although their maximal glycolytic capacity was affected. Importantly, following OM treatment, the absence of a reserve glycolytic capacity in the galactose cells even in the presence of glucose (Figure 3.5B and 3.5D) suggests that these cells cannot utilise glycolysis as efficiently as glucose-cultured cells.

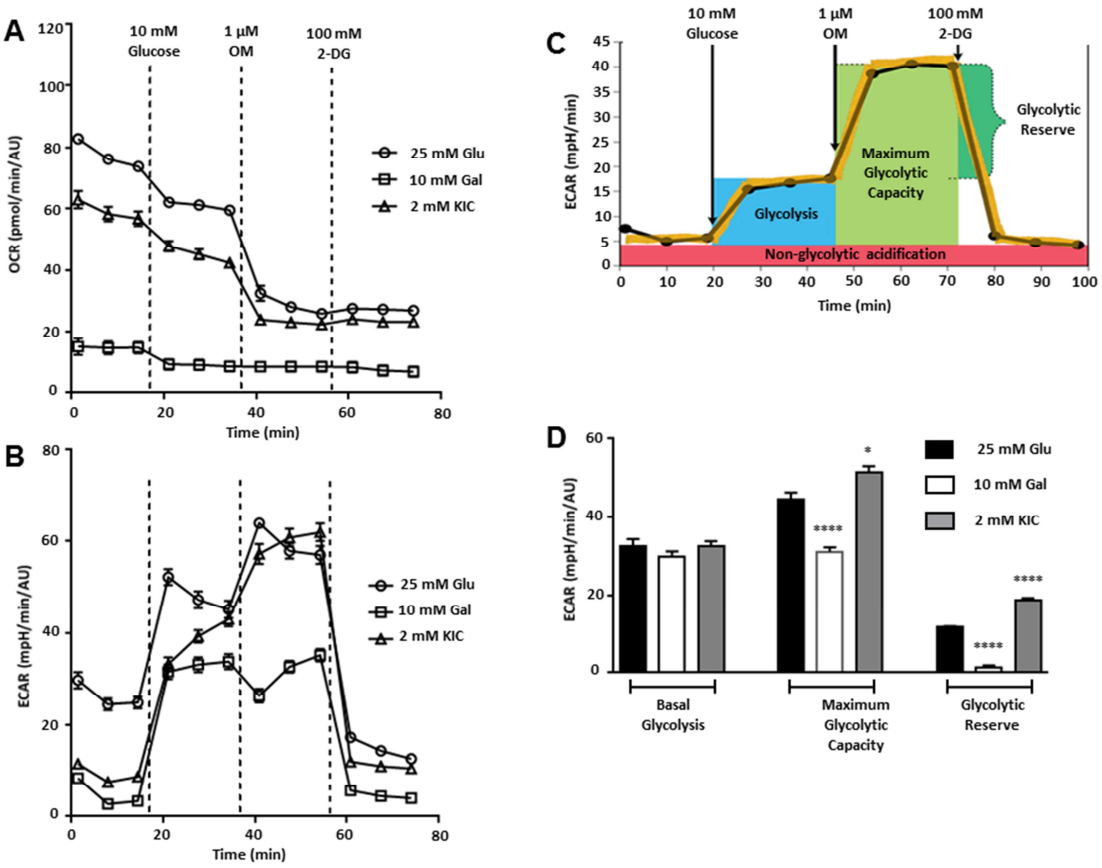

Figure 3.5 - MIA PaCa-2 cells cultured in galactose or KIC exhibit functional glycolysis

MIA PaCa-2 cells were cultured in standard media containing glucose (Glu, 25 mM) or nominal glucose-free media containing galactose (10 mM Gal) and KIC (2 mM) for a minimum of 3 passages and 21 days. Cells were then assayed using an XFe96 extracellular flux analyser performing an XF Glycolysis Stress Test. This assay involved the sequential addition of glucose (10 mM), oligomycin (OM, 1 µM) and 2-deoxyglucose (2-DG, 100 mM) to reveal the various components of glycolytic metabolism. Extracellular acidification rate (ECAR, ***A***) and O_2 consumption rate (OCR, ***B***) were measured in glucose (open circles), galactose (open squares) and KIC (open triangles) throughout the XF Glycolysis Stress Test. ***C*** – Cartoon (supplied by Seahorse Bioscience) depicting a typical XF Glycolysis Stress Test and accompanying measurement of mitochondrial metabolic parameters. All calculations were made using the third baseline measurement and the third measurement post-addition of each drug. ***D*** – Mean ± SEM measurements from one experiment for each metabolic parameter in glucose (n=7) galactose (n=8) and KIC (n=6). All measurements were normalised to protein content using a sulforhodamine B assay for protein content, measured in absorbance units (AU). *, p<0.05;**, p <0.01; ***, p <0.001; ****, p<0.0001, all statistical comparisons made between galactose or KIC-cultured cells and glucose-cultured cells (one-way ANOVA with post-hoc Bonferroni test for multiple comparisons).

3.4.4 - Culture of MIA PaCa-2 cells in galactose or KIC attenuates the effects of IAA on resting $[Ca^{2+}]_i$

Since culturing PDAC cells in either galactose or KIC resulted in an apparent switch in their metabolic phenotype from a highly glycolytic phenotype to one more reliant on mitochondrial metabolism, we next wanted to assess whether this could be translated to the effects of both glycolytic and mitochondrial inhibitors on resting $[Ca^{2+}]_i$ in these cells. We have previously shown that glucose-cultured PDAC cells exhibit an irreversible $[Ca^{2+}]_i$ overload in response to glycolytic inhibitors, while mitochondrial inhibitors had no effect. We speculated that this $[Ca^{2+}]_i$ overload was due to ATP depletion, and in the present study hypothesised that the reversal in the sensitivity of our galactose and KIC-cultured PDAC cells to ATP depletion by metabolic inhibitors (Figures 3.2 and 3.3) might result in a corresponding reversal in the $[Ca^{2+}]_i$ overload response.

To measure $[Ca^{2+}]_i$ we employed fura-2 fluorescence imaging in cells continuously perfused with HEPES-PSS. Due to the reversal of their effects on ATP observed in the previous assays, OM (10 µM), AM (0.5 µM), IAA (2 mM) and BrPy (500 mM) were selected for use in our resting $[Ca^{2+}]_i$ assays. Metabolic inhibitors were applied for 20 minutes, followed by 15 minutes washout and a subsequent treatment with ATP (100 µM) to activate a purinergic receptor-induced $[Ca^{2+}]_i$ response, thereby testing for post-treatment recovery. Cells eliciting an increase in $[Ca^{2+}]_i$ of 100nM or greater in response to ATP were considered viable. To quantify $[Ca^{2+}]_i$ overload responses, the area under the curve (AUC) and the maximum increase in $[Ca^{2+}]_i$ (max-$\Delta[Ca^{2+}]_i$) were measured during the initial 20 minute treatment period. Differences between treatment groups were assessed using a Kruskal-Wallis test with a post-hoc Dunn's test or a one-way ANOVA with a post hoc Bonferroni test.

These experiments revealed a partial reversal in the sensitivity of MIA PaCa-2 cells to glycolytic and mitochondrial inhibitors with respect to $[Ca^{2+}]_i$ overload. Galactose and KIC-cultured MIA PaCa-2 cells exhibited dramatically reduced $[Ca^{2+}]_i$ overload responses following treatment with glycolytic inhibitors compared to those in their glucose-cultured counterparts. Galactose cultured MIA PaCa-2 cells treated with IAA (Figure 3.6Biii) exhibited a reduced AUC (27 ± 5 µM.s, n=12, Figure 3.5C) and max-$\Delta[Ca^{2+}]_i$ (76 ± 11 nM, n=12, Figure 3.6D) compared to glucose-cultured cells (Figures 3.6Aiii, 3.6C and 3.6D. AUC, 195 + 27 µM.s, P<0.0001, n=6; max-$\Delta[Ca^{2+}]_i$, 299 ± 34 nM, P<0.0001, n=6). Similarly, KIC-cultured cells treated with IAA (Figure 3.7Biii) also exhibited a significantly smaller AUC (21 ± 5 µM.s, n=5, Figure 3.7C) and max-$\Delta[Ca^{2+}]_i$ (46 ± 13nM, n=5, Figure 3.7D) compared to glucose-cultured cells (Figures 3.7Aiii, 3.7C and 3.7D. AUC, 195 ± 29 µM.s, P<0.001, n=6; max-$\Delta[Ca^{2+}]_i$, 299 ± 34 nM, P<0.0001, n=6). However, no significant difference in AUC or max-$\Delta[Ca^{2+}]_i$ was found between galactose-cultured and glucose-cultured cells treated with BrPy (Figures 3.6Aiv, 3.6Biv, 3.6C and 3.6D). On the other hand, KIC-cultured cells exhibited significantly smaller $[Ca^{2+}]_i$, responses following BrPy treatment (Figures 3.7Biv, 3.7C and 3.7D. AUC, 68 ± 22 µM.s, n=4; max-$\Delta[Ca^{2+}]_i$, 175 ± 34 nM, n=4) in comparison to glucose-cultured cells (Figures 3.7Aiv, 3.7C and 3.7D. AUC, 285

± 46 µM.s, P<0.0001, n=6; max-Δ[Ca^{2+}]$_i$, 587 ± 86 nM, P<0.0001, n=6). However, no differences were observed in the effects of OM or AM on resting [Ca^{2+}]$_i$ between either galactose (OM, n=8; AM, n=10; Figures 3.6Bi and 3.6Bii) or KIC-cultured cells (OM, n=5; AM, n=4; Figures 3.7Bi and 3.7Bii) and glucose cultured MIA PaCa-2 cells (AM, n=7; OM, n=5; Figures 3.6Ai, 3.6Aii, 3.7Ai, 3.7Aii), as measured by max-Δ[Ca^{2+}]$_i$ and AUC (galactose, 3.6C and 3.6D; KIC, Figures 3.7C and 3.7D).

Responses to ATP following treatment to mitochondrial inhibitors were also significantly decreased in KIC cultured cells; a decrease in post-treatment recovery was observed in KIC-cultured cells treated with AM (0 ± 0 %, n=4, Figure 3.7E) compared to their glucose-cultured counterparts (81 ± 12 %, P<0.01, n=7, Figure 3.7E). However, no significant difference in post-treatment ATP response was observed between KIC or galactose cultured cells and glucose-cultured cells in any of the other treatment groups.

Despite the lack of effect of mitochondrial inhibitors on resting [Ca^{2+}]$_i$ in KIC and galactose-cultured MIA PaCa-2 cells, the reduced [Ca^{2+}]$_i$ overload responses following glycolytic inhibition supports the hypothesis that ATP derived from glycolysis is crucial for maintenance of a low resting [Ca^{2+}]$_i$. in highly glycolytic MIA PaCa-2 cells.

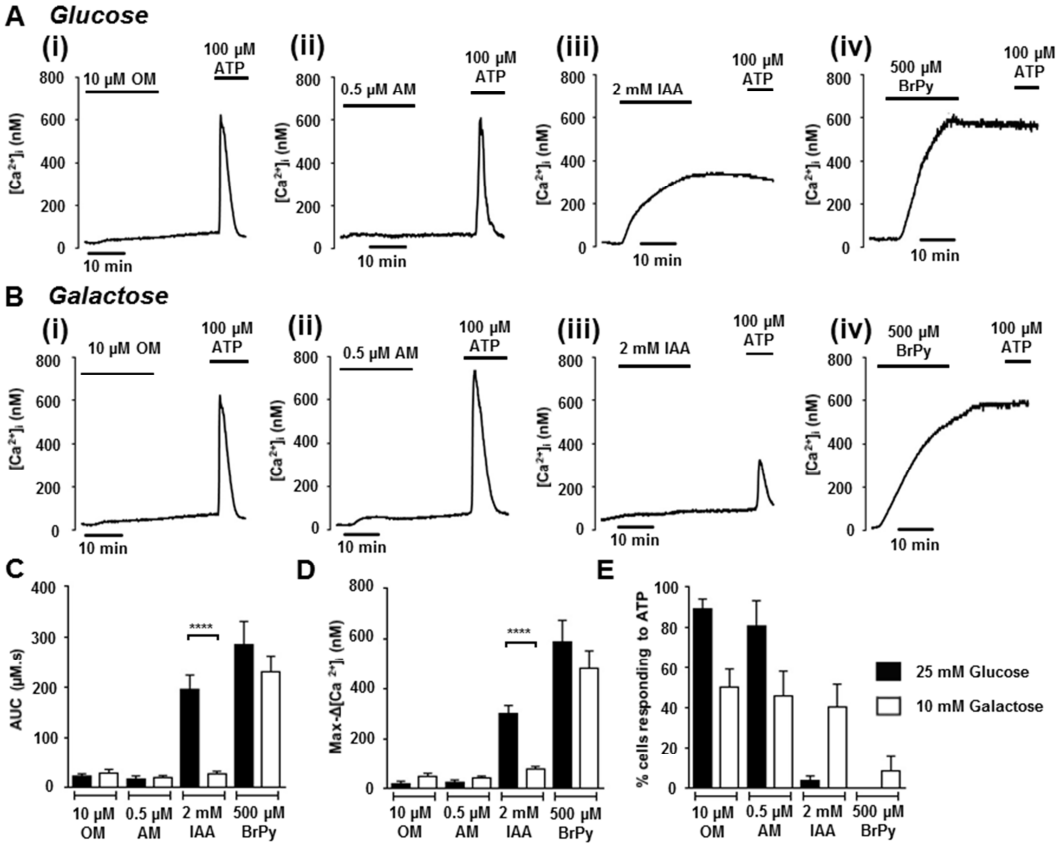

Figure 3.6 - Culture of MIA PaCa-2 cells in 10 mM galactose attenuates the effects of IAA on resting $[Ca^{2+}]_i$

MIA PaCa-2 cells were cultured in standard Dulbecco's modified Eagle's medium containing glucose (25 mM) or nominal glucose-free media containing 10 mM galactose for a minimum of 3 passages and 21 days. Using fura-2 fluorescence imaging, $[Ca^{2+}]_i$ concentration was measured while cells were treated for 20 min with various metabolic inhibitors, followed by 15 minutes washout and subsequent stimulation with the purinergic agonist, ATP (100 μM) to test for cell viability. ***A -*** representative traces showing the effects of mitochondrial (oligomycin, OM, 10 μM, **A(*i*)**; antimycin, AM, 0.5 μM, ***A(ii)***) or glycolytic inhibitors (iodoacetate, IAA, 2 mM, ***A(iii)***; 3-bromopyruvate, BrPy, 500 μM, ***A(iv)***) on resting $[Ca^{2+}]_i$ in glucose-cultured cells. ***B -*** representative traces showing the effects of mitochondrial (OM, 10 μM, **B(*i*)**; AM, 0.5 μM, ***B(ii)***) or glycolytic inhibitors (IAA, 2 mM, ***B(iii)***; BrPy, 500 μM, ***B(iv)***) on resting $[Ca^{2+}]_i$ in galactose-cultured cells. Responses were quantified by measuring the area under the curve (AUC, ***C***) for the 20-min treatment with drug and maximum change in $[Ca^{2+}]_i$ during this period (Max-$\Delta[Ca^{2+}]_i$, ***D***). Recovery from metabolic inhibitor treatment was assessed by measuring the % cells that subsequently responded to ATP ($\Delta[Ca^{2+}]_i$>100 nM, ***E***). Data presented are mean % ATP ± S.E.M, n=6-12 for all conditions. *,p<0.05; **,p<0.01; ***,p<0.001; ****, p<0.0001 (***C*** and ***D***, one-way ANOVA with post-hoc Bonferroni test for multiple comparisons; ***E***, Kruskal-Wallis test with post-hoc Dunn's test for multiple comparisons).

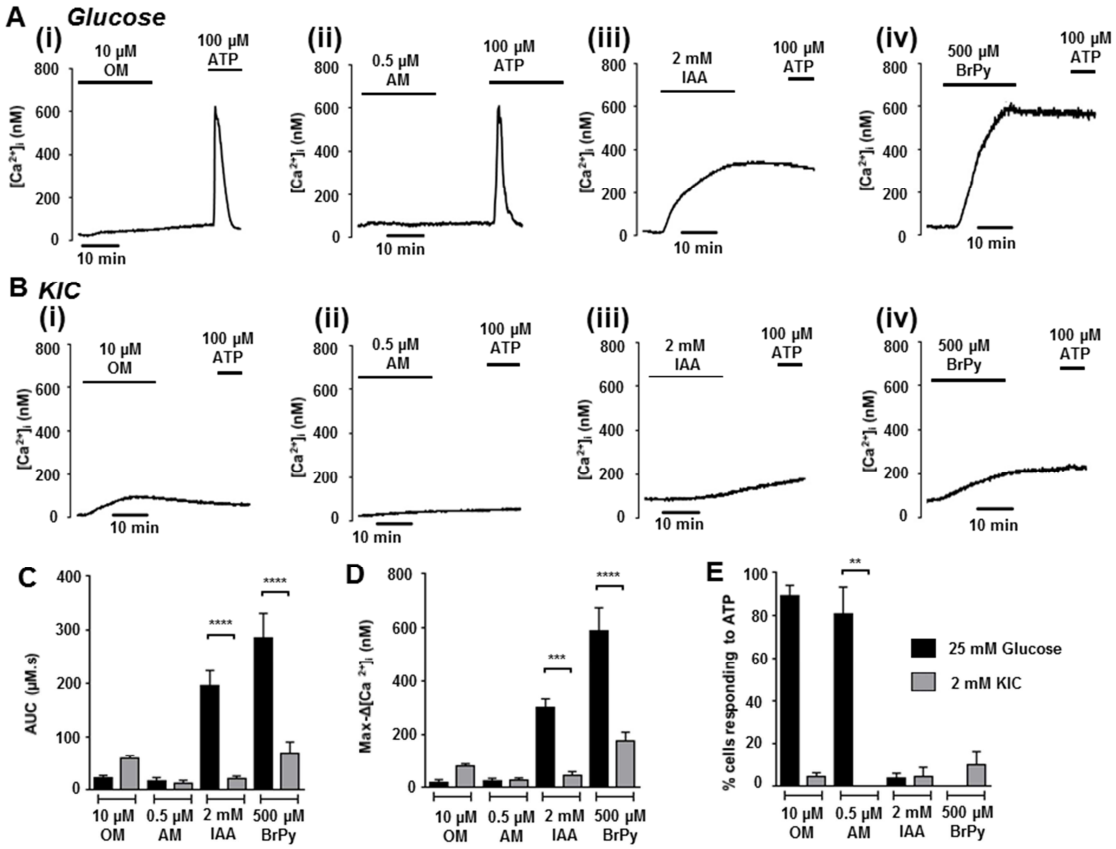

Figure 3.7 - Culture of MIA PaCa-2 cells in 2 mM KIC attenuates the effects of IAA on resting $[Ca^{2+}]_i$

MIA PaCa-2 cells were cultured in standard media containing glucose (25 mM) or nominal glucose-free media containing KIC (2 mM) for a minimum of 3 passages and 21 days. Using fura-2 fluorescence imaging, $[Ca^{2+}]_i$ concentration was measured while cells were treated for 20 min with various metabolic inhibitors, followed by 15 minutes washout and subsequent stimulation with the purinergic agonist, ATP (100 µM) to test for cell viability. ***A -*** representative traces showing the effects of mitochondrial (oligomycin, OM, 10 µM ***A(i)***; antimycin A, AM, 0.5 µM, ***A(ii)***) or a glycolytic inhibitors (iodoacetate, IAA, 2 mM, ***A(iii)***; 3-bromopyruvate, BrPy, 500 µM, ***A(iv)***) on resting $[Ca^{2+}]_i$ in glucose-cultured cells. ***B -*** representative traces showing the effects of mitochondrial (oligomycin, OM, 10 µM ***B(i)***; AM, 0.5 µM, ***B(ii)***) or a glycolytic inhibitors (IAA, 2 mM, ***B(iii)***; BrPy, 500 µM, ***B(iv)***) on resting $[Ca^{2+}]_i$ in KIC-cultured cells. Responses were quantified by measuring the area under the curve (AUC, ***C***) for the 20-min treatment with drug and maximum change in $[Ca^{2+}]_i$ during this period (Max-$\Delta[Ca^{2+}]_i$, ***D***). Recovery from metabolic inhibitor treatment was assessed by measuring the % cells that subsequently responded to ATP ($\Delta[Ca^{2+}]_i$>100 nM, ***E***). *,p<0.05; **,p<0.01; ***,p<0.001; ****, p<0.0001 (***C*** and ***D***, one-way ANOVA with post hoc Bonferroni test for multiple comparisons; ***E***, Kruskal-Wallis test with post hoc Dunn's test for multiple comparisons). Data presented are mean % ATP ± S.E.M, n=4-7 for all conditions.

3.4.5 - IAA-induced inhibition of the PMCA is attenuated in galactose and KIC-cultured PDAC cells

Our previous study demonstrated that inhibitors of glycolytic metabolism compromise $[Ca^{2+}]_i$ clearance, and therefore inhibit PMCA activity (*Chapter 2*, James et al., 2013). Following on from this work, we wanted to test whether KIC or galactose-cultured PDAC cells were less sensitive to glycolytic inhibitor-induced inhibition of the PMCA by using our *in situ* $[Ca^{2+}]_i$ clearance assay. To test this, we selected IAA (2 mM), since its effects on ATP and resting $[Ca^{2+}]_i$ in PDAC cells were profoundly attenuated following their culture in nominal-glucose free media supplemented with galactose or KIC.

To measure PMCA activity we employed an *in situ* $[Ca^{2+}]_i$ clearance assay in which functionally and pharmacologically isolated PMCA activity can be measured (Mankad et al., 2012). This approach was modified in our more recent study to eliminate metabolic inhibitor-induced attenuation of store operated Ca^{2+} entry (SOCE) and thus the steady-state $[Ca^{2+}]_i$ from which $[Ca^{2+}]_i$ clearance can be measured (James et al., 2013). In this previous study we also established that the PMCA is the major Ca^{2+} efflux pathway in PANC-1 and MIA PaCa-2 cell lines and that this *in situ* $[Ca^{2+}]_i$ clearance assay reflects PMCA activity. Briefly, cells were treated with cyclopiazonic acid (CPA) in the absence of extracellular Ca^{2+} and the presence of 1 mM EGTA to inhibit the sarcoplasmic/endoplasmic reticulum Ca^{2+} ATPase (SERCA), resulting in a transient increase in $[Ca^{2+}]_i$ as the ER Ca^{2+} stores depleted. This caused SOCE upon perfusion with 20 mM Ca^{2+}, and at the peak of $[Ca^{2+}]_i$ increase 1 mM La^{3+} in a Ca^{2+}-free/EGTA free solution was applied to inhibit both Ca^{2+} influx and efflux and "clamp" $[Ca^{2+}]_i$ high within the cell for 5 minutes. The inhibition of Ca^{2+} efflux by La^{3+} was rapidly removed by the addition of 1 mM EGTA to rapidly chelate all La^{3+}, resulting in rapid $[Ca^{2+}]_i$ clearance via the PMCA. This influx/clearance phase was repeated a second time in the presence or absence of metabolic inhibitors, thereby adopting a paired experimental design to control for cell-to-cell variability. By applying metabolic inhibitors at the peak of the $[Ca^{2+}]_i$ response for a sufficient period of time (5 minutes) rather than prior to addition of 20 mM Ca^{2+}, this approach isolated the effects of test reagents on $[Ca^{2+}]_i$ clearance and eliminated the confounding effects of test reagent inhibition of SOCE, which would otherwise result in a significantly reduced $[Ca^{2+}]_i$ plateau from which to measure $[Ca^{2+}]_i$ clearance rate. $[Ca^{2+}]_i$ clearance was quantified by measuring the linear clearance rate over 60 seconds from the same starting fura-2 value in both phases. The clearance rate during the second clearance phase was then normalised to that of the first (%). Similarly, relative recovery was measured by normalising (%) the degree of recovery achieved during the second clearance phase to that of the first (see *3.8.1 – Measurement of relative recovery of $[Ca^{2+}]_i$ during in situ $[Ca^{2+}]_i$ clearance assays*), again from the same fura-2 ratio value. All statistical comparisons were performed using a Mann Whitney U test.

In control galactose-cultured cells (Figure 3.8Bi), $[Ca^{2+}]_i$ clearance rate was significantly slowed during the second clearance phase (68 ± 6%, n=5, $P<0.05$, Figure 3.8D) compared to glucose-cultured cells (91 ± 5 %, n=9, Figure 3.8Ai). Relative recovery was also lower in control

galactose cultured cells (90 ± 3%, P<0.05, n=5) compared to control glucose-cultured cells (107 ± 4%, n=9, Figure 3.8E). However, no significant differences in $[Ca^{2+}]_i$ clearance rate or relative recovery were found between control KIC (Figure 3.8Ci) and control glucose-cultured cells (Figure 3.8Ai, 3.8D and 8E), suggesting that metabolism of KIC provides sufficient ATP to fuel the PMCA.

Despite our previous work indicating that IAA causes a significant decrease in $[Ca^{2+}]_i$ clearance rate in glucose-cultured MIA PaCa-2 cells (see *Chapter 2*, James et al., 2013), IAA had no effect on $[Ca^{2+}]_i$ clearance rate in galactose-cultured MIA PaCa-2 cells (Figures 3.8Bi, 3.8Bii and 3.8D). Similarly, IAA had no effect on $[Ca^{2+}]_i$ clearance rate in KIC-cultured cells (Figures 3.8Ci, 3.8Cii and 3.8D). In contrast, consistent with our previous study, IAA treatment induced a profound decrease in $[Ca^{2+}]_i$ clearance rate in glucose-cultured cells (45 ± 5%, n=11, Figure 3.8Aii) compared to untreated control cells (91 ± 5%, n=9, P<0.0001, Figures 3.8Ai and 3.8D). Furthermore, relative $[Ca^{2+}]_i$ clearance rate during the second $[Ca^{2+}]_i$ clearance phase was actually significantly higher in IAA-treated galactose (69 ± 2%, n=5, P<0.05) and KIC-cultured cells (81 ± 7%, n=4, P<0.05) than that in the IAA-treated glucose-cultured cells (Figure 3.8E).

In addition to IAA having no effect on $[Ca^{2+}]_i$ clearance in galactose or KIC-cultured cells, IAA treatment also had no effect on recovery during the second influx/clearance phase relative to the first when compared to untreated control cells (Figure 3.8E). However, IAA significantly attenuated relative recovery in glucose-cultured cells (72 ±3%, n=11, Figure 3.8E) compared to untreated glucose-cultured cells (107 ± 4%, n=9, P<0.0001, Figure 3.8E). Furthermore, similar to $[Ca^{2+}]_i$ clearance rate, relative recovery was significantly higher in IAA-treated galactose (91 ± 1%, n=5, P<0.001) and KIC-cultured cells (91 ± 4%, n=4, P<0.01) than that in IAA-treated glucose-cultured cells (72 ± 3%, n=11, Figure 3.8E).

Taken together, these data indicate that despite a progressive time-dependent run-down in $[Ca^{2+}]_i$ clearance rate (and thus PMCA activity), galactose and KIC-cultured MIA PaCa-2 cells become effectively resistant to the PMCA inhibition by IAA. In light of the previous results described in the present study, this is likely due to cytosolic ATP levels being preserved in the face of glycolytic inhibition due to a switch towards mitochondrial metabolism and a decreased reliance on glycolysis in KIC and galactose-cultured MIA PaCa-2 cells.

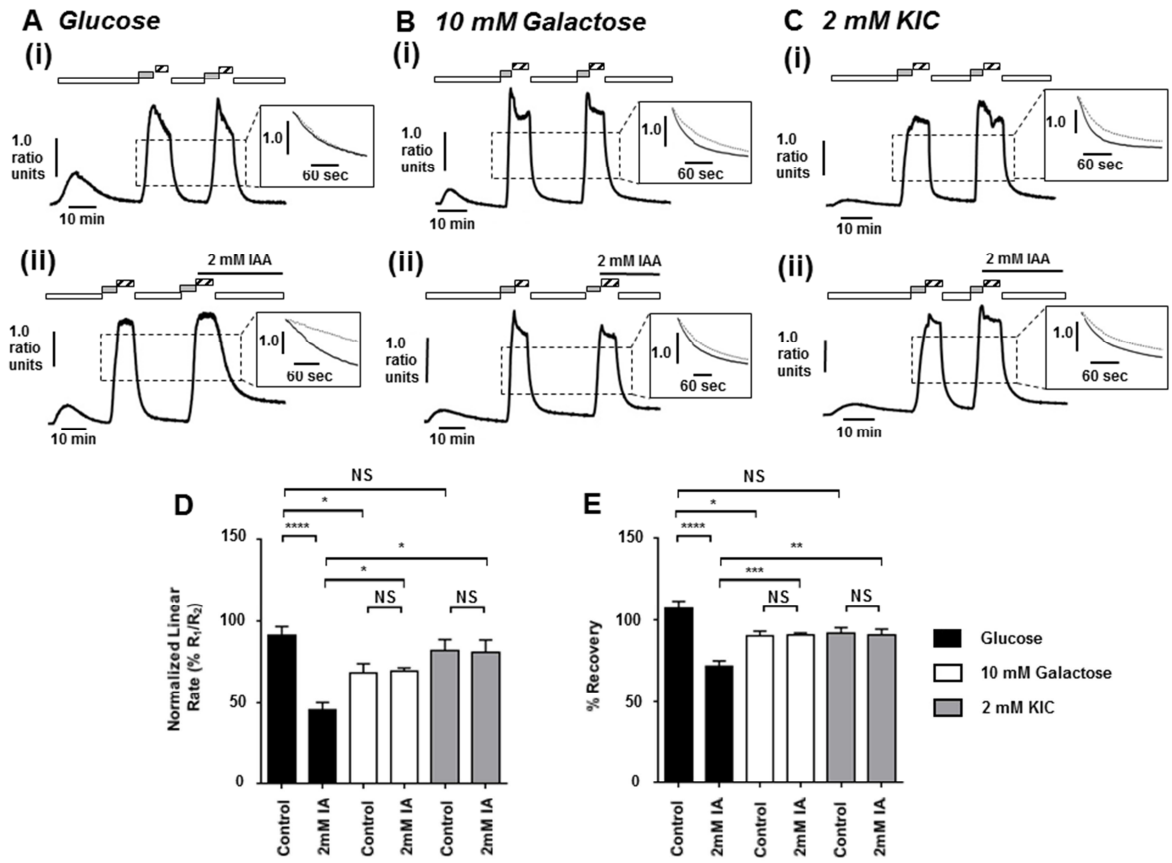

Figure 3.8 - IAA-induced inhibition of the PMCA is attenuated in galactose and KIC-cultured PDAC cells.

A – C, representative traces showing the *in situ* $[Ca^{2+}]_i$ clearance assay (PMCA activity) in fura-2-loaded MIA PaCa-2 cells that had been grown in either glucose-containing (25 mM, ***Ai***) or nominal glucose-free media supplemented with 10 mM galactose (***Bi***) or 2 mM KIC (***Ci***) for a minimum of 3 passages and 21 days. CPA (30 µM) was applied in the absence of external Ca^{2+} with 1 mM EGTA (white box) or 20 mM Ca^{2+} (grey box) to induce store-operated Ca^{2+} influx. 1 mM La^{3+} was then applied at the peak of Ca^{2+} influx (striped box). Subsequent removal of external La^{3+} with 1 mM EGTA after 5 min allowed $[Ca^{2+}]_i$ clearance. This influx-clearance phase was repeated either in the presence of absence of 2 mM IAA. Ca^{2+} influx was induced before application of test reagents to isolate their effects on $[Ca^{2+}]_i$ clearance. Representative traces show the effects of IAA on $[Ca^{2+}]_i$ clearance in cells cultured in 25 mM glucose (***Aii***), 10 mM galactose (***Bii***) and 2 mM KIC (***Cii***). Each inset trace shows expanded time courses comparing the second clearance phase (grey trace) with the first (black trace). Linear clearance rate over 60 seconds during the second clearance phase was normalized to that of the first (% relative clearance). Relative recovery during the second clearance phase was normalized (%) to that of the first influx/clearance phase. Both clearance and recovery were calculated from a standardized $[Ca^{2+}]_i$ value. ***D***, mean normalized linear rate (± S.E.M.),. ***E***, mean recovery (± S.E.M.), n=4-12 for all conditions. *, p<0.05;**, p <0.01; ***, p <0.001; ****, p<0.0001 (Mann-Whitney *U* test), compared with control.

3.5 - Discussion

We have previously demonstrated that inhibition of glycolysis in cultured human PDAC cell lines (PANC-1 and MIA PaCa-2) results in ATP depletion and an inability to maintain a low resting $[Ca^{2+}]_i$ that is most likely due to inhibition of the PMCA (*Chapter 2*, James et al., 2013). To further interrogate the glycolytic ATP dependency of $[Ca^{2+}]_i$ regulation by the PMCA, the current study aimed to "switch" highly glycolytic MIA PaCa-2 cells towards mitochondrial metabolism by culturing in low glucose conditions supplemented with either galactose or α-ketoisocaproate (KIC). The relative sensitivity of these cells to mitochondrial and glycolytic inhibitors was then tested on a number of key functional readouts, including ATP depletion, oxygen consumption rate (OCR), extracellular acidification rate (ECAR), cytosolic $[Ca^{2+}]_i$ overload and PMCA activity. Culture in either 10 mM galactose or 2 mM KIC in nominal glucose-free conditions resulted in a marked decrease in proliferation rate and extracellular acidification rate, indicating that the Warburg phenotype can be at least partially reversed under these culture conditions. Moreover, these "switched" cells also became less sensitive to ATP depletion by glycolytic inhibitors and more sensitive to that caused by inhibition of mitochondrial metabolism. Furthermore, KIC and galactose-cultured MIA PaCa-2 cells became resistant to $[Ca^{2+}]_i$ overload or inhibition of the PMCA when glycolysis was inhibited by IAA. As such, the results support those of our previous study (*Chapter 2*, James et al., 2013), strengthening the hypothesis that glycolytic ATP is particularly critical for PMCA function in normal PDAC cells that exhibit a high glycolytic rate. On the other hand, these results indicate that this is less critical in cells that rely more on mitochondrial metabolism, such as non-cancerous cells or PDAC cells cultured in glucose-deprived conditions that are supplemented with KIC or galactose. The clear reversal in the sensitivity of KIC or galactose-cultured cells to IAA-induced $[Ca^{2+}]_i$ overload and PMCA inhibition suggests that an increased reliance on mitochondrial metabolism can maintain PMCA activity in the face of glycolytic inhibition in these cells. Conversely, despite these PDAC cells exhibiting a degree of metabolic adaptation to altered substrate conditions by slowing glycolytic flux, highly glycolytic PDAC cells were exquisitely sensitive to an acute challenge by glycolytic inhibitors. These findings suggest that PDAC cells exhibiting the Warburg phenotype, such as those in a hypoxic tumour core, are vulnerable to ATP depletion, $[Ca^{2+}]_i$ overload and PMCA inhibition following treatment with glycolytic inhibitors, while cells dependent on mitochondrial metabolism are resistant. These findings corroborate our hypothesis that eliminating the glycolytic ATP supply to the PMCA may be a novel therapeutic strategy for selectively killing highly glycolytic PDAC cells.

The luciferase and GO-ATeam based assays first revealed that culturing PDAC cells in galactose or KIC reversed the relative sensitivity of these cells to ATP depletion by mitochondrial and glycolytic inhibitors over 20 minutes. These findings are supported by those of previous studies. When cultured in galactose medium, HeLa cells increase the expression of mitochondrial respiratory chain proteins (Rossignol et al., 2004), while HepG2 and HLF-a cells cultured in galactose medium have both been shown to exhibit an increased reliance on mitochondrial ATP production (Bellance et al., 2009, Marroquin et al., 2007). It is important to

note, however, that in the present study the switch towards mitochondrial metabolism likely occurs due to relative decrease in glycolytic flux rather than its complete cessation. This is because glycolysis is functional but slowed when cells are cultured in galactose (Bustamante and Pedersen, 1977), and a small amount (~0.5 mM) of glucose remains in both KIC and galactose media due to FCS supplementation. Nevertheless, all imaging experiments were performed in conditions devoid of extracellular glucose. It is also likely that glutamine metabolism contributes significantly to ATP production in KIC and galactose cells. Glutamine has been shown to be a significant fuel for oxidative ATP production in MCF7 cells cultured in glucose medium (Guppy et al., 2002), and it has previously been demonstrated that following culture in galactose medium 98% of the ATP utilised in HeLa cells for growth is derived from glutamine (Reitzer et al., 1979). Moreover, the switch in metabolism observed in KIC and galactose-cultured cells suggests that PDAC cells exhibit a degree of metabolic adaptability when substrate availability changes over time, and retain functional mitochondria that can fuel ATP production should certain conditions prevail.

In addition to the changes in ATP sensitivity revealed by the luciferase and GO-ATeam based assays, extracellular flux measurements (OCR and ECAR) of PDAC cells revealed that under the conditions of nominal glucose-free culture supplemented with galactose or KIC, MIA PaCa-2 cells showed a marked decrease in ECAR, indicating that the rate of glycolysis was significantly reduced. Furthermore, while their basal OCR was significantly less than that of glucose-cultured cells in the XF Cell Mito Stress Test, no increase the ECAR was observed in galactose and KIC-cultured cells in response to blockade of mitochondrial ATP synthesis by OM. This indicates that these cells possess no glycolytic reserve under these glucose-deprived culture conditions. In contrast, their glucose-cultured counterparts could compensate following OM treatment by increasing glycolytic flux, presumably to maintain ATP. The notion that MIA PaCa-2 cells cultured in KIC or galactose media cannot increase glycolysis to compensate for loss of mitochondrial ATP production is supported by the ATP depleting effects of OM in our luciferase and GO-ATeam ATP assays. On the other hand, while both culture conditions decreased ECAR, KIC and galactose supplementation had different effects on respiration rate (OCR). Basal OCR in cells cultured in galactose was significantly reduced, most likely because galactose enters the glycolytic cascade from the Leloir pathway at a slower rate than glucose enters glycolysis (Bustamante and Pedersen, 1977), resulting in a slowed overall metabolic rate (both OCR and ECAR). On the other hand, OCR was relatively well maintained in KIC cells, suggesting that KIC is a better substrate than galactose for switching highly glycolytic cancer cells back towards mitochondrial metabolism when deprived of glucose. This is likely due to conversion of KIC in the mitochondria into the respiratory substrates α-ketoglutarate (Lenzen et al., 1985, Malaisse et al., 1981), acetyl CoA and the ketone body acetoacetate (Noda and Ichihara, 1974, MacDonald et al., 2005), which can then be utilised by mitochondrial metabolism as an alternative mitochondrial fuel. Similarly, glucose deprivation coupled with an altered availability of ketone bodies has previously been explored as a potential treatment avenue for cancer. This “ketogenic diet” aims to elevate the circulating levels of ketone bodies while limiting

carbohydrate availability (Seyfried et al., 2003, Abdelwahab et al., 2012, Otto et al., 2008) and has been shown to slow glycolytic flux by reprogramming metabolism, leading to reduced cell survival in pancreatic cancer cell lines (Shukla et al., 2014). These results are similar to those of the present study, where conditions of glucose deprivation coupled with supplementation of KIC decreased glycolytic flux, ECAR and proliferation rate. In addition, the decreased proliferation rate in these cells is likely due to a decreased abundance of glycolytic intermediates available for fuelling cell proliferation.

Warburg's initial observations led him to hypothesise that upregulated glycolysis in cancer cells stemmed from defects in mitochondrial oxidative phosphorylation (Warburg, 1956). High glycolytic flux is also known to inhibit mitochondrial metabolism in cancer cells (Wu et al., 2007), a phenomenon known as the Crabtree Effect (Crabtree, 1929). However, it is now appreciated that mitochondria in cancer are indeed functional (Pedersen, 2007) and that while mitochondrial defects may contribute to oncogenic transformation, they are unlikely to be the main underlying cause of the Warburg phenotype (Frezza and Gottlieb, 2009). Indeed, the results of the present study indicate that MIA PaCa-2 cells retain functional mitochondria and a high basal respiratory capacity, despite also exhibiting a high glycolytic rate. While it is now appreciated that mitochondria can contribute to ATP production in cancer cells, until recently the predominant hypothesis has been that cancer cells upregulate glycolysis to provide the bulk of total cellular ATP. It is now thought that a high glycolytic rate in cancer instead supports cell proliferation by supplying glucose carbon in the form of glycolytic intermediates to anabolic and anapleurotic reactions (DeBerardinis et al., 2008, Kroemer and Pouyssegur, 2008). It is thought that this occurs at the expense of glycolytic ATP production and is facilitated by the low activity dimeric form of the M2 isoform of pyruvate kinase, which attenuates flux through the final, ATP generating reaction of glycolysis (Chaneton and Gottlieb, 2012). However, the large amount of carbon excreted as lactate presents a functional paradox, since these are carbons that could instead be incorporated into cell proliferation rather than excreted. This suggests that the fuelling of anabolic processes is unlikely the sole reason for a high glycolytic rate, and that the high glycolytic rate exhibited by cancer may indeed have a bioenergetic component as well as a predominant biosynthetic component (Frezza and Gottlieb, 2009). Moreover, this may be particularly pertinent when PDAC cells are faced with low O_2 availability within a hypoxic tumour core (Guppy, 2002, Guillaumond et al., 2013). Nevertheless, the degree to which glycolysis contributes to ATP in cancer remains a controversial topic, as the available evidence thus far has been equivocal. While some studies indicate that cancer cells do still derive the majority of ATP from mitochondria, despite upregulated glycolysis (Zu and Guppy, 2004, Guppy et al., 2002, Rodriguez-Enriquez et al., 2006, Martin et al., 1998), other studies suggest that cancer cells generate a larger proportion of ATP from glycolysis (Busk et al., 2008, Nakashima et al., 1984, James et al., 2013, Xu et al., 2005, Bellance et al., 2009). To reconcile the discrepancies, it is likely that cancer cells exhibit a degree of metabolic adaptation with regards to glycolytic and mitochondrial ATP production when the abundance of metabolic substrates changes. A cancer cell's metabolic phenotype will likely be influenced by its energetic requirements,

hypoxia within the tumour microenvironment, substrate availability and genetic heterogeneity within the tumour (Rodriguez-Enriquez et al., 2008). Indeed, it has been suggested that metabolic heterogeneity and adaptation to varying O_2 concentrations within a tumour can in fact promote cancer cell survival and proliferation (Sonveaux et al., 2008, Semenza, 2008).

The notion that cancer cells can adapt certain facets of their metabolism to maintain ATP production is supported by the current study, where both MIA PaCa-2 and PANC-1 cells could adapt to survive in nominal glucose-free conditions, but in doing so became sensitive to ATP depletion by inhibitors of mitochondrial metabolism. Moreover, this is also supported by the observation that ECAR rapidly increased following the blockade of mitochondrial ATP production with OM in glucose-cultured MIA PaCa-2 cells, suggesting that these cells could rapidly upregulate glycolytic flux within minutes or even seconds to compensate for the loss of mitochondrial ATP synthesis. Nevertheless, in the current study, the glycolytic inhibitors BrPy and IAA both caused a dramatic drop in cytosolic ATP in PDAC cells cultured in glucose. This suggests that while highly glycolytic PDAC cells are resistant to mitochondrial inhibitors and can compensate for their effects in order to maintain ATP, they are exquisitely sensitive to ATP depletion induced by glycolytic inhibitors. Importantly, the glycolytic inhibitor-induced ATP depletion was markedly attenuated in those cells cultured in galactose or KIC. A high glycolytic flux therefore appears to be essential for the ATP-depleting action of both BrPy and IAA, and supports the notion that glucose-cultured PDAC cells derive a large proportion of ATP from glycolysis rather than mitochondrial metabolism. Importantly, however, the different effects of glycolytic inhibitors on ATP in glucose vs KIC and galactose-cultured cells indicate that while PDAC cells can slowly adapt to survive changes in substrate availability, highly glycolytic PDAC cells are vulnerable to acute glycolytic inhibition. Critically, the IAA-induced ATP depletion in highly glycolytic cells was complemented by a corresponding inability to control resting $[Ca^{2+}]_i$ or maintain PMCA activity, which would be cytotoxic. Therefore, while highly glycolytic PDAC cells may exhibit some metabolic plasticity in order to adapt to changing substrate availability or mitochondrial impairment, they appear unable to adapt to counter acute glycolytic inhibition in order to maintain $[Ca^{2+}]_i$ homeostasis. This, coupled with their exquisite sensitivity to glycolytic inhibition compared to KIC and galactose cultured cells, has important implications for the potential selective targeting of cells at a hypoxic PDAC tumour core.

Despite these findings, not all metabolic inhibitors produced such a clear cut reversal of responses as observed with IAA. A similar reversal in ATP depletion was observed following treatment of KIC and galactose-cultured cells with BrPy, and KIC cultured cells became relatively resistant to $[Ca^{2+}]_i$ overload following treatment with BrPy. Despite this, in galactose-cultured cells, the BrPy induced $[Ca^{2+}]_i$ overload was substantial and very similar to glucose-cultured cells, yet this was not reflected in the ATP assays. In fact, BrPy induced significantly less ATP depletion than OM in galactose-cultured cells, yet OM did not cause $[Ca^{2+}]_i$ overload under these conditions, suggesting a disconnection between $[Ca^{2+}]_i$ overload and ATP depletion. It is therefore tempting to speculate that BrPy can cause $[Ca^{2+}]_i$ overload via an ATP-depletion independent mechanism. Importantly, evidence suggests that PMCA inhibition and

$[Ca^{2+}]_i$ overload can follow depolarisation of the mitochondria without accompanying ATP depletion (Baggaley et al., 2008). Indeed, BrPy has been reported to depolarise the mitochondrial membrane potential (ΔΨm, Ihrlund et al., 2008) and to induce dissociation of hexokinase from VDAC (Chen et al., 2009). Moreover, BrPy has been shown to induce the release of proapoptotic factors from the mitochondria (Chen et al., 2009); factors implicated in apoptosis such as caspases and calpain cleave and inactivate the PMCA (Schwab et al., 2002, Brown and Dean, 2007), however these processes may occur over a much longer time course than that required for initiation of BrPy-induced $[Ca^{2+}]_i$ overload (~2 min). A more likely candidate may be increased ROS production following BrPy treatment (Kim et al., 2008), since oxidative stress is known to inhibit PMCA activity (Baggaley et al., 2008). Nevertheless, the effects of BrPy are less clear cut due to the numerous additional effects that BrPy has on the cell other than solely blockade of glycolytic flux through HK.

Surprisingly, in glucose-cultured cells, 10 mM 2-DG had no effect on ATP over 20 minutes using either GO-ATeam or luciferase-based measurements of ATP. It is possible that 2-DG requires longer to inhibit glycolysis at 10 mM when glucose is present due to competition for the same uptake transporters and the HK active site. On the other hand, the effects of 2-DG on KIC and galactose-cultured cells are more difficult to reconcile. While in the luciferase-based experiments 2-DG had no effect on ATP in PANC-1 cells from any of the three culture conditions, 2-DG induced rapid ATP depletion in both KIC and galactose MIA PaCa-2 cells in both the GO-ATeam and luciferase based ATP assays. In the case of the galactose-cultured cells, similar to glucose-cultured cells, it is possible that 2-DG competes for the same hexose transporters on the plasma membrane as these substrates, thereby slowing its uptake. Given the low basal metabolic rate of galactose-cultured cells (both mitochondrial and glycolytic), this alone may be sufficient to cause ATP depletion. Moreover, since galactose is converted to glucose-6-phosphate via the three-step Leloir pathway (Garrett and Grisham, 2013), inhibition of glucose-6-phosphate isomerase by 2-DG-6-P following its conversion from 2-DG (Wick et al., 1957) could also prevent further metabolism of galactose-derived glucose-6-phosphate through glycolysis. This would further limit pyruvate supply to the mitochondria in cells that already exhibited an attenuated glycolytic rate due to galactose culture (Bustamante and Pedersen, 1977). Finally, it is possible that inhibition of mitochondria-bound hexokinase by 2-DG results in indirect effect on mitochondrial metabolism in addition to blocking glycolytic flux, which may explain its effects in KIC-cultured cells. Therefore, similarly to BrPy, 2-DG may affect mitochondrial metabolism in a fashion that KIC and galactose-cultured MIA PaCa-2 cells are exquisitely sensitive to, especially given the former's greater reliance on mitochondrial ATP production relative to glycolysis.

Following the marked OM and AM-induced ATP depletion observed in galactose and KIC-cultured cells, the lack of effect in the resting $[Ca^{2+}]_i$ experiments came as a surprise. It is important to note, however, that in the current study the starting absolute ATP concentration within cells is not known. A higher resting ATP concentration in our KIC and galactose-cultured cells could explain the lack of effect of mitochondrial inhibitors on resting $[Ca^{2+}]_i$ and $[Ca^{2+}]_i$

clearance. While mitochondrial inhibitors induced a significant decrease in ATP in both KIC and galactose-cultured cells, these cells may exhibit a much higher starting ATP concentration than their glucose-cultured counterparts, meaning the degree of ATP depletion may not be sufficient to cause PMCA inhibition. For example, a 50% decrease in ATP under one culture condition may be insufficient to reach the critical threshold ATP concentration at which the PMCA is affected. However, under a different culture condition, cells might present with a much lower starting ATP concentration, and an equivalent % decrease in ATP might be sufficient to inhibit the PMCA. Previous studies aiming to determine the absolute ATP content of cells cultured in glucose free medium have yielded conflicting results, with one suggesting cellular ATP rose by 50% in the absence of glucose (Rodriguez-Enriquez et al., 2006), while another suggested that cells cultured in galactose have a considerably lower ATP content than that in their glucose-cultured counterparts (Bellance et al., 2009). Additionally, studies in multicellular tumour spheroids indicate that cancer cells exhibit metabolic plasticity, and have a significantly higher ATP content when the majority of ATP is derived via oxidative phosphorylation (Rodriguez-Enriquez et al., 2008). Thus, different starting ATP concentrations might account for the lack of effect of certain drugs in the resting $[Ca^{2+}]_i$ experiments, despite an apparent effect on ATP in the luciferase and GO-ATeam assays. Nevertheless, the regulation of the PMCA by ATP is complex (Echarte et al., 2007), and the ATP sensitivity of the PMCA can be dynamically regulated by $[Mg^{2+}]_i$, $[Ca^{2+}]_i$, calmodulin and the phospholipid composition of the plasma membrane (Rossi and Rega, 1989, Zhang et al., 2009). Therefore, the absolute concentration to which ATP would need to decrease to in order to affect PMCA activity in living cells is not clear and likely more complex than originally thought following cell-free assays.

In addition to the absolute ATP sensitivity of the PMCA, it is possible that the source (glycolysis vs oxidative phosphorylation) and temporal distribution of ATP production has an important bearing on the vulnerability of the PMCA to ATP depletion following metabolic inhibition. In intact human erythrocytes, a complex of glycolytic enzymes has been shown to be associated with the plasma membrane in close proximity to the plasma membrane (Puchulu-Campanella et al., 2013, Campanella et al., 2005). Moreover, in inside-out smooth muscle plasma membrane vesicles, the supply of glycolytic substrates has been shown to maintain PMCA activity. This suggests that an endogenous glycolytic cascade fuels PMCA activity by providing a submembrane pool of glycolytically-derived ATP in the absence of mitochondria (Paul et al., 1989). Furthermore, extensions of this work found that the PMCA preferentially uses this endogenous glycolytic ATP supply to clear $[Ca^{2+}]_i$ instead of exogenous ATP supplemented into the assay buffer (Hardin et al., 1992). Interestingly, in the present study, a modest but significant decrease in $[Ca^{2+}]_i$ clearance rate was observed during the second influx/clearance phase in control KIC and galactose cells. In light of these previous studies (Hardin et al., 1992, Paul et al., 1989), this decrease in PMCA rate may reflect the lack of a rapid local glycolytic ATP supply at the plasma membrane. Moreover, it is likely that ATP is rapidly consumed by the PMCA under the conditions of our *in situ* $[Ca^{2+}]_i$ clearance assay, and in the absence of a privileged local supply of glycolytic ATP the rate of ATP diffusion from the mitochondria may

limit the maximum achievable $[Ca^{2+}]_i$ clearance rate in these assays. In this instance, when ATP is being rapidly consumed by the PMCA the mitochondria cannot adequately replenish submembrane ATP fast enough, and therefore the maximum rate of $[Ca^{2+}]_i$ clearance by the PMCA cannot be maintained. Importantly, however, despite this modest reduction in $[Ca^{2+}]_i$ clearance rate, KIC or galactose-cultured cells could still recover to a low resting $[Ca^{2+}]_{i.}$ after an influx/clearance challenge, suggesting that mitochondrial ATP production allows galactose and KIC-cultured cells to maintain $[Ca^{2+}]_i$ homeostasis, albeit with a slightly slowed PMCA.

In contrast to galactose and KIC-cultured cells, in the present study IAA significantly inhibited PMCA activity in glucose-cultured cells, as previously described (*Chapter 2*, James et al., 2013). Given the apparent lack of effect of IAA in galactose and KIC-cultured cells, we attribute the IAA-induced PMCA inhibition in glucose-cultured cells to profound depletion of glycolytically-derived ATP, as evidenced by our luciferase and GO-ATeam assays. This seems to happen despite these cells exhibiting an apparently high respiratory rate, providing further evidence that PDAC cells exhibiting the Warburg phenotype are exquisitely sensitive to glycolytic inhibition, and that the PMCA is critically reliant on a glycolytic ATP supply for $[Ca^{2+}]_i$ clearance when glycolytic flux is high. We propose that the glycolytic regulation of the PMCA in PDAC is a cancer-specific weakness that can be exploited, and may be an effective and previously untapped therapeutic locus for the selective treatment of highly glycolytic PDAC cells.

3.6 - Acknowledgements

We thank Prof. M. Dunne for use of the BioTek Synergy HT luminescent multi-plate reader, and Peter March and the University of Manchester Bioimaging Facility for their help with the microscopy performed for the transfection work.

3.7 - References

ABDELWAHAB, M. G., FENTON, K. E., PREUL, M. C., RHO, J. M., LYNCH, A., STAFFORD, P. & SCHECK, A. C. 2012. The ketogenic diet is an effective adjuvant to radiation therapy for the treatment of malignant glioma. *PloS one,* 7**,** e36197.

AMIN, Z., THEIS, B., RUSSELL, R. C., HOUSE, C., NOVELLI, M. & LEES, W. R. 2006. Diagnosing pancreatic cancer: the role of percutaneous biopsy and CT. *Clin Radiol,* 61**,** 996-1002.

BAGGALEY, E. M., ELLIOTT, A. C. & BRUCE, J. I. 2008. Oxidant-induced inhibition of the plasma membrane Ca^{2+}-ATPase in pancreatic acinar cells: role of the mitochondria. *Am J Physiol Cell Physiol,* 295**,** C1247-60.

BELLANCE, N., BENARD, G., FURT, F., BEGUERET, H., SMOLKOVA, K., PASSERIEUX, E., DELAGE, J. P., BASTE, J. M., MOREAU, P. & ROSSIGNOL, R. 2009. Bioenergetics of lung tumors: alteration of mitochondrial biogenesis and respiratory capacity. *Int J Biochem Cell Biol,* 41**,** 2566-77.

BRINI, M. & CARAFOLI, E. 2009. Calcium pumps in health and disease. *Physiol Rev,* 89**,** 1341-78.

BROWN, C. S. & DEAN, W. L. 2007. Regulation of plasma membrane Ca^{2+}-ATPase in human platelets by calpain. *Platelets,* 18**,** 207-11.

BRUCE, J. I. & ELLIOTT, A. C. 2007. Oxidant-impaired intracellular Ca^{2+} signaling in pancreatic acinar cells: role of the plasma membrane Ca^{2+}-ATPase. *Am J Physiol Cell Physiol,* 293**,** C938-50.

BUSK, M., HORSMAN, M. R., KRISTJANSEN, P. E., VAN DER KOGEL, A. J., BUSSINK, J. & OVERGAARD, J. 2008. Aerobic glycolysis in cancers: implications for the usability of oxygen-responsive genes and fluorodeoxyglucose-PET as markers of tissue hypoxia. *Int J Cancer,* 122**,** 2726-34.

BUSTAMANTE, E. & PEDERSEN, P. L. 1977. High aerobic glycolysis of rat hepatoma cells in culture: role of mitochondrial hexokinase. *Proc Natl Acad Sci U S A*, 74**,** 3735-9.

CAMPANELLA, M. E., CHU, H. & LOW, P. S. 2005. Assembly and regulation of a glycolytic enzyme complex on the human erythrocyte membrane. *Proc Natl Acad Sci U S A*, 102**,** 2402-7.

CHANETON, B. & GOTTLIEB, E. 2012. Rocking cell metabolism: revised functions of the key glycolytic regulator PKM2 in cancer. *Trends Biochem Sci,* 37**,** 309-16.

CHEN, W. & GUERON, M. 1992. The inhibition of bovine heart hexokinase by 2-deoxy-D-glucose-6-phosphate: characterization by ^{31}P NMR and metabolic implications. *Biochimie,* 74**,** 867-73.

CHEN, Z., ZHANG, H., LU, W. & HUANG, P. 2009. Role of mitochondria-associated hexokinase II in cancer cell death induced by 3-bromopyruvate. *Biochim Biophys Acta,* 1787**,** 553-60.

CRABTREE, H. G. 1929. Observations on the carbohydrate metabolism of tumours. *Biochem J,* 23**,** 536-45.

DEBERARDINIS, R. J., LUM, J. J., HATZIVASSILIOU, G. & THOMPSON, C. B. 2008. The biology of cancer: metabolic reprogramming fuels cell growth and proliferation. *Cell Metab,* 7**,** 11-20.

ECHARTE, M. M., ROSSI, R. C. & ROSSI, J. P. 2007. Phosphorylation of the plasma membrane calcium pump at high ATP concentration. On the mechanism of ATP hydrolysis. *Biochemistry,* 46**,** 1034-41.

FREZZA, C. & GOTTLIEB, E. 2009. Mitochondria in cancer: not just innocent bystanders. *Semin Cancer Biol,* 19**,** 4-11.

GARRETT, R. & GRISHAM, C. M. 2013. *Biochemistry,* Belmont, CA, Brooks/Cole, Cengage Learning.

GATENBY, R. A. & GILLIES, R. J. 2004. Why do cancers have high aerobic glycolysis? *Nat Rev Cancer,* 4**,** 891-9.

GILLIES, R. J. & GATENBY, R. A. 2007. Adaptive landscapes and emergent phenotypes: why do cancers have high glycolysis? *J Bioenerg Biomembr,* 39**,** 251-7.

GUILLAUMOND, F., LECA, J., OLIVARES, O., LAVAUT, M. N., VIDAL, N., BERTHEZENE, P., DUSETTI, N. J., LONCLE, C., CALVO, E., TURRINI, O., IOVANNA, J. L., TOMASINI, R. & VASSEUR, S. 2013. Strengthened glycolysis under hypoxia supports tumor symbiosis and hexosamine biosynthesis in pancreatic adenocarcinoma. *Proc Natl Acad Sci U S A,* 110**,** 3919-24.

GUPPY, M. 2002. The hypoxic core: a possible answer to the cancer paradox. *Biochem Biophys Res Commun,* 299**,** 676-80.

GUPPY, M., LEEDMAN, P., ZU, X. & RUSSELL, V. 2002. Contribution by different fuels and metabolic pathways to the total ATP turnover of proliferating MCF-7 breast cancer cells. *Biochem J,* 364**,** 309-15.

HANAHAN, D. & WEINBERG, R. A. 2011. Hallmarks of cancer: the next generation. *Cell,* 144**,** 646-74.

HARDIN, C. D., RAEYMAEKERS, L. & PAUL, R. J. 1992. Comparison of endogenous and exogenous sources of ATP in fueling Ca^{2+} uptake in smooth muscle plasma membrane vesicles. *J Gen Physiol,* 99**,** 21-40.

HUTTON, J. C., SENER, A. & MALAISSE, W. J. 1979. The metabolism of 4-methyl-2-oxopentanoate in rat pancreatic islets. *Biochem J,* 184**,** 291-301.

IHRLUND, L. S., HERNLUND, E., KHAN, O. & SHOSHAN, M. C. 2008. 3-Bromopyruvate as inhibitor of tumour cell energy metabolism and chemopotentiator of platinum drugs. *Mol Oncol,* 2**,** 94-101.

JAMES, A. D., CHAN, A., ERICE, O., SIRIWARDENA, A. K. & BRUCE, J. I. 2013. Glycolytic ATP fuels the plasma membrane calcium pump critical for pancreatic cancer cell survival. *J Biol Chem,* 288**,** 36007-19.

KAFTAN, E. J., XU, T., ABERCROMBIE, R. F. & HILLE, B. 2000. Mitochondria shape hormonally induced cytoplasmic calcium oscillations and modulate exocytosis. *J Biol Chem,* 275**,** 25465-70.

WARBURG, O. H. & DICKENS, F., 1930. *The metabolism of tumours: investigations from the Kaiser Wilhelm Institute for Biology, Berlin-Dahlem,* London, Constable and Co.

KIM, J. S., AHN, K. J., KIM, J. A., KIM, H. M., LEE, J. D., LEE, J. M., KIM, S. J. & PARK, J. H. 2008. Role of reactive oxygen species-mediated mitochondrial dysregulation in 3-bromopyruvate induced cell death in hepatoma cells : ROS-mediated cell death by 3-BrPA. *J Bioenerg Biomembr,* 40**,** 607-18.

KO, Y. H., PEDERSEN, P. L. & GESCHWIND, J. F. 2001. Glucose catabolism in the rabbit VX2 tumor model for liver cancer: characterization and targeting hexokinase. *Cancer Lett,* 173**,** 83-91.

KO, Y. H., SMITH, B. L., WANG, Y., POMPER, M. G., RINI, D. A., TORBENSON, M. S., HULLIHEN, J. & PEDERSEN, P. L. 2004. Advanced cancers: eradication in all cases using 3-bromopyruvate therapy to deplete ATP. *Biochem Biophys Res Commun,* 324**,** 269-75.

KOONG, A. C., MEHTA, V. K., LE, Q. T., FISHER, G. A., TERRIS, D. J., BROWN, J. M., BASTIDAS, A. J. & VIERRA, M. 2000. Pancreatic tumors show high levels of hypoxia. *Int J Radiat Oncol Biol Phys,* 48**,** 919-22.

KROEMER, G. & POUYSSEGUR, J. 2008. Tumor cell metabolism: cancer's Achilles' heel. *Cancer Cell,* 13**,** 472-82.

LENZEN, S., SCHMIDT, W. & PANTEN, U. 1985. Transamination of neutral amino acids and 2-keto acids in pancreatic B-cell mitochondria. *J Biol Chem,* 260**,** 12629-34.

LOOS, M., KLEEFF, J., FRIESS, H. & BUCHLER, M. W. 2008. Surgical treatment of pancreatic cancer. *Ann N Y Acad Sci,* 1138**,** 169-80.

MACDONALD, M. J., FAHIEN, L. A., BROWN, L. J., HASAN, N. M., BUSS, J. D. & KENDRICK, M. A. 2005. Perspective: emerging evidence for signaling roles of mitochondrial anaplerotic products in insulin secretion. *Am J Physiol Endocrinol Metab,* 288**,** E1-15.

MAGEE, B. A., POTEZNY, N., ROFE, A. M. & CONYERS, R. A. 1979. The inhibition of malignant cell growth by ketone bodies. *Aust J Exp Biol Med Sci,* 57**,** 529-39.

MALAISSE, W. J., SENER, A., MALAISSE-LEGAE, F., HUTTON, J. C. & CHRISTOPHE, J. 1981. The stimulus-secretion coupling of amino acid-induced insulin release. Metabolic interaction of L-glutamine and 2-ketoisocaproate in pancreatic islets. *Biochim Biophys Acta,* 677**,** 39-49.

MANKAD, P., JAMES, A., SIRIWARDENA, A. K., ELLIOTT, A. C. & BRUCE, J. I. 2012. Insulin protects pancreatic acinar cells from cytosolic calcium overload and inhibition of plasma membrane calcium pump. *J Biol Chem,* 287**,** 1823-36.

MARROQUIN, L. D., HYNES, J., DYKENS, J. A., JAMIESON, J. D. & WILL, Y. 2007. Circumventing the Crabtree effect: replacing media glucose with galactose increases susceptibility of HepG2 cells to mitochondrial toxicants. *Toxicol Sci,* 97**,** 539-47.

MARTIN, M., BEAUVOIT, B., VOISIN, P. J., CANIONI, P., GUERIN, B. & RIGOULET, M. 1998. Energetic and morphological plasticity of C6 glioma cells grown on 3-D support; effect of transient glutamine deprivation. *J Bioenerg Biomembr,* 30**,** 565-78.

MATHUPALA, S. P., KO, Y. H. & PEDERSEN, P. L. 2009. Hexokinase-2 bound to mitochondria: cancer's stygian link to the "Warburg Effect" and a pivotal target for effective therapy. *Semin Cancer Biol,* 19**,** 17-24.

NAKANO, M., IMAMURA, H., NAGAI, T. & NOJI, H. 2011. Ca^{2+} regulation of mitochondrial ATP synthesis visualized at the single cell level. *ACS Chem Biol,* 6**,** 709-15.

NAKASHIMA, R. A., PAGGI, M. G. & PEDERSEN, P. L. 1984. Contributions of glycolysis and oxidative phosphorylation to adenosine 5'-triphosphate production in AS-30D hepatoma cells. *Cancer Res,* 44**,** 5702-6.

NODA, C. & ICHIHARA, A. 1974. Control of ketogenesis from amino acids. II. Ketone bodies formation from alpha-ketoisocaproate, the keto-analogue of leucine, by rat liver mitochondria. *J Biochem,* 76**,** 1123-30.

OTTO, C., KAEMMERER, U., ILLERT, B., MUEHLING, B., PFETZER, N., WITTIG, R., VOELKER, H. U., THIEDE, A. & COY, J. F. 2008. Growth of human gastric cancer cells in nude mice is delayed by a ketogenic diet supplemented with omega-3 fatty acids and medium-chain triglycerides. *BMC Cancer,* 8**,** 122.

PAUL, R. J., HARDIN, C. D., RAEYMAEKERS, L., WUYTACK, F. & CASTEELS, R. 1989. Preferential support of Ca^{2+} uptake in smooth muscle plasma membrane vesicles by an endogenous glycolytic cascade. *FASEB J,* 3**,** 2298-301.

PEDERSEN, P. L. 2007. Warburg, me and Hexokinase 2: Multiple discoveries of key molecular events underlying one of cancers' most common phenotypes, the "Warburg Effect", i.e., elevated glycolysis in the presence of oxygen. *J Bioenerg Biomembr,* 39**,** 211-22.

PELICANO, H., MARTIN, D. S., XU, R. H. & HUANG, P. 2006. Glycolysis inhibition for anticancer treatment. *Oncogene,* 25**,** 4633-46.

PUCHULU-CAMPANELLA, E., CHU, H., ANSTEE, D. J., GALAN, J. A., TAO, W. A. & LOW, P. S. 2013. Identification of the components of a glycolytic enzyme metabolon on the human red blood cell membrane. *J Biol Chem,* 288**,** 848-58.

REITZER, L. J., WICE, B. M. & KENNELL, D. 1979. Evidence that glutamine, not sugar, is the major energy source for cultured HeLa cells. *J Biol Chem,* 254**,** 2669-76.

ROBINSON, B. H., PETROVA-BENEDICT, R., BUNCIC, J. R. & WALLACE, D. C. 1992. Nonviability of cells with oxidative defects in galactose medium: a screening test for affected patient fibroblasts. *Biochem Med Metab Biol,* 48**,** 122-6.

RODRIGUEZ-ENRIQUEZ, S., GALLARDO-PEREZ, J. C., AVILES-SALAS, A., MARIN-HERNANDEZ, A., CARRENO-FUENTES, L., MALDONADO-LAGUNAS, V. & MORENO-SANCHEZ, R. 2008. Energy metabolism transition in multi-cellular human tumor spheroids. *J Cell Physiol,* 216**,** 189-97.

RODRIGUEZ-ENRIQUEZ, S., VITAL-GONZALEZ, P. A., FLORES-RODRIGUEZ, F. L., MARIN-HERNANDEZ, A., RUIZ-AZUARA, L. & MORENO-SANCHEZ, R. 2006. Control of cellular proliferation by modulation of oxidative phosphorylation in human and rodent fast-growing tumor cells. *Toxicol Appl Pharmacol,* 215**,** 208-17.

ROSSI, J. P. & REGA, A. F. 1989. A study to see whether phosphatidylserine, partial proteolysis and EGTA substitute for calmodulin during activation of the Ca^{2+}-ATPase from red cell membranes by ATP. *Biochim Biophys Acta,* 996**,** 153-9.

ROSSIGNOL, R., GILKERSON, R., AGGELER, R., YAMAGATA, K., REMINGTON, S. J. & CAPALDI, R. A. 2004. Energy substrate modulates mitochondrial structure and oxidative capacity in cancer cells. *Cancer Res,* 64**,** 985-93.

SCHMIDT, M. M. & DRINGEN, R. 2009. Differential effects of iodoacetamide and iodoacetate on glycolysis and glutathione metabolism of cultured astrocytes. *Front Neuroenergetic,* 1**,** 1.

SCHWAB, B. L., GUERINI, D., DIDSZUN, C., BANO, D., FERRANDO-MAY, E., FAVA, E., TAM, J., XU, D., XANTHOUDAKIS, S., NICHOLSON, D. W., CARAFOLI, E. & NICOTERA, P. 2002. Cleavage of plasma membrane calcium pumps by caspases: a link between apoptosis and necrosis. *Cell Death Differ,* 9**,** 818-31.

SEMENZA, G. L. 2008. Tumor metabolism: cancer cells give and take lactate. *J Clin Invest,* 118**,** 3835-7.

SEYFRIED, T. N., SANDERSON, T. M., EL-ABBADI, M. M., MCGOWAN, R. & MUKHERJEE, P. 2003. Role of glucose and ketone bodies in the metabolic control of experimental brain cancer. *Br J Cancer,* 89**,** 1375-82.

SHCHEPINA, L. A., PLETJUSHKINA, O. Y., AVETISYAN, A. V., BAKEEVA, L. E., FETISOVA, E. K., IZYUMOV, D. S., SAPRUNOVA, V. B., VYSSOKIKH, M. Y., CHERNYAK, B. V. & SKULACHEV, V. P. 2002. Oligomycin, inhibitor of the F_0 part of H^+-ATP-synthase, suppresses the TNF-induced apoptosis. *Oncogene,* 21**,** 8149-57.

SHUKLA, S. K., GEBREGIWORGIS, T., PUROHIT, V., CHAIKA, N. V., GUNDA, V., RADHAKRISHNAN, P., MEHLA, K., PIPINOS, II, POWERS, R., YU, F. & SINGH, P. K. 2014. Metabolic reprogramming induced by ketone bodies diminishes pancreatic cancer cachexia. *Cancer Metab,* 2**,** 18.

SHULGA, N., WILSON-SMITH, R. & PASTORINO, J. G. 2010. Sirtuin-3 deacetylation of cyclophilin D induces dissociation of hexokinase II from the mitochondria. *J Cell Sci,* 123**,** 894-902.

SLATER, E. C. 1973. The mechanism of action of the respiratory inhibitor, antimycin. *Biochim Biophys Acta,* 301**,** 129-54.

SONVEAUX, P., VEGRAN, F., SCHROEDER, T., WERGIN, M. C., VERRAX, J., RABBANI, Z. N., DE SAEDELEER, C. J., KENNEDY, K. M., DIEPART, C., JORDAN, B. F., KELLEY, M. J., GALLEZ, B., WAHL, M. L., FERON, O. & DEWHIRST, M. W. 2008. Targeting lactate-fueled respiration selectively kills hypoxic tumor cells in mice. *J Clin Invest,* 118**,** 3930-42.

WARBURG, O. 1956. On the origin of cancer cells. *Science,* 123**,** 309-14.

WICK, A. N., DRURY, D. R., NAKADA, H. I. & WOLFE, J. B. 1957. Localization of the primary metabolic block produced by 2-deoxyglucose. *J Biol Chem,* 224**,** 963-9.

WU, M., NEILSON, A., SWIFT, A. L., MORAN, R., TAMAGNINE, J., PARSLOW, D., ARMISTEAD, S., LEMIRE, K., ORRELL, J., TEICH, J., CHOMICZ, S. & FERRICK, D. A. 2007. Multiparameter metabolic analysis reveals a close link between attenuated mitochondrial bioenergetic function and enhanced glycolysis dependency in human tumor cells. *Am J Physiol Cell Physiol,* 292**,** C125-36.

XU, R. H., PELICANO, H., ZHANG, H., GILES, F. J., KEATING, M. J. & HUANG, P. 2005. Synergistic effect of targeting mTOR by rapamycin and depleting ATP by inhibition of glycolysis in lymphoma and leukemia cells. *Leukemia,* 19**,** 2153-8.

ZHANG, J., XIAO, P. & ZHANG, X. 2009. Phosphatidylserine externalization in caveolae inhibits Ca^{2+} efflux through plasma membrane Ca^{2+}-ATPase in ECV304. *Cell Calcium,* 45**,** 177-84.

ZU, X. L. & GUPPY, M. 2004. Cancer metabolism: facts, fantasy, and fiction. *Biochem Biophys Res Commun,* 313**,** 459-65.

3.8 - Chapter 3 Supplementary Methods and Results

3.8.1 - Measurement of relative recovery of $[Ca^{2+}]_i$ during in situ *$[Ca^{2+}]_i$ clearance assays*

As previously mentioned in *2.8.4 - Measurement of % recovery of $[Ca^{2+}]_i$ to baseline*, recovery of $[Ca^{2+}]_i$ in our *in situ* $[Ca^{2+}]_i$ clearance assay can be assessed by measuring the degree of recovery during the second clearance phase to the post-CPA response baseline. This method is appropriate to calculate the recovery of $[Ca^{2+}]_i$ to baseline during the second influx/clearance phase provided the recovery during the first control influx/clearance phase is unaffected. However, cells cultured in glucose-free media containing α-ketoisocaproate or galactose did not completely recover $[Ca^{2+}]_i$ to baseline following the first, control influx/clearance phase. As a result, the measurement of recovery to the post-CPA response baseline would not distinguish between drug-induced effects on recovery during the second influx/clearance phase and the effects of the culture conditions apparent in the first influx/clearance phase. Thus a different method of measuring recovery is required which would control for any effect on recovery during the first clearance phase, In this case, recovery during the second influx/clearance phase relative to that of the first is a better indicator of recovery than absolute recovery to the post-CPA, pre influx/clearance phase baseline. Therefore, in the present study, the recovery during the second influx/clearance phase was normalised to that of the first (%), with both measurements beginning at the same fura-2 ratio value, to give relative recovery (Supplementary Figure 3.1).

3.8.2 - Amplification and validation of GO-ATeam Plasmid

GO-ATeam plasmid (pcDNA-GO-ATeam1) was supplied by Imamura and colleagues (Nakano et al., 2011). This plasmid was constructed from the pcDNA3.1 plasmid (Invitrogen, Supplementary Figure 3.2A). Upon receiving the plasmid, we first transformed competent *E.coli* cells (DH5α™, Invitrogen) using heat shock. Plasmid DNA (50 ng) was added to 50 µl competent cell solution, and following 10 minutes incubation on ice, cells were incubated at 42°C in a waterbath for 45 seconds before returning to incubation on ice for a further 2 minutes. Cells were then incubated in 1 ml antibiotic free lysogeny broth (LB, 172 mM NaCl, 1 % (w/v) Tryptone, 0.5 % (w/v) yeast extract) at 37°C (200 rpm) for 1 hour, and 100 µl of the cell suspension was subsequently spread on pre-warmed LB agar plates (LB + 1 % (w/v) agar) containing ampicillin (1 µg/ml, Sigma) and grown overnight at 37°C. Between 5 and 10 colonies were then screened for the presence of the plasmid. Briefly, *E. coli* from each colony were grown in 3 ml LB broth containing ampicillin, at which point glycerol stocks were prepared for each colony and the plasmid DNA isolated and amplified using a mini-preparation kit, according to manufacturer's instructions (QIAprep Spin Miniprep Kit, QIAGEN). The DNA content of each preparation was then quantified using a Nanodrop 2000 spectrophotometer (Thermo Scientific), and one preparation selected to use for amplification and transfection based on its purity and

concentration. Glycerol stocks were prepared for long term storage of E coli cells by adding 300 µl of 50 % glycerol to 700 µl of transformed *E coli* suspension in LB.

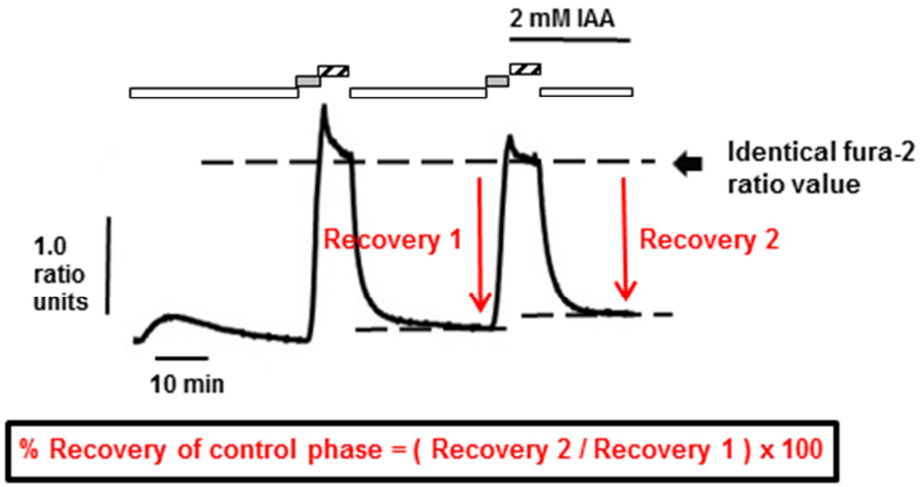

Supplementary Figure 3.1 - Measurement of relative recovery in an *in situ* $[Ca^{2+}]_i$ clearance assay

In our *in situ* $[Ca^{2+}]_i$ clearance assay, 30 µM cyclopiazonic acid (CPA) was applied in the absence of external Ca^{2+} with 1 mM EGTA (*white box*), or 20 mM Ca^{2+} (*grey box*) to induce store-operated Ca^{2+} influx. 1 mM La^{3+} was then applied at the peak of Ca^{2+} influx (*striped box*). Subsequent removal of external La^{3+} and readdition of 1 mM EGTA after 5 minutes allowed $[Ca^{2+}]_i$ clearance. This influx-clearance phase was repeated and metabolic inhibitors applied during this second influx-clearance phase. Recovery from Ca^{2+} influx in our *in situ* $[Ca^{2+}]_i$ clearance assay was measured as the *relative % recovery* which normalises recovery during the second clearance phase (Recovery 2) to that of the first (Recovery 1). Recovery 1 and Recovery 2 are measured from an identical fura-2 ratio value between their two respective recovery values.

After selection of the plasmid DNA sample to be carried forward for amplification and transfection, a restriction digest was performed followed by analysis by agarose gel electrophoresis to assess pcDNA-GO-ATeam1. This was to check that the plasmid DNA vector and the GO-ATeam insert were the correct size, and that the GO-ATeam insert was present in the correct position within pcDNA-GO-ATeam1. A 1 % agarose gel was prepared using 1x TAE (40 mM **T**ris base, 20 mM **a**cetic acid and 1 mM **E**DTA) buffer containing 0.001 % ethidium bromide. Reaction mixtures for each sample were prepared using 500 ng pcDNA, 2.5 µl 10x SuRE/Cut Buffer B (Roche) 1 U restriction endonuclease (0.5 µl), and made up to 25 µl. These were then incubated at 37°C for 1 hour, at which point the reaction was inactivated by incubating the sample at 65°C for 20 minutes. Samples were then diluted in 6x loading buffer containing 30% glycerol and 0.25% bromophenol blue to give 20% loading buffer in each sample immediately prior to loading sample into the gel. HindIII and XhoI restriction endonucleases (Roche) were used to either cut the pcDNA-GO-ATeam1 at one site adjacent to the GO-ATeam insert (HindIII alone) or at both at either side of the GO-ATeam insert to excise the GO-ATeam sequence (HindIII and XhoI in combination). Similarly, HindIII was used to

prepare a single-site restriction digest of the pcDNA3.1 vector. In addition to these single and double restriction digest samples, uncut pcDNA-GO-ATeam1 and uncut pcDNA3.1 (Vector) were run alongside a molecular weight ladder (HyperLadder I, Bioline) The results are presented in Supplementary Figure 3.2B and indicate that all DNA fragments were at their expected positions and at the correct sizes. Sequencing was performed by GATC Biotech using the CMV forward and BGH reverse primers, which confirmed the plasmid sequence was correct.

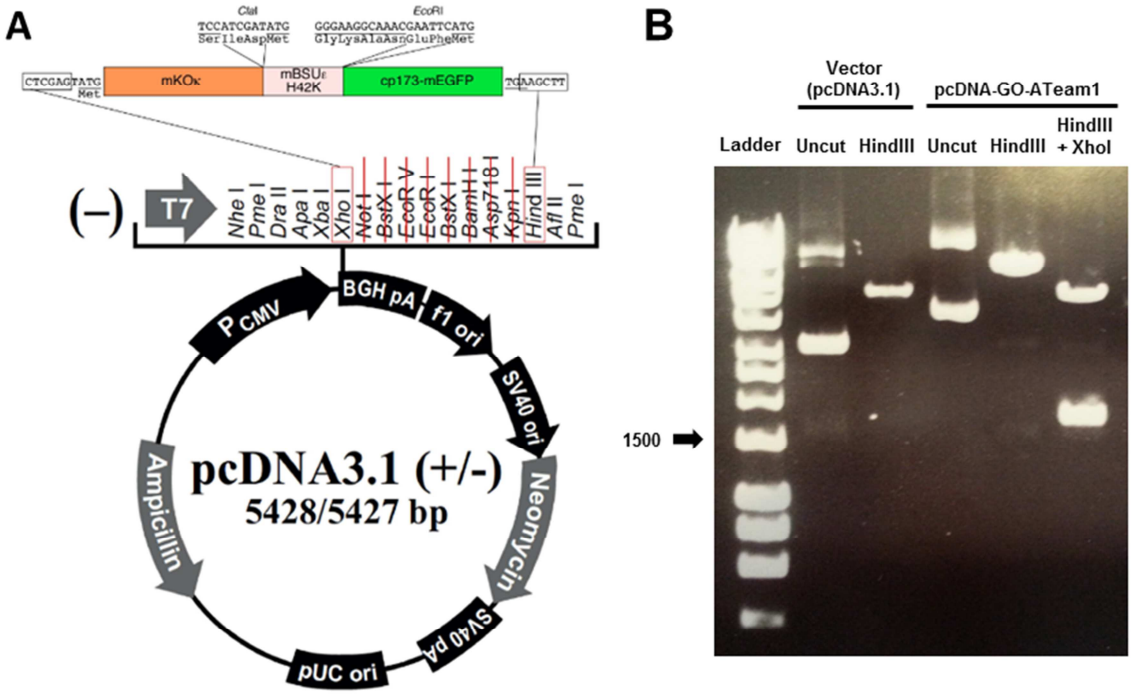

Supplementary Figure 3.2 - The pcDNA3.1 plasmid and GO-ATeam insert

A, a diagram showing the GO-ATeam sequence insertion point on the pcDNA3.1 plasmid vector. Used with permission of H. Imamura. **B**, agarose gel electrophoresis confirmed that the sequence inserted into the pcDNA3.1 plasmid between Xho I and Hind III corresponded to the expected size of the GO-ATeam sequence, 1806 bp.

3.8.3 - Generation of MIA PaCa-2 cells stably expressing GO-ATeam

MIA PaCa-2 cells stably expressing GO-ATeam were selected using the neomycin resistance system, using resistance to the antibiotic G418 (Sigma) to select for stably transfected cells. To select the appropriate concentration of G418 to use to select for resistant cells, MIA PaCa-2 cells were seeded out at a constant density (1 x 10^5 cells/ml) into 12 well culture plates (Corning), and following 24 hours culture were treated with varying concentrations of G418 (0, 125, 250, 500, 750 and 1000 µg/ml) for 9 days. Since G418 is labile at 37°C, the media containing G418 was changed every day, also to remove dead cells. The concentration of G418

which showed complete cell death after 7 days (500 µg/ml) was selected for use generating stably transfected MIA PaCa-2 cells.

pcDNA-GO-ATeam1 (Supplementary Figure 3.2A) was amplified for transfections in MIA PaCa-2 cells using the glycerol stocks of transformed bacteria described above and a midi-preparation kit according to manufacturer's instructions (Plasmid Midi Kit, QIAGEN). To generate MIA PaCa-2 cells stably expressing GO-ATeam, MIA PaCa-2 cells were first seeded out at a constant density (1 x 10^5 cells/ml) into 12 well culture plates (Corning). After 24 hours post-seeding, cells were transfected with pcDNA-GO-ATeam1 using GeneCellin™ (BioCellChallenge) according to the manufacturer's instructions. At 24 hours post-transfection, the cell culture media was subsequently changed for standard medium (DMEM, D6429, Sigma, supplemented with 10% FBS, 100 units/ml penicillin and 100 µg/ml streptomycin) containing 500 µg/ml G418, and cells were cultured under these conditions for 21 days, with the G418 containing medium being changed every 2 days. At this point, colonies expressing GO-ATeam were selected using a Zeiss Axio Observer D1 microscope fitted with an Axiocam CCD camera and FITC filter set (Zeiss), isolated using PYREX® cloning cylinders (Corning), and routinely cultured as normal.

3.8.4 - GO-ATeam FRET imaging of cytosolic ATP

To measure GO-ATeam fluorescence, one of the previously described imaging systems that had been used to measure fura-2 fluorescence was used, with some changes made to the optical hardware. Supplementary Figure 3.3 depicts the setup used to measure GO-ATeam fluorescence. This system was comprised of a Nikon TE2000 microscope fitted with a x40 oil immersion objective (numerical aperture 1.3), a CoolSNAP HQ interline progressive-scan CCD camera (Roper Scientific Photometrics, Tucson, AZ), and a monochromator illumination system with a xenon arc lamp light source (Cairn Research, Kent, UK). In order to measure GO-ATeam fluorescence, the microscrope was equipped with a FITC/TRITC dichroic (505 nm) and a 59004m ET FITC/TRITC dual band emission filter to separate excitation light from emission light. Emitted light was then simultaneously collected at 510 nm and above 560 nm using an OptoSplit Image Splitter equipped with a JC1 565 nm dichroic (Cairn Research, Kent, UK), which allowed light at the two emission wavelengths to be captured on two separate halves of the CCD camera chip. The Optosplit drop-in software within Metafluor separated the different regions on the CCD camera, and treated these as separate images.

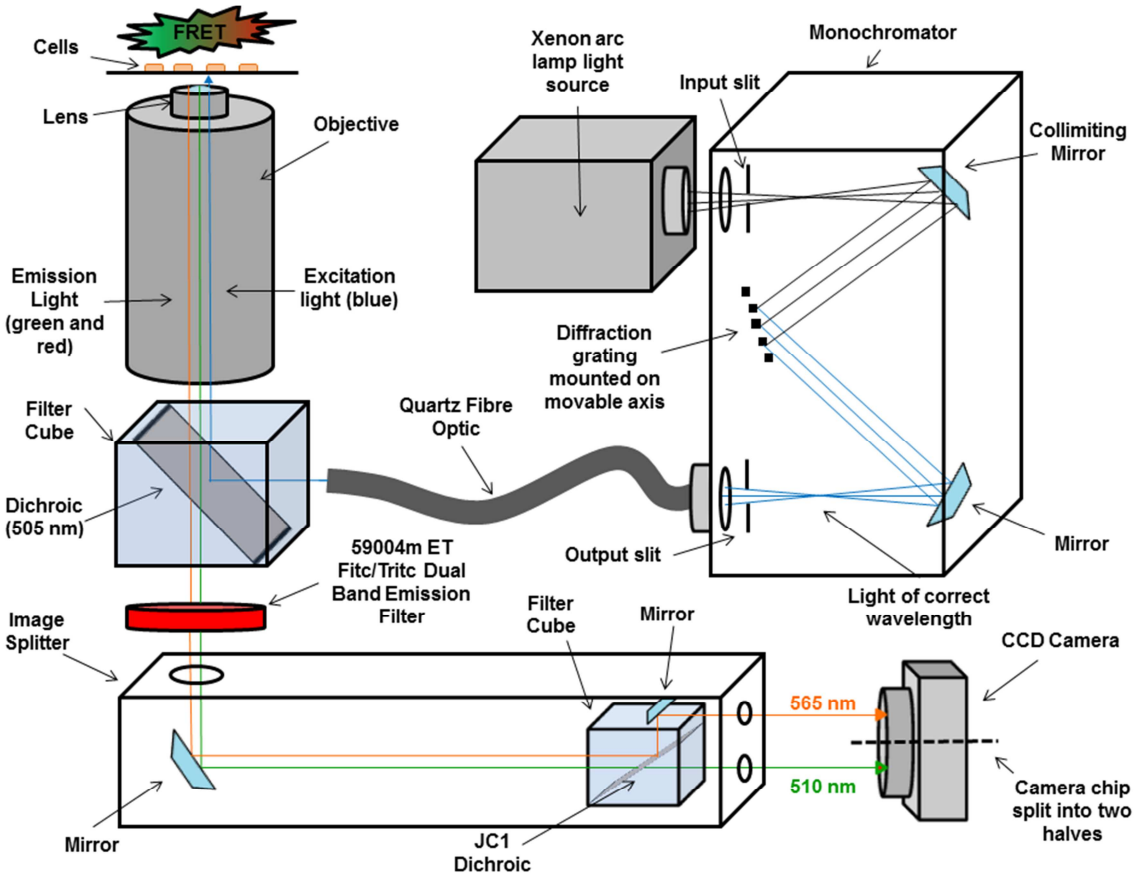

Supplementary Figure 3.3 - An inverted microscope system for GO-ATeam FRET microscopy

Within a monochromator system, light generated by a xenon arc lamp light source was first collimited using a collimiting mirror before being separated using a mobile diffraction grating. Using a mirror, this light was reflected through the output slit at the correct excitation wavelength (λ, 470 nm). This light was carried to the microscope using a quartz fibre optic cable, where a dichroic mirror (505 nm) reflected it up through an objective to excite the cells. Light emitted at both FRET wavelengths (510 nm, green, and 565 nm, orange) following excitation of GO-ATeam was then carried back through the objective and passed through the dichroic mirror and a FITC/TRITC dual band emission filter. Emission light then entered an Optosplit image splitter, where it was reflected and then separated using a JC1 dichroic into the two separate emission wavelengths, 565 nm and 510 nm. This light was detected using a charged coupled device (CCD) camera system, with the detection chip split into two halves in order to detect each wavelength separately.

3.9 - Supplemental References

NAKANO, M., IMAMURA, H., NAGAI, T. & NOJI, H. 2011. Ca^{2+} regulation of mitochondrial ATP synthesis visualized at the single cell level. *ACS Chem Biol,* 6**,** 709-15.

Chapter 4 - Regulation of the Plasma Membrane Calcium Pump by Membrane-Bound Glycolytic Enzymes in Pancreatic Cancer

Andrew James[‡1], James Wong[‡], Bobby Chow[‡], Joseph Dent[‡], Jonathan Briggs[‡], Hannah Tierney[‡], Raga Dakhel[‡], Hiromi Imamura[¶], Donald Ward[‡], and Jason Bruce[‡]

From the [‡] Faculty of Life Sciences, The University of Manchester, Michael Smith Building, Oxford Road, Manchester, M13 9PT, United Kingdom, and [¶] PRESTO, Japan Science and Technology Agency, Japan.

4.1 - Abstract

Pancreatic ductal adenocarcinoma (PDAC) is an aggressive cancer with limited treatment options. We have previously identified that the plasma membrane calcium ATPase, which extrudes cytosolic Ca^{2+} in order to maintain a low intracellular Ca^{2+} concentration ($[Ca^{2+}]_i$) and thus cell survival, is critically reliant on glycolytically-derived ATP in human PDAC cells exhibiting the Warburg effect. Moreover, previous studies suggest that glycolytic enzymes dynamically associate with the plasma membrane. Whilst it is not known whether this phenomenon occurs in PDAC, this could provide a privileged ATP supply to the PMCA and be key to its glycolytic dependency, and therefore may be an important therapeutic locus. The present study sought to determine whether glycolytic enzymes associate with the plasma membrane in PDAC and whether this is regulated by tyrosine phosphorylation. Using cell surface biotinylation assays with subsequent western blot analysis, we show that the key glycolytic enzymes LDHA, PFKP, GAPDH, PFKFB3 and PKM2 associate with the plasma membrane in MIA PaCa-2 cells. Furthermore, western blots following tyrosine kinase inhibition with genistein (150 µM) and tyrphostin A23 (50 µM) or tyrosine phosphatase inhibition with pervanadate (10 µM) tentatively suggest that this membrane association may be regulated by tyrosine phosphorylation. However, while both genistein and tyrphostin A23 slowed PMCA activity during an *in situ* $[Ca^{2+}]_i$ clearance assay, measurement of cytosolic ATP indicated that this was not likely due to ATP depletion. Further research is required to characterise the regulation of glycolytic enzyme association with the plasma membrane in PDAC and whether this influences PMCA activity.

4.2 - Introduction

While significant advances have been made in cancer treatment, pancreatic cancer has proven notoriously difficult to combat with conventional chemotherapy and prognosis for patients remains extremely poor. At present, pancreatic cancer is the fourth leading cause of cancer-related death in the United States with a 5 year survival rate of only 6% (Siegel et al., 2014). Pancreatic ductal adenocarcinoma (PDAC) accounts for around 85% of reported pancreatic malignancies, and commonly arises from the epithelial exocrine tissue within the head of the pancreas (Alexakis et al., 2004). In the case of PDAC, tumour resection remains the most common course of action. However, since PDAC commonly progresses to metastasis in the absence of noticeable clinical symptoms, only 15–20% of patients present with resectable disease (Amin et al., 2006). Nevertheless, of those patients undergoing surgical resection, only 20% survive beyond 5 years (Li et al., 2004). These bleak statistics clearly illustrate that novel treatment approaches are required to combat this unsolved global health problem.

One potential target for treating PDAC that is currently the focus of intense research is altered cell metabolism in cancer (Tennant et al., 2010). In particular, cancer cells exhibit a high glycolytic rate even when oxygen is abundant, a phenomenon first observed by Otto Warburg in the 1920s that subsequently became known as the “Warburg Effect” (Warburg, 1956). A high glycolytic rate is vital for the rapid proliferation of PDAC cells as it provides an abundance of glucose carbons in the form of glycolytic intermediates for anabolic processes and cell proliferation (Gillies and Gatenby, 2007, Kroemer and Pouyssegur, 2008). Though glycolysis is not an energetically favourable means of generating ATP in comparison to mitochondrial oxidative phosphorylation due to its poor yield of ATP per glucose molecule consumed, glycolysis is a rapid means of generating ATP (Pfeiffer et al., 2001) that can be maintained despite the hypoxic conditions within a tumour (Koong et al., 2000). Proteomic studies have revealed that PDAC exhibits key metabolic changes that promote the Warburg phenotype (Zhou et al., 2012), and targeting tumour energy metabolism may therefore hold promise as an effective therapeutic intervention for PDAC. Indeed, studies have shown that pharmacological inhibition of glycolysis depletes ATP levels in highly glycolytic cells (including those derived from pancreatic cancer) and can prevent tumour progression in xenograft models of cancer (James et al., 2013, Le et al., 2010, Ko et al., 2004).

Following the upregulation of glycolysis in PDAC, one might expect that those processes critically dependent on a robust ATP supply may be affected due to a change in the relative contributions of glycolysis and mitochondrial metabolism to ATP generation. One such process is the ATP-dependent extrusion of cytosolic calcium (Ca^{2+}) by the plasma membrane calcium ATPase (PMCA), which is crucial for maintaining a low intracellular Ca^{2+} concentration ($[Ca^{2+}]_i$, ~100 nM). This is critical for cell survival; impaired PMCA activity is catastrophic for a cell, as it inevitably leads to a sustained and irreversible $[Ca^{2+}]_i$ overload that ultimately results in cell death (Brini and Carafoli, 2009). We have previously shown that the PMCA utilises a supply of glycolytically-derived ATP in PDAC, and that glycolytic inhibition results in PMCA inhibition and

$[Ca^{2+}]_i$ overload (James et al., 2013, *Chapter 2*). Furthermore, our follow up study showed that the sensitivity of the PMCA in PDAC to glycolytic inhibition was significantly attenuated when glycolysis was slowed, suggesting that the critical reliance of the PMCA on glycolytically-derived ATP in PDAC cells is specific to those cells exhibiting the Warburg phenotype (*Chapter 3*). We therefore suggested that the glycolytic ATP supply to the PMCA might be a weakness that could be exploited selectively in PDAC cells exhibiting a high glycolytic rate, as these cells appear exquisitely sensitive to the loss of a glycolytic ATP supply to the PMCA.

Evidence suggests that glycolytic enzymes can colocalise with the plasma membrane and may be functionally coupled to ATP-consuming pumps such as the PMCA and the Na^+/K^+ ATPase, thereby providing them with a privileged ATP supply. A large body of evidence indicates that glycolytic enzymes associate with the plasma membrane in erythrocytes via interactions with anion exchanger 1 (AE1), also known as band 3, in a tyrosine kinase dependent fashion (Puchulu-Campanella et al., 2013, Campanella et al., 2005, Campanella et al., 2008). However, AE1 expression is largely restricted to erythrocytes. Nevertheless, early functional studies showed that the PMCA has its own glycolytic ATP supply in porcine smooth muscle cells (Hardin et al., 1992, Paul et al., 1989). More recently, however, the glycolytic enzyme PKM2 has been shown to associate with the membrane-associated mucin 1 (MUC1) in 3Y1 fibroblasts in a tyrosine kinase dependent manner (Kosugi et al., 2011). Moreover, MUC1 has been shown to promote the glycolytic phenotype in pancreatic cancer (Chaika et al., 2012), and is aberrantly overexpressed in PDAC (Hinoda et al., 2003). It is not currently known whether glycolytic enzymes associate at the plasma membrane in PDAC, and whether this is dynamically regulated. Nevertheless, it is tempting to speculate that the plasma membrane localisation of glycolytic enzymes proximal to the PMCA in PDAC may be an important therapeutic locus in highly glycolytic cancer cells.

Based on these previous studies, the present study sought to determine whether enzymes involved in the glycolytic cascade associate with the plasma membrane in the human PDAC cell line, MIA PaCa-2, and whether any association was dynamically regulated by tyrosine kinase activity. Furthermore, since membrane association of glycolytic enzymes in other cell types is known to affect their activity, the effects of tyrosine kinase inhibitors were assessed on PMCA activity and cytosolic [ATP]. We report for the first time that glycolytic enzymes associate with the plasma membrane in MIA PaCa-2 cells, potentially providing the PMCA with a privileged ATP supply. Tyrosine kinase inhibitors slowed PMCA activity, but did not decrease global cytosolic [ATP]. These results confirm the presence of membrane-bound glycolytic enzymes in PDAC that are proximal to the PMCA; however, it remains unclear whether this membrane association is regulated in a tyrosine kinase-dependent fashion and whether this regulates PMCA function.

4.3 - Experimental Procedures

4.3.1 - Cell culture

MIA Paca-2 cells (American Type Culture Collection) were grown in Dulbecco's Modified Essential Media (DMEM, D6429, Sigma), supplemented with 10% foetal bovine serum, 100 U/ml penicillin and 100 µg/ml streptomycin in a humidified atmosphere of air/CO2 (95%:5%) at 37°C. Cells were used until passage 30, at which point they were discarded.

4.3.2 - Preparation of test reagents

Stocks of pervanadate (PV) were prepared from orthovanadate monomers by adding excess H_2O_2, which was incubated for 15 minutes at room temperature before being quenched with excess catalase (Sigma, see *4.7.1 – Preparation of pervanadate*). Stocks of genistein and Tyrphostin A23 were both prepared in DMSO. HEPES-buffered physiological saline solution (HEPES-PSS; 138 mM NaCl, 4.7 mM KCl, 1.28 mM $CaCl_2$, 0.56 mM $MgCl_2$, 5.5 mM glucose, 10 mM HEPES, pH 7.4) was used in all imaging experiments. Phosphate buffered saline (PBS) used in the biotinylation assays was prepared using Thermo Scientific BupH Phosphate Buffered Saline Packs (Pierce, 0.1M sodium phosphate, 0.15M NaCl, pH 7.2). Aliquots were stored at -20°C, and were defrosted and added to the appropriate solutions immediately prior to assay.

4.3.3 - Western blotting

Proteins were separated by SDS-PAGE on 6, 7.5 and 10 % resolving gels (see *4.7.3 – Gel preparation for western blot*) using a SE300 miniVE Integrated Vertical Electrophoresis and Blotting Unit (Hoefer) with running buffer (25 mM Tris base, 192 mM glycine, 0.1% SDS). Prestained SDS-PAGE standards (#161-0318, Bio-Rad) were used to determine molecular weight of bands. After resolving a gel, proteins were transferred onto a nitrocellulose membrane (Amersham Protran Premium 0.45 µm NC) using a Trans-Blot® SD semi-dry electrophoretic transfer cell (Bio-Rad) and transfer buffer (25 mM Tris base, 192 mM glycine, 20% methanol and 0.1% SDS). Nitrocellulose membranes were then blocked for 1 hour in either 5% BSA or milk in Tween Tris buffered saline (Tween TBS, pH 7.6, 20 mM Tris base, 138 mM NaCl, 0.15% Tween 20) at room temperature. Membranes were then washed and blotted with primary antibody overnight at 4°C in Tween TBS containing 5% BSA or milk. The following day the membranes were again washed in Tween TBS prior to applying the appropriate secondary antibody for 1 hour at room temperature. Following a final wash in Tween TBS, the nitrocellulose membranes were incubated in ECL reagent (Western Lightning Plus, Perkin Elmer) at room temperature, exposed to x-ray film (CL-XPosure, Pierce) and developed. Primary antibodies supplied by Cell Signalling Technology were PKM2 (D78A4) XP®, PKM1/2

(C103A3), GAPDH (D16H11) XP®, PDH (C54G1), HKI (C35C4), HKII (C64G5), LDHA (C4B5), PFKP (D4B2) and PFKFB3 (D7H4Q). Similarly, PMCA4 and PMCA NS primary antibodies were supplied by Cell Signalling, while the anti-phosphotyrosine (PY20) primary antibody was supplied by Sigma. Secondary antibodies used were HRP-linked anti-rabbit (Cell Signalling Technology) and HRP-linked anti-mouse (Dako). The MUC1 (BC-2) antibody was kindly donated by Professor John Aplin (Hey et al., 1995).

4.3.4 - Phosphotyrosine western blot sample preparation

To test the effects of tyrosine kinase inhibitors on global tyrosine phosphorylation using an antiphosphotyrosine antibody (PY20), MIA PaCa-2 cells were first seeded at a constant density in 35 mm diameter tissue culture-treated dishes (Corning) and allowed to grow until 90% confluent. Cells were then treated with test reagents (genistein, 50 and 150 µM, tyrphostin A23, 10 and 50 µM, and pervanadate, PV, 10 µM) in either cell culture media or PBS for 15 minutes at 37°C, and then rinsed with PBS twice on ice and lysed using a RadioImmune Precipitation Assay (RIPA) buffer, containing 50 mM Trizma® base (Sigma), 1 mM EDTA, 1 mM EGTA, 0.1 mM vanadate, 1 mM NaF, 40 mM $Na_4P_2O_7$, 1% Triton X-100, 0.1% SDS, and cOmplete EDTA-free protease inhibitors (Roche Applied Science). A BCA assay (Pierce) was performed on all samples using a Nanodrop 2000 (Thermo Scientific) and equal protein concentrations loaded for each condition.

4.3.5 - Isolation of plasma membrane proteins

MIA PaCa-2 cells were cultured in 75cm^3 vented cap flasks (Corning) until 90% confluent at which point proteins found within or associated with the plasma membrane were isolated using a biotinylation-based Pierce Cell Surface Protein Isolation Kit (see *4.7.2 – Isolation of membrane bound proteins using cell surface biotinylation assay*, Thermo Fisher). Four flasks were used per condition. Cells were first treated with test reagents which were subsequently removed prior to labelling cells with the supplied biotinylation reagent. Following labelling, cells were lysed using the supplied lysis buffer supplemented with cOmplete EDTA-free protease inhibitors (Roche Applied Science). The protein isolation of the biotinylated (membrane) fraction was then performed according to manufacturer's instructions. Briefly, this involved lysis sample sonication (5 x 1 second bursts) followed by 30 minutes treatment with lysis buffer on ice with repeat vortex steps every 5 minutes, centrifugation of lysate (10000 x g at 4°C) and transfer of the clarified supernatant to an elution column containing NeutrAvidin™ agarose beads (Thermo Scientific). The sample was then incubated at room temperature for 1 hour on a rocking platform, after which the unbound proteins (the non-biotinylated fraction) were eluted. The non-biotinylated eluent was retained as this fraction contained the non-membrane bound or cytosolic proteins. The column was rinsed and the biotinylated fraction eluted using 1x SDS sample buffer (62.5mM Tris HCl; pH 6.8, 2% SDS; 10% Glycerol; 1% β-mercaptoethanol)

supplemented with dithiothreitol (DTT, 50 mM). 5x SDS sample buffer without DTT was added to non-biotinylated fraction sample to give 1x SDS sample buffer and both the biotinylated and non-biotinylated fractions were boiled at 95 °C for 5 min, at which point they were analysed by western blot as described above.

In the assays comparing protein abundance in biotinylated vs non-biotinylated fraction after treatment with either tyrosine kinase inhibitors or pervanadate, cells were seeded at an identical cell density 2 days prior to sample preparation to ensure each flask contained the same cell mass on the day of the assay. Cells were first treated with genistein (150 µM) and tyrphostin A23 (50 µM) in combination (G+T) or PV (10 µM) in PBS for 15 minutes at 37°C. Following treatment, cells were rinsed twice with cold PBS on ice and the biotinylation protocol performed. Following fraction separation, a BCA protein assay (Pierce) was performed on the non-biotinylated fraction samples using a Nanodrop 2000 (Thermo Scientific). Samples were analysed by western blot as described above.

4.3.6 - Fura-2 fluorescence imaging

To measure $[Ca^{2+}]_i$ clearance, MIA PaCa-2 cells were seeded onto glass coverslips and allowed to adhere overnight before being loaded with fura-2 AM (4 µM) for 40 minutes at room temperature. These cells were mounted on an imaging system, as previously described (James et al., 2013). This system employed a Nikon Diaphot microscope fitted with a x40 oil immersion objective (numerical aperture 1.3) and an Orca CCD camera (Hamamatsu). Both microscope systems used in this study (one for GO-ATeam FRET imaging, the other for fura-2 fluorescence imaging) employed a monochromator illumination system (Cairn Research,Kent, UK) controlled by MetaFluor image acquisition and analysis software (Molecular Devices, Downingtown, PA). Cells were continually perfused with HEPES-PSS by means of a gravity-operated perfusion system (Harvard Apparatus). Cells were excited at 340 nm and 380 nm (50 ms exposure) and excitation light separated from emitted light using a 400 nm dichroic with a 505LP filter. All experiments were performed at room temperature (22°C).

4.3.7 - GO-ATeam FRET imaging

To measure cytosolic ATP, MIA PaCa-2 cells were stably transfected using the FRET-based ATP reporter, GO-ATeam (Nakano et al., 2011) as previously described (*Chapter 3*). These cells were then seeded onto glass coverslips and allowed to adhere overnight before being mounted onto an imaging system. This system included a Nikon TE2000 microscope with a x40 oil immersion objective (numerical aperture 1.3), and background subtracted images were acquired using a CoolSNAP HQ interline progressive-scan CCD camera (Roper Scientific Photometrics, Tucson, AZ). Cells were perfused with HEPES-PSS using gravity-operated perfusion systems (Harvard Apparatus). Cells were excited at 470 nm (500 ms exposure), and emitted light separated from excitation light using a 505 nm dichroic fitted with a dual band

emission filter (59004m ET FITC/TRITC Dual Emitter). Simultaneous collection of light emitted at 510 nm and above 560 nm was made possible using an OptoSplit Image Splitter fitted with a JC1 565 nm dichroic (Cairn Research, Kent, UK). All experiments were performed at room temperature (22°C).

4.3.8 - Data analysis

Background subtracted images of a field-of-view of cells were acquired every 5 seconds for each emission (GO-ATeam) or excitation (fura-2) wavelength. All analysis was performed using Microsoft Excel and Graphpad Prism 6, and presented data represent the means ± SEM of the indicated number (n) of experimental repeats.

In order to calculate ATP (%) in the GO-ATeam experiments (See Figure 4.4A), we first calculated the maximum decrease in GO-ATeam FRET ratio (ΔR_{max}) from the pretreatment baseline (R_0) following treatment with the ATP depletion cocktail, as this drug combination was assumed to cause 100% ATP depletion, thus giving the dynamic range of the experiment. ΔR_{max} was calculated by subtracting the minimum steady-state ratio observed following treatment with the ATP depletion cocktail (R_{min}) from the baseline ratio prior to drug addition (R_0, the mean of the 10 values immediately prior to application of test reagent). R_{min} was then subtracted from all FRET ratio values throughout the experiment, and these corrected values were then normalised to ΔR_{max} (%). These values were averaged across all cells in an assay to give the experimental mean % ATP for all time points throughout the assay. ATP depletion at 0, 5, 10, 15 and 20 minutes treatment with the test reagent was then compared to that in untreated control cells. Statistical comparisons were performed using a two-way ANOVA with a post hoc Bonferroni test for multiple comparisons.

To calculate $[Ca^{2+}]_i$ clearance rate, the linear rate (60 seconds) during the second influx/clearance phase (fura-2 ratio units/second) was normalised (%) to that of the first clearance phase, with both measurements beginning at the same starting fura-2 ratio value. Similarly, relative recovery during the second clearance phase was normalised (%) to that of the first, again measured from a standardised fura-2 ratio value. In instances where recovery was 100% across treatment groups, clearance was also assessed by measuring the relative time constant (tau, τ) for each clearance phase. This involved fitting the clearance curves to a single exponential decay from the same starting fura-2 ratio value, and normalising the time constant (tau, τ) of the second clearance phase to that of the first. Since the τ represents the time constant (in seconds) and is the reciprocal of the rate constant (in $seconds^{-1}$), the inverse of the τ during the second clearance phase (τ_2) must be normalised (%) to that of the first (τ_1), or $((1/\tau_2)/(1/\tau_1)) \times 100$. This can be simplified as $(\tau_1/\tau_2) \times 100$ to give the relative τ %. Differences in $[Ca^{2+}]_i$ clearance rate (as assessed by measuring both the linear rate and the time constant of a single exponential decay) and relative recovery were then statistically assessed between treatment groups using a Mann Whitney U test.

4.4 - Results

4.4.1 - Key glycolytic enzymes associate with plasma membrane proteins in MIA PaCa-2 cells

To determine whether glycolytic enzymes associate with the plasma membrane, cell membranes from MIA PaCa-2 cells were isolated using a cell surface biotinylation assay. Briefly, this method involved labelling the external envelope of the plasma membrane with a biotinylation reagent (Sulfo-NHS-SS-Biotin) that binds to primary amines (such as the side-chain of lysine) within the extracellular domains of transmembrane proteins. This reagent does not cross the plasma membrane and therefore only labels proteins from the extracellular envelope. Thus, following cell lysis, the labelled plasma membrane (and anything associated with it) could be immobilised and separated from the cytosolic fraction using NeutrAvidin^{TM} agarose beads and then eluted using dithiothreitol (DTT, 50 mM). Subsequently, the biotin-labelled membrane fraction could be western blotted at low (10 µl) and high (30 µl) volumes alongside the retained non-biotinylated fraction containing cytosolic and organelle-associated protein (10 µg), with whole cell lysates from MIA PaCa-2 cells (5 µg) included as a positive control.

Before assessing whether glycolytic enzymes are found in the biotinylated fraction, we first confirmed that this fraction is enriched with proteins typically only found at the plasma membrane. We therefore probed biotinylated and non-biotinylated fractions from MIA PaCa-2 cells for the PMCA using a nonspecific antibody for all PMCA isoforms (PMCA NS) and antibodies specific for PMCA4. As expected, bands were found at ~140 kDa in the biotinylated fraction and whole cell lysate for both PMCA NS and PMCA4 (Figure 4.1). Only a faint band was observed within the non-biotinylated fraction for both PMCA NS and PMCA4, most likely due to protein in the process of either being trafficked to or endocytosed from the plasma membrane, or a minor contamination by unlabelled transmembrane proteins. These results confirmed the presence of PMCA and specifically PMCA4 in MIA PaCa-2 cells, and also confirmed that by using this method the biotinylated fraction is enriched with proteins that are known to be typically only expressed at the plasma membrane.

Using western blotting, we next assessed the expression profile of key glycolytic enzymes within biotinylated vs non-biotinylated fractions from MIA PaCa-2 cells (Figure 4.1), again using whole cell lysates as a positive control. This included western blot for hexokinase I (HKI, 102 kDa), lactate dehydrogenase A (LDHA, 37 kDa), phosphofructokinase, platelet (PFKP, 80 kDa), glyceraldehyde 3-phosphate dehydrogenase (GAPDH, 37 kDa), 6-phosphofructo-2-kinase/fructose-2,6-biphosphatase 3 (PFKFB3, 60 kDa), pyruvate kinase muscle 2 (PKM2, 60 kDa) and pyruvate kinase muscle 1 and 2 isoform nonspecific (PKM1/2, 60 kDa). Bands at the appropriate molecular weight were detected for LDHA, PFKP, GAPDH, PFKFB3 and PKM2 within the whole cell lysate and both biotinylated and non-biotinylated fractions. These results confirm that these enzymes all associate with proteins at the plasma membrane in MIA PaCa-2 cells, as well as being found within the non-biotinylated fraction.

However, following western blot for and hexokinase II (HKII, 102 kDa), bands were detected at the appropriate molecular weight in both the whole cell lysate and the non-biotinylated fraction, but not the biotinylated fraction. Similarly, pyruvate dehydrogenase (PDH, 43 kDa) was only detected in the non-biotinylated fraction. While this indicates that MIA PaCa-2 cells do indeed express HKII and PDH, the absence of PDH within the whole cell lysate was surprising and was potentially due to low protein abundance. However, as expected, these results indicate that PDH does not associate with the plasma membrane. PDH and HKII are proteins found within or associated to the mitochondria, and the lack of bands within the biotinylated fraction suggests that this fraction is specific for proteins associated with the plasma membrane. Furthermore, these results indicate that, following this separation method, the biotinylated fraction is not contaminated with proteins from the non-biotinylated fraction.

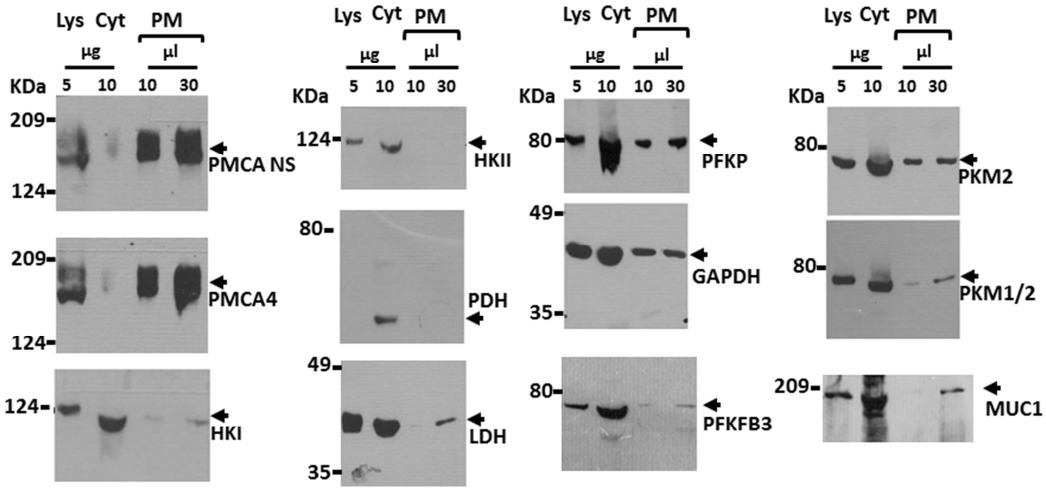

Figure 4.1 – Glycolytic enzymes are associated with the plasma membrane in MIA PaCa-2 cells.

Using a cell surface biotinylation assay, plasma membrane was isolated from MIA PaCa-2 cells. Biotinylated fractions (representing the plasma membrane, PM, 10 and 30 µl) were blotted against non-biotinylated fractions (representing the cytosol fraction, Cyt, 10 µg) and whole cell lysates (Lys, 5 µg). Representative western blots are presented using antibodies against PMCA NS (PMCA isoform nonspecific), PMCA4 (PMCA isoform 4), hexokinase I (HKI), hexokinase II (HKII), pyruvate dehydrogenase (PDH), lactate dehydrogenase (LDH), phosphofructokinase platelet isoform (PFKP), glyceraldehyde 3-phosphate dehydrogenase (GAPDH), 6-phosphofructo-2-kinase/fructose-2,6-biphosphatase 3 (PFKFB3), pyruvate kinase M2 isoform (PKM2), pyruvate kinase M1 and M2 nonspecific (PKM1/2) and mucin 1 (MUC1).

Evidence suggests that PKM2 can associate with mucin 1 (MUC1) in a tyrosine kinase-dependent fashion (Kosugi et al., 2011), thereby potentially providing a candidate binding site for a glycolytic enzymes at the plasma membrane in PDAC. Therefore, we aimed to determine whether MUC1 is expressed in the plasma membrane of MIA PaCa-2 cells, since it may act to anchor glycolytic enzymes to the plasma membrane. The MUC1 (BC-2) antibody binds a 5 amino acid epitope present within the 20 amino acid tandem repeat region of the MUC1 core protein (Xing et al., 1990, Xing et al., 1989). Following western blot for MUC1, bands were

observed just below the 209 kDa weight marker in the MIA PaCa-2 whole cell lysate and both biotinylated and non-biotinylated fractions (Figure 4.1). Surprisingly, numerous bands were observed in the non-biotinylated fraction, potentially due to MUC1 endocytosis, recycling and trafficking to exosomes (Hanisch et al., 2012). Nevertheless, these results confirm that MIA PaCa-2 cells do indeed express MUC1, and that this protein is expressed at the plasma membrane.

4.4.2 - Regulation of glycolytic enzyme membrane association by protein tyrosine phosphorylation

Previous studies have shown that tyrosine kinase-mediated phosphorylation regulates the formation of a submembrane glycolytic enzyme complex in human erythrocytes (Campanella et al., 2005), and also regulates the aforementioned association of PKM2 with MUC1 in 3Y1 fibroblasts expressing the cytoplasmic domain of MUC1 (Kosugi et al., 2011). Therefore, after establishing that glycolytic enzymes are associated with plasma membrane proteins in MIA PaCa-2 cells, we aimed to test whether this membrane association was dynamically regulated by tyrosine phosphorylation.

To test this, we set out to compare the relative protein abundance within the biotinylated vs non-biotinylated fractions following treatment with the tyrosine kinase inhibitors genistein and tyrphostin A23 (to inhibit basal phosphorylation of tyrosine residues) or the tyrosine phosphatase inhibitor pervanadate (to induce maximal tyrosine phosphorylation). However, it was important to first establish the full dynamic range of protein tyrosine phosphorylation in MIA PaCa-2 cells following treatment with these drugs. This was achieved by applying either genistein (50 µM or 150 µM), tyrphostin A23 (10 µM or 50 µM) or pervanadate (PV, 10 µM), followed by whole cell lysis and western blot using an anti-phosphotyrosine antibody (PY20). Whole cell lysates were prepared from MIA PaCa-2 cells treated with test reagents in cell culture media for 15 minutes, and untreated cells were used as a control. Equal protein concentrations (30 µg) were loaded in each lane. Following treatment with pervanadate to inhibit tyrosine phosphatases, western blotting for phorphorylated tyrosine residues revealed numerous large bands due to the unopposed tyrosine kinase-mediated phosphorylation of cellular proteins (Figure 4.2A(i)). However, little difference in signal intensity was observed between the control group and those treated with genistein or tyrphostin A23. This suggests that basal tyrosine phosphorylation is very low in MIA PaCa-2 cells and indistinguishable from that following treatment with these tyrosine kinase inhibitors. This was possibly due to basal tyrosine phosphatase activity being higher than basal tyrosine kinase activity. The low basal tyrosine phosphorylation could also be explained by the fact that experiments were performed in HEPES-PSS and therefore in the absence of serum, which contains numerous growth factors which influence basal tyrosine phosphorylation by activating numerous growth factor receptor-mediated tyrosine kinase pathways. We therefore performed side-by-side experiments with genistein, tyrphostin A23 and PV in both cell culture medium (Figure 4.2A(ii)) and HEPES-PSS.

However to our surprise, band intensities were significantly higher in cells which received drug treatment in HEPES-PSS (Figure 4.2A(i) and 4.2A(ii)). One possible explanation for this is that serum is known to bind drugs, and thus their effective concentration might be reduced in serum-supplemented media. Therefore HEPES-PSS was used as the vehicle in all subsequent drug incubations. Furthermore, to our surprise, 10 µM tyrphostin A23 alone increased tyrosine phosphorylation compared to untreated controls, wheras 50 µM tyrphostin A23 did not. Subsequent experiments therefore used 50 µM tyrphostin A23.

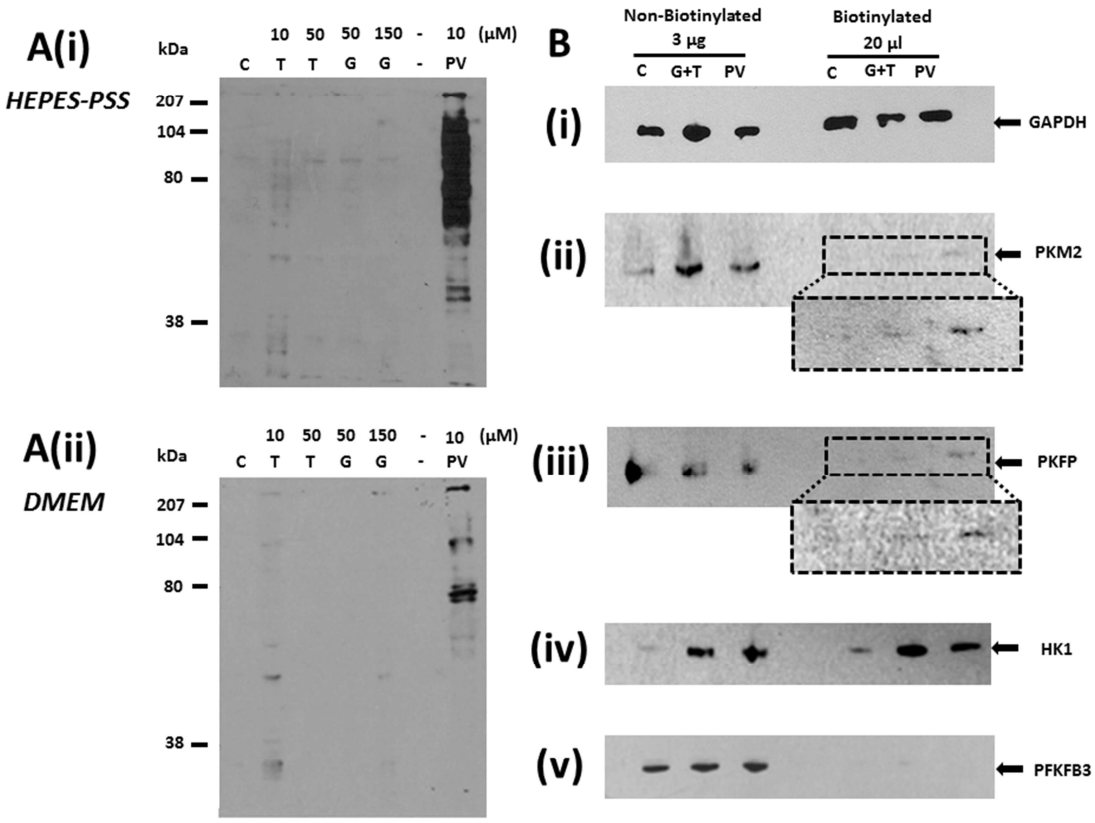

Figure 4.2 - Regulation of glycolytic enzyme membrane association by tyrosine kinase phosphorylation.

A - Western blots showing tyrosine phosphorylation in whole cell lysates from MIA PaCa-2 cells treated for 15 minutes with tyrphostin A23 (T), genistein (G), pervanadate (PV) or vehicle (control, C) at the concentrations indicated. Vehicle for treatment was HEPES-buffered phosphate saline solution (HEPES-PSS, ***A(i)***) or Dulbecco's modified Eagle's medium with supplements (DMEM, ***A(ii)***), with 30 µg protein loaded for each treatment sample. Western blots were carried out using an anti-phosphotyrosine antibody (PY20). ***B -*** Using HEPES-PSS as the vehicle, MIA PaCa-2 cells were treated with genistein (150 µM) and tyrphostin A23 (50 µM) in combination (G+T), with PV (10 µM) or HEPES-PSS alone (control, C). A biotinylation-based assay was then used to separate the plasma membrane fraction (Biotinylated) and cytosolic fraction (Non-biotinylated), and western blots performed using primary antibodies against key glycolytic enzymes: ***B(i)***, GAPDH; ***B(i)***, PKM2; ***B(iii)***, PFKP; ***B(iv)***, HK1; ***B(v)***, PFKFB3. 3 µg of sample was loaded for all non-biotinylated fraction samples, while in the absence of a protein assay 20 µl was loaded for all biotinylated fraction samples.

We then tested the relative level of glycolytic enzymes in biotinylated vs non-biotinylated fractions following treatment of MIA PaCa-2 cells with the tyrosine kinase inhibitors or pervanadate (see *4.7.2 – Isolation of membrane bound proteins using cell surface biotinylation assay*). To ensure maximal inhibition of tyrosine kinases (and thus minimum tyrosine phosphorylation), a combination of genistein (150 µM) and tyrphostin A23 (50 µM) was used (G+T). If tyrosine phosphorylation dynamically regulates the association of glycolytic enzymes with the plasma membrane, we would expect to see corresponding and opposite changes in glycolytic enzyme abundance in the biotinylated vs non-biotinylated fractions following treatment with PV (10 µM) vs genistein and tyrophostin A23 (G+T). Since flasks were seeded at an identical cell density for each drug treatment, it was assumed that each flask would contain the same number of cells (and thus protein content) at the start of each drug treatment. However, it must be noted that protein concentration could not be determined for the biotinylated fractions due to the presence of DTT at the elution step of fraction separation. Nevertheless, protein concentration was determined for the non-biotinylated fraction, and 3 µg protein was loaded for each non-biotinylated sample. It was also anticipated that there would be significantly less protein in the biotinylated fractions; therefore, a roughly tenfold higher volume (equated to 20 µl) was loaded for all biotinylated samples. Importantly, in the absence of a protein assay, this volume (20 µl) was kept constant for all biotinylated fraction samples.

Following combination treatment with G+T, the band intensity for GAPDH increased within the non-biotinylated fraction with a corresponding decrease in the biotinylated fraction (Figure 4.2B(i)), compared to PV. However, no change was observed following treatment with PV compared to control, despite PV causing maximum tyrosine phosphorylation of cellular protein. These results suggest that inhibition of tyrosine kinase activity may lead to a decrease in membrane-associated GAPDH and that tyrosine phosphatase inhibition does not increase the abundance of GAPDH at the membrane, compared to control conditions.

With regards G+T and PV treatment, qualitatively similar results were obtained when identical blots were re-probed for PKM2 and PFKP (Figure 4.2B(ii) and 4.2B(iii)), however only very faint bands were detected in the biotinylated fractions, which may reflect low protein abundance. Nevertheless, there appears to be an increase in the non-biotinylated fraction following treatment with G+T compared to treatment with PV, and a corresponding increase in the biotinylated fraction following treatment with PV compared to treatment with G+T. On the other hand, in comparison to PV treatment, HKI (Figure 4.2B(iv)) was enriched in the biotinylated fraction following treatment with G+T; this corresponded with an increase in the non-biotinylated fraction following PV treatment compared to G+T treatment. However, in contrast to the results presented in Figure 4.1, PFKFB3 could not be detected within the biotinylated fraction during these assays (Figure 4.2B(v)), suggesting that this protein is expressed at a low level at the plasma membrane in MIA PaCa-2 cells.

Similar to GAPDH, the results obtained following western blot for PKM2, PFKP and HKI tentatively suggest that these glycolytic enzymes all dynamically associate with the plasma

membrane in a tyrosine kinase-dependent manner. Nevertheless, care must be taken when interpreting these data since the protein concentrations in the biotinylated samples could not be determined and due to band intensities being close to detection limits. This meant that results were highly variable and inconsistent in repeat experiments, and therefore may present a major confounding factor. Thus, the observed changes in protein abundance in the biotinylated fraction could be due to a difference in protein concentration between samples, rather than the effect of drug induced membrane association/dissociation. Nevertheless, protein concentration could be determined for the non-biotinylated fractions and the amount loaded standardised; although tenuous, these results broadly fit with the hypothesis that tyrosine phosphorylation status controls the translocation of these glycolytic enzymes to and from the cytosol to the plasma membrane.

4.4.3 - The tyrosine kinase inhibitors reduce PMCA activity in MIA PaCa-2 cells

Membrane association of glycolytic enzymes may be an important factor in maintaining a glycolytic ATP supply to the PMCA in PDAC, and thus their dissociation from the plasma membrane could be expected to impact on PMCA for numerous reasons. The proximity of a glycolytic metabolon to glucose transporters might be important in maintaining a high availability of glucose for rapid metabolism by HKI, while the proximity of LDHA to monocarboxylate transporters (MCT) might facilitate lactic acid efflux, thereby maintaining LDHA activity. Moreover, the LDHA reaction generates NAD^+, and thus its activity at the plasma membrane may be important for providing NAD^+ to membrane-bound GAPDH. In addition, consumption of ATP by the PMCA might be important for maintaining a high glycolytic rate. A high cytosolic concentration of ATP ($[ATP]_i$, ~5 mM) is known to allosterically inhibit PFK activity (Dobson et al., 1986, Sola-Penna et al., 2010), and since the PMCA is a major consumer of cytosolic ATP, colocalisation of the PMCA and PFK1 might be expected to maintain the concentration of ATP below the inhibitory threshold, thereby maintaining glycolytic flux. Moreover, the major ATP generating enzyme of the glycolytic cascade is PKM2, which has been shown to have low catalytic activity when bound to the plasma membrane protein MUC1 (Kosugi et al., 2011). Thus global ATP might be expected to increase upon the dissociation of PKM2 from the membrane and the stabilisation of its more active tetrameric form (Christofk et al., 2008a). Nevertheless, the loss of a local ATP production may become a limiting factor for PMCA activity. Consequently, we next aimed to assess whether inhibition of tyrosine phosphorylation (and thus by extrapolation, inhibition of glycolytic enzyme association with the plasma membrane) would have any functional effect on PMCA activity.

MIA PaCa-2 cells were treated with genistein (50 µM and 100 µM) or tyrphostin A23 (50 µM), and the PMCA activity and relative recovery of resting $[Ca^{2+}]_i$ measured. To achieve this we employed an *in situ* $[Ca^{2+}]_i$ clearance assay as previously described (*Chapter 2* and *Chapter 3*, Samad et al., 2014, Mankad et al., 2012, James et al., 2013), in which PMCA activity is pharmacologically and functionally isolated and can be measured. Briefly, cells were treated

with cyclopiazonic acid (CPA) to inhibit the sarcoplasmic/endoplasmic reticulum Ca^{2+}-ATPase (SERCA), causing depletion of the ER Ca^{2+} stores in the absence of external Ca^{2+} and presence of 1 mM EGTA. Subsequent repeated treatment with either 20 mM Ca^{2+} or zero external Ca^{2+} induced rapid Ca^{2+} influx and clearance phases. The rate of Ca^{2+} clearance, due to PMCA activity, can be quantified during each Ca^{2+} clearance phase. Test reagents and manoeuvres can then be applied during the second influx/clearance phase, beginning 2 minutes prior to Ca^{2+} influx, and the rate of clearance and degree of recovery during the second clearance phase are normalised (%) to the first influx/clearance (control) phase. Linear $[Ca^{2+}]_i$ clearance rate (60 seconds) and relative recovery are both measured from the same fura-2 fluorescence value. This paired experimental design controls for cell-to-cell and time-dependent variations in $[Ca^{2+}]_i$ clearance, which under the conditions of this assay is achieved almost solely via the PMCA in MIA PaCa-2 cells, as established previously (James et al., 2013).

In untreated control cells, linear $[Ca^{2+}]_i$ clearance rate during the second influx/clearance phase was on average 105 ± 5 % of the first (Figures 4.3A and 4.3E, n=6). Genistein caused a significant concentration-dependent decrease in relative linear $[Ca^{2+}]_i$ clearance when compared to corresponding control cells (50 µM genistein, 63 ± 2 %, Figures 4.3B and 4.3E, n=4, $P<0.01$; 100 µM genistein, 42 ± 2 %, Figures 4.3C and 4.3E, n=3, $P<0.05$). In contrast to genistein, 50 µM tyrphostin A23 had no significant effect on linear $[Ca^{2+}]_i$ clearance rate (Figures 4.3D and 4.3E, n=3) compared to control cells. However, neither genistein or tyrphostin A23 had any effect on relative recovery (Figure 4.3F), and cells achieved complete clearance of $[Ca^{2+}]_i$ following treatment with either drug.

Since treatment with either genistein or tyrphostin A23 had no effect on the degree of relative recovery, it was valid to fit the clearance curves to a single exponential decay and compare their relative time constants (τ). To achieve this, starting from the same fura-2 value in each phase, both clearance phases were fitted to a single exponential decay. However, because τ is a time constant (in seconds), it is the reciprocal of the rate constant (in seconds-1). Thus the inverse of the τ during the second influx/clearance phase (τ_2) must be normalised (%) to that of the first (τ_1). This is simplifed as τ_1/τ_2 (relative τ %, see *4.3.8 – Data analysis*). In control cells, relative τ during the second clearance phase was 107 ± 4 % of the first (Figure 4.3A and 4.3G, n=6). Similar to that observed following the linear clearance rate analysis, genistein caused a significant concentration-dependent decrease in relative τ during the second clearance phase when compared to untreated control cells (50 µM genistein, 60 ± 2 %, Figure 4.3B and 4.3G, n=4, $P<0.01$; 100 µM genistein, 38 ± 2 %, Figure 4.3C and 4.3G, n=3, $P<0.05$). However, in contrast to the linear clearance rate analysis, treatment with tyrphostin A23 induced a significant decrease in relative τ during the second clearance phase (84 ± 4 %, Figure 4.3D and 4.3G, n=4, $P<0.05$). These results indicate that tyrphostin A23 does indeed slow PMCA activity, albeit not to the same degree relative to genistein. Taken together, these data indicate that treatment with tyrosine kinase inhibitors slow PMCA activity. However, these cells could still fully recover $[Ca^{2+}]_i$, indicating that the PMCA could still maintain a low resting $[Ca^{2+}]_i$ despite treatment with these drugs.

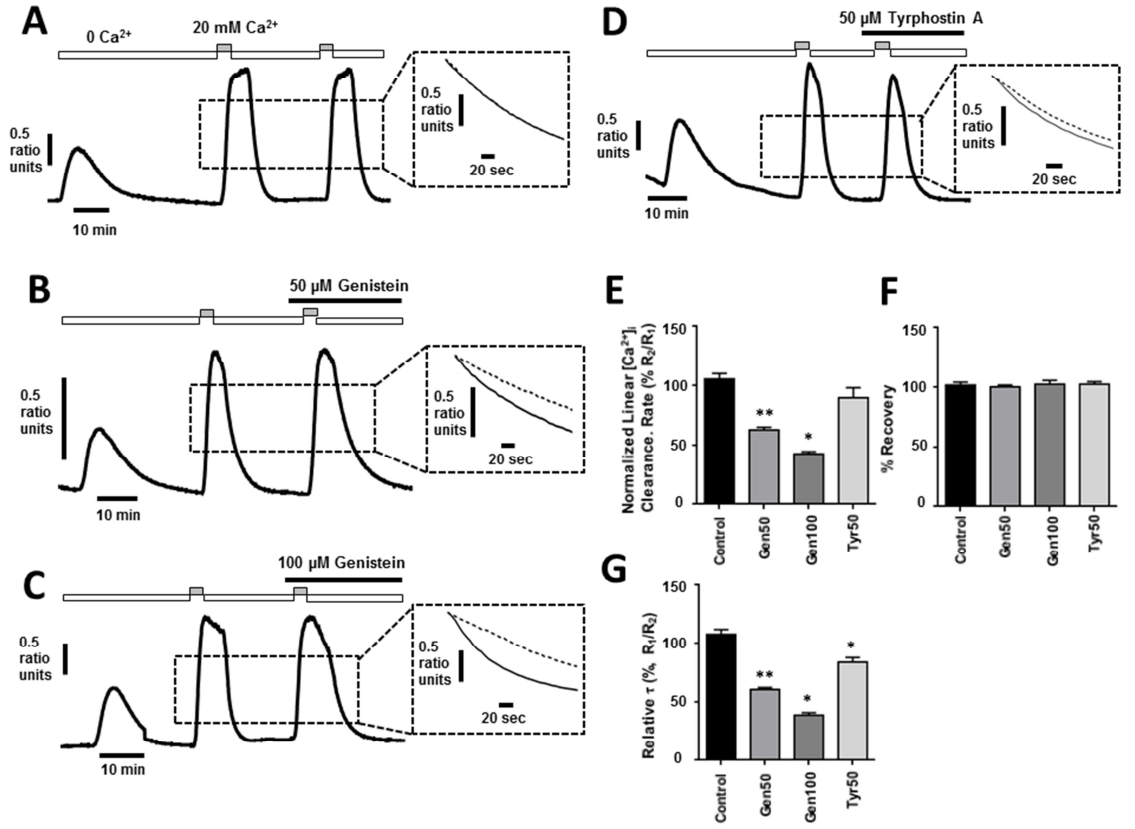

Figure 4.3 - The tyrosine kinase inhibitors genistein and tyrphostin A23 inhibit PMCA activity in MIA PaCa-2 cells.

A–D, representative traces showing the *in situ* $[Ca^{2+}]_i$ clearance assay (PMCA activity) in fura-2-loaded MIA-PaCa-2 cells. The cells were treated with 30 µM cyclopiazonic acid (CPA) in the absence of external Ca^{2+} with 1mM EGTA (*white box*) to block SERCA activity and deplete the ER Ca^{2+} store, at which point cells were treated with 20mM Ca^{2+} (*grey box*) to induce store-operated Ca^{2+} influx. Subsequent removal of external Ca^{2+} allowed $[Ca^{2+}]_i$ clearance. This influx-clearance phase was repeated using a paired experimental design and tyrosine kinase inhibitors were applied during the second influx-clearance phase, starting 2 minutes prior to Ca^{2+} influx. The inset of each trace shows expanded time courses comparing the second (dotted trace) with the first clearance phase (black trace) in the presence of each inhibitor. ***A,*** time-matched control; ***B***, 50 µM genistein (Gen50); ***C***, 100 µM genistein (Gen100); ***D***, 50 µM tyrphostin A23 (Tyr50). For the second clearance phase in each experiment, both the linear clearance rate over 60 seconds (in the presence of each drug) and the rate constant when fitted to a single exponential decay (derived from the time constant, τ) were normalized to those of the first clearance phase to give normalized linear $[Ca^{2+}]_i$ clearance rate (R_2/R_1) and relative τ (%, τ_1/τ_2). Similarly, relative recovery during the second clearance phase was calculated and normalised (%) to that of the first clearance phase. All measurements were taken from the same fura-2 value in both clearance phases. ***E***, mean normalised linear $[Ca^{2+}]_i$ clearance rate (±S.E.M). ***F***, mean percentage recovery (±S.E.M). ***G***, mean relative τ (±S.E.M), n=3-6 for all conditions. *, $p<0.05$; **, $p<0.01$; ***, $p<0.001$ (Mann-Whitney U), compared with time-matched control experiments (*white bar).*

4.4.4 - Genistein-induced decrease in $[Ca^{2+}]_i$ clearance rate in MIA PaCa-2 cells is independent of global ATP depletion

Since treatment with the tyrosine kinase inhibitor genistein significantly inhibited PMCA activity, we next tested whether this was due to an effect on the cytosolic ATP concentration ($[ATP]_i$). To achieve this we employed MIA PaCa-2 cells stably expressing GO-ATeam (*Chapter 3*), a recombinant FRET reporter for $[ATP]_i$ (Nakano et al., 2011). Using GO-ATeam FRET microscopy, cells were treated with 50 or 100 µM genistein for 20 minutes, followed by treatment with an ATP depletion cocktail containing oligomycin (10 µM), antimycin A (0.5 µM), 2-deoxyglucose (10 mM) and iodoacetate (2 mM) to induce maximal ATP depletion. To measure % ATP, R_{min} was subtracted from all GO-ATeam FRET ratio values, and these values were normalised (%) to ΔR_{max} (R_{min} subtracted from R_0, Figure 4.4A, see *4.3.8 – Data analysis*).

While no difference in $[ATP]_i$ was observed between control and treated cells at the onset of treatment (0 min), to our surprise, treatment of MIA PaCa-2 cells with either 50 or 100 µM genistein caused a significant increase in $[ATP]_i$ at all other timepoints (5, 10, 15 and 20 minutes, Figure 4.4B). At 10 minutes treatment, 50 µM genistein caused a significant and sustained increase in $[ATP]_i$ (115 ± 2 %, Figure 4.4B, n=5, P<0.0001), as did 100 µM (118 ± 3 %, Figure 4.4B, n=5, P<0.0001), compared to $[ATP]_i$ in time-matched control cells (94 ± 2 %, Figure 4.4B, n=7). It is therefore unlikely that the decrease in PMCA activity induced by genistein in our $[Ca^{2+}]_i$ clearance assays was due to a decrease in global $[ATP]_i$.

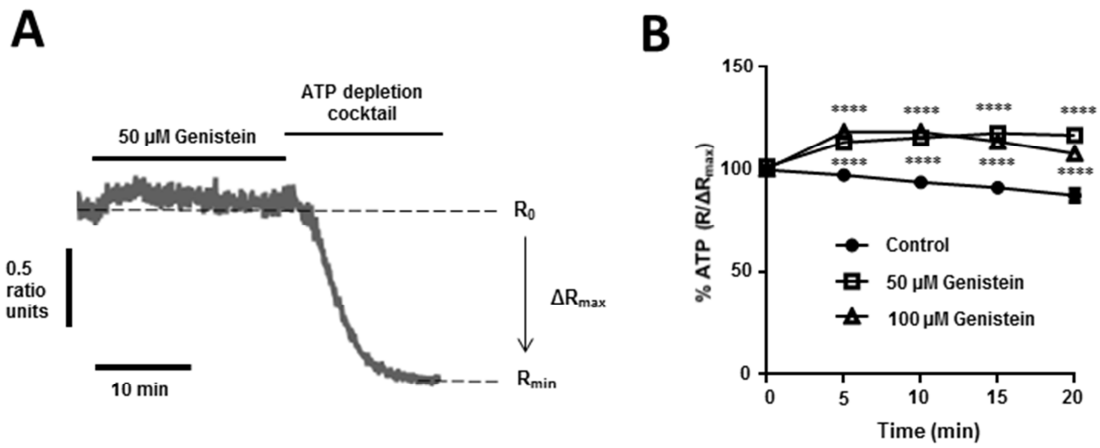

Figure 4.4 - GO-ATeam FRET imaging reveals the effects of genistein on ATP in MIA PaCa-2 cells.

MIA PaCa-2 cells stably expressing the ATP probe GO-Ateam were treated with genistein (50 and 100 µM) and cytosolic [ATP] measured using GO-Ateam FRET imaging. Cells were treated with genistein for 20 minutes before maximal ATP depletion was induced using an ATP depletion cocktail containing inhibitors of both glycolysis and mitochondrial metabolism (oligomycin, 10 µM; antimycin A, 0.5 µM, 2-deoxyglucose, 10 mM; iodoacetate, 2 mM). ***A***, a representative trace showing a cell treated with genistein (50 µM). ATP depletion (%) was calculated by first subtracting the minimum ratio observed after ATP depletion cocktail addition (R_{min}) from the FRET ratio values at 0, 5, 10, 15 and 20 minutes genistein treatment. These values were then normalised to the difference between the mean of the 10 FRET ratio values immediately prior to drug addition (R_0) and the R_{min} (ΔR_{max}). ***B***, % ATP in genistein-treated and untreated control cells at 0, 5, 10, 15 and 20 minutes drug treatment. *,p0.05; **,p0.01; ***,p0.001; ****,p0.001. Data presented are mean % ATP ± S.E.M, n=5-7 for all conditions. Statistical comparisons were made to untreated control cells using a two-way ANOVA with post hoc Bonferroni test for multiple comparisons.

4.5 - Discussion

To our knowledge, the present study is the first to show that the glycolytic enzymes HKI, LDH, PFKP, GAPDH, PFKFB3 and PKM2 are all found within the plasma membrane fraction of biotinylated human PDAC cells (MIA PaCa-2), strongly suggesting that these enzymes associate with plasma membrane proteins. Moreover, preliminary evidence presented here suggests that some of these glycolytic enzymes may dynamically associate with the membrane in a tyrosine phosphorylation-dependent manner. While the putative binding site for these enzymes is currently unknown, in the present study, the membrane-associated protein mucin 1 was also found in the membrane fraction; MUC1 is highly expressed in advanced PDAC (Hinoda et al., 2003), drives the highly glycolytic phenotype (Chaika et al., 2012), and importantly has been shown to bind to and regulate the key glycolytic enzyme pyruvate kinase isoform M2 (PKM2, Kosugi et al., 2011). These data provide the first insight into a possible submembrane glycolytic cascade that may be important for the fuelling of ion transporters in PDAC.

The notion of a membrane-bound complex of glycolytic enzymes is not new. A large body of evidence indicates that glycolytic enzymes form a complex at the plasma membrane of erythrocytes, and that the binding site of this complex is anion exchanger 1 (AE1), also known as band 3 (Campanella et al., 2005, Campanella et al., 2008, Puchulu-Campanella et al., 2013). This allows for the formation of a "pool" of glycolytically-derived ATP that is trapped within cytoskeletal elements (Chu et al., 2012). Studies using [γ-^{32}P]ATP have shown that this submembrane pool of glycolytic ATP is used preferentially to fuel the Na^+/K^+ ATPase and the PMCA over bulk cytosolic ATP (Hoffman et al., 2009). This submembrane pool of ATP alone was sufficient to support the transport of Ca^{2+} into inside-out isolated erythrocyte plasma membrane vesicles, which is a measure of PMCA activity. Since erythrocytes do not contain mitochondria and are therefore obligated to derive their ATP from glycolysis, evidence suggesting that glycolytic ATP is important for PMCA activity in erythrocytes is to be expected. However, these data provide convincing evidence that the localisation of a privileged glycolytic ATP supply is critical for PMCA function in red blood cells. Given the apparent importance of a local glycolytic ATP supply for ion transporter function in erythrocytes, it is tempting to speculate that a similar phenomenon may be observed in cancer cells that exhibit a highly glycolytic phenotype.

Although the membrane-bound glycolytic enzyme complex found at AE1 in erythrocytes is relatively well characterised, AE1 expression is largely restricted to erythrocytes, and the putative binding sites for glycolytic enzyme association with the plasma membrane in other cell types remain poorly understood. Nevertheless, evidence suggests that similar complexes of membrane-associated glycolytic enzymes may be important for generating a submembrane ATP pool and regulating ion channels and transporters in other cell types. For example, glycolytic enzymes have been found associated to K_{ATP} channels in membrane fractions from

rat heart, and further studies in COS7L cells transfected with Kir6.2 suggest that these glycolytic enzymes regulate the function of K_{ATP} channels by generating ATP (Dhar-Chowdhury et al., 2005). More recent studies have also shown that the migration of highly glycolytic endothelial cells requires a submembrane glycolytic ATP pool at the leading edge of lamellipodia that is dependent on the expression of PFKFB3, which acts to activate the glycolytic cascade (De Bock et al., 2013). These findings have potentially important implications for $[Ca^{2+}]_i$ homeostasis given the absence of mitochondria from lamellipodia in migratory cells coupled with the key role Ca^{2+} plays in migration and metastasis (Prevarskaya et al., 2011). Moreover, a large body of evidence indicates that glycolysis couples to and regulates the Na^+/K^+ ATPase in numerous cell types other than erythrocytes, including cardiac and smooth muscle cells (reviewed in Ueda and Ikemoto, 2007) and cultured tumour cells (Balaban and Bader, 1984). In light of these findings, it would be reasonable to propose that the PMCA may also be fuelled by a submembrane ATP pool in these cells, since in erythrocytes the submembrane ATP pool is apparently shared by both the Na^+/K^+ ATPase and the PMCA. Indeed, studies using inside-out plasma membrane vesicles from porcine smooth muscle cells have shown that when glycolytic substrates are supplied, PMCA activity can be fuelled by an endogenous glycolytic cascade from aldolase onwards (Paul et al., 1989). Moreover, further investigations found that the PMCA preferentially uses ATP generated by these putative membrane-associated glycolytic enzymes to fuel Ca^{2+} efflux despite the presence of exogenously-supplemented ATP (Hardin et al., 1992). These results clearly resemble those obtained from erythrocytes, suggesting that a similar submembrane ATP supply fuelling Ca^{2+} transport across the plasma membrane may be more common across cell types than previously thought.

While the putative membrane association sites are not known for the glycolytic enzymes identified in the present study, one possible candidate is MUC1. The present study indicated that MUC1 is expressed in PDAC cell lines, consistent with previous studies using human PDAC tumour samples (Hinoda et al., 2003). Moreover, studies using 3Y1 fibroblasts have shown that PKM2 can associate with the cytoplasmic domain of MUC1 (Kosugi et al., 2011), and that this interaction is dynamically regulated by tyrosine phosphorylation, similar to the glycolytic enzyme association to AE1 in erythrocytes (Campanella et al., 2005). We therefore sought to determine whether the membrane association of the identified glycolytic enzymes in MIA PaCa-2 cells was dynamically regulated by tyrosine phosphorylation. These initial results tentatively suggest that global protein tyrosine phosphorylation can dynamically regulate the association of glycolytic enzymes to and from the membrane. Specifically, GAPDH, PKM2 and PFKP appeared to become more abundant in the cytosol following inhibition of tyrosine kinases (and vice versa for tyrosine phosphatase inhibition), suggesting that tyrosine kinase activity promotes membrane association of these enzymes. The opposite is true of HK1, which appeared to become enriched in the biotinylated fraction following treatment with tyrosine kinase inhibitors. However, these preliminary results require further verification, and numerous sources of error and alternative explanations for these observations certainly remain. It is possible that differences in cell growth may have resulted in inconsistencies in cell mass at the

beginning of the experiments, despite flasks being seeded at a constant density, and inconsistent protein solubilisation and separation could have further impacted on protein yields across samples. Indeed, inconsistencies in total protein abundance (biotinylated and non-biotinylated) were observed between the treatment groups and untreated control cell samples. Therefore, while the current method is capable of identifying the presence or absence of a protein within isolated membrane fractions, it may not be sufficiently reliable for quantitatively assessing relative changes in protein abundance in the biotinylated vs non-biotinylated fractions from different preparations.

Notwithstanding the cautious interpretation of the data obtained from these biotinylation-based assays, it is tempting to speculate that such a dynamic tyrosine kinase-mediated association of glycolytic enzymes with the plasma membrane might have a functional effect on PMCA activity. Since the PMCA appears to be reliant on a glycolytic ATP supply in highly glycolytic PDAC cells (*Chapter 2* and *Chapter 3*, James et al., 2013), the dissociation of glycolytic enzymes from the plasma membrane following inhibition of tyrosine kinases may be expected to impact on $[Ca^{2+}]_i$ clearance. We therefore also aimed to determine whether inhibition of tyrosine kinase activity had any effect on $[Ca^{2+}]_i$ clearance via the PMCA. Genistein caused a significant concentration-dependent decrease in PMCA activity in MIA PaCa-2 cells. Tyrphostin A23 also significantly inhibited PMCA activity at 50 µM, although to a lesser degree than genistein. Nevertheless, cells treated with either genistein or tyrphostin A23 were able to fully recover $[Ca^{2+}]_i$ to baseline levels, suggesting that while PMCA activity was slowed, these drugs do not prevent MIA PaCa-2 cells from recovering a low resting $[Ca^{2+}]_i$. Furthermore, genistein did not decrease $[ATP]_i$ in MIA PaCa-2 cells, but rather increased $[ATP]_i$ in comparison to untreated control cells. Together with the recovery data, this suggests that genistein exerts its effects on the PMCA via a mechanism other than ATP depletion. Interestingly, tyrosine phosphorylation of the PMCA is associated with a decrease in PMCA activity (Bozulic et al., 2007), and genistein has been shown to eliminate all tyrosine phosphorylation of the PMCA (Dean et al., 1997). Thus, one would expect genistein or tyrphostin A23 to increase PMCA activity if operating via this mechanism, however, in the present study genistein induced a concentration-dependent decrease in PMCA activity. However, while genistein is often used as a tyrosine kinase inhibitor (Akiyama et al., 1987), other studies suggest that high concentrations of genistein can also inhibit serine/threonine kinases (O'Dell et al., 1991) with an IC_{50} of around 185 µM. Importantly, the C-terminus of the PMCA contains sites that are the target of phosphorylation by protein kinase C (Monteith et al., 1998, Penniston and Enyedi, 1998) and protein kinase A (Strehler and Zacharias, 2001), and phosphorylation at this site confers an increase in PMCA activity (Neyses et al., 1985, Smallwood et al., 1988, Zylinska et al., 1998). While the concentrations of genistein used in the present study was selected to be below the threshold for appreciable serine/threonine kinase inhibition, the IC_{50} values for genistein were determined using i*n vitro* assays rather than whole cell assays (O'Dell et al., 1991). It is therefore possible that genistein still exerted an effect on PKC regulation in live cells that led to the observed decrease in PMCA activity.

The observation that genistein increased global $[ATP]_i$ in MIA PaCa-2 cells came as somewhat of a surprise considering that genistein caused a decrease in PMCA activity. Given the increase in global [ATP]i coupled with PMCA inhibition following genistein treatment, it seems unlikely that the ATP consumption by the PMCA maintains the activity of PFK by keeping submembrane [ATP] below the PFK inhibitory threshold. The dissociation of PFK from the plasma membrane following inhibition of tyrosine kinases would be expected to slow PFK activity if proximal ATP consumption by the PMCA was important to prevent the allosteric inhibition of membrane-bound PFK by high concentrations of ATP (Sola-Penna et al., 2010). Similarly, if this were the case, one would not expect to see an increase in [ATP]i concomitant with a significant decrease in PMCA activity, as was observed following treatment with genistein. Moreover, if localisation of glycolytic enzymes to the plasma membrane to glucose transporters and MCTs were important for maintaining glycolytic flux, one would not expect to see a potential increase in glycolytic flux upon their dissociation from the plasma membrane. However, a possible explanation for the increase in global $[ATP]_i$ following genstein treatment is that the dissociation of PKM2 from the plasma membrane may induce an increase in ATP generation by PKM2. Importantly, PKM2 association with MUC1 has been shown to decrease the catalytic activity of PKM2 (Kosugi et al., 2011). The low-activity dimeric state of PKM2 is thought to be a key factor in maintaining the Warburg phenotype, as the a low catalytic activity of dimeric PKM2 is thought to increase the availability of upstream glycolytic intermediates to anabolic processes by slowing glycolytic flux (Christofk et al., 2008a). Furthermore, the association of PKM2 with MUC1 appears to be dependent on tyrosine phosphorylation of the MUC1 cytoplasmic domain (Kosugi et al., 2011). It is possible that blocking tyrosine kinase activity prevents the phosphorylation of the required tyrosine residues on the MUC1 cytoplasmic domain for PKM2 association. This would allow PKM2 to dissociate from the MUC1, enter the bulk cytosol and oligermerise to form its high activity tetrameric state, thus increasing $[ATP]_i$. Indeed, the western blot data presented within the present study tentatively support the notion that PKM2 dissociates from the plasma membrane upon tyrosine kinase inhibition. While speculative, this would explain the observed increase in global $[ATP]_i$ following genistein treatment in the GO-ATeam experiments. In addition, it is worth noting that PKM2 itself is known to be inactivated by tyrosine phosphorylation (Christofk et al., 2008b), which destabilises the more active, tetrameric state and disrupts the activation of PKM2 by its allosteric activator fructose-1,6-bisphosphate (Hitosugi et al., 2009). This provides another explanation for the increase in $[ATP]_i$ following genistein treatment, since genistein would be expected to relieve this inhibition by preventing tyrosine phosphorylation of PKM2. Nevertheless, while global $[ATP]_i$ may rise following PKM2 dissociation from the plasma membrane, in this scenario ATP generation would no longer be in close proximity to the PMCA. This relocation of the ATP generating site may be enough to limit $[Ca^{2+}]_i$, clearance rate, given that ATP would need to diffuse to the PMCA rather than it being generated proximally in the submembrane compartment. Thus, the low activity MUC1-bound PKM2 may generate sufficient ATP to fuel the PMCA provided this glycolytic ATP supply is in close proximity. Therefore, it may not be the rate of glycolytic ATP production that is a limiting factor for PMCA activity, but instead its availability from within the submembrane pool.

In summary, the present study indicates that glycolytic enzymes associate with the plasma membrane in PDAC, and provides preliminary evidence that this process might be dynamically regulated by tyrosine phosphorylation. As such, these data present the possibility of a glycolytic enzyme metabolon proximal to ATP consuming pumps at the plasma membrane in PDAC. It is therefore tempting to speculate that this membrane-bound glycolytic metabolon might be important for the glycolytic dependency of the PMCA in PDAC (*Chapter 2* and *Chapter 3,* James et al., 2013), and therefore might be an attractive therapeutic target for selectively targeting highly glycolytic PDAC cells. Further research is therefore required to fully characterise the mechanisms by which these glycolytic enzymes associate with the plasma membrane in PDAC and to determine whether they regulate the ATP-dependent ion transporters critical for cancer cell survival.

4.6 - References

AKIYAMA, T., ISHIDA, J., NAKAGAWA, S., OGAWARA, H., WATANABE, S., ITOH, N., SHIBUYA, M. & FUKAMI, Y. 1987. Genistein, a specific inhibitor of tyrosine-specific protein kinases. *J Biol Chem,* 262**,** 5592-5.

ALEXAKIS, N., HALLORAN, C., RARATY, M., GHANEH, P., SUTTON, R. & NEOPTOLEMOS, J. P. 2004. Current standards of surgery for pancreatic cancer. *Br J Surg,* 91**,** 1410-27.

AMIN, Z., THEIS, B., RUSSELL, R. C., HOUSE, C., NOVELLI, M. & LEES, W. R. 2006. Diagnosing pancreatic cancer: the role of percutaneous biopsy and CT. *Clin Radiol,* 61**,** 996-1002.

BALABAN, R. S. & BADER, J. P. 1984. Studies on the relationship between glycolysis and (Na^+ $^+$ K^+)-ATPase in cultured cells. *Biochim Biophys Acta,* 804**,** 419-26.

BOZULIC, L. D., MALIK, M. T. & DEAN, W. L. 2007. Effects of plasma membrane Ca^{2+} -ATPase tyrosine phosphorylation on human platelet function. *J Thromb Haemost,* 5**,** 1041-6.

BRINI, M. & CARAFOLI, E. 2009. Calcium pumps in health and disease. *Physiol Rev,* 89**,** 1341-78.

CAMPANELLA, M. E., CHU, H. & LOW, P. S. 2005. Assembly and regulation of a glycolytic enzyme complex on the human erythrocyte membrane. *Proc Natl Acad Sci U S A,* 102**,** 2402-7.

CAMPANELLA, M. E., CHU, H., WANDERSEE, N. J., PETERS, L. L., MOHANDAS, N., GILLIGAN, D. M. & LOW, P. S. 2008. Characterization of glycolytic enzyme interactions with murine erythrocyte membranes in wild-type and membrane protein knockout mice. *Blood,* 112**,** 3900-6.

CHAIKA, N. V., GEBREGIWORGIS, T., LEWALLEN, M. E., PUROHIT, V., RADHAKRISHNAN, P., LIU, X., ZHANG, B., MEHLA, K., BROWN, R. B., CAFFREY, T., YU, F., JOHNSON, K. R., POWERS, R., HOLLINGSWORTH, M. A. & SINGH, P. K. 2012. MUC1 mucin stabilizes and activates hypoxia-inducible factor 1 alpha to regulate metabolism in pancreatic cancer. *Proc Natl Acad Sci U S A,* 109**,** 13787-92.

CHRISTOFK, H. R., VANDER HEIDEN, M. G., HARRIS, M. H., RAMANATHAN, A., GERSZTEN, R. E., WEI, R., FLEMING, M. D., SCHREIBER, S. L. & CANTLEY, L. C. 2008a. The M2 splice isoform of pyruvate kinase is important for cancer metabolism and tumour growth. *Nature,* 452**,** 230-3.

CHRISTOFK, H. R., VANDER HEIDEN, M. G., WU, N., ASARA, J. M. & CANTLEY, L. C. 2008b. Pyruvate kinase M2 is a phosphotyrosine-binding protein. *Nature,* 452**,** 181-6.

CHU, H., PUCHULU-CAMPANELLA, E., GALAN, J. A., TAO, W. A., LOW, P. S. & HOFFMAN, J. F. 2012. Identification of cytoskeletal elements enclosing the ATP pools that fuel human red blood cell membrane cation pumps. *Proc Natl Acad Sci U S A,* 109**,** 12794-9.

DE BOCK, K., GEORGIADOU, M., SCHOORS, S., KUCHNIO, A., WONG, B. W., CANTELMO, A. R., QUAEGEBEUR, A., GHESQUIERE, B., CAUWENBERGHS, S., EELEN, G., PHNG, L. K., BETZ, I., TEMBUYSER, B., BREPOELS, K., WELTI, J., GEUDENS, I., SEGURA, I., CRUYS, B., BIFARI, F., DECIMO, I., BLANCO, R., WYNS, S., VANGINDERTAEL, J., ROCHA, S., COLLINS, R. T., MUNCK, S., DAELEMANS, D., IMAMURA, H., DEVLIEGER, R., RIDER, M., VAN VELDHOVEN, P. P., SCHUIT, F., BARTRONS, R., HOFKENS, J., FRAISL, P., TELANG, S., DEBERARDINIS, R. J., SCHOONJANS, L., VINCKIER, S., CHESNEY, J., GERHARDT, H., DEWERCHIN, M. & CARMELIET, P. 2013. Role of PFKFB3-driven glycolysis in vessel sprouting. *Cell,* 154**,** 651-63.

DEAN, W. L., CHEN, D., BRANDT, P. C. & VANAMAN, T. C. 1997. Regulation of platelet plasma membrane Ca^{2+}-ATPase by cAMP-dependent and tyrosine phosphorylation. *J Biol Chem,* 272**,** 15113-9.

DHAR-CHOWDHURY, P., HARRELL, M. D., HAN, S. Y., JANKOWSKA, D., PARACHURU, L., MORRISSEY, A., SRIVASTAVA, S., LIU, W., MALESTER, B., YOSHIDA, H. & COETZEE, W. A. 2005. The glycolytic enzymes, glyceraldehyde-3-phosphate dehydrogenase, triose-phosphate isomerase, and pyruvate kinase are components of the K(ATP) channel macromolecular complex and regulate its function. *J Biol Chem,* 280**,** 38464-70.

DOBSON, G. P., YAMAMOTO, E. & HOCHACHKA, P. W. 1986. Phosphofructokinase control in muscle: nature and reversal of pH-dependent ATP inhibition. *Am J Physiol,* 250**,** R71-6.

GILLIES, R. J. & GATENBY, R. A. 2007. Adaptive landscapes and emergent phenotypes: why do cancers have high glycolysis? *J Bioenerg Biomembr,* 39**,** 251-7.

HANISCH, F. G., KINLOUGH, C. L., STAUBACH, C. L. & HUGHEY, R. P. 2012. MUC1 membrane trafficking: protocols for assessing biosynthetic delivery, endocytosis, recycling, and release through exosomes. *Methods Mol Biol*, 842, 123-40

HARDIN, C. D., RAEYMAEKERS, L. & PAUL, R. J. 1992. Comparison of endogenous and exogenous sources of ATP in fueling Ca^{2+} uptake in smooth muscle plasma membrane vesicles. *J Gen Physiol,* 99**,** 21-40.

HEY, N. A., LI, T. C., DEVINE, P. L., GRAHAM, R. A., SARAVELOS, H. & APLIN, J. D. 1995. MUC1 in secretory phase endometrium: expression in precisely dated biopsies and flushings from normal and recurrent miscarriage patients. *Hum Reprod,* 10**,** 2655-62.

HINODA, Y., IKEMATSU, Y., HORINOCHI, M., SATO, S., YAMAMOTO, K., NAKANO, T., FUKUI, M., SUEHIRO, Y., HAMANAKA, Y., NISHIKAWA, Y., KIDA, H., WAKI, S., OKA, M., IMAI, K. & YONEZAWA, S. 2003. Increased expression of MUC1 in advanced pancreatic cancer. *J Gastroenterol,* 38**,** 1162-6.

HITOSUGI, T., KANG, S., VANDER HEIDEN, M. G., CHUNG, T. W., ELF, S., LYTHGOE, K., DONG, S., LONIAL, S., WANG, X., CHEN, G. Z., XIE, J., GU, T. L., POLAKIEWICZ, R. D., ROESEL, J. L., BOGGON, T. J., KHURI, F. R., GILLILAND, D. G., CANTLEY, L. C., KAUFMAN, J. & CHEN, J. 2009. Tyrosine phosphorylation inhibits PKM2 to promote the Warburg effect and tumor growth. *Sci Signal,* 2**,** ra73.

HOFFMAN, J. F., DODSON, A. & PROVERBIO, F. 2009. On the functional use of the membrane compartmentalized pool of ATP by the Na^{+} and Ca^{++} pumps in human red blood cell ghosts. *J Gen Physiol,* 134**,** 351-61.

JAMES, A. D., CHAN, A., ERICE, O., SIRIWARDENA, A. K. & BRUCE, J. I. 2013. Glycolytic ATP fuels the plasma membrane calcium pump critical for pancreatic cancer cell survival. *J Biol Chem,* 288**,** 36007-19.

KO, Y. H., SMITH, B. L., WANG, Y., POMPER, M. G., RINI, D. A., TORBENSON, M. S., HULLIHEN, J. & PEDERSEN, P. L. 2004. Advanced cancers: eradication in all cases using 3-bromopyruvate therapy to deplete ATP. *Biochem Biophys Res Commun,* 324**,** 269-75.

KOONG, A. C., MEHTA, V. K., LE, Q. T., FISHER, G. A., TERRIS, D. J., BROWN, J. M., BASTIDAS, A. J. & VIERRA, M. 2000. Pancreatic tumors show high levels of hypoxia. *Int J Radiat Oncol Biol Phys,* 48**,** 919-22.

KOSUGI, M., AHMAD, R., ALAM, M., UCHIDA, Y. & KUFE, D. 2011. MUC1-C oncoprotein regulates glycolysis and pyruvate kinase M2 activity in cancer cells. *PloS one,* 6**,** e28234.

KROEMER, G. & POUYSSEGUR, J. 2008. Tumor cell metabolism: cancer's Achilles' heel. *Cancer Cell,* 13**,** 472-82.

LE, A., COOPER, C. R., GOUW, A. M., DINAVAHI, R., MAITRA, A., DECK, L. M., ROYER, R. E., VANDER JAGT, D. L., SEMENZA, G. L. & DANG, C. V. 2010. Inhibition of lactate dehydrogenase A induces oxidative stress and inhibits tumor progression. *Proc Natl Acad Sci U S A,* 107**,** 2037-42.

LI, D., XIE, K., WOLFF, R. & ABBRUZZESE, J. L. 2004. Pancreatic cancer. *Lancet,* 363**,** 1049-57.

MANKAD, P., JAMES, A., SIRIWARDENA, A. K., ELLIOTT, A. C. & BRUCE, J. I. 2012. Insulin protects pancreatic acinar cells from cytosolic calcium overload and inhibition of plasma membrane calcium pump. *J Biol Chem,* 287**,** 1823-36.

MONTEITH, G. R., WANIGASEKARA, Y. & ROUFOGALIS, B. D. 1998. The plasma membrane calcium pump, its role and regulation: new complexities and possibilities. *J Pharmacol Toxicol Methods,* 40**,** 183-90.

NAKANO, M., IMAMURA, H., NAGAI, T. & NOJI, H. 2011. Ca^{2+} regulation of mitochondrial ATP synthesis visualized at the single cell level. *ACS Chem Biol,* 6**,** 709-15.

NEYSES, L., REINLIB, L. & CARAFOLI, E. 1985. Phosphorylation of the Ca^{2+}-pumping ATPase of heart sarcolemma and erythrocyte plasma membrane by the cAMP-dependent protein kinase. *J Biol Chem,* 260**,** 10283-7.

O'DELL, T. J., KANDEL, E. R. & GRANT, S. G. 1991. Long-term potentiation in the hippocampus is blocked by tyrosine kinase inhibitors. *Nature,* 353**,** 558-60.

PAUL, R. J., HARDIN, C. D., RAEYMAEKERS, L., WUYTACK, F. & CASTEELS, R. 1989. Preferential support of Ca^{2+} uptake in smooth muscle plasma membrane vesicles by an endogenous glycolytic cascade. *FASEB J,* 3**,** 2298-301.

PENNISTON, J. T. & ENYEDI, A. 1998. Modulation of the plasma membrane Ca^{2+} pump. *J Membr Biol,* 165**,** 101-9.

PFEIFFER, T., SCHUSTER, S. & BONHOEFFER, S. 2001. Cooperation and competition in the evolution of ATP-producing pathways. *Science,* 292**,** 504-7.

PREVARSKAYA, N., SKRYMA, R. & SHUBA, Y. 2011. Calcium in tumour metastasis: new roles for known actors. *Nat Rev Cancer,* 11**,** 609-18.

PUCHULU-CAMPANELLA, E., CHU, H., ANSTEE, D. J., GALAN, J. A., TAO, W. A. & LOW, P. S. 2013. Identification of the components of a glycolytic enzyme metabolon on the human red blood cell membrane. *J Biol Chem,* 288**,** 848-58.

SAMAD, A., JAMES, A., WONG, J., MANKAD, P., WHITEHOUSE, J., PATEL, W., ALVES-SIMOES, M., SIRIWARDENA, A. K. & BRUCE, J. I. 2014. Insulin protects pancreatic acinar cells from palmitoleic acid-induced cellular injury. *J Biol Chem*, 289, 23582-95

SIEGEL, R., MA, J., ZOU, Z. & JEMAL, A. 2014. Cancer statistics, 2014. *CA Cancer J Clin,* 64**,** 9-29.

SMALLWOOD, J. I., GUGI, B. & RASMUSSEN, H. 1988. Regulation of erythrocyte Ca^{2+} pump activity by protein kinase C. *J Biol Chem,* 263**,** 2195-202.

SOLA-PENNA, M., DA SILVA, D., COELHO, W. S., MARINHO-CARVALHO, M. M. & ZANCAN, P. 2010. Regulation of mammalian muscle type 6-phosphofructo-1-kinase and its implication for the control of the metabolism. *IUBMB life,* 62**,** 791-6.

STREHLER, E. E. & ZACHARIAS, D. A. 2001. Role of alternative splicing in generating isoform diversity among plasma membrane calcium pumps. *Physiol Rev,* 81**,** 21-50.

TENNANT, D. A., DURAN, R. V. & GOTTLIEB, E. 2010. Targeting metabolic transformation for cancer therapy. *Nat Rev Cancer,* 10**,** 267-77.

UEDA, T., & IKEMOTO, A. 2007. 4.1 Cytoplasmic glycolytic enzymes. synaptic vesicle-associated glycolytic ATP-generating enzymes: coupling to neurotransmitter accumulation. In: GIBSON, G. E. & DIENEL, G. A. eds. *Handbook of Neurochemistry and Molecular Neurobiology*. New York, Springer pp. 241-259.

WARBURG, O. 1956. On the origin of cancer cells. *Science,* 123**,** 309-14.

XING, P. X., REYNOLDS, K., TJANDRA, J. J., TANG, X. L. & MCKENZIE, I. F. 1990. Synthetic peptides reactive with anti-human milk fat globule membrane monoclonal antibodies. *Cancer Res,* 50**,** 89-96.

XING, P. X., TJANDRA, J. J., STACKER, S. A., TEH, J. G., THOMPSON, C. H., MCLAUGHLIN, P. J. & MCKENZIE, I. F. 1989. Monoclonal antibodies reactive with mucin expressed in breast cancer. *Immunol Cell Biol,* 67 (Pt 3)**,** 183-95.

ZHOU, W., CAPELLO, M., FREDOLINI, C., RACANICCHI, L., PIEMONTI, L., LIOTTA, L. A., NOVELLI, F. & PETRICOIN, E. F. 2012. Proteomic analysis reveals Warburg effect and anomalous metabolism of glutamine in pancreatic cancer cells. *J Proteome Res,* 11**,** 554-63.

ZYLINSKA, L., GUERINI, D., GROMADZINSKA, E. & LACHOWICZ, L. 1998. Protein kinases A and C phosphorylate purified Ca^{2+}-ATPase from rat cortex, cerebellum and hippocampus. *Biochim Biophys Acta,* 1448**,** 99-108.

4.7 - Supplementary Methods and Results

4.7.1 - Preparation of pervanadate

Prior to the biotinylation assay, cells were first treated with genistein (G, 150 µM) and tyrphostin A23 (T, 50µM) in combination (G+T) or pervanadate (PV, 10 µM) in PBS for 15 minutes at 37°C. To prepare 10 µM PV, a 330 µL of a 45.5 mM stock of orthovanadate (monomers only) was added into 170 µL H_2O_2 (1.51x dilution), resulting in 30 mM orthovanadate in H_2O_2. This was incubated at room temperature for 15 minutes at which time the residual H_2O_2 was quenched with 10 mg/ml catalase. Providing that H_2O_2 fully converts the orthovanadate monomers to the PV form in a 1:1 ratio, this gave a 30 mM solution PV. This could then be diluted to give 10 µM PV. Owing to the instability of PV, the solution was either used immediately or frozen in aliquots for future use (Kadota et al., 1987).

4.7.2 - Isolation of membrane bound proteins using cell surface biotinylation assay

To isolate membrane-associated proteins from the cytosolic fraction, a biotinylation-based Pierce Cell Surface Protein Isolation Kit (Thermo Fisher) was used according to the manufacturer's instructions. MIA PaCa-2 cells were first seeded into 75 cm^3 vented cap flasks (Corning) at a constant cell density 2 days prior to the biotinylation assay to ensure each flask contained the same cell mass when the membrane fraction was isolated. At 90% confluence, the membrane fraction was isolated from these cells using the biotinylation protocol (Supplementary Figure 4.1). Four 75 cm^3 flasks were used for each sample. In some cases, cells were treated with various drugs prior to performing the biotinylation protocol.

Following treatment, cells were rinsed twice with 8 ml ice cold phosphate buffered saline (PBS, supplied with the kit). Cells were then labelled with 10 ml of the supplied Sulfo-NHS-SS-Biotin reagent and incubated for 30 minutes at 4°C on a rocking platform, after which the biotinylation reaction was stopped using the supplied quenching solution (500 µl). Cells were then scraped and extracted from the flasks and centrifuged at 500 x g for 3 minutes. The supernatant was discarded and the cells resuspended in 5 ml Tris-buffered saline (TBS, supplied with the kit), before being centrifuged once more at 500 x g for 3 minutes. Again the supernatant was discarded, At this point, cells were lysed using the supplied lysis buffer supplemented with cOmplete EDTA-free protease inhibitor tablets (Roche Applied Science). Samples were vortexed and sonicated (5 x 1 second bursts) followed by 30 minutes lysis on ice with repeat vortex steps every 5 minutes. The lysate was then centrifuged (10000 x g at 4°C) and the clarified supernatant transferred to an elution column containing NeutrAvidin agarose beads (Thermo Scientific). The clarified supernatant was incubated in the column at room temperature for 1 hour on an end-over-end rotating platform, at which point the non-biotinylated fraction was eluted. This non-biotinylated eluent was retained as this fraction contained the non-membrane bound proteins. A BCA protein assay (Pierce) was then performed on the non-biotinylated

fraction samples using a Nanodrop 2000 (Thermo Scientific). The column was then rinsed three times with wash buffer supplied in the kit, after which the biotinylated fraction was eluted using 1x SDS sample buffer (62.5mM Tris HCl; pH 6.8, 2% SDS; 10% Glycerol; 1% β-mercaptoethanol) supplemented with dithiothreitol (DTT, 50mM). Similarly, 5x SDS sample buffer without DTT was added to the non-biotinylated fraction sample to give 1x SDS sample buffer, to prepare the sample for western blot. Both fractions were then boiled at 95 °C for 5 min and analysed by western blot.

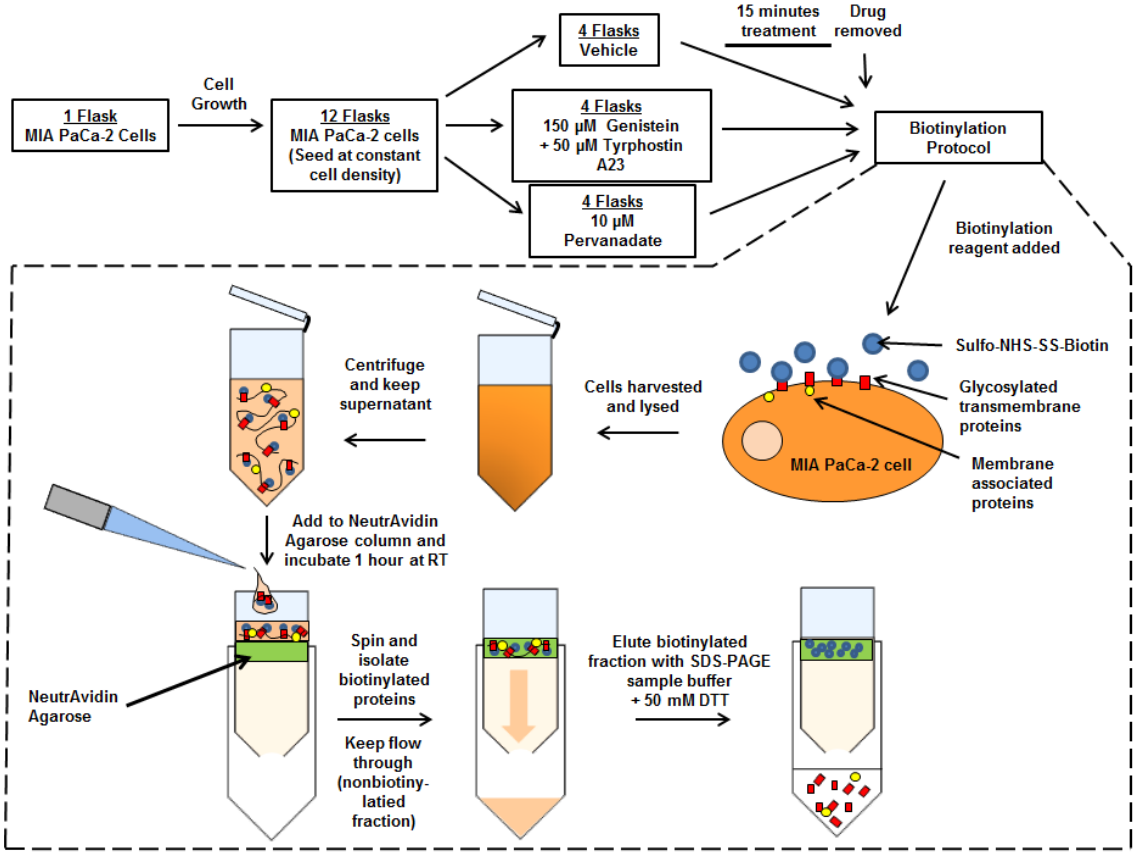

Supplementary Figure 4.1 - Isolation of plasma membrane-associated proteins from cultured cells following drug treatment

To isolate the plasma-membrane and any associated proteins, a cell surface biotinylation assay was used. MIA PaCa-2 cells were first seeded into 12 flasks (75 cm^3) at a constant density. Once cells had reached 95% confluence, cells were treated for 15 minutes at 37 °C with either vehicle (phosphate buffered saline, PBS), a combination of 150 µM genistein and 50 µM tyrphostin A23, or 10 µM pervanadate, with 4 flasks in each treatment group. At this point, cells were rinsed twice with ice cold PBS, and the membrane-fraction isolated using the biotinylation assay protocol. This involved the labelling of glycosolated transmembrane proteins using Sulfo-NHS-SS-Biotin Briefly, biotin-labelled cells were lysed, and the cell lysate clarified by centrifugation at 10000 x g before being added to a NeutrAvidin Agarose column. This column was incubated for an hour at room temperature using an end-over-end rotating mixer before the biotinylated and non-biotinylated fractions were separated by centrifugation. Labelled proteins bound to the NeutrAvidin Agarose column were eluted using 1x SDS-PAGE sample buffer containing 50 mM dithiothreitol (DTT). Samples were then analysed using western blot analysis.

4.7.3 - Gel preparation for western blot

Resolving and stacking gels for western blot analysis were prepared as described in Supplementary Table 4.7.1.

	Volume (ml) required for gel			
	10%	7.5%	6%	Stacking
1M Tris, pH 6.8	0	0	0	0.625
1M Tris, pH 8.8	7.5	7.5	7.5	0
40 % Acrylamide/Bis Solution	5	3.7	3	0.5
H_2O	6.78	8.075	8.91	3.716
Sodium dodecyl sulfate (SDS) 20%	0.1	0.1	0.1	0.025
Tetramethylethylenediamine (TEMED)	0.025	0.025	0.025	0.0125
Ammonium persulfate (10%)	0.6	0.6	0.6	0.15

Supplementary Table 4.7.1 – Recipes for 6, 7.5 and 10 % gels for western blot analysis

4.8 - Supplemental References

KADOTA, S., FANTUS, I. G., DERAGON, G., GUYDA, H. J., HERSH, B. & POSNER, B. I. 1987. Peroxide(s) of vanadium: a novel and potent insulin-mimetic agent which activates the insulin receptor kinase. *Biochem Biophys Res Commun,* 147**,** 259-66.

Chapter 5 - Concluding Discussion and Future Work

Despite pancreatic ductal adenocarcinoma (PDAC) being the 5th most common cause of cancer-related death, there is no effective treatment or imminent cure (Krejs, 2010). Aside from surgical intervention, the current treatment options for PDAC (including gemcitibine, FOLFIRINOX and radiotherapy) only extend median survival by a few months (Conroy et al., 2011a, Conroy et al., 2011b, Warsame and Grothey, 2012), and therefore there is a clear unmet clinical need for novel ways to combat this disease. This thesis provides evidence for an entirely novel putative coupling between glycolytic ATP production and the plasma membrane Ca^{2+} ATPase (PMCA) which may be critical for the growth and survival of PDAC tumours, and therefore may be a weakness that can be exploited therapeutically.

Recent years have seen an increased research focus on the role of altered metabolism (Cairns et al., 2011) and ion transport (Lang and Stournaras, 2014) in cancer cells, with the aim of identifying new druggable targets. Nevertheless, whilst there have been significant advances in our understanding of how ion transporters and channels contribute to cancer progression, little is known about the metabolic regulation of ATP dependent ion transporters in tumours exhibiting metabolic transformation. The data presented within this thesis provides the first insight into the regulation of the PMCA by glycolytically-derived ATP in PDAC. In line with the results of previous studies (Zhou et al., 2011, Zhou et al., 2012, Mikuriya et al., 2007, Chaika et al., 2012b), we established that PDAC cell lines (particular MIA PaCa-2 cells) exhibit a highly glycolytic phenotype characteristic of the Warburg phenotype. Moreover, the data presented in *Chapter 2* and *Chapter 3* together indicate that, in these highly glycolytic PDAC cells, glycolytic ATP is critically important for PMCA activity and the maintenance of a low resting cytosolic Ca^{2+} concentration ($[Ca^{2+}]_i$). This work is expanded upon in *Chapter 3*, where MIA PaCa-2 cells became significantly less sensitive to the effects of glycolytic inhibitors on PMCA activity and resting $[Ca^{2+}]_i$ when their metabolic phenotype was manipulated such that they exhibited a lower glycolytic rate and an increased reliance on mitochondrial metabolism. Additionally, the data presented in *Chapter 4* is the first to show that numerous key glycolytic enzymes associate with the plasma membrane in PDAC cells, presenting the possibility of a submembrane glycolytic metabolon that may provide a privileged ATP supply to cation pumps at the plasma membrane. Taken together, these data indicate that the PMCA in PDAC cells exhibiting the Warburg phenotype is exquisitely sensitive to glycolytic inhibition in comparison to cells exhibiting a more normal metabolic phenotype. As such, the glycolytic regulation of the PMCA in PDAC may provide an effective means to target highly glycolytic PDAC cells selectively while leaving healthy cells unharmed. Furthermore, the presence of glycolytic enzymes at the plasma membrane may represent an important therapeutic locus for novel treatment strategies, since these enzymes may be critical to the glycolytic regulation of the PMCA. Future research is required to determine the functional importance of the glycolytic dependency of the PMCA to the progression of PDAC, and to determine the structure-function relationships membrane-bound glycolytic enzymes in facilitating this.

The importance of PMCA activity to the survival of PDAC cells is highlighted by the fact our data (*Chapter 2*) indicates that the PMCA is the main and most important mechanism for extruding Ca^{2+} from human PDAC cell lines (PANC-1 and MIA PaCa-2). During our *in situ* $[Ca^{2+}]_i$ clearance assays, substitution of all Na^+ within the external buffer with N-methyl D-glucamine (Na^+ free/NMDG) had no effect on $[Ca^{2+}]_i$ clearance rate, ruling out the possibility that the Na^+/Ca^{2+} exchanger contributes significantly to $[Ca^{2+}]_i$ clearance in these cells. Moreover, application of external La^{3+} profoundly inhibited of $[Ca^{2+}]_i$ clearance. Since La^{3+} ion is charged, it cannot freely cross the plasma membrane, and therefore exerts its effects at the extracellular side of the plasma membrane. As such, we could therefore also rule out intracellular $[Ca^{2+}]_i$ clearance pathways (such as mitochondrial Ca^{2+} uptake) as being major contributors to $[Ca^{2+}]_i$ clearance. This left the PMCA as the predominant means by which MIA PaCa-2 and PANC-1 cells clear $[Ca^{2+}]_i$, and any effects on $[Ca^{2+}]_i$ clearance could be attributed to effects on PMCA activity. This effectively leaves the PMCA as the "final gatekeeper" to maintaining a low $[Ca^{2+}]_i$ in PDAC cells. As such, unimpaired PMCA activity is crucial for PDAC cell survival, and underlines the glycolytic regulation of the PMCA as a potential anticancer target.

Since the PMCA is ubiquitously expressed and is important for maintaining a low resting $[Ca^{2+}]_i$ in all cells (Strehler and Zacharias, 2001b), any chemotherapeutic agent that aimed to compromise PMCA activity in PDAC would need to do so selectively. Moreover, the data in this thesis suggests that the metabolic phenotype of PDAC cells may provide a means to successfully achieve this selectivity. While *Chapter 2* established that glycolytic inhibition induced ATP depletion, $[Ca^{2+}]_i$ overload and inhibition of PMCA activity, it was not known whether these observations were exclusive to those cells exhibiting a highly glycolytic phenotype, or whether cells exhibiting a lower glycolytic rate and an increased reliance upon mitochondrial metabolism would respond in a similar fashion. However, when addressed in *Chapter 3*, MIA PaCa-2 cells cultured in nominal glucose-free media supplemented with KIC or galactose were significantly less sensitive to the effects of iodoacetate (IAA) on ATP depletion, $[Ca^{2+}]_i$ overload and PMCA inhibition, and IAA had no effect on the ability of these cells to recover $[Ca^{2+}]_i$ compared to control cells. Moreover, following culture in nominal glucose-free media supplemented with KIC or galactose, cells were sensitised to ATP depletion by mitochondrial inhibitors such as antimycin A (AM) and oligomycin (OM), and were less sensitive to the ATP depleting effects of the glycolytic inhibitors 3-bromopyruvate (BrPy) and IAA compared to their glucose-cultured counterparts. In addition, extracellular flux (XF) assays established that culture in either KIC or galactose slowed the high glycolytic rate of MIA PaCa-2 cells, and in the case of KIC, preserved a high mitochondrial respiration rate. To our knowledge, this study is the first to show that a reversal in the Warburg phenotype can be been achieved using nominal glucose-free media supplemented with KIC. Taken together with the data presented in *Chapter 2*, these findings suggest that the high glycolytic rate in PDAC cells is a prerequisite for their exquisite sensitivity to inhibition of glycolytic ATP production. Crucially, however, this sensitivity to glycolytic inhibitors was not observed when the high glycolytic rate

was attenuated, suggesting that targeting the metabolic phenotype of PDAC may represent an effective means to compromise $[Ca^{2+}]_i$ clearance via the PMCA selectively in PDAC.

While the data strongly imply that glycolytic ATP depletion results in $[Ca^{2+}]_i$ overload and PMCA activity, the absolute concentration to which ATP would be required to deplete to in order to inhibit the PMCA is unknown. Cell-free assays indicate that the ATP sensitivity of the PMCA is influenced by factors including calmodulin, the phospholipid composition of the plasma membrane and changes in $[Mg^{2+}]_i$ and $[Ca^{2+}]_i$ (Rossi and Rega, 1989, Zhang et al., 2009, Richards et al., 1978), and until recently the lack of reliable methods for measuring changes in cellular $[ATP]_i$ in live cells has limited our ability to reliably probe the regulation of ATP dependent processes such as the PMCA. However, this has been recently addressed with the ATeam recombinant ATP indicators (Imamura et al., 2009). Furthermore, the more recent GO-ATeam FRET reporter was developed to have a minimal overlap with fura-2 emission spectra and is, in contrast to firefly luciferase (Seliger and McElroy, 1964), insensitive to pH within the physiological range (Nakano et al., 2011). GO-ATeam has therefore provided the first means of measuring cytosolic $[ATP]_i$ and $[Ca^{2+}]_i$ simultaneously in intact, living cells. Moreover, in order to investigate the critical $[ATP]_i$ threshold at which PMCA becomes inhibited and $[Ca^{2+}]_i$ overload is initiated, a logical future extension of the present work would be to use GO-ATeam to simultaneously measure $[ATP]_i$ and $[Ca^{2+}]_i$ during an *in situ* $[Ca^{2+}]_i$. clearance assay in human PDAC cell lines (PANC-1 and MIA PaCa-2). Furthermore, it would also be desirable to calibrate the $[ATP]_i$ by permeabilising cells to known extracellular concentrations of ATP, for example using α-toxin (Tarasov et al., 2006) or beta-escin (Konishi and Watanabe, 1995), in a similar method to that used to calibrate $[Ca^{2+}]_i$. Previous studies have also shown the GO-ATeam can be targeted to specific subcellular compartments; for example, the measurement of [ATP] within the mitochondrial matrix was made possible using a GO-ATeam construct targeted to the mitochondria (Nakano et al., 2011). This raises the possibility of using a GO-ATeam targeted to the submembrane compartment to measure ATP levels proximal to the PMCA and to determine whether changes in a submembrane pool of ATP influence its activity. Furthermore, the present body of work indicates that GO-ATeam can be stably expressed in transfected PDAC cell lines. Importantly, this may provide the opportunity to measure $[ATP]_i$ in xenografted PDAC tumour cells *in vivo* using GO-ATeam. For example, dorsal window chamber intravital microscopy could be used to visualize PDAC cells stably expressing GO-ATeam that had been grafted into nude mice (Nu/Nu). Moreover, this technique could be extended to other recombinant reporters for $[Ca^{2+}]_i$ and cell death, such as GECO (Zhao et al., 2011), GCaMP (Muto et al., 2011), and IMS-RP-GFP (Earley et al., 2012), allowing changes in ATP to be correlated to changes in $[Ca^{2+}]_i$ and cell viability in *in vivo* xenograft models of cancer.

The data in this thesis is also the first to show that numerous key glycolytic enzymes are found associated with the plasma membrane in human PDAC cells (MIA PaCa-2). Membrane-bound glycolytic enzymes have previously been shown to be important for fuelling ATP-dependent cation pumps in erythrocytes (Campanella et al., 2008, Campanella et al., 2005, Puchulu-Campanella et al., 2013, Chu et al., 2012) and for maintaining Ca^{2+} transport via the PMCA in

inside-out plasma membrane vesicles from porcine smooth muscle cells (Hardin et al., 1992, Paul et al., 1989). Furthermore, it is known that membrane association can affect the activity of glycolytic enzymes (Kosugi et al., 2011). Similarly, in *Chapter 4*, we show that glycolytic enzymes associate with the plasma membrane in human PDAC cell lines. Using a biotinylation based assay to isolate plasma membrane-associated proteins, hexokinase I (HKI), lactate dehydrogenase (LDH), phosphofructokinase (PFK), glyceraldehyde 3-phosphate dehydrogenase (GAPDH), 6-phosphofructo-2-kinase/fructose-2,6-biphosphatase 3 (PFKFB3) and pyruvate kinase M2 (PKM2) were all shown to be present in the biotinylated fraction using western blot. Since the PMCA is exquisitely sensitive to depletion of glycolytic ATP in highly glycolytic PDAC cells, these findings raise the possibility that PMCA activity in PDAC is regulated by glycolytic ATP derived from a local, submembrane glycolytic metabolon (Figure 6.1). Moreover, it could be hypothesised that this would provide the PMCA with a rapid and privileged ATP supply and that high glucose availability and lactate efflux efficiency from nearby membrane-bound transporters could facilitate an efficient ATP-generating locus for maintaining PMCA activity. Furthermore, the aberrant expression of glycolytic enzymes in PDAC (Chaika et al., 2012b, Zhou et al., 2011, Zhou et al., 2012) may provide a further means to selectively target this metabolon (and by extension, the PMCA) in PDAC.

We also provide preliminary evidence that the membrane association of these glycolytic enzymes may be regulated in a tyrosine phosphorylation-dependent fashion. While this dynamic regulation of membrane association requires further verification, the data are consistent with similar mechanisms where glycolytic enzymes associate with anion exchanger 1 (AE1) in erythrocytes (Campanella et al., 2005, Campanella et al., 2008, Chu et al., 2012, Puchulu-Campanella et al., 2013) and by which PKM2 associates with MUC1 in 3Y1 fibroblasts (Kosugi et al., 2011). Nevertheless, the putative binding sites of these enzymes remain unknown, and future work is required to identify physical and functional nature of the protein-protein interactions that facilitate glycolytic enzyme association with proteins found in the plasma membrane. An early candidate for this putative binding domain is MUC1, which is a transmembrane protein that has previously been shown to bind PKM2 (Kosugi et al., 2011) and is overexpressed in PDAC (Hinoda et al., 2003) and, in the present study, was found to be expressed in MIA PaCa-2 cells. Future studies are required to determine whether the plasma-membrane association of glycolytic enzymes observed in the present study occurs via an interaction with MUC1. This could be achieved by performing a co-immunoprecipitation of MUC1 from human PDAC cell lines or tumour samples followed by western blot for glycolytic enzymes and analysis of associated proteins by mass spectrometry. Similarly, the identification of key plasma membrane binding proteins could be achieved by co-immunoprecipitation of glycolytic enzymes from plasma membrane fractions followed by analysis by mass spectrometry and subsequent confirmation by western blot.

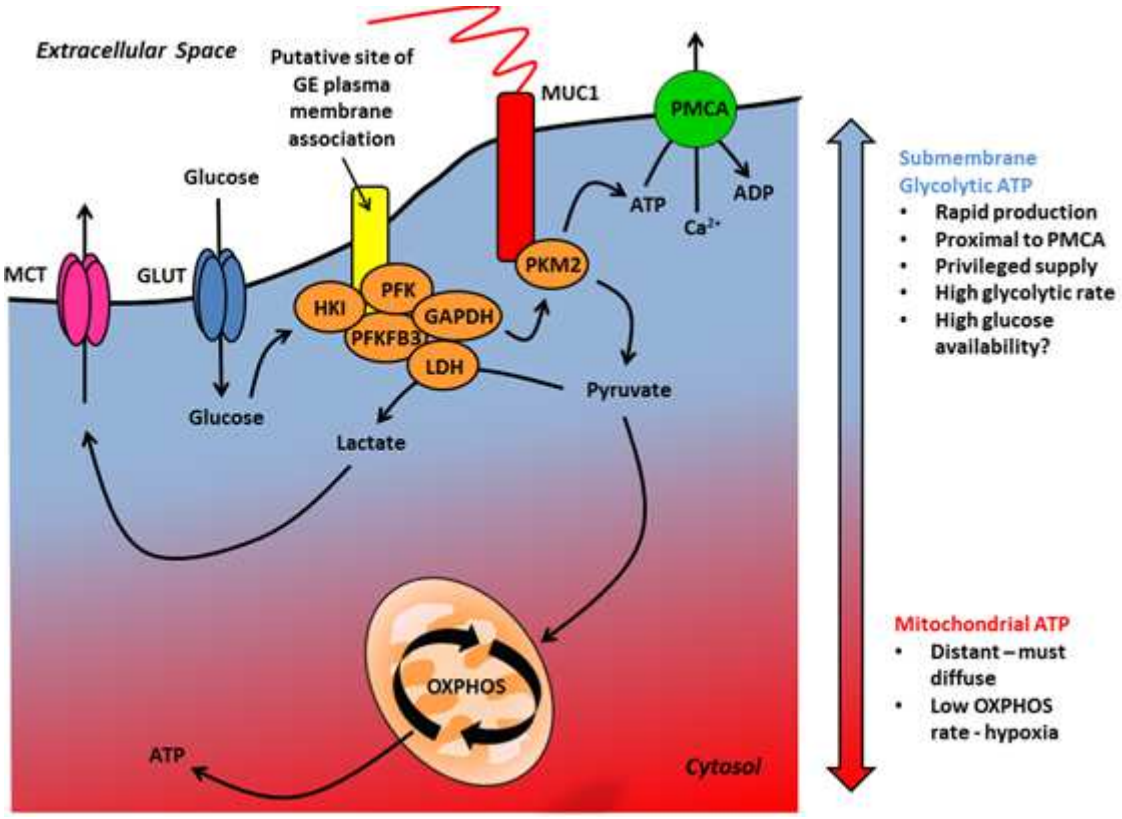

Figure 5.1 - Diagram depicting a hypothetical submembrane glycolytic ATP supply to the plasma membrane Ca^{2+} ATPase in PDAC.

The results presented in this thesis raise the the possibility that the PMCA in PDAC is regulated by a local, submembrane glycolytic metabolon. In this hypothetical model, putative associations with plasma membrane proteins (such as the reported interaction between PKM2 and MUC1) allows membrane-bound glycolytic enzymes to provide the PMCA with a privelidged and rapid supply of submembrane glycolytic ATP (blue shading). Glucose availability for this submembrane glycolytic cascade might be expected to be high given its close proximity to glucose transporters (GLUT), with efficient efflux of lactate via nearby monocaboxylate transporters (MCT) facilitating glycolytic flux. In contrast, ATP derived from oxidative phosphorylation (OXPHOS, red shading) appears to be less important for PMCA activity in PDAC. This is potentially due to the upregulation of glycolysis coupled with a lower relative contribution of mitochondrial metabolism to ATP production. Furthermore, mitochondrial ATP might be less accessible as a PMCA fuel source, and may be required to diffuse larger distances compared to that derived from the submembrane mitochondrial metabolon.

Following identification of those proteins involved in facilitating glycolytic enzyme association with the plasma membrane, the putative binding domains could be identified using site-directed mutagenesis. The importance of these glycolytic enzymes and their putative regulatory binding proteins could be further investigated by assessing the effects of doxycycline-induced gene deletion on functional readouts such as cytosolic $[Ca^{2+}]_i$ overload, PMCA activity, ATP depletion, cell death and cell proliferation. Furthermore, changes in glycolytic enzyme activity following association with putative regulatory plasma membrane proteins could be assessed using i*n vitro* enzyme-linked NADH absorbance assays of cytosolic vs membrane-associated enzyme activity, for example, for PKM2, PFK1 and PFKFB3 (Smallbone et al., 2013, Marin-Hernandez et al., 2011). Together these studies would provide a foundation from which to design small molecule

drugs with which to disrupt or modulate the functional coupling of this submembrane glycolytic cascade with ATP driven pumps, which may be expected to impair PMCA activity.

To conclude, we propose that the regulation of the PMCA by glycolytic ATP in PDAC is critical for tumour growth and survival, and that this may be an “Achilles heel” that can be therapeutically targeted to selectively kill cancer cells while sparing healthy cells. This work provides a platform for future studies to further characterise the relationship between the Warburg phenotype, glycolytic ATP and $[Ca^{2+}]_i$ homeostasis in PDAC, and to dissect the functional relationships of the enzymes and proteins key in facilitating this.

Chapter 6 - References

AGUIRRE, A. J., BARDEESY, N., SINHA, M., LOPEZ, L., TUVESON, D. A., HORNER, J., REDSTON, M. S. & DEPINHO, R. A. 2003. Activated Kras and Ink4a/Arf deficiency cooperate to produce metastatic pancreatic ductal adenocarcinoma. *Genes Dev,* 17**,** 3112-26.

AKAKURA, N., KOBAYASHI, M., HORIUCHI, I., SUZUKI, A., WANG, J., CHEN, J., NIIZEKI, H., KAWAMURA, K., HOSOKAWA, M. & ASAKA, M. 2001. Constitutive expression of hypoxia-inducible factor-1alpha renders pancreatic cancer cells resistant to apoptosis induced by hypoxia and nutrient deprivation. *Cancer Res,* 61**,** 6548-54.

ALARCON, R., KOUMENIS, C., GEYER, R. K., MAKI, C. G. & GIACCIA, A. J. 1999. Hypoxia induces p53 accumulation through MDM2 down-regulation and inhibition of E6-mediated degradation. *Cancer Res,* 59**,** 6046-51.

ALBERTS, B. 2004. *Essential cell biology,* New York, NY, Garland Science Pub.

ALTOMARE, D. A., TANNO, S., DE RIENZO, A., KLEIN-SZANTO, A. J., SKELE, K. L., HOFFMAN, J. P. & TESTA, J. R. 2002. Frequent activation of AKT2 kinase in human pancreatic carcinomas. *J Cell Biochem,* 87**,** 470-6.

AMIN, Z., THEIS, B., RUSSELL, R. C., HOUSE, C., NOVELLI, M. & LEES, W. R. 2006. Diagnosing pancreatic cancer: the role of percutaneous biopsy and CT. *Clin Radiol,* 61**,** 996-1002.

ANKORINA-STARK, I., AMSTRUP, J. & NOVAK, I. 2002. Regulation of the Na^+/Ca^{2+} exchanger in rat pancreatic ducts. *J Membr Biol,* 186**,** 43-53.

ARMSTRONG, C. T., ANDERSON, J. L. & DENTON, R. M. 2014. Studies on the regulation of the human E1 subunit of the 2-oxoglutarate dehydrogenase complex, including the identification of a novel calcium-binding site. *Biochem J,* 459**,** 369-81.

ASANO, T., YAO, Y., ZHU, J., LI, D., ABBRUZZESE, J. L. & REDDY, S. A. 2004. The PI 3-kinase/Akt signaling pathway is activated due to aberrant Pten expression and targets transcription factors NF-kappaB and c-Myc in pancreatic cancer cells. *Oncogene,* 23**,** 8571-80.

AUNG, C. S., KRUGER, W. A., PORONNIK, P., ROBERTS-THOMSON, S. J. & MONTEITH, G. R. 2007. Plasma membrane Ca^{2+}-ATPase expression during colon cancer cell line differentiation. *Biochem Biophys Res Commun,* 355**,** 932-6.

BACHEM, M. G., SCHUNEMANN, M., RAMADANI, M., SIECH, M., BEGER, H., BUCK, A., ZHOU, S., SCHMID-KOTSAS, A. & ADLER, G. 2005. Pancreatic carcinoma cells induce fibrosis by stimulating proliferation and matrix synthesis of stellate cells. *Gastroenterology,* 128**,** 907-21.

BANSAL, P. & SONNENBERG, A. 1995. Pancreatitis is a risk factor for pancreatic cancer. *Gastroenterology,* 109**,** 247-51.

BARDEESY, N., AGUIRRE, A. J., CHU, G. C., CHENG, K. H., LOPEZ, L. V., HEZEL, A. F., FENG, B., BRENNAN, C., WEISSLEDER, R., MAHMOOD, U., HANAHAN, D., REDSTON, M. S., CHIN, L. & DEPINHO, R. A. 2006a. Both p16(Ink4a) and the p19(Arf)-p53 pathway constrain progression of pancreatic adenocarcinoma in the mouse. *Proc Natl Acad Sci U S A,* 103**,** 5947-52.

BARDEESY, N., CHENG, K. H., BERGER, J. H., CHU, G. C., PAHLER, J., OLSON, P., HEZEL, A. F., HORNER, J., LAUWERS, G. Y., HANAHAN, D. & DEPINHO, R. A. 2006b. Smad4 is dispensable for normal pancreas development yet critical in progression and tumor biology of pancreas cancer. *Genes Dev,* 20**,** 3130-46.

BARDEESY, N. & DEPINHO, R. A. 2002. Pancreatic cancer biology and genetics. *Nat Rev Cancer,* 2**,** 897-909.

BAUGHMAN, J. M., PEROCCHI, F., GIRGIS, H. S., PLOVANICH, M., BELCHER-TIMME, C. A., SANCAK, Y., BAO, X. R., STRITTMATTER, L., GOLDBERGER, O., BOGORAD, R. L.,

KOTELIANSKY, V. & MOOTHA, V. K. 2011. Integrative genomics identifies MCU as an essential component of the mitochondrial calcium uniporter. *Nature,* 476**,** 341-5.

BAUTISTA, D. M., SIEMENS, J., GLAZER, J. M., TSURUDA, P. R., BASBAUM, A. I., STUCKY, C. L., JORDT, S. E. & JULIUS, D. 2007. The menthol receptor TRPM8 is the principal detector of environmental cold. *Nature,* 448**,** 204-8.

BEHROOZ, A. & ISMAIL-BEIGI, F. 1999. Stimulation of Glucose Transport by Hypoxia: Signals and Mechanisms. *News Physiol Sci,* 14**,** 105-110.

BELLACOSA, A., CHAN, T. O., AHMED, N. N., DATTA, K., MALSTROM, S., STOKOE, D., MCCORMICK, F., FENG, J. & TSICHLIS, P. 1998. Akt activation by growth factors is a multiple-step process: the role of the PH domain. *Oncogene,* 17**,** 313-25.

BENSAAD, K., TSURUTA, A., SELAK, M. A., VIDAL, M. N., NAKANO, K., BARTRONS, R., GOTTLIEB, E. & VOUSDEN, K. H. 2006. TIGAR, a p53-inducible regulator of glycolysis and apoptosis. *Cell,* 126**,** 107-20.

BERLIOCCHI, L., BANO, D. & NICOTERA, P. 2005. Ca^{2+} signals and death programmes in neurons. *Philos Trans R Soc Lond B Biol Sci,* 360**,** 2255-8.

BERRIDGE, M. J. 2009. Inositol trisphosphate and calcium signalling mechanisms. *Biochim Biophys Acta,* 1793**,** 933-40.

BERRIDGE, M. J., BOOTMAN, M. D. & LIPP, P. 1998. Calcium--a life and death signal. *Nature,* 395**,** 645-8.

BERRIDGE, M. J., BOOTMAN, M. D. & RODERICK, H. L. 2003. Calcium signalling: dynamics, homeostasis and remodelling. *Nat Rev Mol Cell Biol,* 4**,** 517-29.

BERRIDGE, M. J., LIPP, P. & BOOTMAN, M. D. 2000. The versatility and universality of calcium signalling. *Nat Rev Mol Cell Biol,* 1**,** 11-21.

BERRINGTON DE GONZALEZ, A., SWEETLAND, S. & SPENCER, E. 2003. A meta-analysis of obesity and the risk of pancreatic cancer. *Br J Cancer,* 89**,** 519-23.

BHARDWAJ, V., RIZVI, N., LAI, M. B., LAI, J. C. & BHUSHAN, A. 2010. Glycolytic enzyme inhibitors affect pancreatic cancer survival by modulating its signaling and energetics. *Anticancer Res,* 30**,** 743-9.

BIERIE, B. & MOSES, H. L. 2006. Tumour microenvironment: TGFbeta: the molecular Jekyll and Hyde of cancer. *Nat Rev Cancer,* 6**,** 506-20.

BLAUSTEIN, M. P. & LEDERER, W. J. 1999. Sodium/calcium exchange: its physiological implications. *Physiol Rev,* 79**,** 763-854.

BLUM, R. & KLOOG, Y. 2014. Metabolism addiction in pancreatic cancer. *Cell Death Dis,* 5**,** e1065.

BOBARYKINA, A. Y., MINCHENKO, D. O., OPENTANOVA, I. L., MOENNER, M., CARO, J., ESUMI, H. & MINCHENKO, O. H. 2006. Hypoxic regulation of PFKFB-3 and PFKFB-4 gene expression in gastric and pancreatic cancer cell lines and expression of PFKFB genes in gastric cancers. *Acta Biochim Pol,* 53**,** 789-99.

BOOTMAN, M., NIGGLI, E., BERRIDGE, M. & LIPP, P. 1997. Imaging the hierarchical Ca^{2+} signalling system in HeLa cells. *J Physiol,* 499 (Pt 2)**,** 307-14.

BRAGADIN, M., POZZAN, T. & AZZONE, G. F. 1979. Kinetics of Ca^{2+} carrier in rat liver mitochondria. *Biochemistry,* 18**,** 5972-8.

BRAND, K. A. & HERMFISSE, U. 1997. Aerobic glycolysis by proliferating cells: a protective strategy against reactive oxygen species. *FASEB J,* 11**,** 388-95.

BRINI, M. 2009. Plasma membrane Ca^{2+}-ATPase: from a housekeeping function to a versatile signaling role. *Pflugers Arch,* 457**,** 657-64.

BRISTOW, R. G. & HILL, R. P. 2008. Hypoxia and metabolism. Hypoxia, DNA repair and genetic instability. *Nat Rev Cancer,* 8**,** 180-92.

BRUCE, J. 2010. Plasma membrane calcium pump regulation by metabolic stress. *World J Biol Chem,* 1**,** 221-8.

BRUCE, J. I., STRAUB, S. V. & YULE, D. I. 2003. Crosstalk between cAMP and Ca^{2+} signaling in non-excitable cells. *Cell Calcium,* 34**,** 431-44.

BRUGGE, W. R., LAUWERS, G. Y., SAHANI, D., FERNANDEZ-DEL CASTILLO, C. & WARSHAW, A. L. 2004. Cystic neoplasms of the pancreas. *N Engl J Med,* 351**,** 1218-26.

BUCHLER, P., REBER, H. A., BUCHLER, M., SHRINKANTE, S., BUCHLER, M. W., FRIESS, H., SEMENZA, G. L. & HINES, O. J. 2003. Hypoxia-inducible factor 1 regulates vascular endothelial growth factor expression in human pancreatic cancer. *Pancreas,* 26**,** 56-64.

BUDD, S. L. & NICHOLLS, D. G. 1996. A reevaluation of the role of mitochondria in neuronal Ca^{2+} homeostasis. *J Neurochem,* 66**,** 403-11.

BURNASHEV, N. 1998. Calcium permeability of ligand-gated channels. *Cell Calcium,* 24**,** 325-32.

BYGRAVE, F. L. & BENEDETTI, A. 1996. What is the concentration of calcium ions in the endoplasmic reticulum? *Cell Calcium,* 19**,** 547-51.

CAIRNS, R. A., HARRIS, I. S. & MAK, T. W. 2011. Regulation of cancer cell metabolism. *Nat Rev Cancer,* 11**,** 85-95.

CAMELLO, C., LOMAX, R., PETERSEN, O. H. & TEPIKIN, A. V. 2002. Calcium leak from intracellular stores--the enigma of calcium signalling. *Cell Calcium,* 32**,** 355-61.

CAMPANELLA, M. E., CHU, H. & LOW, P. S. 2005. Assembly and regulation of a glycolytic enzyme complex on the human erythrocyte membrane. *Proc Natl Acad Sci U S A,* 102**,** 2402-7.

CAMPANELLA, M. E., CHU, H., WANDERSEE, N. J., PETERS, L. L., MOHANDAS, N., GILLIGAN, D. M. & LOW, P. S. 2008. Characterization of glycolytic enzyme interactions with murine erythrocyte membranes in wild-type and membrane protein knockout mice. *Blood,* 112**,** 3900-6.

CANCER RESEARCH UK. 2014. All Cancers Combined Key Stats. [online] Available at: http://publications.cancerresearchuk.org/downloads/Product/CS_KF_ALLCANCERS.pdf [Accessed 16 Jan. 2015].

CANTO, M. I., GOGGINS, M., HRUBAN, R. H., PETERSEN, G. M., GIARDIELLO, F. M., YEO, C., FISHMAN, E. K., BRUNE, K., AXILBUND, J., GRIFFIN, C., ALI, S., RICHMAN, J., JAGANNATH, S., KANTSEVOY, S. V. & KALLOO, A. N. 2006. Screening for early pancreatic neoplasia in high-risk individuals: a prospective controlled study. *Clin Gastroenterol Hepatol,* 4**,** 766-81; quiz 665.

CARAFOLI, E. 1991. Calcium pump of the plasma membrane. *Physiol Rev,* 71**,** 129-53.

CARAFOLI, E. 1994. Biogenesis: plasma membrane calcium ATPase: 15 years of work on the purified enzyme. *FASEB J,* 8**,** 993-1002.

CARAFOLI, E., SANTELLA, L., BRANCA, D. & BRINI, M. 2001. Generation, control, and processing of cellular calcium signals. *Crit Rev Biochem Mol Biol,* 36**,** 107-260.

CARAFOLI, E., TIOZZO, R., LUGLI, G., CROVETTI, F. & KRATZING, C. 1974. The release of calcium from heart mitochondria by sodium. *J Mol Cell Cardiol,* 6**,** 361-71.

CARDENAS-NAVIA, L. I., MACE, D., RICHARDSON, R. A., WILSON, D. F., SHAN, S. & DEWHIRST, M. W. 2008. The pervasive presence of fluctuating oxygenation in tumors. *Cancer Res,* 68**,** 5812-9.

CARIDE, A. J., FILOTEO, A. G., PENHEITER, A. R., PASZTY, K., ENYEDI, A. & PENNISTON, J. T. 2001a. Delayed activation of the plasma membrane calcium pump by a sudden increase in Ca^{2+}: fast pumps reside in fast cells. *Cell Calcium,* 30**,** 49-57.

CARIDE, A. J., PENHEITER, A. R., FILOTEO, A. G., BAJZER, Z., ENYEDI, A. & PENNISTON, J. T. 2001b. The plasma membrane calcium pump displays memory of past calcium spikes. Differences between isoforms 2b and 4b. *J Biol Chem,* 276**,** 39797-804.

CARRASCO, S. & MEYER, T. 2010. Cracking CRAC. *Nat Cell Biol,* 12**,** 416-8.

CASTRO, J., RUMINOT, I., PORRAS, O. H., FLORES, C. M., HERMOSILLA, T., VERDUGO, E., VENEGAS, F., HARTEL, S., MICHEA, L. & BARROS, L. F. 2006. ATP steal between cation pumps: a mechanism linking Na^+ influx to the onset of necrotic Ca^{2+} overload. *Cell Death Differ,* 13**,** 1675-85.

CATERINA, M. J., SCHUMACHER, M. A., TOMINAGA, M., ROSEN, T. A., LEVINE, J. D. & JULIUS, D. 1997. The capsaicin receptor: a heat-activated ion channel in the pain pathway. *Nature,* 389**,** 816-24.

CATTERALL, W. A., PEREZ-REYES, E., SNUTCH, T. P. & STRIESSNIG, J. 2005. International Union of Pharmacology. XLVIII. Nomenclature and structure-function relationships of voltage-gated calcium channels. *Pharmacol Rev,* 57**,** 411-25.

CHAIKA, N. V., GEBREGIWORGIS, T., LEWALLEN, M. E., PUROHIT, V., RADHAKRISHNAN, P., LIU, X., ZHANG, B., MEHLA, K., BROWN, R. B., CAFFREY, T., YU, F., JOHNSON, K. R., POWERS, R., HOLLINGSWORTH, M. A. & SINGH, P. K. 2012a. MUC1 mucin stabilizes and activates hypoxia-inducible factor 1 alpha to regulate metabolism in pancreatic cancer. *Proc Natl Acad Sci U S A,* 109**,** 13787-92.

CHAIKA, N. V., YU, F., PUROHIT, V., MEHLA, K., LAZENBY, A. J., DIMAIO, D., ANDERSON, J. M., YEH, J. J., JOHNSON, K. R., HOLLINGSWORTH, M. A. & SINGH, P. K. 2012b. Differential expression of metabolic genes in tumor and stromal components of primary and metastatic loci in pancreatic adenocarcinoma. *PLoS One,* 7**,** e32996.

CHEN, W. & GUERON, M. 1992. The inhibition of bovine heart hexokinase by 2-deoxy-D-glucose-6-phosphate: characterization by ^{31}P NMR and metabolic implications. *Biochimie,* 74**,** 867-73.

CHENG, J. Q., RUGGERI, B., KLEIN, W. M., SONODA, G., ALTOMARE, D. A., WATSON, D. K. & TESTA, J. R. 1996. Amplification of AKT2 in human pancreatic cells and inhibition of AKT2 expression and tumorigenicity by antisense RNA. *Proc Natl Acad Sci U S A,* 93**,** 3636-41.

CHOW, J. Y., DONG, H., QUACH, K. T., VAN NGUYEN, P. N., CHEN, K. & CARETHERS, J. M. 2008. TGF-beta mediates PTEN suppression and cell motility through calcium-dependent PKC-alpha activation in pancreatic cancer cells. *Am J Physiol Gastrointest Liver Physiol,* 294**,** G899-905.

CHRISTOFK, H. R., VANDER HEIDEN, M. G., HARRIS, M. H., RAMANATHAN, A., GERSZTEN, R. E., WEI, R., FLEMING, M. D., SCHREIBER, S. L. & CANTLEY, L. C. 2008a. The M2 splice isoform of pyruvate kinase is important for cancer metabolism and tumour growth. *Nature,* 452**,** 230-3.

CHRISTOFK, H. R., VANDER HEIDEN, M. G., WU, N., ASARA, J. M. & CANTLEY, L. C. 2008b. Pyruvate kinase M2 is a phosphotyrosine-binding protein. *Nature,* 452**,** 181-6.

CHU, H., PUCHULU-CAMPANELLA, E., GALAN, J. A., TAO, W. A., LOW, P. S. & HOFFMAN, J. F. 2012. Identification of cytoskeletal elements enclosing the ATP pools that fuel human red blood cell membrane cation pumps. *Proc Natl Acad Sci U S A,* 109**,** 12794-9.

CLAPHAM, D. E. 2003. TRP channels as cellular sensors. *Nature,* 426**,** 517-24.

CLAPHAM, D. E. 2007. Calcium signaling. *Cell,* 131**,** 1047-58.

CONROY, T., DESSEIGNE, F., YCHOU, M., BOUCHE, O., GUIMBAUD, R., BECOUARN, Y., ADENIS, A., RAOUL, J. L., GOURGOU-BOURGADE, S., DE LA FOUCHARDIERE, C., BENNOUNA, J., BACHET, J. B., KHEMISSA-AKOUZ, F., PERE-VERGE, D., DELBALDO, C., ASSENAT, E., CHAUFFERT, B., MICHEL, P., MONTOTO-GRILLOT, C. & DUCREUX, M. 2011a. FOLFIRINOX versus gemcitabine for metastatic pancreatic cancer. *N Engl J Med,* 364**,** 1817-25.

CONROY, T., GAVOILLE, C. & ADENIS, A. 2011b. Metastatic pancreatic cancer: old drugs, new paradigms. *Curr Opin Oncol,* 23**,** 390-5.

CRIDDLE, D. N., GERASIMENKO, J. V., BAUMGARTNER, H. K., JAFFAR, M., VORONINA, S., SUTTON, R., PETERSEN, O. H. & GERASIMENKO, O. V. 2007. Calcium signalling and pancreatic cell death: apoptosis or necrosis? *Cell Death Differ,* 14**,** 1285-94.

CSORDAS, G., RENKEN, C., VARNAI, P., WALTER, L., WEAVER, D., BUTTLE, K. F., BALLA, T., MANNELLA, C. A. & HAJNOCZKY, G. 2006. Structural and functional features and significance of the physical linkage between ER and mitochondria. *J Cell Biol,* 174**,** 915-21.

CUI, Y., TIAN, M., ZONG, M., TENG, M., CHEN, Y., LU, J., JIANG, J., LIU, X. & HAN, J. 2009a. Proteomic analysis of pancreatic ductal adenocarcinoma compared with normal adjacent pancreatic tissue and pancreatic benign cystadenoma. *Pancreatology,* 9**,** 89-98.

CUI, Y., ZHANG, D., JIA, Q., LI, T., ZHANG, W. & HAN, J. 2009b. Proteomic and tissue array profiling identifies elevated hypoxia-regulated proteins in pancreatic ductal adenocarcinoma. *Cancer Invest,* 27**,** 747-55.

CULLEN, P. J. & LOCKYER, P. J. 2002. Integration of calcium and Ras signalling. *Nat Rev Mol Cell Biol,* 3**,** 339-48.

CURI, R., NEWSHOLME, P. & NEWSHOLME, E. A. 1988. Metabolism of pyruvate by isolated rat mesenteric lymphocytes, lymphocyte mitochondria and isolated mouse macrophages. *Biochem J,* 250**,** 383-8.

CURRY, M. C., LUK, N. A., KENNY, P. A., ROBERTS-THOMSON, S. J. & MONTEITH, G. R. 2012. Distinct regulation of cytoplasmic calcium signals and cell death pathways by different plasma membrane calcium ATPase isoforms in MDA-MB-231 breast cancer cells. *J Biol Chem,* 287**,** 28598-608.

DAVID, C. J., CHEN, M., ASSANAH, M., CANOLL, P. & MANLEY, J. L. 2010. HnRNP proteins controlled by c-Myc deregulate pyruvate kinase mRNA splicing in cancer. *Nature,* 463**,** 364-8.

DE BOCK, K., GEORGIADOU, M., SCHOORS, S., KUCHNIO, A., WONG, B. W., CANTELMO, A. R., QUAEGEBEUR, A., GHESQUIERE, B., CAUWENBERGHS, S., EELEN, G., PHNG, L. K., BETZ, I., TEMBUYSER, B., BREPOELS, K., WELTI, J., GEUDENS, I., SEGURA, I., CRUYS, B., BIFARI, F., DECIMO, I., BLANCO, R., WYNS, S., VANGINDERTAEL, J., ROCHA, S., COLLINS, R. T., MUNCK, S., DAELEMANS, D., IMAMURA, H., DEVLIEGER, R., RIDER, M., VAN VELDHOVEN, P. P., SCHUIT, F., BARTRONS, R., HOFKENS, J., FRAISL, P., TELANG, S., DEBERARDINIS, R. J., SCHOONJANS, L., VINCKIER, S., CHESNEY, J., GERHARDT, H., DEWERCHIN, M. & CARMELIET, P. 2013. Role of PFKFB3-driven glycolysis in vessel sprouting. *Cell,* 154**,** 651-63.

DE STEFANI, D., RAFFAELLO, A., TEARDO, E., SZABO, I. & RIZZUTO, R. 2011. A forty-kilodalton protein of the inner membrane is the mitochondrial calcium uniporter. *Nature,* 476**,** 336-40.

DEBERARDINIS, R. J., LUM, J. J., HATZIVASSILIOU, G. & THOMPSON, C. B. 2008a. The biology of cancer: metabolic reprogramming fuels cell growth and proliferation. *Cell Metab,* 7**,** 11-20.

DEBERARDINIS, R. J., MANCUSO, A., DAIKHIN, E., NISSIM, I., YUDKOFF, M., WEHRLI, S. & THOMPSON, C. B. 2007. Beyond aerobic glycolysis: transformed cells can engage in glutamine metabolism that exceeds the requirement for protein and nucleotide synthesis. *Proc Natl Acad Sci U S A,* 104**,** 19345-50.

DEBERARDINIS, R. J., SAYED, N., DITSWORTH, D. & THOMPSON, C. B. 2008b. Brick by brick: metabolism and tumor cell growth. *Curr Opin Genet Dev,* 18**,** 54-61.

DECUYPERE, J. P., MONACO, G., BULTYNCK, G., MISSIAEN, L., DE SMEDT, H. & PARYS, J. B. 2011. The IP(3) receptor-mitochondria connection in apoptosis and autophagy. *Biochim Biophys Acta,* 1813**,** 1003-13.

DENTON, R. M., RANDLE, P. J. & MARTIN, B. R. 1972. Stimulation by calcium ions of pyruvate dehydrogenase phosphate phosphatase. *Biochem J,* 128**,** 161-3.

DENTON, R. M., RICHARDS, D. A. & CHIN, J. G. 1978. Calcium ions and the regulation of NAD^+-linked isocitrate dehydrogenase from the mitochondria of rat heart and other tissues. *Biochem J,* 176**,** 899-906.

DEPREZ, J., VERTOMMEN, D., ALESSI, D. R., HUE, L. & RIDER, M. H. 1997. Phosphorylation and activation of heart 6-phosphofructo-2-kinase by protein kinase B and other protein kinases of the insulin signaling cascades. *J Biol Chem,* 272**,** 17269-75.

DI CRISTOFANO, A. & PANDOLFI, P. P. 2000. The multiple roles of PTEN in tumor suppression. *Cell,* 100**,** 387-90.

DI LEVA, F., DOMI, T., FEDRIZZI, L., LIM, D. & CARAFOLI, E. 2008. The plasma membrane Ca^{2+} ATPase of animal cells: structure, function and regulation. *Arch Biochem Biophys,* 476**,** 65-74.

DI MAGLIANO, M. P. & LOGSDON, C. D. 2013. Roles for KRAS in pancreatic tumor development and progression. *Gastroenterology,* 144**,** 1220-9.

DISTLER, M., AUST, D., WEITZ, J., PILARSKY, C., GR, #XFC & TZMANN, R. 2014. Precursor Lesions for Sporadic Pancreatic Cancer: PanIN, IPMN, and MCN. *Biomed Res Int,* 2014**,** 11.

DOLMAN, N. J. & TEPIKIN, A. V. 2006. Calcium gradients and the Golgi. *Cell Calcium,* 40**,** 505-12.

DOLMETSCH, R. E., XU, K. & LEWIS, R. S. 1998. Calcium oscillations increase the efficiency and specificity of gene expression. *Nature,* 392**,** 933-6.

DOLPHIN, A. C. 2006. A short history of voltage-gated calcium channels. *Br J Pharmacol,* 147 Suppl 1**,** S56-62.

DONG, H., SHIM, K. N., LI, J. M., ESTREMA, C., ORNELAS, T. A., NGUYEN, F., LIU, S., RAMAMOORTHY, S. L., HO, S., CARETHERS, J. M. & CHOW, J. Y. 2010. Molecular mechanisms underlying Ca^{2+}-mediated motility of human pancreatic duct cells. *Am J Physiol Cell Physiol,* 299**,** C1493-503.

DONG, X., LI, Y., CHANG, P., TANG, H., HESS, K. R., ABBRUZZESE, J. L. & LI, D. 2011a. Glucose metabolism gene variants modulate the risk of pancreatic cancer. *Cancer Prev Res (Phila),* 4**,** 758-66.

DONG, X., TANG, H., HESS, K. R., ABBRUZZESE, J. L. & LI, D. 2011b. Glucose metabolism gene polymorphisms and clinical outcome in pancreatic cancer. *Cancer,* 117**,** 480-91.

DUCHEN, M. R. 1999. Contributions of mitochondria to animal physiology: from homeostatic sensor to calcium signalling and cell death. *J Physiol,* 516 (Pt 1)**,** 1-17.

DUCHEN, M. R. 2000. Mitochondria and calcium: from cell signalling to cell death. *J Physiol,* 529 Pt 1**,** 57-68.

DUNHAM, E. T. & GLYNN, I. M. 1961. Adenosinetriphosphatase activity and the active movements of alkali metal ions. *J Physiol,* 156**,** 274-93.

DURR, G., STRAYLE, J., PLEMPER, R., ELBS, S., KLEE, S. K., CATTY, P., WOLF, D. H. & RUDOLPH, H. K. 1998. The medial-Golgi ion pump Pmr1 supplies the yeast secretory pathway with Ca^{2+} and Mn^{2+} required for glycosylation, sorting, and endoplasmic reticulum-associated protein degradation. *Mol Biol Cell,* 9**,** 1149-62.

DUVEL, K., YECIES, J. L., MENON, S., RAMAN, P., LIPOVSKY, A. I., SOUZA, A. L., TRIANTAFELLOW, E., MA, Q., GORSKI, R., CLEAVER, S., VANDER HEIDEN, M. G., MACKEIGAN, J. P., FINAN, P. M., CLISH, C. B., MURPHY, L. O. & MANNING, B. D. 2010. Activation of a metabolic gene regulatory network downstream of mTOR complex 1. *Mol Cell,* 39**,** 171-83.

EARLEY, S., VINEGONI, C., DUNHAM, J., GORBATOV, R., FERUGLIO, P. F. & WEISSLEDER, R. 2012. *In vivo* imaging of drug-induced mitochondrial outer membrane permeabilization at single-cell resolution. *Cancer Res,* 72**,** 2949-56.

EBERT, B. L., FIRTH, J. D. & RATCLIFFE, P. J. 1995. Hypoxia and mitochondrial inhibitors regulate expression of glucose transporter-1 via distinct Cis-acting sequences. *J Biol Chem,* 270**,** 29083-9.

EBERT, M. P., FEI, G., SCHANDL, L., MAWRIN, C., DIETZMANN, K., HERRERA, P., FRIESS, H., GRESS, T. M. & MALFERTHEINER, P. 2002. Reduced PTEN expression in the pancreas overexpressing transforming growth factor-beta 1. *Br J Cancer,* 86**,** 257-62.

ECHARTE, M. M., ROSSI, R. C. & ROSSI, J. P. 2007. Phosphorylation of the plasma membrane calcium pump at high ATP concentration. On the mechanism of ATP hydrolysis. *Biochemistry,* 46**,** 1034-41.

ELSTROM, R. L., BAUER, D. E., BUZZAI, M., KARNAUSKAS, R., HARRIS, M. H., PLAS, D. R., ZHUANG, H., CINALLI, R. M., ALAVI, A., RUDIN, C. M. & THOMPSON, C. B. 2004. Akt stimulates aerobic glycolysis in cancer cells. *Cancer Res,* 64**,** 3892-9.

ELWESS, N. L., FILOTEO, A. G., ENYEDI, A. & PENNISTON, J. T. 1997. Plasma membrane Ca^{2+} pump isoforms 2a and 2b are unusually responsive to calmodulin and Ca^{2+}. *J Biol Chem,* 272**,** 17981-6.

FADOK, V. A., VOELKER, D. R., CAMPBELL, P. A., COHEN, J. J., BRATTON, D. L. & HENSON, P. M. 1992. Exposure of phosphatidylserine on the surface of apoptotic lymphocytes triggers specific recognition and removal by macrophages. *J Immunol,* 148**,** 2207-16.

FALCHETTO, R., VORHERR, T., BRUNNER, J. & CARAFOLI, E. 1991. The plasma membrane Ca^{2+} pump contains a site that interacts with its calmodulin-binding domain. *J Biol Chem,* 266**,** 2930-6.

FALCHETTO, R., VORHERR, T. & CARAFOLI, E. 1992. The calmodulin-binding site of the plasma membrane Ca^{2+} pump interacts with the transduction domain of the enzyme. *Protein Sci,* 1**,** 1613-21.

FANTIN, V. R., ST-PIERRE, J. & LEDER, P. 2006. Attenuation of LDH-A expression uncovers a link between glycolysis, mitochondrial physiology, and tumor maintenance. *Cancer cell,* 9**,** 425-34.

FEDORENKO, O. A., POPUGAEVA, E., ENOMOTO, M., STATHOPULOS, P. B., IKURA, M. & BEZPROZVANNY, I. 2014. Intracellular calcium channels: inositol-1,4,5-trisphosphate receptors. *Eur J Pharmacol,* 739**,** 39-48.

FEIG, C., GOPINATHAN, A., NEESSE, A., CHAN, D. S., COOK, N. & TUVESON, D. A. 2012. The pancreas cancer microenvironment. *Clin Cancer Res,* 18**,** 4266-76.

FENG, Z., HU, W., DE STANCHINA, E., TERESKY, A. K., JIN, S., LOWE, S. & LEVINE, A. J. 2007. The regulation of AMPK beta1, TSC2, and PTEN expression by p53: stress, cell and tissue specificity, and the role of these gene products in modulating the IGF-1-AKT-mTOR pathways. *Cancer Res,* 67**,** 3043-53.

FISCHER, K., HOFFMANN, P., VOELKL, S., MEIDENBAUER, N., AMMER, J., EDINGER, M., GOTTFRIED, E., SCHWARZ, S., ROTHE, G., HOVES, S., RENNER, K., TIMISCHL, B., MACKENSEN, A., KUNZ-SCHUGHART, L., ANDREESEN, R., KRAUSE, S. W. & KREUTZ, M. 2007. Inhibitory effect of tumor cell-derived lactic acid on human T cells. *Blood,* 109**,** 3812-9.

FLEMING, J. B., SHEN, G. L., HOLLOWAY, S. E., DAVIS, M. & BREKKEN, R. A. 2005. Molecular consequences of silencing mutant K-ras in pancreatic cancer cells: justification for K-ras-directed therapy. *Mol Cancer Res,* 3**,** 413-23.

FLORIDI, A., BRUNO, T., MICCADEI, S., FANCIULLI, M., FEDERICO, A. & PAGGI, M. G. 1998. Enhancement of doxorubicin content by the antitumor drug lonidamine in resistant Ehrlich ascites tumor cells through modulation of energy metabolism. *Biochem Pharmacol,* 56**,** 841-9.

FLORIDI, A., PAGGI, M. G., MARCANTE, M. L., SILVESTRINI, B., CAPUTO, A. & DE MARTINO, C. 1981. Lonidamine, a selective inhibitor of aerobic glycolysis of murine tumor cells. *J Natl Cancer Ins,* 66**,** 497-9.

FREZZA, C. & GOTTLIEB, E. 2009. Mitochondria in cancer: not just innocent bystanders. *Semin Cancer Biol,* 19**,** 4-11.

FRIESS, H., YAMANAKA, Y., BUCHLER, M., EBERT, M., BEGER, H. G., GOLD, L. I. & KORC, M. 1993. Enhanced expression of transforming growth factor beta isoforms in pancreatic cancer correlates with decreased survival. *Gastroenterology,* 105**,** 1846-56.

FRISCHAUF, I., SCHINDL, R., DERLER, I., BERGSMANN, J., FAHRNER, M. & ROMANIN, C. 2008. The STIM/Orai coupling machinery. *Channels,* 2**,** 261-8.

FUCHS, C. S., COLDITZ, G. A., STAMPFER, M. J., GIOVANNUCCI, E. L., HUNTER, D. J., RIMM, E. B., WILLETT, W. C. & SPEIZER, F. E. 1996. A prospective study of cigarette smoking and the risk of pancreatic cancer. *Arch Intern Med,* 156**,** 2255-60.

FUNASAKA, T. & RAZ, A. 2007. The role of autocrine motility factor in tumor and tumor microenvironment. *Cancer Metastasis Rev,* 26**,** 725-35.

GALIONE, A. & CHUANG, K. T. 2012. Pyridine nucleotide metabolites and calcium release from intracellular stores. *Adv Exp Med Biol,* 740**,** 305-23.

GAMBHIR, S. S. 2002. Molecular imaging of cancer with positron emission tomography. *Nat Rev Cancer,* 2**,** 683-93.

GAO, P., TCHERNYSHYOV, I., CHANG, T. C., LEE, Y. S., KITA, K., OCHI, T., ZELLER, K. I., DE MARZO, A. M., VAN EYK, J. E., MENDELL, J. T. & DANG, C. V. 2009. c-Myc suppression of miR-23a/b enhances mitochondrial glutaminase expression and glutamine metabolism. *Nature,* 458**,** 762-5.

GATENBY, R. A., GAWLINSKI, E. T., GMITRO, A. F., KAYLOR, B. & GILLIES, R. J. 2006. Acid-mediated tumor invasion: a multidisciplinary study. *Cancer Res,* 66**,** 5216-23.

GATENBY, R. A. & GILLIES, R. J. 2004. Why do cancers have high aerobic glycolysis? *Nat Rev Cancer,* 4**,** 891-9.

GILLIES, R. J. & GATENBY, R. A. 2007. Adaptive landscapes and emergent phenotypes: why do cancers have high glycolysis? *J Bioenerg Biomembr,* 39**,** 251-7.

GIUNTI, R., GAMBERUCCI, A., FULCERI, R., BANHEGYI, G. & BENEDETTI, A. 2007. Both translocon and a cation channel are involved in the passive Ca^{2+} leak from the endoplasmic reticulum: a mechanistic study on rat liver microsomes. *Arch Biochem Biophys,* 462**,** 115-21.

GLANCY, B. & BALABAN, R. S. 2012. Role of mitochondrial Ca^{2+} in the regulation of cellular energetics. *Biochemistry,* 51**,** 2959-73.

GORDAN, J. D. & SIMON, M. C. 2007. Hypoxia-inducible factors: central regulators of the tumor phenotype. *Curr Opin Genet Dev,* 17**,** 71-7.

GOTTLIEB, E. & TOMLINSON, I. P. 2005. Mitochondrial tumour suppressors: a genetic and biochemical update. *Nat Rev Cancer,* 5**,** 857-66.

GOTTLOB, K., MAJEWSKI, N., KENNEDY, S., KANDEL, E., ROBEY, R. B. & HAY, N. 2001. Inhibition of early apoptotic events by Akt/PKB is dependent on the first committed step of glycolysis and mitochondrial hexokinase. *Genes Dev,* 15**,** 1406-18.

GREEN, D. R. 1998. Apoptotic pathways: the roads to ruin. *Cell,* 94**,** 695-8.

GREWE, M., GANSAUGE, F., SCHMID, R. M., ADLER, G. & SEUFFERLEIN, T. 1999. Regulation of cell growth and cyclin D1 expression by the constitutively active FRAP-p70s6K pathway in human pancreatic cancer cells. *Cancer Res,* 59**,** 3581-7.

GROCHOLA, L. F., TAUBERT, H., GREITHER, T., BHANOT, U., UDELNOW, A. & WURL, P. 2011. Elevated transcript levels from the MDM2 P1 promoter and low p53 transcript levels are associated with poor prognosis in human pancreatic ductal adenocarcinoma. *Pancreas,* 40**,** 265-70.

GROMADZINSKA, E., LACHOWICZ, L., WALKOWIAK, B. & ZYLINSKA, L. 2001. Calmodulin effect on purified rat cortical plasma membrane Ca^{2+}-ATPase in different phosphorylation states. *Biochim Biophys Acta,* 1549**,** 19-31.

GUDJONSSON, B. 2009. Pancreatic cancer: survival, errors and evidence. *Eur J Gastroenterol Hepatol,* 21**,** 1379-82.

GUERRA, C., MIJIMOLLE, N., DHAWAHIR, A., DUBUS, P., BARRADAS, M., SERRANO, M., CAMPUZANO, V. & BARBACID, M. 2003. Tumor induction by an endogenous K-ras oncogene is highly dependent on cellular context. *Cancer Cell,* 4**,** 111-20.

GUERTIN, D. A. & SABATINI, D. M. 2007. Defining the role of mTOR in cancer. *Cancer Cell,* 12**,** 9-22.

GUILLAUMOND, F., LECA, J., OLIVARES, O., LAVAUT, M. N., VIDAL, N., BERTHEZENE, P., DUSETTI, N. J., LONCLE, C., CALVO, E., TURRINI, O., IOVANNA, J. L., TOMASINI, R. & VASSEUR, S. 2013. Strengthened glycolysis under hypoxia supports tumor symbiosis and hexosamine biosynthesis in pancreatic adenocarcinoma. *Curr Opin Genet Dev,* 110**,** 3919-24.

GYSIN, S., SALT, M., YOUNG, A. & MCCORMICK, F. 2011. Therapeutic strategies for targeting ras proteins. *Genes Cancer,* 2**,** 359-72.

HAHN, S. A., SCHUTTE, M., HOQUE, A. T., MOSKALUK, C. A., DA COSTA, L. T., ROZENBLUM, E., WEINSTEIN, C. L., FISCHER, A., YEO, C. J., HRUBAN, R. H. & KERN, S. E. 1996. DPC4, a candidate tumor suppressor gene at human chromosome 18q21.1. *Science,* 271**,** 350-3.

HANAHAN, D. & WEINBERG, R. A. 2011. Hallmarks of cancer: the next generation. *Cell,* 144**,** 646-74.

HANSEN, M. R., KRABBE, S., ANKORINA-STARK, I. & NOVAK, I. 2009. Purinergic receptors stimulate Na^+/Ca^{2+} exchange in pancreatic duct cells: possible role of proteins handling and transporting Ca^{2+}. *Cell Physiol Biochem,* 23**,** 387-96.

HAO, L., RIGAUD, J. L. & INESI, G. 1994. Ca^{2+}/H^+ countertransport and electrogenicity in proteoliposomes containing erythrocyte plasma membrane Ca-ATPase and exogenous lipids. *J Biol Chem,* 269**,** 14268-75.

HARA, K., MARUKI, Y., LONG, X., YOSHINO, K., OSHIRO, N., HIDAYAT, S., TOKUNAGA, C., AVRUCH, J. & YONEZAWA, K. 2002. Raptor, a binding partner of target of rapamycin (TOR), mediates TOR action. *Cell,* 110**,** 177-89.

HARDIN, C. D., RAEYMAEKERS, L. & PAUL, R. J. 1992. Comparison of endogenous and exogenous sources of ATP in fueling Ca^{2+} uptake in smooth muscle plasma membrane vesicles. *J Gen Physio,* 99**,** 21-40.

HARRISON, M. L., RATHINAVELU, P., ARESE, P., GEAHLEN, R. L. & LOW, P. S. 1991. Role of band 3 tyrosine phosphorylation in the regulation of erythrocyte glycolysis. *J Biol Chem,* 266**,** 4106-11.

HASSAN, M. M., BONDY, M. L., WOLFF, R. A., ABBRUZZESE, J. L., VAUTHEY, J. N., PISTERS, P. W., EVANS, D. B., KHAN, R., CHOU, T. H., LENZI, R., JIAO, L. & LI, D. 2007. Risk factors for pancreatic cancer: case-control study. *Am J Gastroenterol,* 102**,** 2696-707.

HELMLINGER, G., YUAN, F., DELLIAN, M. & JAIN, R. K. 1997. Interstitial pH and pO_2 gradients in solid tumors *in vivo*: high-resolution measurements reveal a lack of correlation. *Nat Med,* 3**,** 177-82.

HENNESSY, B. T., SMITH, D. L., RAM, P. T., LU, Y. & MILLS, G. B. 2005. Exploiting the PI3K/AKT pathway for cancer drug discovery. *Nat Rev Drug Discov,* 4**,** 988-1004.

HEZEL, A. F., GURUMURTHY, S., GRANOT, Z., SWISA, A., CHU, G. C., BAILEY, G., DOR, Y., BARDEESY, N. & DEPINHO, R. A. 2008. Pancreatic LKB1 deletion leads to acinar polarity defects and cystic neoplasms. *Mol Cell Biol,* 28**,** 2414-25.

HEZEL, A. F., KIMMELMAN, A. C., STANGER, B. Z., BARDEESY, N. & DEPINHO, R. A. 2006. Genetics and biology of pancreatic ductal adenocarcinoma. *Genes Dev,* 20**,** 1218-49.

HILL, R., CALVOPINA, J. H., KIM, C., WANG, Y., DAWSON, D. W., DONAHUE, T. R., DRY, S. & WU, H. 2010. PTEN loss accelerates KrasG12D-induced pancreatic cancer development. *Cancer Res,* 70**,** 7114-24.

HINGORANI, S. R., PETRICOIN, E. F., MAITRA, A., RAJAPAKSE, V., KING, C., JACOBETZ, M. A., ROSS, S., CONRADS, T. P., VEENSTRA, T. D., HITT, B. A., KAWAGUCHI, Y., JOHANN, D., LIOTTA, L. A., CRAWFORD, H. C., PUTT, M. E., JACKS, T., WRIGHT, C. V., HRUBAN, R. H., LOWY, A. M. & TUVESON, D. A. 2003. Preinvasive and invasive ductal pancreatic cancer and its early detection in the mouse. *Cancer Cell,* 4**,** 437-50.

HINGORANI, S. R., WANG, L., MULTANI, A. S., COMBS, C., DERAMAUDT, T. B., HRUBAN, R. H., RUSTGI, A. K., CHANG, S. & TUVESON, D. A. 2005. $Trp53^{R172H}$ and $Kras^{G12D}$

cooperate to promote chromosomal instability and widely metastatic pancreatic ductal adenocarcinoma in mice. *Cancer Cell,* 7**,** 469-83.

HINODA, Y., IKEMATSU, Y., HORINOCHI, M., SATO, S., YAMAMOTO, K., NAKANO, T., FUKUI, M., SUEHIRO, Y., HAMANAKA, Y., NISHIKAWA, Y., KIDA, H., WAKI, S., OKA, M., IMAI, K. & YONEZAWA, S. 2003. Increased expression of MUC1 in advanced pancreatic cancer. *J Gastroenterol,* 38**,** 1162-6.

HOFER, A. M., CURCI, S., MACHEN, T. E. & SCHULZ, I. 1996. ATP regulates calcium leak from agonist-sensitive internal calcium stores. *FASEB J,* 10**,** 302-8.

HOGAN, P. G., CHEN, L., NARDONE, J. & RAO, A. 2003. Transcriptional regulation by calcium, calcineurin, and NFAT. *Genes Dev,* 17**,** 2205-32.

HOLLOWAY, S., DAVIS, M., JABER, R. & FLEMING, J. 2003. A clinically relevant model of human pancreatic adenocarcinoma identifies patterns of metastasis associated with alterations of the TGF-beta/Smad4 signaling pathway. *Int J Gastrointest Cancer,* 33**,** 61-9.

HONG, S. M., HEAPHY, C. M., SHI, C., EO, S. H., CHO, H., MEEKER, A. K., ESHLEMAN, J. R., HRUBAN, R. H. & GOGGINS, M. 2011. Telomeres are shortened in acinar-to-ductal metaplasia lesions associated with pancreatic intraepithelial neoplasia but not in isolated acinar-to-ductal metaplasias. *Mod Pathol,* 24**,** 256-66.

HORN, H. F. & VOUSDEN, K. H. 2007. Coping with stress: multiple ways to activate p53. *Oncogene,* 26**,** 1306-16.

HRUBAN, R. H., ADSAY, N. V., ALBORES-SAAVEDRA, J., COMPTON, C., GARRETT, E. S., GOODMAN, S. N., KERN, S. E., KLIMSTRA, D. S., KLOPPEL, G., LONGNECKER, D. S., LUTTGES, J. & OFFERHAUS, G. J. 2001. Pancreatic intraepithelial neoplasia: a new nomenclature and classification system for pancreatic duct lesions. *Am J Surg Pathol,* 25**,** 579-86.

HRUBAN, R. H., MAITRA, A., SCHULICK, R., LAHERU, D., HERMAN, J., KERN, S. E. & GOGGINS, M. 2008. Emerging molecular biology of pancreatic cancer. *Gastrointest Cancer Res,* 2**,** S10-5.

HRUBAN, R. H., TAKAORI, K., KLIMSTRA, D. S., ADSAY, N. V., ALBORES-SAAVEDRA, J., BIANKIN, A. V., BIANKIN, S. A., COMPTON, C., FUKUSHIMA, N., FURUKAWA, T., GOGGINS, M., KATO, Y., KLOPPEL, G., LONGNECKER, D. S., LUTTGES, J., MAITRA, A., OFFERHAUS, G. J., SHIMIZU, M. & YONEZAWA, S. 2004. An illustrated consensus on the classification of pancreatic intraepithelial neoplasia and intraductal papillary mucinous neoplasms. *Am J Surg Pathol,* 28**,** 977-87.

HUG, M., PAHL, C. & NOVAK, I. 1996. Evidence for a Na^{+}-Ca^{2+} exchanger in rat pancreatic ducts. *FEBS Lett,* 397**,** 298-302.

HUXLEY, R., ANSARY-MOGHADDAM, A., BERRINGTON DE GONZALEZ, A., BARZI, F. & WOODWARD, M. 2005. Type-II diabetes and pancreatic cancer: a meta-analysis of 36 studies. *Br J Cancer,* 92**,** 2076-83.

HWANG, T. L., LIANG, Y., CHIEN, K. Y. & YU, J. S. 2006. Overexpression and elevated serum levels of phosphoglycerate kinase 1 in pancreatic ductal adenocarcinoma. *Proteomics,* 6**,** 2259-72.

IMAGAWA, T., SMITH, J. S., CORONADO, R. & CAMPBELL, K. P. 1987. Purified ryanodine receptor from skeletal muscle sarcoplasmic reticulum is the Ca^{2+}-permeable pore of the calcium release channel. *J Biol Chem,* 262**,** 16636-43.

IMAMURA, H., NHAT, K. P., TOGAWA, H., SAITO, K., IINO, R., KATO-YAMADA, Y., NAGAI, T. & NOJI, H. 2009. Visualization of ATP levels inside single living cells with fluorescence resonance energy transfer-based genetically encoded indicators. *Proc Natl Acad Sci U S A,* 106**,** 15651-6.

INESI, G., KURZMACK, M. & VERJOVSKI-ALMEIDA, S. 1978. ATPase phosphorylation and calcium ion translocation in the transient state of sarcoplasmic reticulum activity. *Ann N Y Acad Sci,* 307**,** 224-7.

INOKI, K., LI, Y., ZHU, T., WU, J. & GUAN, K. L. 2002. TSC2 is phosphorylated and inhibited by Akt and suppresses mTOR signalling. *Nat Cell Biol,* 4**,** 648-57.

INOKI, K., ZHU, T. & GUAN, K. L. 2003. TSC2 mediates cellular energy response to control cell growth and survival. *Cell,* 115**,** 577-90.

ISHIHARA, H., WANG, H., DREWES, L. R. & WOLLHEIM, C. B. 1999. Overexpression of monocarboxylate transporter and lactate dehydrogenase alters insulin secretory responses to pyruvate and lactate in beta cells. *J Clin Invest,* 104**,** 1621-9.

ITO, D., FUJIMOTO, K., MORI, T., KAMI, K., KOIZUMI, M., TOYODA, E., KAWAGUCHI, Y. & DOI, R. 2006. In vivo antitumor effect of the mTOR inhibitor CCI-779 and gemcitabine in xenograft models of human pancreatic cancer. *Int J Cancer,* 118**,** 2337-43.

IZERADJENE, K., COMBS, C., BEST, M., GOPINATHAN, A., WAGNER, A., GRADY, W. M., DENG, C. X., HRUBAN, R. H., ADSAY, N. V., TUVESON, D. A. & HINGORANI, S. R. 2007. $Kras^{G12D}$ and Smad4/Dpc4 haploinsufficiency cooperate to induce mucinous cystic neoplasms and invasive adenocarcinoma of the pancreas. *Cancer Cell,* 11**,** 229-43.

JAMES, P., MAEDA, M., FISCHER, R., VERMA, A. K., KREBS, J., PENNISTON, J. T. & CARAFOLI, E. 1988. Identification and primary structure of a calmodulin binding domain of the Ca^{2+} pump of human erythrocytes. *J Biol Chem,* 263**,** 2905-10.

JASTER, R. 2004. Molecular regulation of pancreatic stellate cell function. *Mol Cancer,* 3**,** 26.

JEFFERY, D. A., ROUFOGALIS, B. D. & KATZ, S. 1981. The effect of calmodulin on the phosphoprotein intermediate of Mg^{2+}-dependent Ca^{2+}-stimulated adenosine triphosphatase in human erythrocyte membranes. *Biochem J,* 194**,** 481-6.

JEMAL, A., BRAY, F., CENTER, M. M., FERLAY, J., WARD, E. & FORMAN, D. 2011. Global cancer statistics. *CA Cancer J Clin,* 61**,** 69-90.

JIANG, B. H., SEMENZA, G. L., BAUER, C. & MARTI, H. H. 1996. Hypoxia-inducible factor 1 levels vary exponentially over a physiologically relevant range of O_2 tension. *Am J Physiol,* 271**,** C1172-80.

JOUAVILLE, L. S., ICHAS, F., HOLMUHAMEDOV, E. L., CAMACHO, P. & LECHLEITER, J. D. 1995. Synchronization of calcium waves by mitochondrial substrates in Xenopus laevis oocytes. *Nature,* 377**,** 438-41.

JUNG, D. W., BAYSAL, K. & BRIERLEY, G. P. 1995. The sodium-calcium antiport of heart mitochondria is not electroneutral. *J Biol Chem,* 270**,** 672-8.

KATO, M., LI, J., CHUANG, J. L. & CHUANG, D. T. 2007. Distinct structural mechanisms for inhibition of pyruvate dehydrogenase kinase isoforms by AZD7545, dichloroacetate, and radicicol. *Structure,* 15**,** 992-1004.

KENNEDY, A. L., MORTON, J. P., MANOHARAN, I., NELSON, D. M., JAMIESON, N. B., PAWLIKOWSKI, J. S., MCBRYAN, T., DOYLE, B., MCKAY, C., OIEN, K. A., ENDERS, G. H., ZHANG, R., SANSOM, O. J. & ADAMS, P. D. 2011. Activation of the PIK3CA/AKT pathway suppresses senescence induced by an activated RAS oncogene to promote tumorigenesis. *Mol Cell,* 42**,** 36-49.

KIM, J., LEE, J. H. & IYER, V. R. 2008. Global identification of Myc target genes reveals its direct role in mitochondrial biogenesis and its E-box usage *in vivo*. *PloS one,* 3**,** e1798.

KIM, J. W., TCHERNYSHYOV, I., SEMENZA, G. L. & DANG, C. V. 2006. HIF-1-mediated expression of pyruvate dehydrogenase kinase: a metabolic switch required for cellular adaptation to hypoxia. *Cell Metab,* 3**,** 177-85.

KLIMSTRA, D. S. & LONGNECKER, D. S. 1994. K-ras mutations in pancreatic ductal proliferative lesions. *Am J Pathol,* 145**,** 1547-50.

KO, Y. H., SMITH, B. L., WANG, Y., POMPER, M. G., RINI, D. A., TORBENSON, M. S., HULLIHEN, J. & PEDERSEN, P. L. 2004. Advanced cancers: eradication in all cases using 3-bromopyruvate therapy to deplete ATP. *Biochem Biophys Res Commun,* 324**,** 269-75.

KOLE, H. K., RESNICK, R. J., VAN DOREN, M. & RACKER, E. 1991. Regulation of 6-phosphofructo-1-kinase activity in ras-transformed rat-1 fibroblasts. *Arch Biochem Biophys,* 286**,** 586-90.

KONDOH, H., LLEONART, M. E., BERNARD, D. & GIL, J. 2007. Protection from oxidative stress by enhanced glycolysis; a possible mechanism of cellular immortalization. *Histol Histopathol,* 22**,** 85-90.

KONISHI, M. & WATANABE, M. 1995. Molecular size-dependent leakage of intracellular molecules from frog skeletal muscle fibers permeabilized with beta-escin. *Pflugers Arch,* 429**,** 598-600.

KOONG, A. C., MEHTA, V. K., LE, Q. T., FISHER, G. A., TERRIS, D. J., BROWN, J. M., BASTIDAS, A. J. & VIERRA, M. 2000. Pancreatic tumors show high levels of hypoxia. *Int J Radiat Oncol Biol Phys,* 48**,** 919-22.

KOPACH, O., KRUGLIKOV, I., PIVNEVA, T., VOITENKO, N. & FEDIRKO, N. 2008. Functional coupling between ryanodine receptors, mitochondria and Ca^{2+} ATPases in rat submandibular acinar cells. *Cell Calcium,* 43**,** 469-81.

KOSUGI, M., AHMAD, R., ALAM, M., UCHIDA, Y. & KUFE, D. 2011. MUC1-C oncoprotein regulates glycolysis and pyruvate kinase M2 activity in cancer cells. *PloS One,* 6**,** e28234.

KREJS, G. J. 2010. Pancreatic cancer: epidemiology and risk factors. *Dig Dis,* 28**,** 355-8.

KRISTIAN, T., PIVOVAROVA, N. B., FISKUM, G. & ANDREWS, S. B. 2007. Calcium-induced precipitate formation in brain mitochondria: composition, calcium capacity, and retention. *J Neurochem,* 102**,** 1346-56.

KROEMER, G. & POUYSSEGUR, J. 2008. Tumor cell metabolism: cancer's Achilles' heel. *Cancer Cell,* 13**,** 472-82.

KUPZIG, S., WALKER, S. A. & CULLEN, P. J. 2005. The frequencies of calcium oscillations are optimized for efficient calcium-mediated activation of Ras and the ERK/MAPK cascade. *Proc Natl Acad Sci U S A,* 102**,** 7577-82.

LANG, F. & STOURNARAS, C. 2014. Ion channels in cancer: future perspectives and clinical potential. *Philos Trans R Soc Lond B Biol Sci,* 369**,** 20130108.

LARDNER, A. 2001. The effects of extracellular pH on immune function. *J Leukoc Biol,* 69**,** 522-30.

LE, A., COOPER, C. R., GOUW, A. M., DINAVAHI, R., MAITRA, A., DECK, L. M., ROYER, R. E., VANDER JAGT, D. L., SEMENZA, G. L. & DANG, C. V. 2010. Inhibition of lactate dehydrogenase A induces oxidative stress and inhibits tumor progression. *Proc Natl Acad Sci U S A,* 107**,** 2037-42.

LE, A., RAJESHKUMAR, N. V., MAITRA, A. & DANG, C. V. 2012. Conceptual framework for cutting the pancreatic cancer fuel supply. *Clin Cancer Res,* 18**,** 4285-90.

LEE, W. J., ROBERTS-THOMSON, S. J., HOLMAN, N. A., MAY, F. J., LEHRBACH, G. M. & MONTEITH, G. R. 2002. Expression of plasma membrane calcium pump isoform mRNAs in breast cancer cell lines. *Cellular Signal,* 14**,** 1015-22.

LEE, W. J., ROBERTS-THOMSON, S. J. & MONTEITH, G. R. 2005. Plasma membrane calcium-ATPase 2 and 4 in human breast cancer cell lines. *Biochem Biophys Res Commun,* 337**,** 779-83.

LEHOTSKY, J., RAEYMAEKERS, L., MISSIAEN, L., WUYTACK, F., DE SMEDT, H. & CASTEELS, R. 1992. Stimulation of the catalytic cycle of the Ca^{2+} pump of porcine plasma-membranes by negatively charged phospholipids. *Biochim Biophys Acta,* 1105**,** 118-24.

LEVINE, A. J. & OREN, M. 2009. The first 30 years of p53: growing ever more complex. *Nat Rev Cancer,* 9**,** 749-58.

LI, D., XIE, K., WOLFF, R. & ABBRUZZESE, J. L. 2004. Pancreatic cancer. *Lancet,* 363**,** 1049-57.

LI, F., WANG, Y., ZELLER, K. I., POTTER, J. J., WONSEY, D. R., O'DONNELL, K. A., KIM, J. W., YUSTEIN, J. T., LEE, L. A. & DANG, C. V. 2005. Myc stimulates nuclearly encoded mitochondrial genes and mitochondrial biogenesis. *Mol Cell Biol,* 25**,** 6225-34.

LI, J., CUBBON, R. M., WILSON, L. A., AMER, M. S., MCKEOWN, L., HOU, B., MAJEED, Y., TUMOVA, S., SEYMOUR, V. A., TAYLOR, H., STACEY, M., O'REGAN, D., FOSTER, R., PORTER, K. E., KEARNEY, M. T. & BEECH, D. J. 2011. Orai1 and CRAC channel dependence of VEGF-activated Ca^{2+} entry and endothelial tube formation. *Circ Res,* 108**,** 1190-8.

LI, X., FANG, P., MAI, J., CHOI, E. T., WANG, H. & YANG, X. F. 2013. Targeting mitochondrial reactive oxygen species as novel therapy for inflammatory diseases and cancers. *J Hematol Oncol,* 6**,** 19.

LINCK, B., QIU, Z., HE, Z., TONG, Q., HILGEMANN, D. W. & PHILIPSON, K. D. 1998. Functional comparison of the three isoforms of the Na^{+}/Ca^{2+} exchanger (NCX1, NCX2, NCX3). *Am J Physiol,* 274**,** C415-23.

LIOU, J., KIM, M. L., HEO, W. D., JONES, J. T., MYERS, J. W., FERRELL, J. E., JR. & MEYER, T. 2005. STIM is a Ca^{2+} sensor essential for Ca^{2+}-store-depletion-triggered Ca2+ influx. *Curr Biol,* 15**,** 1235-41.

LIU, H., HU, Y. P., SAVARAJ, N., PRIEBE, W. & LAMPIDIS, T. J. 2001. Hypersensitization of tumor cells to glycolytic inhibitors. *Biochemistry,* 40**,** 5542-7.

LIU, H., SAVARAJ, N., PRIEBE, W. & LAMPIDIS, T. J. 2002. Hypoxia increases tumor cell sensitivity to glycolytic inhibitors: a strategy for solid tumor therapy (Model C). *Biochem Pharmacol,* 64**,** 1745-51.

LOEWITH, R. 2011. A brief history of TOR. *Biochem Soc Trans,* 39**,** 437-42.

LOOS, M., KLEEFF, J., FRIESS, H. & BUCHLER, M. W. 2008. Surgical treatment of pancreatic cancer. *Ann N Y Acad Sci,* 1138**,** 169-80.

LOW, P. S., ALLEN, D. P., ZIONCHECK, T. F., CHARI, P., WILLARDSON, B. M., GEAHLEN, R. L. & HARRISON, M. L. 1987. Tyrosine phosphorylation of band 3 inhibits peripheral protein binding. *J Biol Chem,* 262**,** 4592-6.

LUM, J. J., BUI, T., GRUBER, M., GORDAN, J. D., DEBERARDINIS, R. J., COVELLO, K. L., SIMON, M. C. & THOMPSON, C. B. 2007. The transcription factor HIF-1alpha plays a critical role in the growth factor-dependent regulation of both aerobic and anaerobic glycolysis. *Genes Dev,* 21**,** 1037-49.

LUO, W., HU, H., CHANG, R., ZHONG, J., KNABEL, M., O'MEALLY, R., COLE, R. N., PANDEY, A. & SEMENZA, G. L. 2011. Pyruvate kinase M2 is a PHD3-stimulated coactivator for hypoxia-inducible factor 1. *Cell,* 145**,** 732-44.

MA, W., SUNG, H. J., PARK, J. Y., MATOBA, S. & HWANG, P. M. 2007. A pivotal role for p53: balancing aerobic respiration and glycolysis. *J Bioenerg Biomembr,* 39**,** 243-6.

MACLENNAN, D. H. 1970. Purification and properties of an adenosine triphosphatase from sarcoplasmic reticulum. *J Biol Chem,* 245**,** 4508-18.

MACLENNAN, D. H. & KRANIAS, E. G. 2003. Phospholamban: a crucial regulator of cardiac contractility. *Nat Rev Mol Cell Biol,* 4**,** 566-77.

MAHER, J. C., KRISHAN, A. & LAMPIDIS, T. J. 2004. Greater cell cycle inhibition and cytotoxicity induced by 2-deoxy-D-glucose in tumor cells treated under hypoxic vs aerobic conditions. *Cancer Chemother Pharmacol,* 53**,** 116-22.

MAITRA, A., ADSAY, N. V., ARGANI, P., IACOBUZIO-DONAHUE, C., DE MARZO, A., CAMERON, J. L., YEO, C. J. & HRUBAN, R. H. 2003. Multicomponent analysis of the pancreatic adenocarcinoma progression model using a pancreatic intraepithelial neoplasia tissue microarray. *Mod Pathol,* 16**,** 902-12.

MALUMBRES, M. & BARBACID, M. 2003. RAS oncogenes: the first 30 years. *Nat Rev Cancer,* 3**,** 459-65.

MARCHI, S. & PINTON, P. 2014. The mitochondrial calcium uniporter complex: molecular components, structure and physiopathological implications. *J Physiol,* 592**,** 829-39.

MARIN-HERNANDEZ, A., GALLARDO-PEREZ, J. C., RODRIGUEZ-ENRIQUEZ, S., ENCALADA, R., MORENO-SANCHEZ, R. & SAAVEDRA, E. 2011. Modeling cancer glycolysis. *Biochim Biophys Acta,* 1807**,** 755-67.

MASCHEK, G., SAVARAJ, N., PRIEBE, W., BRAUNSCHWEIGER, P., HAMILTON, K., TIDMARSH, G. F., DE YOUNG, L. R. & LAMPIDIS, T. J. 2004. 2-deoxy-D-glucose increases the efficacy of adriamycin and paclitaxel in human osteosarcoma and non-small cell lung cancers *in vivo*. *Cancer Res,* 64**,** 31-4.

MASSAGUE, J. 2008. TGFbeta in Cancer. *Cell,* 134**,** 215-30.

MATHUPALA, S. P., KO, Y. H. & PEDERSEN, P. L. 2006. Hexokinase II: cancer's double-edged sword acting as both facilitator and gatekeeper of malignancy when bound to mitochondria. *Oncogene,* 25**,** 4777-86.

MATHUPALA, S. P., REMPEL, A. & PEDERSEN, P. L. 2001. Glucose catabolism in cancer cells: identification and characterization of a marked activation response of the type II hexokinase gene to hypoxic conditions. *J Biol Chem,* 276**,** 43407-12.

MATOBA, S., KANG, J. G., PATINO, W. D., WRAGG, A., BOEHM, M., GAVRILOVA, O., HURLEY, P. J., BUNZ, F. & HWANG, P. M. 2006. p53 regulates mitochondrial respiration. *Science,* 312**,** 1650-3.

MAYO, L. D. & DONNER, D. B. 2002. The PTEN, Mdm2, p53 tumor suppressor-oncoprotein network. *Trends Biochem Sci,* 27**,** 462-7.

MAZUREK, S., BOSCHEK, C. B., HUGO, F. & EIGENBRODT, E. 2005. Pyruvate kinase type M2 and its role in tumor growth and spreading. *Semin Cancer Biol,* 15**,** 300-8.

MCBRIDE, H. M., NEUSPIEL, M. & WASIAK, S. 2006. Mitochondria: more than just a powerhouse. *Curr Biol,* 16**,** R551-60.

MCCORMACK, J. G. & DENTON, R. M. 1979. The effects of calcium ions and adenine nucleotides on the activity of pig heart 2-oxoglutarate dehydrogenase complex. *Biochem J,* 180**,** 533-44.

MCCORMACK, J. G., HALESTRAP, A. P. & DENTON, R. M. 1990. Role of calcium ions in regulation of mammalian intramitochondrial metabolism. *Physiol Rev,* 70**,** 391-425.

MICHELAKIS, E. D., WEBSTER, L. & MACKEY, J. R. 2008. Dichloroacetate (DCA) as a potential metabolic-targeting therapy for cancer. *Br J Cancer,* 99**,** 989-94.

MICHELANGELI, F., OGUNBAYO, O. A. & WOOTTON, L. L. 2005. A plethora of interacting organellar Ca^{2+} stores. *Curr Opin Cell Biol,* 17**,** 135-40.

MIKOSHIBA, K. 2007. The IP_3 receptor/Ca^{2+} channel and its cellular function. *Biochem Soc Symp***,** 9-22.

MIKURIYA, K., KURAMITSU, Y., RYOZAWA, S., FUJIMOTO, M., MORI, S., OKA, M., HAMANO, K., OKITA, K., SAKAIDA, I. & NAKAMURA, K. 2007. Expression of glycolytic enzymes is increased in pancreatic cancerous tissues as evidenced by proteomic profiling by two-dimensional electrophoresis and liquid chromatography-mass spectrometry/mass spectrometry. *Int J Oncol,* 30**,** 849-55.

MILANICK, M. A. 1990. Proton fluxes associated with the Ca pump in human red blood cells. *Am J Physiol,* 258**,** C552-62.

MOLE, D. R., BLANCHER, C., COPLEY, R. R., POLLARD, P. J., GLEADLE, J. M., RAGOUSSIS, J. & RATCLIFFE, P. J. 2009. Genome-wide association of hypoxia-inducible factor (HIF)-1alpha and HIF-2alpha DNA binding with expression profiling of hypoxia-inducible transcripts. *J Biol Chem,* 284**,** 16767-75.

MOLLENHAUER, J., ROETHER, I. & KERN, H. F. 1987. Distribution of extracellular matrix proteins in pancreatic ductal adenocarcinoma and its influence on tumor cell proliferation in vitro. *Pancreas,* 2**,** 14-24.

MONTEITH, G. R., DAVIS, F. M. & ROBERTS-THOMSON, S. J. 2012. Calcium channels and pumps in cancer: changes and consequences. *J Biol Chem,* 287**,** 31666-73.

MONTEITH, G. R., MCANDREW, D., FADDY, H. M. & ROBERTS-THOMSON, S. J. 2007. Calcium and cancer: targeting Ca^{2+} transport. *Nat Rev Cancer,* 7**,** 519-30.

MONTEITH, G. R., WANIGASEKARA, Y. & ROUFOGALIS, B. D. 1998. The plasma membrane calcium pump, its role and regulation: new complexities and possibilities. *J Pharmacol Toxicol Methods,* 40**,** 183-90.

MOORE, P. S., SIPOS, B., ORLANDINI, S., SORIO, C., REAL, F. X., LEMOINE, N. R., GRESS, T., BASSI, C., KLOPPEL, G., KALTHOFF, H., UNGEFROREN, H., LOHR, M. & SCARPA, A. 2001. Genetic profile of 22 pancreatic carcinoma cell lines. Analysis of K-ras, p53, p16 and DPC4/Smad4. *Virchows Archiv,* 439**,** 798-802.

MORRIS, J. P. T., WANG, S. C. & HEBROK, M. 2010. KRAS, Hedgehog, Wnt and the twisted developmental biology of pancreatic ductal adenocarcinoma. *Nat Rev Cancer,* 10**,** 683-95.

MORRISH, F., ISERN, N., SADILEK, M., JEFFREY, M. & HOCKENBERY, D. M. 2009. c-Myc activates multiple metabolic networks to generate substrates for cell-cycle entry. *Oncogene,* 28**,** 2485-91.

MORRISH, F., NERETTI, N., SEDIVY, J. M. & HOCKENBERY, D. M. 2008. The oncogene c-Myc coordinates regulation of metabolic networks to enable rapid cell cycle entry. *Cell Cycle,* 7**,** 1054-66.

MUALLEM, S., BEEKER, T. & PANDOL, S. J. 1988. Role of Na^{+}/Ca^{2+} exchange and the plasma membrane Ca^{2+} pump in hormone-mediated Ca^{2+} efflux from pancreatic acini. *J Membr Biol,* 102**,** 153-62.

MUALLEM, S. & KARLISH, S. J. 1981. Studies on the mechanism of regulation of the red-cell Ca^{2+} pump by calmodulin and ATP. *Biochim Biophys Acta,* 647**,** 73-86.

MUTO, A., OHKURA, M., KOTANI, T., HIGASHIJIMA, S., NAKAI, J. & KAWAKAMI, K. 2011. Genetic visualization with an improved GCaMP calcium indicator reveals spatiotemporal activation of the spinal motor neurons in zebrafish. *Proc Natl Acad Sci U S A,* 108**,** 5425-30.

NAKANO, M., IMAMURA, H., NAGAI, T. & NOJI, H. 2011. Ca^{2+} regulation of mitochondrial ATP synthesis visualized at the single cell level. *ACS Chem Biol,* 6**,** 709-15.

NEYSES, L., REINLIB, L. & CARAFOLI, E. 1985. Phosphorylation of the Ca^{2+}-pumping ATPase of heart sarcolemma and erythrocyte plasma membrane by the cAMP-dependent protein kinase. *J Biol Chem,* 260**,** 10283-7.

NIGGLI, V., ADUNYAH, E. S. & CARAFOLI, E. 1981a. Acidic phospholipids, unsaturated fatty acids, and limited proteolysis mimic the effect of calmodulin on the purified erythrocyte Ca^{2+}-ATPase. *J Biol Chem,* 256**,** 8588-92.

NIGGLI, V., ADUNYAH, E. S., PENNISTON, J. T. & CARAFOLI, E. 1981b. Purified (Ca^{2+}-Mg^{2+})-ATPase of the erythrocyte membrane. Reconstitution and effect of calmodulin and phospholipids. *J Biol Chem,* 256**,** 395-401.

NIGGLI, V., SIGEL, E. & CARAFOLI, E. 1982. The purified Ca^{2+} pump of human erythrocyte membranes catalyzes an electroneutral Ca^{2+}-H^{+} exchange in reconstituted liposomal systems. *J Biol Chem,* 257**,** 2350-6.

OCEANDY, D., CARTWRIGHT, E. J., EMERSON, M., PREHAR, S., BAUDOIN, F. M., ZI, M., ALATWI, N., VENETUCCI, L., SCHUH, K., WILLIAMS, J. C., ARMESILLA, A. L. & NEYSES, L. 2007. Neuronal nitric oxide synthase signaling in the heart is regulated by the sarcolemmal calcium pump 4b. *Circulation,* 115**,** 483-92.

OKOROKOV, A. L. & MILNER, J. 1999. An ATP/ADP-dependent molecular switch regulates the stability of p53-DNA complexes. *Mol Cell Biol,* 19**,** 7501-10.

ONG, H. L., LIU, X., SHARMA, A., HEGDE, R. S. & AMBUDKAR, I. S. 2007. Intracellular Ca^{2+} release via the ER translocon activates store-operated calcium entry. *Pflugers Archiv,* 453**,** 797-808.

ORLOVA, K. A. & CRINO, P. B. 2010. The tuberous sclerosis complex. *Ann N Y Acad Sci,* 1184**,** 87-105.

ORRENIUS, S., ZHIVOTOVSKY, B. & NICOTERA, P. 2003. Regulation of cell death: the calcium-apoptosis link. *Nat Rev Mol Cell Biol,* 4**,** 552-65.

OSTHUS, R. C., SHIM, H., KIM, S., LI, Q., REDDY, R., MUKHERJEE, M., XU, Y., WONSEY, D., LEE, L. A. & DANG, C. V. 2000. Deregulation of glucose transporter 1 and glycolytic gene expression by c-Myc. *J Biol Chem,* 275**,** 21797-800.

PAREKH, A. B. 2003. Mitochondrial regulation of intracellular Ca^{2+} signaling: more than just simple Ca^{2+} buffers. *News Physiol Sci,* 18**,** 252-6.

PATEL, S., RAMAKRISHNAN, L., RAHMAN, T., HAMDOUN, A., MARCHANT, J. S., TAYLOR, C. W., & BRAILOIU, E. (2011). The endo-lysosomal system as an NAADP-sensitive acidic Ca^{2+} store: role for the two-pore channels. *Cell Calcium*, 50, 157-167.

PATERGNANI, S., SUSKI, J. M., AGNOLETTO, C., BONONI, A., BONORA, M., DE MARCHI, E., GIORGI, C., MARCHI, S., MISSIROLI, S., POLETTI, F., RIMESSI, A., DUSZYNSKI, J., WIECKOWSKI, M. R. & PINTON, P. 2011. Calcium signaling around Mitochondria Associated Membranes (MAMs). *Cell Commun Signal,* 9**,** 19.

PATRON, M., CHECCHETTO, V., RAFFAELLO, A., TEARDO, E., VECELLIO REANE, D., MANTOAN, M., GRANATIERO, V., SZABO, I., DE STEFANI, D. & RIZZUTO, R. 2014. MICU1 and MICU2 finely tune the mitochondrial Ca^{2+} uniporter by exerting opposite effects on MCU activity. *Mol Cell,* 53**,** 726-37.

PAUL, R. J., HARDIN, C. D., RAEYMAEKERS, L., WUYTACK, F. & CASTEELS, R. 1989. Preferential support of Ca^{2+} uptake in smooth muscle plasma membrane vesicles by an endogenous glycolytic cascade. *FASEB J,* 3**,** 2298-301.

PEDERSEN, P. L. 2007. Warburg, me and Hexokinase 2: Multiple discoveries of key molecular events underlying one of cancers' most common phenotypes, the "Warburg Effect", i.e., elevated glycolysis in the presence of oxygen. *J Bioenerg Biomembr,* 39**,** 211-22.

PELENGARIS, S., KHAN, M. & EVAN, G. 2002. c-MYC: more than just a matter of life and death. *Nat Rev Cancer,* 2**,** 764-76.

PELICANO, H., MARTIN, D. S., XU, R. H. & HUANG, P. 2006. Glycolysis inhibition for anticancer treatment. *Oncogene,* 25**,** 4633-46.

PENNISTON, J. T. & ENYEDI, A. 1998. Modulation of the plasma membrane Ca^{2+} pump. *J Membr Biol,* 165**,** 101-9.

PEROCCHI, F., GOHIL, V. M., GIRGIS, H. S., BAO, X. R., MCCOMBS, J. E., PALMER, A. E. & MOOTHA, V. K. 2010. MICU1 encodes a mitochondrial EF hand protein required for Ca^{2+} uptake. *Nature,* 467**,** 291-6.

PETERSEN, G. M. & HRUBAN, R. H. 2003. Familial pancreatic cancer: where are we in 2003? *J Natl Cancer Ins,* 95**,** 180-1.

PFEIFFER, T., SCHUSTER, S. & BONHOEFFER, S. 2001. Cooperation and competition in the evolution of ATP-producing pathways. *Science,* 292**,** 504-7.

PINTON, P., GIORGI, C., SIVIERO, R., ZECCHINI, E. & RIZZUTO, R. 2008. Calcium and apoptosis: ER-mitochondria Ca^{2+} transfer in the control of apoptosis. *Oncogene,* 27**,** 6407-18.

PLAS, D. R. & THOMPSON, C. B. 2005. Akt-dependent transformation: there is more to growth than just surviving. *Oncogene,* 24**,** 7435-42.

POUYSSEGUR, J., DAYAN, F. & MAZURE, N. M. 2006. Hypoxia signalling in cancer and approaches to enforce tumour regression. *Nature,* 441**,** 437-43.

PRAKRIYA, M., FESKE, S., GWACK, Y., SRIKANTH, S., RAO, A. & HOGAN, P. G. 2006. Orai1 is an essential pore subunit of the CRAC channel. *Nature,* 443**,** 230-3.

PREVARSKAYA, N., SKRYMA, R. & SHUBA, Y. 2011. Calcium in tumour metastasis: new roles for known actors. *Nat Rev Cancer,* 11**,** 609-18.

PUCHULU-CAMPANELLA, E., CHU, H., ANSTEE, D. J., GALAN, J. A., TAO, W. A. & LOW, P. S. 2013. Identification of the components of a glycolytic enzyme metabolon on the human red blood cell membrane. *J Biol Chem,* 288**,** 848-58.

PUTNEY, J. W., JR. 1986. A model for receptor-regulated calcium entry. *Cell Calcium,* 7**,** 1-12.

RACKER, E., RESNICK, R. J. & FELDMAN, R. 1985. Glycolysis and methylaminoisobutyrate uptake in rat-1 cells transfected with ras or myc oncogenes. *Proc Natl Acad Sci U S A,* 82**,** 3535-8.

REDSTON, M. S., CALDAS, C., SEYMOUR, A. B., HRUBAN, R. H., DA COSTA, L., YEO, C. J. & KERN, S. E. 1994. p53 mutations in pancreatic carcinoma and evidence of common involvement of homocopolymer tracts in DNA microdeletions. *Cancer Res,* 54**,** 3025-33.

RIBICZEY, P., TORDAI, A., ANDRIKOVICS, H., FILOTEO, A. G., PENNISTON, J. T., ENOUF, J., ENYEDI, A., PAPP, B. & KOVACS, T. 2007. Isoform-specific up-regulation of plasma membrane Ca^{2+}ATPase expression during colon and gastric cancer cell differentiation. *Cell Calcium,* 42**,** 590-605.

RICHARDS, D. E., REGA, A. F. & GARRAHAN, P. J. 1978. Two classes of site for ATP in the Ca^{2+}-ATPase from human red cell membranes. *Biochim Biophys Acta,* 511**,** 194-201.

RIZZUTO, R., MARCHI, S., BONORA, M., AGUIARI, P., BONONI, A., DE STEFANI, D., GIORGI, C., LEO, S., RIMESSI, A., SIVIERO, R., ZECCHINI, E. & PINTON, P. 2009. Ca^{2+} transfer from the ER to mitochondria: when, how and why. *Biochim Biophys Acta,* 1787**,** 1342-51.

ROBERTS-THOMSON, S. J., CURRY, M. C. & MONTEITH, G. R. 2010. Plasma membrane calcium pumps and their emerging roles in cancer. *World J Biol Chem,* 1**,** 248-53.

ROBEY, R. B. & HAY, N. 2009. Is Akt the "Warburg kinase"?-Akt-energy metabolism interactions and oncogenesis. *Semin Cancer Biol,* 19**,** 25-31.

RODERICK, H. L. & COOK, S. J. 2008. Ca^{2+} signalling checkpoints in cancer: remodelling Ca^{2+} for cancer cell proliferation and survival. *Nat Rev Cancer,* 8**,** 361-75.

RODRIGUEZ-ENRIQUEZ, S., GALLARDO-PEREZ, J. C., AVILES-SALAS, A., MARIN-HERNANDEZ, A., CARRENO-FUENTES, L., MALDONADO-LAGUNAS, V. & MORENO-SANCHEZ, R. 2008. Energy metabolism transition in multi-cellular human tumor spheroids. *J Cell Physiol,* 216**,** 189-97.

RONG, Y., WU, W., NI, X., KUANG, T., JIN, D., WANG, D. & LOU, W. 2013. Lactate dehydrogenase A is overexpressed in pancreatic cancer and promotes the growth of pancreatic cancer cells. *Tumour Biol,* 34**,** 1523-30.

ROOS, J., DIGREGORIO, P. J., YEROMIN, A. V., OHLSEN, K., LIOUDYNO, M., ZHANG, S., SAFRINA, O., KOZAK, J. A., WAGNER, S. L., CAHALAN, M. D., VELICELEBI, G. & STAUDERMAN, K. A. 2005. STIM1, an essential and conserved component of store-operated Ca^{2+} channel function. *J Cell Biol,* 169**,** 435-45.

ROSEN, L. B., GINTY, D. D., WEBER, M. J. & GREENBERG, M. E. 1994. Membrane depolarization and calcium influx stimulate MEK and MAP kinase via activation of Ras. *Neuron,* 12**,** 1207-21.

ROSSI, J. P. & REGA, A. F. 1989. A study to see whether phosphatidylserine, partial proteolysis and EGTA substitute for calmodulin during activation of the Ca^{2+}-ATPase from red cell membranes by ATP. *Biochim Biophys Acta,* 996**,** 153-9.

RUGGERI, B. A., HUANG, L., WOOD, M., CHENG, J. Q. & TESTA, J. R. 1998. Amplification and overexpression of the AKT2 oncogene in a subset of human pancreatic ductal adenocarcinomas. *Mol Carcinog,* 21**,** 81-6.

RUTTER, G. A., PRALONG, W. F. & WOLLHEIM, C. B. 1992. Regulation of mitochondrial glycerol-phosphate dehydrogenase by Ca^{2+} within electropermeabilized insulin-secreting cells (INS-1). *Biochim Biophys Acta,* 1175**,** 107-13.

SAITO, K., UZAWA, K., ENDO, Y., KATO, Y., NAKASHIMA, D., OGAWARA, K., SHIBA, M., BUKAWA, H., YOKOE, H. & TANZAWA, H. 2006. Plasma membrane Ca^{2+} ATPase isoform 1 down-regulated in human oral cancer. *Oncol Rep,* 15**,** 49-55.

SALVADOR, J. M., INESI, G., RIGAUD, J. L. & MATA, A. M. 1998. Ca2+ transport by reconstituted synaptosomal ATPase is associated with H^+ countertransport and net charge displacement. *J Biol Chem,* 273**,** 18230-4.

SARBASSOV, D. D., ALI, S. M. & SABATINI, D. M. 2005a. Growing roles for the mTOR pathway. *Curr Opin Cell Biol,* 17**,** 596-603.

SARBASSOV, D. D., GUERTIN, D. A., ALI, S. M. & SABATINI, D. M. 2005b. Phosphorylation and regulation of Akt/PKB by the rictor-mTOR complex. *Science,* 307**,** 1098-101.

SCHATZMANN, H. J. 1966. ATP-dependent Ca++-extrusion from human red cells. *Experientia,* 22**,** 364-5.

SCHEFFZEK, K., AHMADIAN, M. R., KABSCH, W., WIESMULLER, L., LAUTWEIN, A., SCHMITZ, F. & WITTINGHOFER, A. 1997. The Ras-RasGAP complex: structural basis for GTPase activation and its loss in oncogenic Ras mutants. *Science,* 277**,** 333-8.

SCHEK, N., HALL, B. L. & FINN, O. J. 1988. Increased glyceraldehyde-3-phosphate dehydrogenase gene expression in human pancreatic adenocarcinoma. *Cancer Res,* 48**,** 6354-9.

SCHILD, C., WIRTH, M., REICHERT, M., SCHMID, R. M., SAUR, D. & SCHNEIDER, G. 2009. PI3K signaling maintains c-myc expression to regulate transcription of E2F1 in pancreatic cancer cells. *Mol Carcinog,* 48**,** 1149-58.

SCHMIDT, M. M. & DRINGEN, R. 2009. Differential effects of iodoacetamide and iodoacetate on glycolysis and glutathione metabolism of cultured astrocytes. *Front Neuroenergetics,* 1**,** 1.

SCHUH, K., ULDRIJAN, S., TELKAMP, M., ROTHLEIN, N. & NEYSES, L. 2001. The plasmamembrane calmodulin-dependent calcium pump: a major regulator of nitric oxide synthase I. *J Cell Biol,* 155**,** 201-5.

SCHUTTE, M., HRUBAN, R. H., GERADTS, J., MAYNARD, R., HILGERS, W., RABINDRAN, S. K., MOSKALUK, C. A., HAHN, S. A., SCHWARTE-WALDHOFF, I., SCHMIEGEL, W., BAYLIN, S. B., KERN, S. E. & HERMAN, J. G. 1997. Abrogation of the Rb/p16 tumor-suppressive pathway in virtually all pancreatic carcinomas. *Cancer Res,* 57**,** 3126-30.

SEAGROVES, T. N., RYAN, H. E., LU, H., WOUTERS, B. G., KNAPP, M., THIBAULT, P., LADEROUTE, K. & JOHNSON, R. S. 2001. Transcription factor HIF-1 is a necessary mediator of the pasteur effect in mammalian cells. *Mol Cell Biol,* 21**,** 3436-44.

SEIDLER, N. W. 2013. Compartmentation of GAPDH. *Adv Exp Med Biol,* 985**,** 61-101.

SEIDLER, N. W., JONA, I., VEGH, M. & MARTONOSI, A. 1989. Cyclopiazonic acid is a specific inhibitor of the Ca^{2+}-ATPase of sarcoplasmic reticulum. *J Biol Chem,* 264**,** 17816-23.

SELIGER, H. H. & MCELROY, W. D. 1964. The Colors of Firefly Bioluminescence: Enzyme Configuration and Species Specificity. *Proc Natl Acad Sci U S A,* 52**,** 75-81.

SEMENZA, G. L. 2003. Targeting HIF-1 for cancer therapy. *Nat Rev Cancer,* 3**,** 721-32.

SEMENZA, G. L. 2008. Tumor metabolism: cancer cells give and take lactate. *J Clin Invest,* 118**,** 3835-7.

SEMENZA, G. L. 2010. Defining the role of hypoxia-inducible factor 1 in cancer biology and therapeutics. *Oncogene,* 29**,** 625-34.

SEMENZA, G. L. 2013. HIF-1 mediates metabolic responses to intratumoral hypoxia and oncogenic mutations. *J Clin Invest,* 123**,** 3664-71.

SEMENZA, G. L., JIANG, B. H., LEUNG, S. W., PASSANTINO, R., CONCORDET, J. P., MAIRE, P. & GIALLONGO, A. 1996. Hypoxia response elements in the aldolase A, enolase 1, and lactate dehydrogenase A gene promoters contain essential binding sites for hypoxia-inducible factor 1. *J Biol Chem,* 271**,** 32529-37.

SEMENZA, G. L., ROTH, P. H., FANG, H. M. & WANG, G. L. 1994. Transcriptional regulation of genes encoding glycolytic enzymes by hypoxia-inducible factor 1. *J Biol Chem,* 269**,** 23757-63.

SEMENZA, G. L., SHIMODA, L. A. & PRABHAKAR, N. R. 2006. Regulation of gene expression by HIF-1. *Novartis Found Symp,* 272**,** 2-8; discussion 8-14, 33-6.

SHACKELFORD, D. B. & SHAW, R. J. 2009. The LKB1-AMPK pathway: metabolism and growth control in tumour suppression. *Nat Rev Cancer,* 9**,** 563-75.

SHAH, S. A., POTTER, M. W., RICCIARDI, R., PERUGINI, R. A. & CALLERY, M. P. 2001. FRAP-p70s6K signaling is required for pancreatic cancer cell proliferation. *J Surg Res,* 97**,** 123-30.

SHERR, C. J. 2001. The INK4a/ARF network in tumour suppression. *Nat Rev Mol Cell Biol,* 2**,** 731-7.

SHI, Y. & MASSAGUE, J. 2003. Mechanisms of TGF-beta signaling from cell membrane to the nucleus. *Cell,* 113**,** 685-700.

SHIM, H., DOLDE, C., LEWIS, B. C., WU, C. S., DANG, G., JUNGMANN, R. A., DALLA-FAVERA, R. & DANG, C. V. 1997. c-Myc transactivation of LDH-A: implications for tumor metabolism and growth. *Proc Natl Acad Sci U S A,* 94**,** 6658-63.

SHIMOBAYASHI, M. & HALL, M. N. 2014. Making new contacts: the mTOR network in metabolism and signalling crosstalk. *Nat Rev Mol Cell Biol,* 15**,** 155-62.

SIMMERMAN, H. K. & JONES, L. R. 1998. Phospholamban: protein structure, mechanism of action, and role in cardiac function. *Physiol Rev,* 78**,** 921-47.

SMALLBONE, K., MESSIHA, H. L., CARROLL, K. M., WINDER, C. L., MALYS, N., DUNN, W. B., MURABITO, E., SWAINSTON, N., DADA, J. O., KHAN, F., PIR, P., SIMEONIDIS, E., SPASIC, I., WISHART, J., WEICHART, D., HAYES, N. W., JAMESON, D., BROOMHEAD, D. S., OLIVER, S. G., GASKELL, S. J., MCCARTHY, J. E., PATON, N. W., WESTERHOFF, H. V., KELL, D. B. & MENDES, P. 2013. A model of yeast glycolysis based on a consistent kinetic characterisation of all its enzymes. *FEBS Lett,* 587**,** 2832-41.

SMALLWOOD, J. I., GUGI, B. & RASMUSSEN, H. 1988. Regulation of erythrocyte Ca^{2+} pump activity by protein kinase C. *J Biol Chem,* 263**,** 2195-202.

SMETS, I., CAPLANUSI, A., DESPA, S., MOLNAR, Z., RADU, M., VANDEVEN, M., AMELOOT, M. & STEELS, P. 2004. Ca^{2+} uptake in mitochondria occurs via the reverse action of the Na^{+}/Ca^{2+} exchanger in metabolically inhibited MDCK cells. *Am J Physiol Renal Physiol,* 286**,** F784-94.

SMITH, J. S., IMAGAWA, T., MA, J., FILL, M., CAMPBELL, K. P. & CORONADO, R. 1988. Purified ryanodine receptor from rabbit skeletal muscle is the calcium-release channel of sarcoplasmic reticulum. *J Gen Physio,* 92**,** 1-26.

SON, J., LYSSIOTIS, C. A., YING, H., WANG, X., HUA, S., LIGORIO, M., PERERA, R. M., FERRONE, C. R., MULLARKY, E., SHYH-CHANG, N., KANG, Y., FLEMING, J. B., BARDEESY, N., ASARA, J. M., HAIGIS, M. C., DEPINHO, R. A., CANTLEY, L. C. & KIMMELMAN, A. C. 2013. Glutamine supports pancreatic cancer growth through a KRAS-regulated metabolic pathway. *Nature,* 496**,** 101-5.

SONVEAUX, P., VEGRAN, F., SCHROEDER, T., WERGIN, M. C., VERRAX, J., RABBANI, Z. N., DE SAEDELEER, C. J., KENNEDY, K. M., DIEPART, C., JORDAN, B. F., KELLEY, M. J., GALLEZ, B., WAHL, M. L., FERON, O. & DEWHIRST, M. W. 2008. Targeting lactate-fueled respiration selectively kills hypoxic tumor cells in mice. *J Clin Invest,* 118**,** 3930-42.

SPIVAK-KROIZMAN, T. R., HOSTETTER, G., POSNER, R., AZIZ, M., HU, C., DEMEURE, M. J., VON HOFF, D., HINGORANI, S. R., PALCULICT, T. B., IZZO, J., KIRIAKOVA, G. M., ABDELMELEK, M., BARTHOLOMEUSZ, G., JAMES, B. P. & POWIS, G. 2013. Hypoxia triggers hedgehog-mediated tumor-stromal interactions in pancreatic cancer. *Cancer Res,* 73**,** 3235-47.

STAUFFER, T. P., GUERINI, D. & CARAFOLI, E. 1995. Tissue distribution of the four gene products of the plasma membrane Ca^{2+} pump. A study using specific antibodies. *J Biol Chem,* 270**,** 12184-90.

STEVENS, E. A. & RODRIGUEZ, C. P. 2014. Genomic medicine and targeted therapy for solid tumors. *J Surg Oncol*, 111(1), 38–42

STEWART, T. A., YAPA, K. T. & MONTEITH, G. R. 2014. Altered calcium signaling in cancer cells. *Biochim Biophys Acta*, in press.

STIEHL, D. P., WIRTHNER, R., KODITZ, J., SPIELMANN, P., CAMENISCH, G. & WENGER, R. H. 2006. Increased prolyl 4-hydroxylase domain proteins compensate for decreased oxygen levels. Evidence for an autoregulatory oxygen-sensing system. *J Biol Chem,* 281**,** 23482-91.

STOCK, C. & SCHWAB, A. 2009. Protons make tumor cells move like clockwork. *Pflugers Archiv,* 458**,** 981-92.

STOLL, V., CALLEJA, V., VASSAUX, G., DOWNWARD, J. & LEMOINE, N. R. 2005. Dominant negative inhibitors of signalling through the phosphoinositol 3-kinase pathway for gene therapy of pancreatic cancer. *Gut,* 54**,** 109-16.

STREHLER, E. E. & ZACHARIAS, D. A. 2001a. Role of alternative splicing in generating isoform diversity among plasma membrane calcium pumps. *Physiol Rev,* 81**,** 21-50.

STREHLER, E. E. & ZACHARIAS, D. A. 2001b. Role of alternative splicing in generating isoform diversity among plasma membrane calcium pumps. *Physiol Rev,* 81**,** 21-50.

SUMOZA-TOLEDO, A. & PENNER, R. 2011. TRPM2: a multifunctional ion channel for calcium signalling. *J Physiol,* 589**,** 1515-25.

SZASZ, I., SARKADI, B., SCHUBERT, A. & GARDOS, G. 1978. Effects of lanthanum on calcium-dependent phenomena in human red cells. *Biochim Biophys Acta,* 512**,** 331-40.

SZLUFCIK, K., MISSIAEN, L., PARYS, J. B., CALLEWAERT, G. & DE SMEDT, H. 2006. Uncoupled IP_3 receptor can function as a Ca^{2+}-leak channel: cell biological and pathological consequences. *Biol Cell,* 98**,** 1-14.

TARASOV, A. I., GIRARD, C. A. & ASHCROFT, F. M. 2006. ATP sensitivity of the ATP-sensitive K^+ channel in intact and permeabilized pancreatic beta-cells. *Diabetes,* 55**,** 2446-54.

TENNANT, D. A., DURAN, R. V. & GOTTLIEB, E. 2010. Targeting metabolic transformation for cancer therapy. *Nat Rev Cancer,* 10**,** 267-77.

THASTRUP, O., CULLEN, P. J., DROBAK, B. K., HANLEY, M. R. & DAWSON, A. P. 1990. Thapsigargin, a tumor promoter, discharges intracellular Ca^{2+} stores by specific inhibition of the endoplasmic reticulum Ca^{2+}-ATPase. *Proc Natl Acad Sci U S A* 87**,** 2466-70.

THOMAS, R. C. 2009. The plasma membrane calcium ATPase (PMCA) of neurones is electroneutral and exchanges 2 H^+ for each Ca^{2+} or Ba^{2+} ion extruded. *J Physiol,* 587**,** 315-27.

THUL, R., BELLAMY, T. C., RODERICK, H. L., BOOTMAN, M. D. & COOMBES, S. 2008. Calcium oscillations. *Adv Exp Med Biol,* 641**,** 1-27.

TONG, X., ZHAO, F. & THOMPSON, C. B. 2009. The molecular determinants of de novo nucleotide biosynthesis in cancer cells. *Curr Opin Genet Dev,* 19**,** 32-7.

TSUTSUMI, S., YANAGAWA, T., SHIMURA, T., KUWANO, H. & RAZ, A. 2004. Autocrine motility factor signaling enhances pancreatic cancer metastasis. *Clin Cancer Res,* 10**,** 7775-84.

VAN BAELEN, K., DODE, L., VANOEVELEN, J., CALLEWAERT, G., DE SMEDT, H., MISSIAEN, L., PARYS, J. B., RAEYMAEKERS, L. & WUYTACK, F. 2004. The Ca^{2+}/Mn^{2+} pumps in the Golgi apparatus. *Biochim Biophys Acta,* 1742**,** 103-12.

VAN COPPENOLLE, F., VANDEN ABEELE, F., SLOMIANNY, C., FLOURAKIS, M., HESKETH, J., DEWAILLY, E. & PREVARSKAYA, N. 2004. Ribosome-translocon complex mediates calcium leakage from endoplasmic reticulum stores. *J Cell Sci,* 117**,** 4135-42.

VAN ENGELAND, M., NIELAND, L. J., RAMAEKERS, F. C., SCHUTTE, B. & REUTELINGSPERGER, C. P. 1998. Annexin V-affinity assay: a review on an apoptosis detection system based on phosphatidylserine exposure. *Cytometry,* 31**,** 1-9.

VAN HEEK, N. T., MEEKER, A. K., KERN, S. E., YEO, C. J., LILLEMOE, K. D., CAMERON, J. L., OFFERHAUS, G. J., HICKS, J. L., WILENTZ, R. E., GOGGINS, M. G., DE MARZO, A. M., HRUBAN, R. H. & MAITRA, A. 2002. Telomere shortening is nearly universal in pancreatic intraepithelial neoplasia. *Am J Pathol,* 161**,** 1541-7.

VANDER HEIDEN, M. G. 2011. Targeting cancer metabolism: a therapeutic window opens. *Nat Rev Drug,* 10**,** 671-84.

VANDER HEIDEN, M. G., CANTLEY, L. C. & THOMPSON, C. B. 2009. Understanding the Warburg effect: the metabolic requirements of cell proliferation. *Science,* 324**,** 1029-33.

VANDER HEIDEN, M. G., CHRISTOFK, H. R., SCHUMAN, E., SUBTELNY, A. O., SHARFI, H., HARLOW, E. E., XIAN, J. & CANTLEY, L. C. 2010. Identification of small molecule inhibitors of pyruvate kinase M2. *Biochem Pharmacol,* 79**,** 1118-24.

VAUPEL, P. & MAYER, A. 2007. Hypoxia in cancer: significance and impact on clinical outcome. Cancer *Metastasis Rev,* 26**,** 225-39.

VAUPEL, P., MAYER, A. & HOCKEL, M. 2004. Tumor hypoxia and malignant progression. *Methods Enzymol,* 381**,** 335-54.

VIVANCO, I. & SAWYERS, C. L. 2002. The phosphatidylinositol 3-Kinase AKT pathway in human cancer. *Nat Rev Cancer,* 2**,** 489-501.

VONLAUFEN, A., JOSHI, S., QU, C., PHILLIPS, P. A., XU, Z., PARKER, N. R., TOI, C. S., PIROLA, R. C., WILSON, J. S., GOLDSTEIN, D. & APTE, M. V. 2008. Pancreatic stellate cells: partners in crime with pancreatic cancer cells. *Cancer Res,* 68**,** 2085-93.

VOUSDEN, K. H. & RYAN, K. M. 2009. p53 and metabolism. *Nat Rev Cancer,* 9**,** 691-700.

WANG, G. L. & SEMENZA, G. L. 1993. General involvement of hypoxia-inducible factor 1 in transcriptional response to hypoxia. *Proc Natl Acad Sci U S A,* 90**,** 4304-8.

WANG, H. Q., ALTOMARE, D. A., SKELE, K. L., POULIKAKOS, P. I., KUHAJDA, F. P., DI CRISTOFANO, A. & TESTA, J. R. 2005. Positive feedback regulation between AKT activation and fatty acid synthase expression in ovarian carcinoma cells. *Oncogene,* 24**,** 3574-82.

WANG, L., HARRIS, T. E., ROTH, R. A. & LAWRENCE, J. C., JR. 2007. PRAS40 regulates mTORC1 kinase activity by functioning as a direct inhibitor of substrate binding. *J Biol Chem,* 282**,** 20036-44.

WANG, X., LIU, Y., REN, H., YUAN, Z., LI, S., SHENG, J., ZHAO, T., CHEN, Y., LIU, F., WANG, F., HUANG, H. & HAO, J. 2011. Polymorphisms in the hypoxia-inducible factor-1alpha gene confer susceptibility to pancreatic cancer. *Cancer Biol Ther,* 12**,** 383-7.

WARBURG, O. 1956. On the origin of cancer cells. *Science,* 123**,** 309-14.

WARSAME, R. & GROTHEY, A. 2012. Treatment options for advanced pancreatic cancer: a review. *Expert Rev Anticancer Ther,* 12**,** 1327-36.

WARSHAW, A. L. & FERNANDEZ-DEL CASTILLO, C. 1992. Pancreatic carcinoma. *N Engl J Med,* 326**,** 455-65.

WEHR, A. Y., FURTH, E. E., SANGAR, V., BLAIR, I. A. & YU, K. H. 2011. Analysis of the human pancreatic stellate cell secreted proteome. *Pancreas,* 40**,** 557-66.

WEINSTEIN, I. B. 2000. Disorders in cell circuitry during multistage carcinogenesis: the role of homeostasis. *Carcinogenesis,* 21**,** 857-64.

WICK, A. N., DRURY, D. R., NAKADA, H. I. & WOLFE, J. B. 1957. Localization of the primary metabolic block produced by 2-deoxyglucose. *J Biol Chem,* 224**,** 963-9.

WIEMAN, H. L., WOFFORD, J. A. & RATHMELL, J. C. 2007. Cytokine stimulation promotes glucose uptake via phosphatidylinositol-3 kinase/Akt regulation of Glut1 activity and trafficking. *Mol Biol Cell,* 18**,** 1437-46.

WILENTZ, R. E., IACOBUZIO-DONAHUE, C. A., ARGANI, P., MCCARTHY, D. M., PARSONS, J. L., YEO, C. J., KERN, S. E. & HRUBAN, R. H. 2000. Loss of expression of Dpc4 in pancreatic intraepithelial neoplasia: evidence that DPC4 inactivation occurs late in neoplastic progression. *Cancer Res,* 60**,** 2002-6.

WISE, D. R., DEBERARDINIS, R. J., MANCUSO, A., SAYED, N., ZHANG, X. Y., PFEIFFER, H. K., NISSIM, I., DAIKHIN, E., YUDKOFF, M., MCMAHON, S. B. & THOMPSON, C. B. 2008. Myc regulates a transcriptional program that stimulates mitochondrial

glutaminolysis and leads to glutamine addiction. *Proc Natl Acad Sci U S A,* 105**,** 18782-7.

WISE, D. R. & THOMPSON, C. B. 2010. Glutamine addiction: a new therapeutic target in cancer. *Trends Biochem Sci,* 35**,** 427-33.

WONG, K. K., ENGELMAN, J. A. & CANTLEY, L. C. 2010. Targeting the PI3K signaling pathway in cancer. *Curr Opin Genet Dev,* 20**,** 87-90.

WU, L. J., SWEET, T. B. & CLAPHAM, D. E. 2010. International Union of Basic and Clinical Pharmacology. LXXVI. Current progress in the mammalian TRP ion channel family. *Pharmacol Rev,* 62**,** 381-404.

WULLSCHLEGER, S., LOEWITH, R. & HALL, M. N. 2006. TOR signaling in growth and metabolism. *Cell,* 124**,** 471-84.

WUYTACK, F., RAEYMAEKERS, L. & MISSIAEN, L. 2002. Molecular physiology of the SERCA and SPCA pumps. *Cell Calcium,* 32**,** 279-305.

XU, R. H., PELICANO, H., ZHOU, Y., CAREW, J. S., FENG, L., BHALLA, K. N., KEATING, M. J. & HUANG, P. 2005. Inhibition of glycolysis in cancer cells: a novel strategy to overcome drug resistance associated with mitochondrial respiratory defect and hypoxia. *Cancer Res,* 65**,** 613-21.

XU, X., EHDAIE, B., OHARA, N., YOSHINO, T. & DENG, C. X. 2010a. Synergistic action of Smad4 and Pten in suppressing pancreatic ductal adenocarcinoma formation in mice. *Oncogene,* 29**,** 674-86.

XU, Z., VONLAUFEN, A., PHILLIPS, P. A., FIALA-BEER, E., ZHANG, X., YANG, L., BIANKIN, A. V., GOLDSTEIN, D., PIROLA, R. C., WILSON, J. S. & APTE, M. V. 2010b. Role of pancreatic stellate cells in pancreatic cancer metastasis. *Am J Pathol,* 177**,** 2585-96.

YAMAMOTO, S., TOMITA, Y., HOSHIDA, Y., MOROOKA, T., NAGANO, H., DONO, K., UMESHITA, K., SAKON, M., ISHIKAWA, O., OHIGASHI, H., NAKAMORI, S., MONDEN, M. & AOZASA, K. 2004. Prognostic significance of activated Akt expression in pancreatic ductal adenocarcinoma. *Clin Cancer Res,* 10**,** 2846-50.

YANG, L. & MOSES, H. L. 2008. Transforming growth factor beta: tumor suppressor or promoter? Are host immune cells the answer? *Cancer Res,* 68**,** 9107-11.

YAO, Y., CHOI, J. & PARKER, I. 1995. Quantal puffs of intracellular Ca^{2+} evoked by inositol trisphosphate in Xenopus oocytes. *J Physiol,* 482 (Pt 3)**,** 533-53.

YECIES, J. L. & MANNING, B. D. 2011. Transcriptional control of cellular metabolism by mTOR signaling. *Cancer Res,* 71**,** 2815-20.

YEROMIN, A. V., ZHANG, S. L., JIANG, W., YU, Y., SAFRINA, O. & CAHALAN, M. D. 2006. Molecular identification of the CRAC channel by altered ion selectivity in a mutant of Orai. *Nature,* 443**,** 226-9.

YING, H., ELPEK, K. G., VINJAMOORI, A., ZIMMERMAN, S. M., CHU, G. C., YAN, H., FLETCHER-SANANIKONE, E., ZHANG, H., LIU, Y., WANG, W., REN, X., ZHENG, H., KIMMELMAN, A. C., PAIK, J. H., LIM, C., PERRY, S. R., JIANG, S., MALINN, B., PROTOPOPOV, A., COLLA, S., XIAO, Y., HEZEL, A. F., BARDEESY, N., TURLEY, S. J., WANG, Y. A., CHIN, L., THAYER, S. P. & DEPINHO, R. A. 2011. PTEN is a major tumor suppressor in pancreatic ductal adenocarcinoma and regulates an NF-kappaB-cytokine network. *Cancer Discov,* 1**,** 158-69.

YING, H., KIMMELMAN, A. C., LYSSIOTIS, C. A., HUA, S., CHU, G. C., FLETCHER-SANANIKONE, E., LOCASALE, J. W., SON, J., ZHANG, H., COLOFF, J. L., YAN, H., WANG, W., CHEN, S., VIALE, A., ZHENG, H., PAIK, J. H., LIM, C., GUIMARAES, A. R., MARTIN, E. S., CHANG, J., HEZEL, A. F., PERRY, S. R., HU, J., GAN, B., XIAO, Y., ASARA, J. M., WEISSLEDER, R., WANG, Y. A., CHIN, L., CANTLEY, L. C. & DEPINHO, R. A. 2012. Oncogenic Kras maintains pancreatic tumors through regulation of anabolic glucose metabolism. *Cell,* 149**,** 656-70.

YU, X., CARROLL, S., RIGAUD, J. L. & INESI, G. 1993. H^+ countertransport and electrogenicity of the sarcoplasmic reticulum Ca^{2+} pump in reconstituted proteoliposomes. *Biophys J,* 64**,** 1232-42.

YUN, J., RAGO, C., CHEONG, I., PAGLIARINI, R., ANGENENDT, P., RAJAGOPALAN, H., SCHMIDT, K., WILLSON, J. K., MARKOWITZ, S., ZHOU, S., DIAZ, L. A., JR., VELCULESCU, V. E., LENGAUER, C., KINZLER, K. W., VOGELSTEIN, B. & PAPADOPOULOS, N. 2009. Glucose deprivation contributes to the development of KRAS pathway mutations in tumor cells. *Science,* 325**,** 1555-9.

ZHANG, H., BOSCH-MARCE, M., SHIMODA, L. A., TAN, Y. S., BAEK, J. H., WESLEY, J. B., GONZALEZ, F. J. & SEMENZA, G. L. 2008. Mitochondrial autophagy is an HIF-1-dependent adaptive metabolic response to hypoxia. *J Biol Chem,* 283**,** 10892-903.

ZHANG, H., GAO, P., FUKUDA, R., KUMAR, G., KRISHNAMACHARY, B., ZELLER, K. I., DANG, C. V. & SEMENZA, G. L. 2007. HIF-1 inhibits mitochondrial biogenesis and cellular respiration in VHL-deficient renal cell carcinoma by repression of C-MYC activity. *Cancer Cell,* 11**,** 407-20.

ZHANG, J., XIAO, P. & ZHANG, X. 2009. Phosphatidylserine externalization in caveolae inhibits Ca^{2+} efflux through plasma membrane Ca^{2+}-ATPase in ECV304. *Cell Calcium,* 45**,** 177-84.

ZHANG, J. J., WU, H. S., WANG, L., TIAN, Y., ZHANG, J. H. & WU, H. L. 2010. Expression and significance of TLR4 and HIF-1alpha in pancreatic ductal adenocarcinoma. *World J Gastroenterol,* 16**,** 2881-8.

ZHANG, S. L., YU, Y., ROOS, J., KOZAK, J. A., DEERINCK, T. J., ELLISMAN, M. H., STAUDERMAN, K. A. & CAHALAN, M. D. 2005. STIM1 is a Ca^{2+} sensor that activates CRAC channels and migrates from the Ca^{2+} store to the plasma membrane. *Nature,* 437**,** 902-5.

ZHAO, Y., ARAKI, S., WU, J., TERAMOTO, T., CHANG, Y. F., NAKANO, M., ABDELFATTAH, A. S., FUJIWARA, M., ISHIHARA, T., NAGAI, T. & CAMPBELL, R. E. 2011. An expanded palette of genetically encoded Ca^{2+} indicators. *Science,* 333**,** 1888-91.

ZHOU, W., CAPELLO, M., FREDOLINI, C., PIEMONTI, L., LIOTTA, L. A., NOVELLI, F. & PETRICOIN, E. F. 2011. Proteomic analysis of pancreatic ductal adenocarcinoma cells reveals metabolic alterations. *J Proteome Res,* 10**,** 1944-52.

ZHOU, W., CAPELLO, M., FREDOLINI, C., RACANICCHI, L., PIEMONTI, L., LIOTTA, L. A., NOVELLI, F. & PETRICOIN, E. F. 2012. Proteomic analysis reveals Warburg effect and anomalous metabolism of glutamine in pancreatic cancer cells. *J Proteome Res,* 11**,** 554-63.

ZU, X. L. & GUPPY, M. 2004. Cancer metabolism: facts, fantasy, and fiction. *Biochem Biophys Res Commun,* 313**,** 459-65.

ZYLINSKA, L., GUERINI, D., GROMADZINSKA, E. & LACHOWICZ, L. 1998. Protein kinases A and C phosphorylate purified Ca^{2+}-ATPase from rat cortex, cerebellum and hippocampus. *Biochim Biophys Acta,* 1448**,** 99-108.